Stereo-Controlled Supramolecular Assembly of 4(*R*/*S*)-Aminoproline Based Peptides and Peptide Nucleic Acids

A thesis

submitted in partial fulfillment of the requirements of the degree of

Doctor of Philosophy

By

Madhanagopal B

ID: 20113122

Research Supervisor: Prof. Krishna N. Ganesh



INDIAN INSTITUTE OF SCIENCE EDUCATION AND RESEARCH, PUNE

July 2018

CERTIFICATE

I certify that the work incorporated in the thesis entitled **"Stereo-Controlled Supramolecular Assembly of 4(*R*/*S*)-Aminoproline Based Peptides and Peptide Nucleic Acids"** submitted by **Mr. Madhanagopal B** was carried out by the candidate, under my supervision. The work presented here or any part of it has not been included in any other thesis submitted previously for the award of any degree or diploma from any other university or institution.

Date:

Prof. Krishna N. Ganesh

(Research Supervisor)

DECLARATION

I declare that, this written submission represents my ideas in my own words and where others' ideas have been included, I have adequately cited and referenced the original sources. I also declare that I have adhered to all principles of academic honesty and integrity and have not misrepresented or fabricated or falsified any idea / data / fact/ source in my submission. I understand that violation of the above will be cause for disciplinary action by the Institute and can also evoke penal action from the sources which have thus not been properly cited or from whom proper permission has not been taken when needed.

Date: Madhanagopal B

Acknowledgements

I thank my thesis supervisor Prof. Krishna N. Ganesh for his guidance and support through all these years. His words of support and encouragement have been the most important source of strength for me at all times. I am grateful for the lessons I have learnt from him, by listening to his lectures, by discussing with him, and by simply observing him. He has helped me shed my fear of chemistry. And, for that I will be grateful to him for the rest of my life.

I express my sincere thanks to Prof. H. N. Gopi and Prof. Kundan Sengupta for their suggestions and advice. Their insights and questions in RAC meetings have helped me a great deal to understand my project. I am also thankful to Prof. M. Jayakannan, Prof. Aloke Das, and Prof. Sulabha Kulkarni for their support and for helping me learn to design experiments. I am grateful for the discussions with Prof. Nagaraj Balasubramanian, Prof. Sudha Rajamani and Prof. Sai Krishnan in the first two years. Those interactions were short, but very useful as it helped me find fresh perspectives in the projects. My sincere thanks to Prof. Girish Ratnaparkhi for helping me and advising me several times during my Ph.D. in IISER Pune.

The technical staff in chemistry department (Swati, Mahesh, Megha, Sandip, Yatish and Anil) has been very kind to me all these years. I am greatly indebted to all of them for their help. The support and encouragement from my friends and colleagues in the Nanoscience Unit, Neeraj, Keerthi, Usha, Arthur and Resmi have kept me motivated. I am grateful to them for being there for me whenever I needed them.

I thank my labmates and my seniors for helping me all these years. Especially, Tanpreet, Mahesh, Deepak, Nitin, Satheesh, Vijay and Pradnya had been kind and supportive. I am greatly indebted to Prabhakar, Shahaji, Pramod, Manoj, Iranna, Dhrub, Shiraj. Om Shanker, Pradeep, Rajat and Gaurav for helping me at numerous occasions. I am grateful to all of them for teaching me so many things in the lab.

Finally, I am forever indebted to my parents and my sisters. Their affection and love are the pillars of strength I depend on. I cannot thank them enough, for they keep me sane and they keep me alive.

Madhanagopal B

Contents

Abbreviations ix
Abstract xi

Chapter 1

Introduction

1.0 Introduction 2
1.1 Peptides – Structure and Conformations 3
1.2 Peptide Based Self-Assembly 9
1.3 Peptide Nucleic Acids 20
1.4 Scope of the Thesis 24
1.5 References 29

Section A: Linear Peptides

Chapter 2

Design and Synthesis of 4(*R*/*S*)-Amino and Guanidino Proline Based Peptides

2.1 Introduction 36
2.1.1 Biomolecular Self-Assembly 37
2.1.2 Supramolecular Assembly with Peptides 38
2.1.3 Polyproline Peptides and PP-II Conformation 39
2.1.4 C4(*R*/*S*)-Substituted Prolyl Polypeptides 41
2.2 Rationale 42
2.2.1 Aminoprolyl Peptides 42
2.2.2 Guanidinylprolyl Polypeptides 44
2.3 Objectives 45
2.4 Results and Discussion 45
2.4.1 Synthesis of Monomers 46
2.4.2 Solid Phase Peptide Synthesis 49
2.4.3 Purification and Characterization of Peptides 55
2.5 Summary 56
2.6 Experimental 56
2.7 References 72
2.8 Appendix A 78

Chapter 3

Biophysical Studies of 4(*R/S*)-Amino and Guanidino Proline Based Peptides

3.1 Introduction 94

3.2 Objectives 94

3.3 Results and Discussion 95

3.3.1 Aminoprolyl Polypeptides 95

3.3.1a Effect of Length on (4*S*)-amp_n 96

3.3.1b Effect of Temperature 99

3.3.1c Effect of Solvents 100

3.3.1d SDS Induced PP-II to β Conformational Change 101

3.3.1e Conformation of (4*S*)-amp_9 in Water-in-oil Microemulsion 109

3.3.1f Effect of Lipidation on Conformation of 4(*R*/*S*)-Aminoprolyl Polypeptides 109

3.3.2 Guanidinylprolyl polypeptides 111

3.3.2a pK_a of Guanidinylprolyl Polypeptides 111

3.3.2b Conformational Studies of 4(*R*/*S*)-Guanidinylprolyl Polypeptides 112

3.3.2c Effect of Lipidation on Conformation of 4-Guanidinylprolyl Polypeptides 114

3.3.2d Interaction of Guanidinylprolyl Polypeptides with DNA 118

3.4 Summary 125

3.5 Experimental 127

3.6 References 129

Chapter 4

Self-Assembly Studies of 4(*R*/*S*)-Amino and Guanidino Proline Based Peptides

4.1 Introduction 134

4.2 Objectives 137

4.3 Results and Discussion 138

4.3.1 Aminoprolyl Polypeptides 138

4.3.1a Solvent Dependent Self-assembly of (4*S*)-amp_9 139

4.3.1b Effect of Concentration on Morphology in TFE 143

4.3.1c Time Dependent Change in Morphology of (4*S*)-amp_9 144
4.3.1d Effect of Peptide Length on Morphology of (4*S*)-amp_n 146
4.3.1e Effect of Lipidation on Aminoprolyl Polypeptides 148
4.3.1f Thioflavin-T Fluorescent Assay of Nanofibres of (4*S*)-amp_9 150
4.3.2 Guanidinylprolyl Polypeptides 152
4.3.2a Self-assembly of 4-Guanidinylprolyl Polypeptides 152
4.3.2b Effect of Lipidation on Morphology of Guanidinylprolyl Polypeptides 153
4.4 Summary 155
4.5 Experimental 157
4.6 References 158

Section B: Branched Peptides

Chapter 5

Design, Synthesis, Biophysical Studies and Self Assembly of Branched Polyproline Peptides

5.1 Introduction 164
5.2 Rationale and Objectives 165
5.3 Results and Discussion 168
5.3.1 Synthesis of Branched Peptides 168
5.3.1a Design Considerations and Synthetic Strategies 166
5.3.1b Solid Phase Synthesis of Branched Peptides 171
5.3.1c Purification and Characterization of Peptides 173
5.3.2 Conformational Studies of Branched Peptides 173
5.3.3. Morphological Study of Self-Assembled Branched Polyproline Peptides 175
5.3.3a Solvent Dependent Self-Assembly of (4*S*)-$amp^{\curlywedge}$-$(amp_3)_2$ 176
5.3.3b Solvent Dependent Self-Assembly of (4*R*)-$Amp^{\curlywedge}$-$(amp_3)_2$ 179
5.3.3c Effect of the Chiral Core on Self-Assembly of Branched Peptides 180
5.4 Summary 181
5.5 Experimental 182
5.6 References 188
5.7 Appendix B 190

Chapter 6

Design, Synthesis, Biophysical Studies and Self Assembly of Branched Peptide Nucleic Acids

6.1 Introduction 193

6.2 Rationale and Objectives 195

6.3 Results and Discussion 198

6.3.1 Synthesis of Branched PNA 198

6.3.1a Synthetic Strategies 198

6.3.1b Solid Phase Synthesis 201

6.3.1c Purification and Characterization of Branched PNA 201

6.3.2 Conformational Studies of Branched PNA 202

6.3.2a Effect of pH on the Conformation of Branched PNA 202

6.3.2b Effect of Oligonucleotide dC_{12} 204

6.3.2b Effect of Ag^{+} on Conformation of Branched PNA 206

6.3.3 Morphology of Self-Assembled Branched PNAs 217

6.3.3a Effect of pH on Self-Assembly of Branched PNA 217

6.3.3b Effect of dG_{12} on Self-Assembly of Branched PNA 220

6.3.3c Effect of dC_{12} on Self-Assembly of Branched PNA 222

6.3.3d Effect of Ag^{+} on Self-Assembly of Branched PNA 225

6.4 Summary 234

6.5 Experimental 237

6.6 References 239

6.7 Appendix C 248

Abbreviations

Ac	Acetyl
Ac_2O	Acetic anhydride
Ala	Alanine
AFM	Atomic force microscopy
Amp	(2*S*,4*R*)-Aminoproline
amp	(2*S*,4*S*)-aminoproline
Arg	Arginine
Azp	(2*S*,4*R*)-Azidoproline
azp	(2*S*,4*S*)-azidoproline
$(Boc)_2O$	Boc anhydride
^oC	Degree Celsius
CD	Circular Dichroism
CMPs	Collagen mimetic peptides
Cys	Cysteine
DCM	Dichloromethane
ΔTm	Difference in melting temperature
DIAD	Diisopropyl azodicarboxylate
DIPEA	*N,N*- Diisopropylethylamine
DMF	*N,N*-Dimethylformamide
DMS	Dimethyl sulfate
DNA	Deoxyribonucleic acid
ECM	Extracellular matrix
eq.	equivalents
ESI-MS	Electro Spray Ionization Mass Spectrometry
Et	Ethyl
FESEM	Field Emission Scanning Electron Microscopy
FET	Field Effect Transistor
Fmoc	9-Fluorenylmethoxycaronyl
g	Gram
Glu	Glutamic acid
Gly	Glycine
h	Hours
HBTU	(2-(1H-Benzotriazole-1 -yl)-1,1,3,3-tetramethyl-uronium hexafluorophosphate)
HOBt	N- Hydroxybenzotriazole
HPLC	High Performance Liquid Chromatography
Hyp	(2*S*,4*R*)-Hydroxyproline (*trans*-4-hydroxy-L-proline)
hyp	(2*S*,4*S*)-hydroxyproline (*cis*-4-hydroxy-L-proline)
Hz	Hertz
in situ	In the reaction mixture
in vivo	Within the living organism
in vitro	Outside the living organism
IR	Infra Red
K	Kelvin/ Lysine
Leu	Leucine
Lys	Lysine
M	Molar

MALDI-TOF	Matrix Assisted Laser Desorption Ionization-Time of Flight
MBHA	p-methoxybenzhydrylamine
MeCN	Acetonitrile
MeOH	Methanol
mg	milligram
mL	millilitre
min	minutes
μ	Micron
μL	Microliter
μM	Micromolar
mmol	millimolar
MS	Mass spectrometry
MsCl	methanesulfonylchloride
NaN_3	Sodium azide
nm	Nanometer
NMP	N-Methyl-2-pyrrolidone
NMR	Nuclear Magnetic Resonance
Pd-C	Palladium on carbon
Phe	Phenylalanine
Pro	L-Proline
PNA	Peptide Nucleic Acid
ppm	parts per million
PPII	Polyproline II
PPI	Polyproline I
psi	pound per square inch
R	Rectus
RP	Reverse phase
RNA	Ribonucleic acid
S	Sinister
SPPS	Solid Phase Peptide Synthesis
t-Boc	tert-butyloxycarbonyl
TFA	Trifluoroacetic acid
TFMSA	Trifluoromethane sulfonic acid
TFE	2,2,2-Trifluoroethanol
THF	Tetrahedrofuran
Tm	Melting temperature
Trp	Tryptophan
Tyr	Tyrosine
Val	Valine
v/v	volume to volume ratio
Z	zusammen

Abstract

The thesis entitled "**Stereo-Controlled Supramolecular Assembly of 4(*R*/*S*)-Aminoproline Based Peptides and Peptide Nucleic Acids**" is comprised of studies on design, synthesis of peptides and peptide nucleic acids containing 4(*R*/*S*)-aminoproline and its derivatives, and studies on their conformational properties and self-assembling properties. The work explores the solvent dependent and stereo-specific PP-II - β conformational transitions exhibited by 4(*S*)-aminoprolyl polypeptides, and their assembly into slender nanofibers with left-handed twists. The effect of lipidation and, of replacing C4(*R/S*)-NH_2 with guanidine, on the conformational preference of the polypeptides is investigated. The consequences of these modifications on the morphology of the peptide assemblies are also probed. In order to utilize the rich conformational dynamics of 4(*R/S*)-aminoproline to generate complex self-assembled structures, branched polyproline peptides and branched peptide nucleic acids were synthesized with the trifunctional amino acid, 4(*R/S*)-aminoproline as chiral branching core. The conformational and self-assembly studies show that a variety of complex supramolecular assemblies can be constructed with these motifs. Moreover, under specific conditions, stereo-control over morphology of self-assembled structures can be achieved by altering the stereochemistry at the C4 position of aminoproline.

This thesis is divided into six chapters:

Chapter 1: Introduction

Section A: Linear Peptides

Chapter 2: Design and Synthesis of 4(*R/S*)-Amino and Guanidino Proline Based Peptides

Chapter 3: Biophysical Studies of 4(*R*/*S*)-Amino and Guanidino Proline Based Peptides

Chapter 4: Self-Assembly of 4(*R*/*S*)-Amino/Guanidino Proline Based Peptides

Section B: Branched Peptides

Chapter 5: Design, Synthesis, Biophysical Studies and Self-Assembly of Branched Polyproline Peptides

Chapter 6: Design, Synthesis, Biophysical Studies and Self-Assembly of Branched Peptide Nucleic Acids

---

Chapter 1: Introduction

This chapter gives an overview of the background literature for undertaking the research work in the field of self-assembly of polyproline peptides and peptide nucleic acids.

Among the secondary structures adopted by peptides and proteins, polyproline II conformation (PP-II) has gathered interest in the past few decades as their roles in biological processes such as molecular recognition and protein folding are being unraveled.[1] Oligoprolines with PP-II scaffold has been used to construct various self-assembling systems.[2] Owing to the significance the PP-II conformation holds, several investigations have focused on the conformational stability of PP-II conformation.[3] PP-II is a semi-extended left-handed helix, with all the peptide bonds in *trans* conformation. The solvent exposed backbone is highly solvated. Although the PP-II helix is not stabilized by any intrastrand hydrogen bonds, different stereoelectronic effects have been implicated in their stability. In polyproline peptides, backbone n(O) $\rightarrow$ π^*(CO) interaction favors the *trans* amide bond and contributes to the stability of PP-II.[4] Electron withdrawing substitutions at C4(*R*/*S*) position of the repeating proline residues has significant influence on the peptide backbone.[5] Conformational preference of 4(*R*/*S*)-aminoprolyl polypeptides is influenced by the configuration at C4. Specifically, while PP-II is the preferred conformation in aqueous solvents, 4(*S*)-aminoprolyl polypeptide, (4*S*)-amp_9 adopts β-sheet like conformation in 2,2,2-trifluoroethanol (TFE).[6] (4*R*)-Amp_9 retains its preference for PP-II conformation in all the solvents. Similar behavior was observed in case of 4(*R*/*S*)-hydroxyprolyl polypeptides as

well. Further, lipidated 4(*S*)-hydroxyprolyl polypeptides, (4*S*)-hyp_9 was found to also assemble into nanofibers in TFE, under the conditions where they exhibit β-structure.[7] A switch between intramolecular hydrogen bonding scheme to an intermolecular hydrogen bonding was proposed to explain this unusual stereo-specific conformational properties.

In this thesis, this conformational change is explored further. The effect of the cationic amino and guanidino substitutions on the conformational properties and supramolecular organization of peptides with polyproline backbone is studied systematically. This work also includes attempts made to utilize the rich conformational dynamics of 4(*R*/*S*)-aminoprolines to construct branched polyprolines and branched peptide nucleic acids to gain control over their self-assembly by using 4(*R*/*S*)-aminoprolines as a chiral branch point.

Chapter 2: Design and Synthesis of 4(*R/S*)-Amino and Guanidino Proline Based Peptides

This chapter describes the design and synthesis of 4(*R/S*)-aminoproline monomers and the synthesis of a series of homoligomeric linear peptides used in the present work. The peptides were prepared to probe the stereo-dependent conformational changes and to observe the effect of their conformational behavior in different solvents on their self-assembling properties.

The orthogonally protected monomers, (2*S*,4*R*)-N(1)-t-Boc-N^4-Fmoc-aminoproline **7** and (2*S*,4*S*)-N(1)-t-Boc-N^4-Fmoc-aminoproline **12** (Figure 1) were synthesized from the commercially available *trans*-4(*R*)-hydroxyproline as reported in the literature. These monomers were incorporated into their corresponding homooligomeric peptides (4*S*)-amp_n (**P1-P3**) and (4*R*)-Amp_9 (**P9**) using the standard solid phase peptide synthesis protocol.

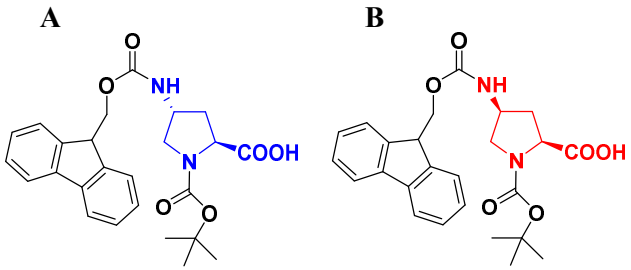
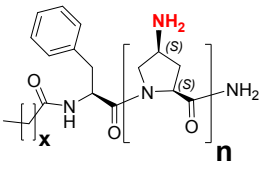
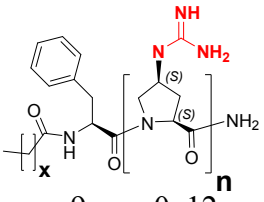
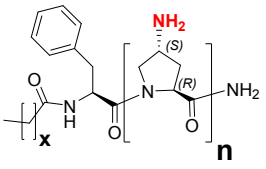
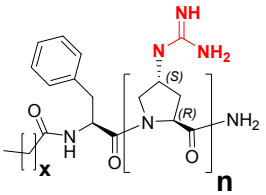


Figure 1: Orthogonally protected aminoproline monomers. (A) (2*S*,4*R*)-N(1)-t-Boc-N^4-Fmoc-aminoproline **7**, (B) (2*S*,4*S*)- N(1)-t-Boc-N^4-Fmoc- aminoproline monomer **12.**

TABLE 1: Linear peptides used in this study

	Peptide	Notation	Structure
P1	Ac- Phe-(***amp***)$_3$-$CONH_2$	(4*S*)-*amp*$_3$	 n = 3, 6, 9 x = 0, 10, 12, 14
P2	Ac- Phe-(***amp***)$_6$-$CONH_2$	(4*S*)-*amp*$_6$	
P3	Ac- Phe-(***amp***)$_9$-$CONH_2$	(4*S*)-*amp*$_9$	
P4	C_{12}- Phe-(***amp***)$_9$-$CONH_2$	(4*S*)-*amp*$_9$–C_{12}	
P5	C_{14}- Phe-(***amp***)$_9$-$CONH_2$	(4*S*)-*amp*$_9$–C_{14}	
P6	C_{16}- Phe-(***amp***)$_9$-$CONH_2$	(4*S*)-*amp*$_9$–C_{16}	
P7	Ac- Phe-(***gndp***)$_9$-$CONH_2$	(4*S*)-*gndp*$_9$	 n = 9; x = 0, 12
P8	C_{14}- Phe-(***gndp***)$_9$-$CONH_2$	(4*S*)-*gndp*$_9$–C_{14}	
P9	Ac- Phe-(***Amp***)$_9$-$CONH_2$	(4*R*)-*Amp*$_9$	 n = 9; x = 0, 12
P10	C_{14}- Phe-(***Amp***)$_9$-$CONH_2$	(4*R*)-*Amp*$_9$–C_{14}	
P11	Ac- Phe-(***Gndp***)$_9$-$CONH_2$	(4*R*)-*Gndp*$_9$	 n = 9; x = 0

The lipidated peptides, (4*S*)-*amp*$_9$–C_{12} (**P4**), (4*S*)-*amp*$_9$–C_{14} (**P5**) and (4*S*)-*amp*$_9$–C_{16} (**P6**), derived from (4*S*)-*amp*$_9$ (**P3**) were obtained by coupling lauric acid (C_{12}), myristic acid (C_{14}), or palmitic acid (C_{16}) respectively to the N-terminal phenyl alanine. On-resin guanidinylation of peptides, (4*S*)-*amp*$_9$ (**P3**) and (4*S*)-*amp*$_9$–C_{14} (**P5**) yielded guanidinylprolyl polypeptides (4*S*)-*gndp*$_9$ (**P7**) and (4*S*)-*gndp*$_9$–C_{14} (**P8**). Similarly, aminoprolyl polypeptides (4*R*)-*Amp*$_9$ (**P9**) and (4*R*)-*Amp*$_9$–C_{14} (**P10**)**,** were prepared from (4*R*)-*Amp* monomer **12**. The peptide (4*R*)-*Amp*$_9$ (**P9**) was guanidinylated on-resin to obtain guanidinylprolyl polypeptide (4*R*)-*Gndp*$_9$ (**P11**). The peptides were cleaved from the solid support resin and purified using RP-HPLC. The purified peptides were then characterized with MALDI-TOF to check their integrity.

Chapter 3: Biophysical Studies of 4(*R*/*S*)-Amino and Guanidino Proline Based Peptides

This chapter deals with investigations into the conformational properties of C4(*S*)-NH_2 substituted aminoprolyl polypeptides (**P1**-**P6**), and guanidinylprolyl polypeptides (**P7**-**P8**) in aqueous buffer and TFE to elucidate stereospecific effects on the secondary structure adopted by polyproline peptides.

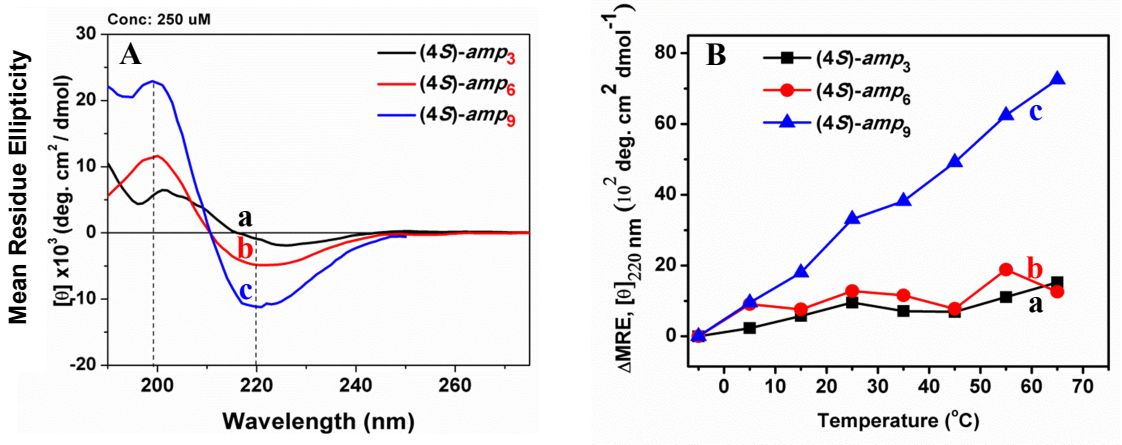


Figure 2: A) CD spectra of 250 µM solution of peptides (4*S*)-*amp*$_3$ (**P1**) (trace **a**), (4*S*)-*amp*$_6$ (**P2**) (trace **b**), (4*S*)-*amp*$_9$ (**P3**) (trace **c**) in TFE. B) Change in the magnitude of MRE at 220 nm with temperature for peptides (4*S*)-*amp*$_3$ (**P1**) (trace **a,** ■), (4*S*)-*amp*$_6$ (**P2**) (trace **b,** ●), (4*S*)-*amp*$_9$ (**P3**) (trace **c,** ▲).

The propensity of the aminoprolyl polypeptides (4*S*)-*amp*$_n$ to form β-like conformation was found to increase with the number of aminoproline residues in the homooligomers as indicated by an increase in the magnitudes of both negative CD band at 220 nm and positive band at 195 nm in TFE (Figure 2A). While the peptides with three and six residues of (4*S*)-*amp* did not show any temperature dependent change in the intensity of their characteristic CD bands in TFE, (4*S*)-*amp*$_9$ showed a linear decrease in the intensity of its CD band at 220 nm and 200 nm (Figure 2B). These observations suggest the plausible involvement of interchain hydrogen bonding in contributing to the stability of the β-sheet like arrangement in TFE.

CD spectra recorded in different solvents showed that the extent to which solvents affect the propensity of (4*S*)-*amp* to adopt β-like structure is dependent on peptide length. While (4*S*)-*amp*$_3$ (**P1**) showed β only in TFE and acetonitrile, the longer peptide (4*S*)-*amp*$_9$ (**P3**) readily adopted β structure in all the alcohols studied.

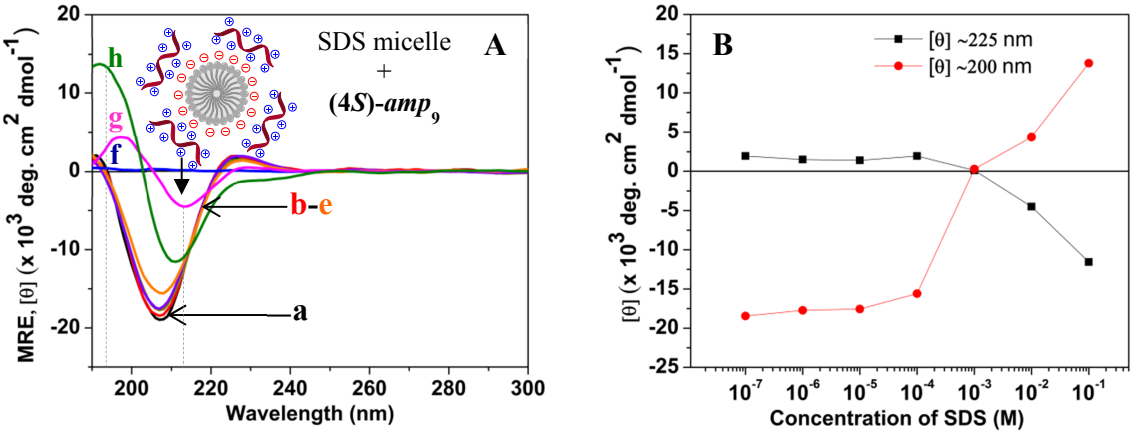


Figure 3: SDS induced conformational changes in peptide (4*S*)-*amp*$_9$ (**P3**). A) CD spectra of the peptide **P3** (100 μM) in the presence of different concentrations of SDS: 0 M (trace **a**); 0.1 μM SDS (trace **b**); 1.0 μM SDS (trace **c**); 10 μM SDS (trace **d**); 100 μM SDS (trace **e**); 1 mM SDS (trace **f**); 10 mM SDS (trace **g**); 100 mM SDS (trace **h**). B) Change in magnitude of CD bands at 225 nm (black ■) and 200 nm (red ●) with concentration of SDS.

The investigations performed with surfactants showed that SDS, in its monomeric state (below cmc), tends to destabilize the secondary structure of the 4(*R*/*S*)-aminoprolyl polypeptides upon interaction with their cationic sidechains (Figure 3). As micelles, SDS was

found to promote the formation of β-like structure in case of (4*S*)-amp_9, (**P3**). These observations suggest that the conformational preference of the aminoprolyl polypeptide is dictated mainly by changes in the solvation of the backbone and changes in the backbone to side-chain hydrogen bonding.

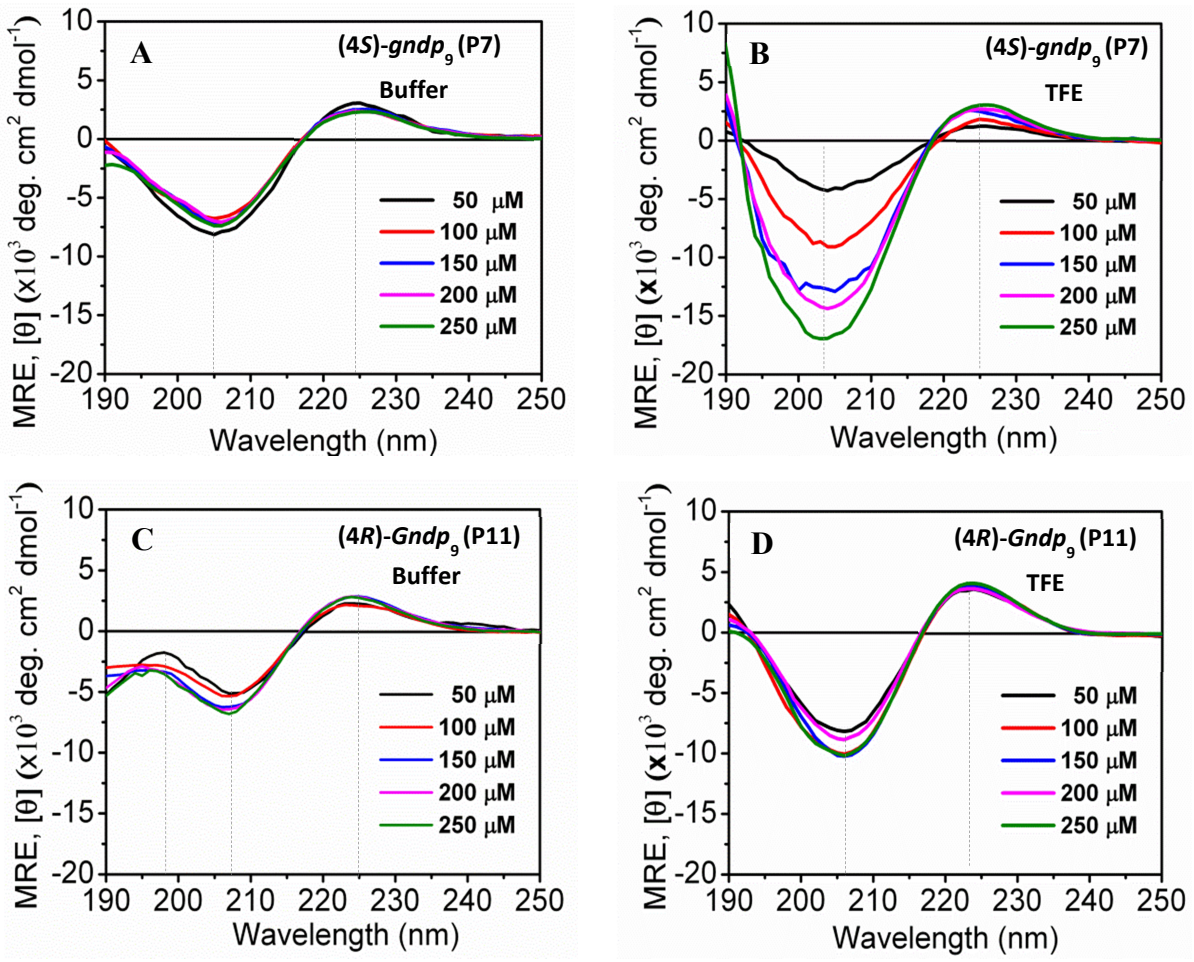


Figure 4: CD spectra of peptides (4*S*)-$gndp_9$ (**P7**) in phosphate buffer (10 mM, pH 7.0) (A) and in TFE (B); (4*R*)-$Gndp_9$, (**P11**) in phosphate buffer (10 mM, pH 7.0) (C) and in TFE (D).

4(*R*/*S*)-Guanidnylprolyl polypeptides did not show any solvent dependent conformational change as their amine derivatives did. They retained PP-II form in both phosphate buffer and TFE (Figure 4). Lipidation of the peptide was shown to destabilize the PP-II form, in the presence of counterions such as sulphates and phosphates. Thus, the present work suggests ways to alter and hence control the backbone conformation of polyproline peptides. With C4(*S*)-NH_2 substitution, the peptide can be tuned from a left

handed PP-II helix to a ribbon-like β-sheet in TFE and in the presence of SDS micelles. With C4(*S*)-guanidine substitution however, the backbone conformation can be altered by conjugation with lipid chain at the N-terminus of the peptide.

Chapter 4: Self-Assembly of 4(*R*/*S*)-Amino/Guanidino Proline Based Peptides

This chapter deals with investigations into the self-assembling properties of C4(*S*)-NH_2 substituted aminoprolyl polypeptides (**P1**-**P6**), and guanidnylprolyl polypeptides (**P7**-**P8**) under different conditions mainly using field emission scanning electron microscopy (FESEM) and atomic force microscopy (AFM) techniques.

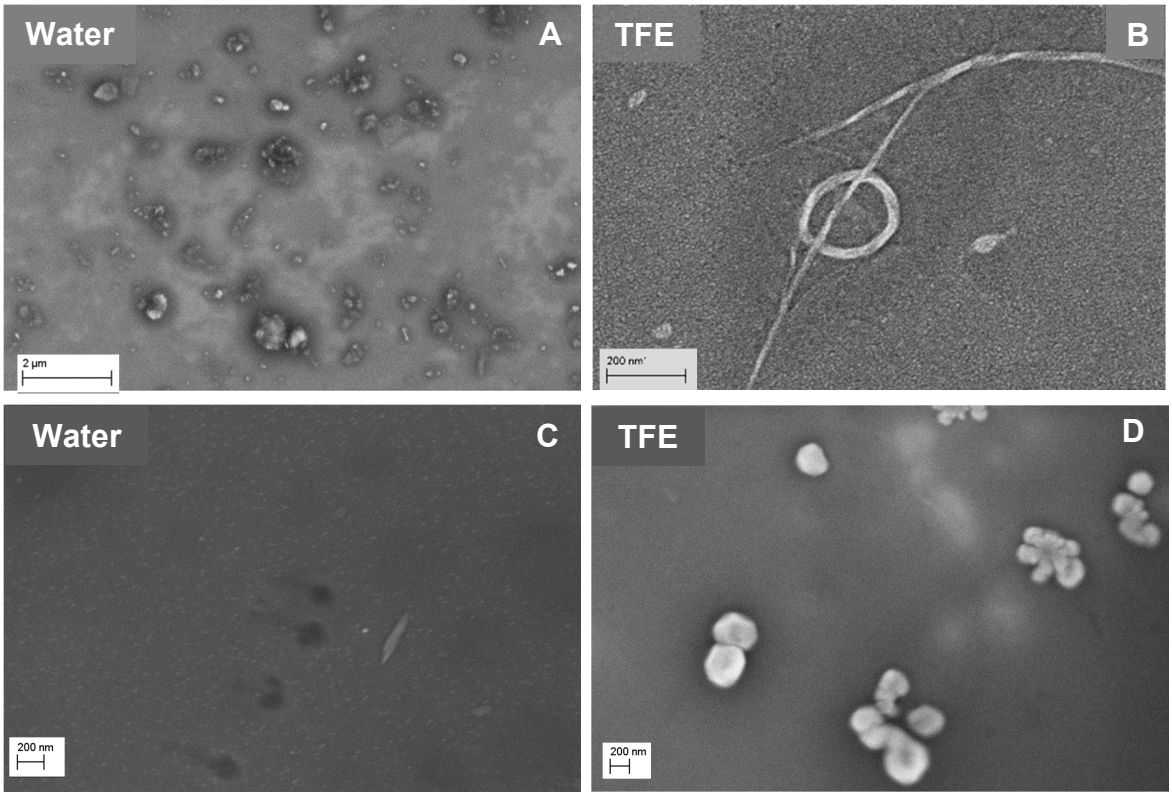


Figure 5: FE-SEM images of morphologies formed by peptide (4*S*)-amp_9 (**P3**) in water (A) and in TFE (B) and peptide (4*R*)-Amp_9 (**P9**) in water (C) and TFE (D).

C4(*S*)-NH_2 substitution on polyproline oligomers were found to confer the peptides with superior self-assembling properties in TFE, in which the peptide showed β-sheet like conformation. The peptide, (4*S*)-amp_9 (**P3**), forms nearly spherical aggregates of size about 50 nm within 1 hour of incubation in TFE. Then, it transforms into mature nanofibres within

a period of about 12 hours under ambient conditions. The fibres were found to have a gentle left-handed twist with a twist angle of about 37°. The fibrils formed were about 2 – 3 nm in height. These fibrils intertwined to form larger left handed helical fibres and bundles of about 30 nm to 60 nm in diameter. The peptide (4*R*)-Amp_9 (**P9**), on the other hand show no characteristic morphology either in water or in TFE (Figure 5).

Shorter peptides (4*S*)-amp_3 (**P1**), and (4*S*)-amp_6 (**P2**) did not form any characteristic morphologies in water or TFE suggesting the involvement of interchain hydrogen-bonding interactions in stabilizing the extended structures formed by the peptides in TFE. N-terminal lipidation of the aminoprolyl polypeptide (4*S*)-amp_9 (**P3**) did not alter the morphological properties of the peptide in TFE.

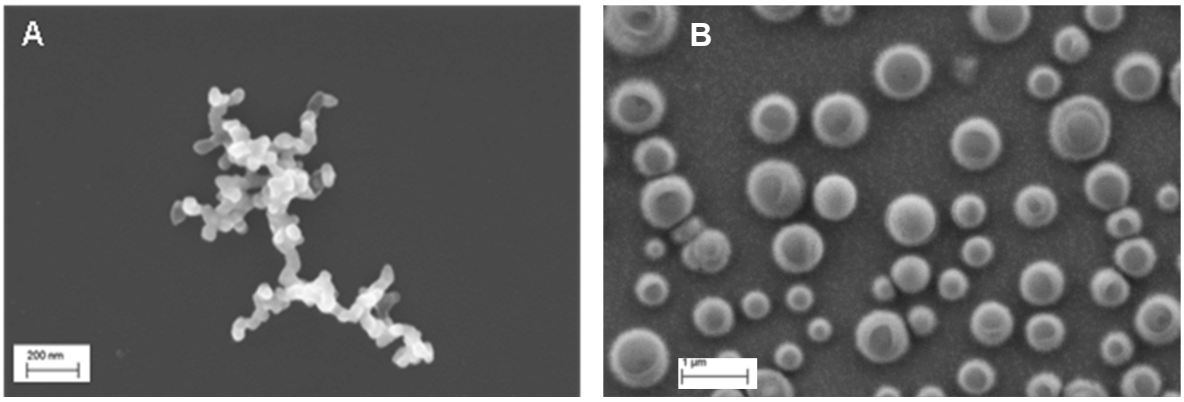
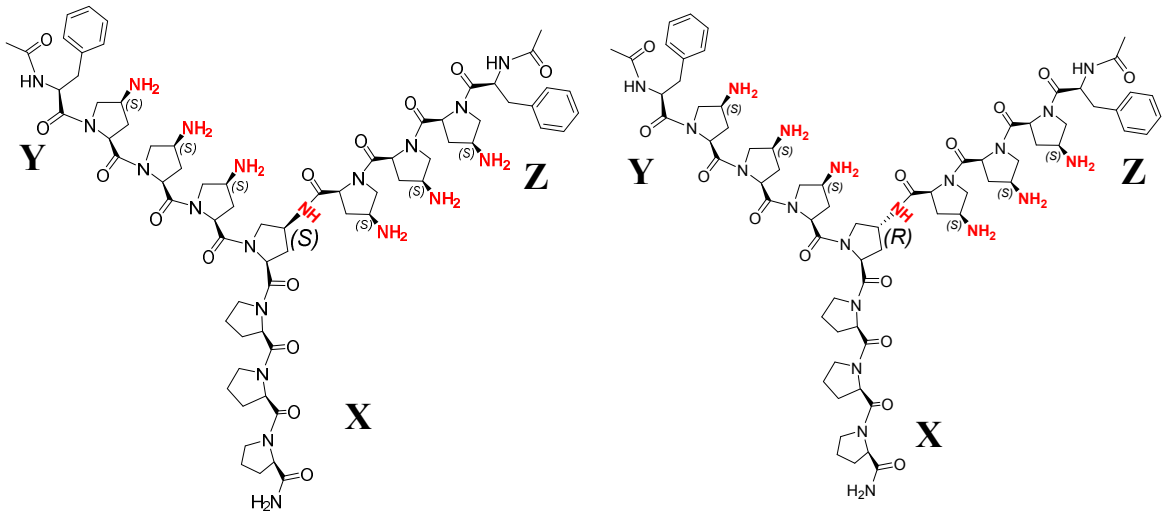


Figure 6: FESEM images of peptides (4*S*)-$gndp_9$ (**P7**) in water (A) (4*S*)-$gndp_9$–C_{14} (**P8**) in phosphate buffer (10 mM, pH 7.0) (B).

Guanidinylprolyl polypeptides (4*S*)-$gndp_9$ (**P7**) and (4*R*)-$Gndp_9$ (**P11**), which did not show solvent dependent conformational change, were found to show no regular morphologies either in water or in TFE (Figure 6A). The myristoylated peptide (4*S*)-$gndp_9$–C_{14} (**P8**) produced spherical particles with multilayered structures (Figure 6B). As cationic peptides, the tendency of the peptides to form spherical particles could make them promising candidate as carriers of drugs and other cargo for drug delivery applications.

Chapter 5: Design, Synthesis, Biophysical Studies and Self-Assembly of Branched Polyproline Peptides

In this chapter, the synthesis, conformational and self-assembling properties of branched polyproline peptides, constructed with (4*S*)-*amp* and (4*R*)-*Amp* residues as the core-branching unit is described.



(4*S*)-*amp*$^{\curlywedge}$-(*amp*$_3$)$_2$ (**P12**) (4*R*)-*Amp*$^{\curlywedge}$-(*amp*$_3$)$_2$ (**P13**)

Figure 7: Branched peptides (**P12-P13**) with three branches X, Y and Z

The branched polyproline peptides (4*S*)-*amp*$^{\curlywedge}$-(*amp*$_3$)$_2$ (**P12**) and (4*R*)-*Amp*$^{\curlywedge}$-(*amp*$_3$)$_2$ (**P13**) were synthesized with 4(*R*/*S*) aminoproline as chiral branching unit (Figure 7). The peptides were designed in such a way that one arm (X) with three prolyl residues contained the free amidated C-terminus and two branches (Y and Z) had acetylated N terminus. The branching peptide arms bearing three (4*S*)-*amp* residues were synthesized from the core 4(*R*/*S*)-aminoprolyl unit simultaneously.

The circular dichroism spectra showed that both the peptides formed PP-II structure in aqueous phoshphate buffer (pH 7.0) (Figure 8). In TFE, the PP-II form was found to be destabilized with the formation of β-sheet like conformation of the aminoprolyl arms Y and Z. In water, the peptides assembled into spherical structures and showed no differences in

their morphology. In TFE, (4*S*)-*amp*$^{\lambda}$-(*amp*$_3$)$_2$ (**P12**) assembled into fibres and (4*R*)-*Amp*$^{\lambda}$-(*amp*$_3$)$_2$ (**P13**) formed irregular spherical aggregates.

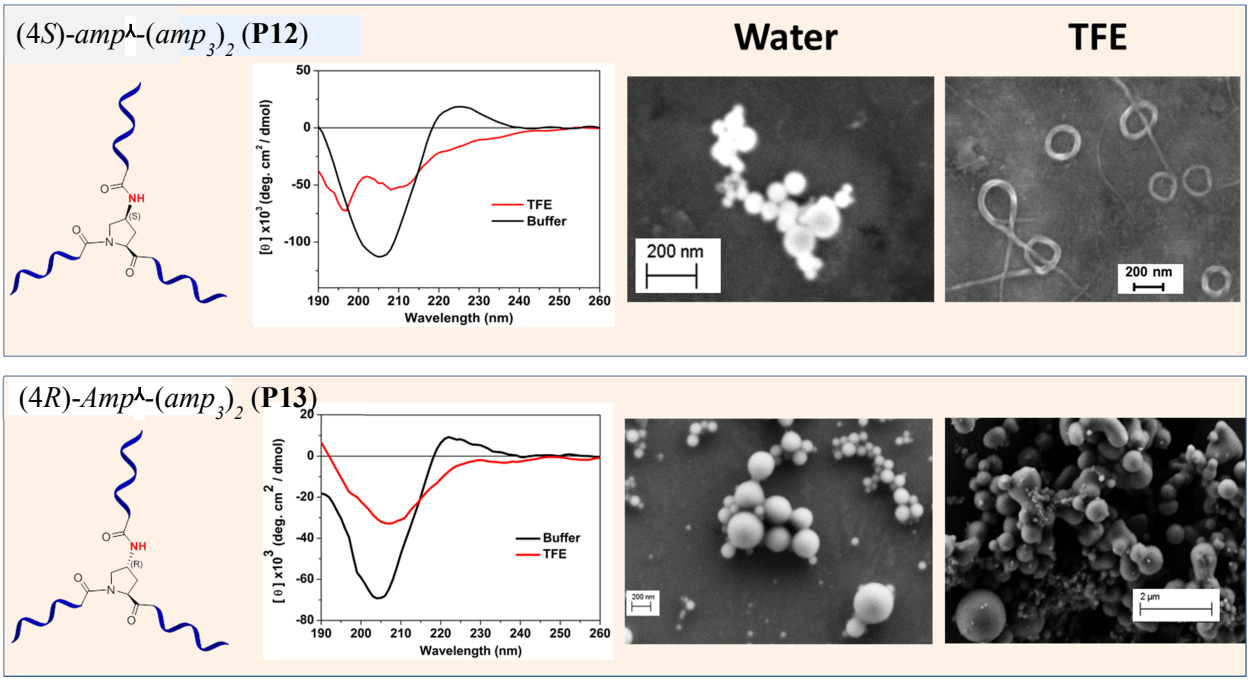


Figure 8: Comparison of CD spectra and morphologies formed by branched peptides (4*S*)-*amp*$^{\lambda}$-(*amp*$_3$)$_2$ (**P12**) and (4*R*)-*Amp*$^{\lambda}$-(*amp*$_3$)$_2$ (**P13**) in different solvents

The change in morphology was attributed to the chiral core effecting the intermolecular interactions between the branched aminoprolyl peptide arms. The results suggested that a branched structure promotes self-assembly of the nanofibers as compared to linear topology, with the morphology dependent on the stereochemistry of the 4(*R*/*S*)-aminoproline at the branching point.

Chapter 6: Design, Synthesis, Biophysical Studies and Self-Assembly of Branched Peptide Nucleic Acids

In this chapter, the synthesis, conformational and self-assembling properties of branched peptide nucleic acids, constructed with (4*S*)-*amp* and (4*R*)-*Amp* residues as the core-branching unit is described.

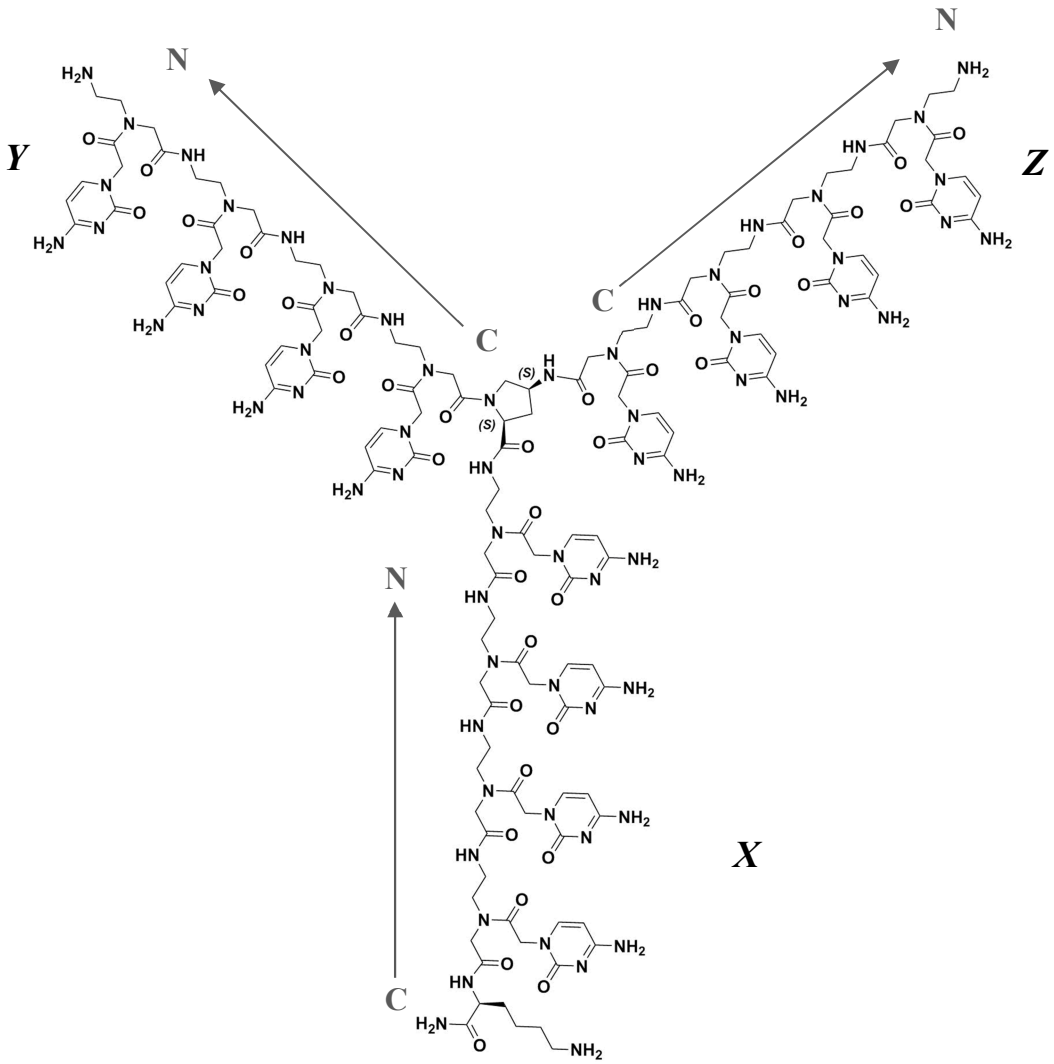


Figure 9: Branched PNA (4*S*)-*amp*$^{\lambda}$-$(C_4)_3$ (**P14**) showing the three branches X, Y and Z. Arrows show the direction of synthesis of different PNA arms.

Branched peptide nucleic acids PNAs (4*S*)-*amp*$^{\lambda}$-$(C_4)_3$ (**P14**) and (4*R*)-*Amp*$^{\lambda}$-$(C_4)_3$ (**P15**) were designed to have three PNA C_4 branches emerging from the chiral (4*S*)-*amp* or (4*R*)-*Amp* core (Figure 9). The conformational properties and self-assembling properties of these dendron like PNA molecules were investigated under different conditions. Since cytosines are known to form i-motif structures[8] (Figure 10B) at acidic pH, studies focused on the effect of pH on the conformation and morphology of the branched PNA and its hybrids with DNA dC_{12}were carried out. As cytosines are also known to have strong affinity for Ag^+ ions[9] (Figure 10C), the effect of this was also probed on the conformation and morphology in

water. From these investigations, the role of chirality and hydrogen bonding rearrangements (Figure 10 D) at the core of the branched PNA in influencing their self-assembling properties (Figure 10 E) is explored.

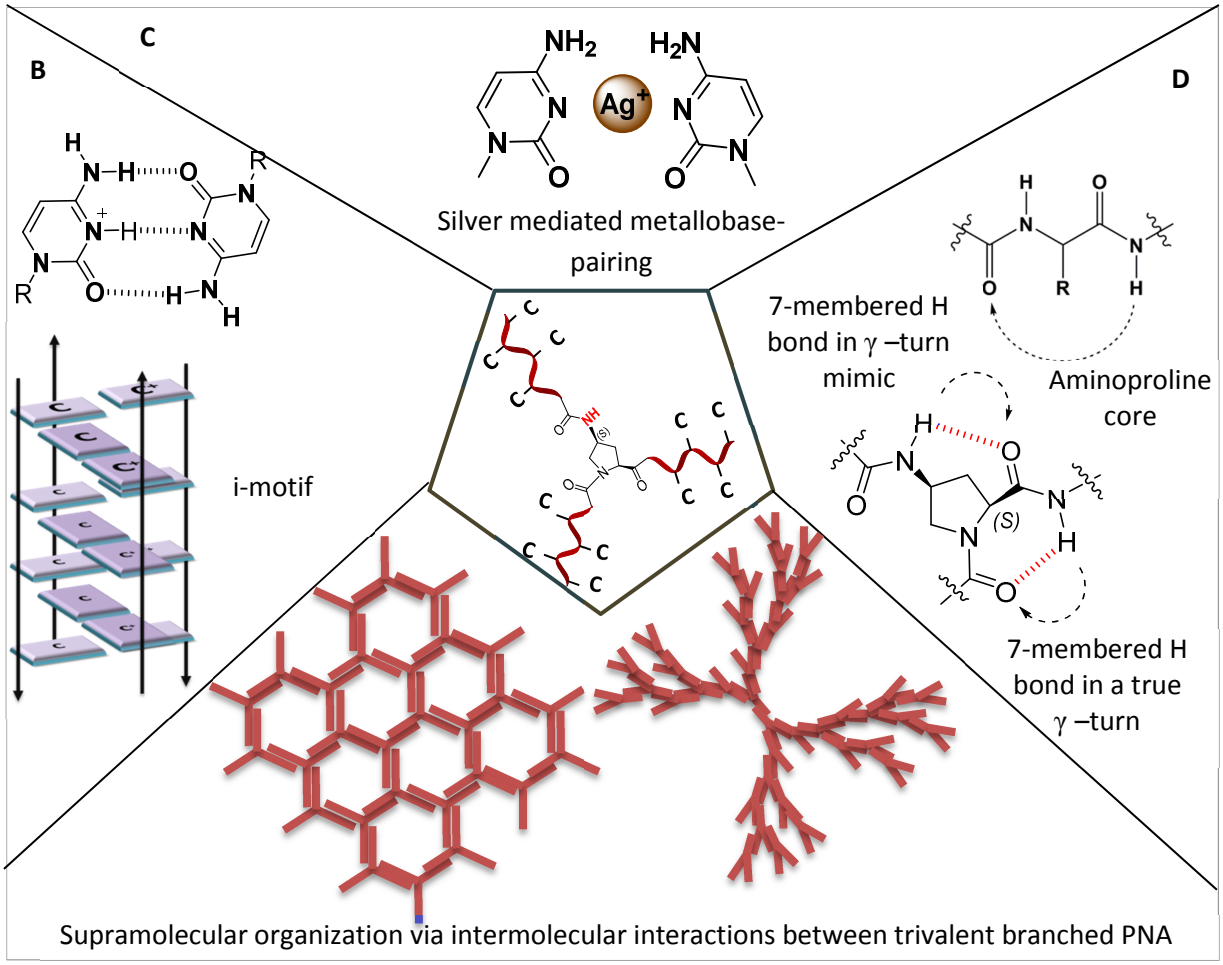
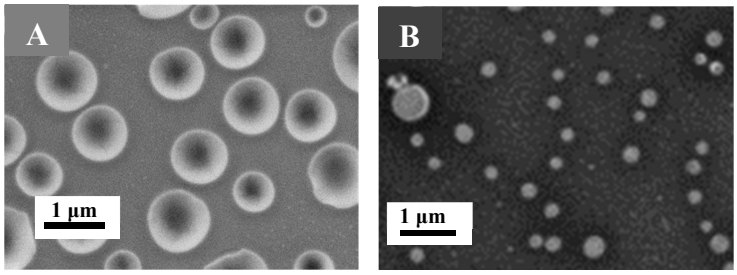


Figure 10: Structural, conformational and self-assembling properties of branched PNA

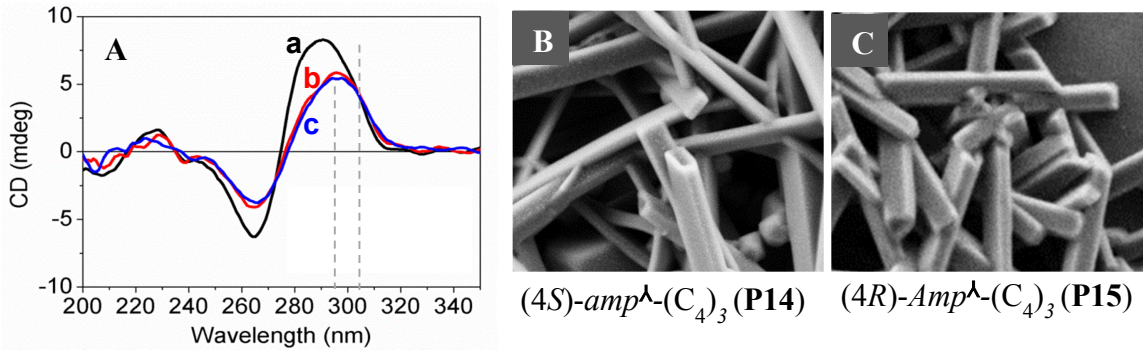
Branched peptide nucleic acids (4*S*)-*amp*$^{\lambda}$-$(C_4)_3$ (**P14**)) and (4*R*)-*Amp*$^{\lambda}$-$(C_4)_3$ (**P15**) were found to assemble into spherical particles at pH 5 (10 mM phosphate buffer) (Figure 11).



(4*S*)-*amp*$^{\curlywedge}$-$(C_4)_3$ (**P14**) (4*R*)-*Amp*$^{\curlywedge}$-$(C_4)_3$ (**P15**)

Figure 11: FESEM images of PNA DNA hybrid of DNA dC_{12} and PNA (4*S*)-*amp*$^{\curlywedge}$-$(C_4)_3$ (**P14**) (A) and (4*R*)-*Amp*$^{\curlywedge}$-$(C_4)_3$ (**P15**) (B) in 10 mM phosphate buffered saline at pH 5.

CD spectroscopic studies revealed that in the presence of dC_{12} at pH 5, the PNAs (4*S*)-*amp*$^{\curlywedge}$-$(C_4)_3$ (**P14**) and (4*R*)-*Amp*$^{\curlywedge}$-$(C_4)_3$ (**P15**) showed a CD spectral band at 295 nm, characteristic of i-motif structures of the PNA:DNA complexes[8] (Figure 12A). These hybrids assembled into hollow rectangular nanotubes. The nanotubes appeared to be crystalline and to have grown from octahedral seed crystals over a period of 5 days (Figure 12B-C).



(4*S*)-*amp*$^{\curlywedge}$-$(C_4)_3$ (**P14**) (4*R*)-*Amp*$^{\curlywedge}$-$(C_4)_3$ (**P15**)

Figure 12: (A) Circular dichroism spectra of DNA dC_{12} only (trace **a**), PNA-DNA dC_{12} hybrid formed by (4*S*)-*amp*$^{\curlywedge}$-$(C_4)_3$ (**P14**) (trace **b**), and (4*R*)-*Amp*$^{\curlywedge}$-$(C_4)_3$ (**P15**) (trace **c**) in 10 mM phosphate buffered saline at pH 5. FESEM images of PNA/DNA hybrid of DNA dC_{12} and PNA (4*S*)-*amp*$^{\curlywedge}$-$(C_4)_3$ (**P14**) (B) and (4*R*)-*Amp*$^{\curlywedge}$-$(C_4)_3$ (**P15**) (C) in 10 mM phosphate buffered saline at pH 5.

The branched PNAs showed chiral core dependent characteristic conformational behavior in the presence of Ag^+ (Figure 13). While both (4*S*)-*amp*$^{\curlywedge}$-$(C_4)_3$ (**P14**) and (4*R*)-*Amp*$^{\curlywedge}$-$(C_4)_3$ (**P15**) formed duplex on addition of silver ions, the PNAs **P14** and **P15** underwent conformational changes within 90 minutes. (4*S*)-*amp*$^{\curlywedge}$-$(C_4)_3$ (**P14**) exhibited a

total reversal of the CD spectra during this period, which indicated a change in the handedness of branched PNAs. In case of PNA (4*R*)-*Amp*$^{\lambda}$-$(C_4)_3$ (**P15**) however, the CD signals gradually obliterated. Stereochemistry dependent intra-molecular H-bonding properties were postulated to orchestrate the reversal of helical handedness of the silver mediated PNA duplexes. The chirality of the core also influenced the self-assembling properties.

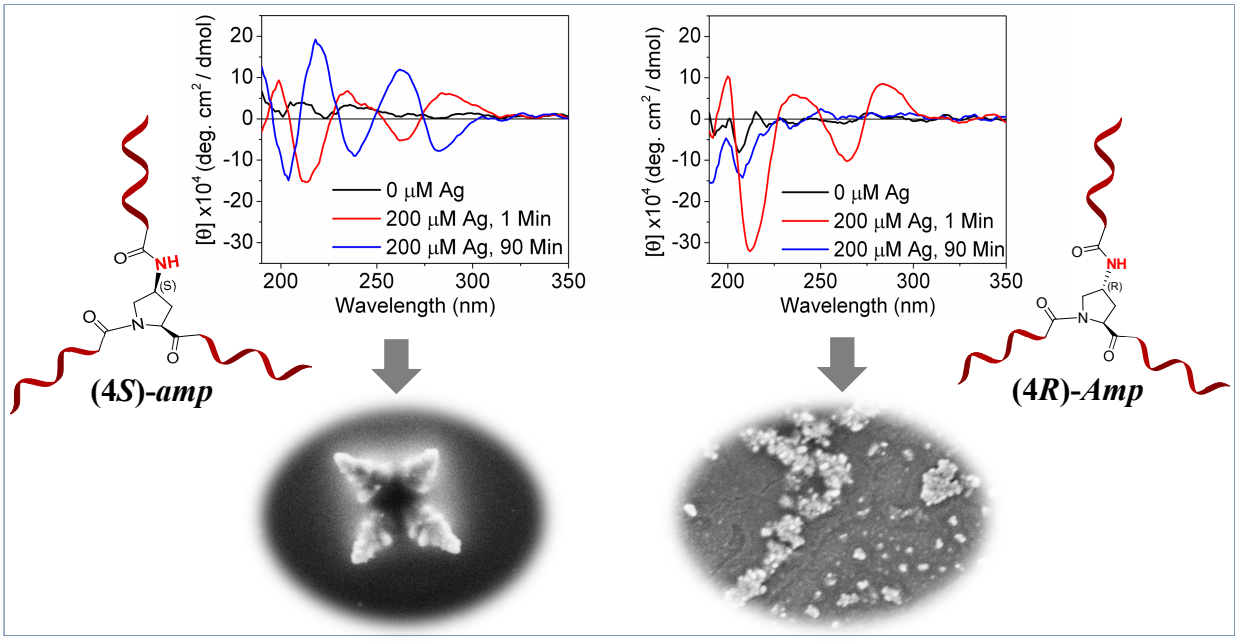


Figure 13: Stereodependent self-assembly of branched PNA

Upon examining the self-assembled structures of the PNA-Ag^+ complex under FESEM, it was found that the configuration at C4 of the chiral aminoproline core controls the morphology of the supramolecular assemblies. A four-point star like morphology was formed by silver complexes with PNA (4*S*)-*amp*$^{\lambda}$-$(C_4)_3$ (**P14**) at equimolar concentration of Ag^+ and cytosines. PNA **P15** (4*R*)-*Amp*$^{\lambda}$-$(C_4)_3$ on the other hand, resulted in irregular aggregates without any characteristic features in the presence of Ag^+. Time dependent study revealed that the nanostars grew as a single entity and not clusters of separately formed elliptical particles.

The branched PNAs, regardless of the chirality of the core were found to also assemble into long molecular wires in the presence of Hg^{2+} ions in water in a period of 2 days (Figure 14).

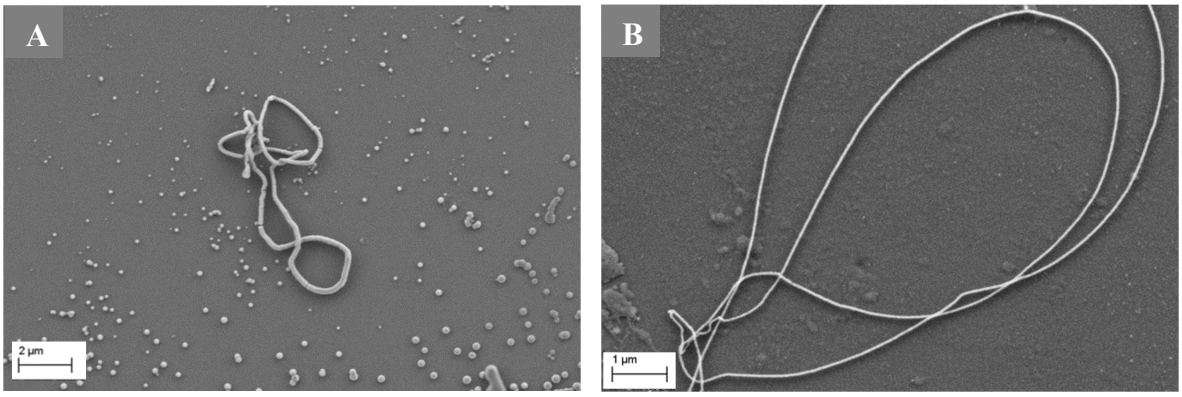


Figure 14: PNA / Hg^{2+} molecular wires formed by PNA (4*S*)-*amp*ʎ-$(C_4)_3$ (**P14**) and by PNA (4*R*)-*Amp*ʎ-$(C_4)_3$ (**P15**) in water.

These studies showed that a chiral control over the conformation and self-assembly could be achieved with these dendron like branched PNA enabled by the rich conformational dynamics of 4(*R*/*S*)-aminoproline. As a novel motif that brings together the strengths of peptide backbone based peptide nanotechnology and sequence dependent nucleic acid nanotechnology, these chiral branched PNA proved to be highly promising as a tool for directed self-assembly, and for construction of dynamic nanodevices as demonstrated by the diverse nanostructures like nanospheres, hollow capsules, nanostars, and nanotubes, formed by these molecules under various conditions.

References

1. a) Adzhubei, A. A.; Sternberg, M. J. E. Left-handed Polyproline II Helices Commonly Occur in Globular Proteins. *J. Mol. Biol*. **1993**, *229*, 472-493. b) Esipova, N. G.; Tumanyan, V. G. Omnipresence of the Polyproline II Helix in Fibrous and Globular Proteins. *Curr. Opin. Struct. Biol.* **2017**, *42*, 41 –49.

2. a) Yoon, Y.; Lim, Y.; Lee, E.; Lee, M.Self-assembly of a peptide rod–coil: a polyproline rod and a cell-penetrating peptide Tat coil. *Chem. Commun.* **2008**, 1892-1894. b)

Lewandowska, U.; Zajaczkowski, W.; Chen, L.; Bouillière, F.; Wang, D.; Koynov, K.; Pisula, W.; Müllen, K.; Wennemers, H. Hierarchical Supramolecular Assembly of Sterically Demanding π-Systems by Conjugation with Oligoprolines. *Angew. Chem. Int. Ed.* **2014**, *53*, 12537 – 12541.

3. a) Shoulders, M. D.; Raines, R. T.; Collagen structure and stability. *Ann. Rev. Biochem*. **2009**, 78, 929-958. b) Bansode, N. D.; Madhanagopal, B.; Sonar, M. V.; Ganesh, K. N. Stereodependent and solvent specific formation of unusual β-structure through side chain-backbone H-bonding in C4(*S*)-(NH_2/OH/NHCHO)-L-prolyl polypeptides. *Peptide Science* **2017**, *108*(*1*), e22981.

4. Horng, J. C.; Raines, R. T. Stereoelectronic Effects on Polyproline Conformation. *Protein Sci.* **2006**, *15*, 74-83.

5. Shoulders, M. D.; Kotch, F. W.; Choudhary, A.; Guzei, I. A.; Raines, R. T. The Aberrance of the 4*S* Diastereomer of 4-Hydroxyproline. *J. Am. Chem. Soc.* **2010**, *132*, 10857-10865.

6. Sonar, M. V.; Ganesh, K. N. Water-induced switching of β-structure to polyproline II conformation in the 4S-aminoproline polypeptide via H-bond rearrangement. *Org. Lett.* **2010***, 12*, 5390–5393.

7. Bansode, N. D.; Sonar, M. V.; Ganesh, K. N. A nanofiber assembly directed by the non-classical antiparallel β-structure from 4*S*-(OH) proline polypeptide. *Chem. Commun*. **2016**, *52*, 4884-4887.

8. Guéron, M.; Leroy, J. The i-motif in nucleic acids. *Curr. Opin. Struct. Biol*. **2000**, *10*, 326–331.

9. Kondo, J.; Tada, Y.; Dairaku, T.; Hattori, Y.; Saneyoshi, H.; Ono, A,; Tanaka, Y. Silver continguous wire: A metallo-DNA nanowire with uninterrupted one-dimensional silver array. *Nat. Chem.* **2017**, *9,* 956-960.

Chapter 1

Introduction

1.0 Introduction

Order holds a unique place in nature. It is in the quest to understand order, its consequences, and its manifestations, that a large portion of scientific enquiry of mankind has been concerned with for many centuries.

Self-assembly is a process that involves organization of simpler building blocks through spontaneous diffusion into complex ordered structures, governed by various non-covalent interactions such as electrostatic, hydrophobic, van der Waals, and hydrogen bonds.[1] A large number of weak interactions in different combinations are often involved in producing stable assemblies. In biomolecular systems, complexity is achieved by hierarchical organization of basic building blocks like amino acids, nucleotides, and sugars and their polymers. The hierarchical self-assembly is an overarching feature that underlies all the structure of complex cellular organelles and their functions.[2] The hallmarks of these biomolecular architectures are their molecular recognition and reproducibility. The nano-assemblies such as viral capsids,[3] amyloid fibres,[4] flagella,[5] and ribosomes,[6] etc., involve periodic arrangement of biopolymers such as proteins and nucleic acids. Their formation is dependent on the conformation of individual macromolecule as much as it depends on the ensemble of weak interactions holding them together. Our ability to emulate nature to generate sophisticated supramolecular assemblies with an excellent degree of control and predictability over specific molecular interactions and the overall architecture of the complexes is greatly limited by the gaps in our understanding of the process of molecular self-assembly. A lack of detailed understanding of general principles outlining the interconnection between the structure and morphology of the self-assembled structure is one of the major impediments in the rational design of synthetic biomolecular nano-assemblies and fabrication of artificial nanodevices inspired by them.

1.1 Peptides – Structure and Conformations

1.1.1 Structure of Peptides

Proteins are linear polymers made up of 20 proteinogenic amino acids in different sequences. In proteins and polypeptides, the monomeric α-amino acid units are linked by peptide bonds and hence the polypeptide backbone has three main chain dihedral angles: (i) φ (*phi*), the torsion angle between C_α -N (ii) ψ (*psi*), the torsion angle about the bond between carbonyl carbon and C_α, (iii) ω, the angle about the amide bond (Figure 1.1).

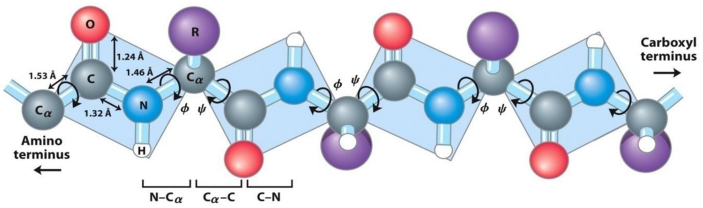


Figure 1.1: Polypeptide backbone showing the main chain torsion angles.[7]

These main chain dihedral angles define the relative positions of the adjacent planar peptide bonds. The conformation of a polypeptide chain is therefore determined by these torsional angles. The preferred torsion angles for φ and ψ depend primarily on the nature of the α- substituent. Thus, the conformation adopted by a polypeptide chain is dependent on the amino acid sequence.[8]

1.1.2 Peptide Secondary Structures

Different non-covalent interactions among the amino acid residues in segments of a peptide chain result in ordered structures with repetitive dihedral angles (φ and ψ). These secondary structures often exhibit specific hydrogen bonding patterns between the main chain atoms in the peptide backbone. The most common secondary structures are α-helix and β-sheets. Other structures include polyproline helix (PP-II), 3_{10} helix, and π-helix. These secondary structural motifs are usually connected by turns of different kinds.

1.1.2a. *α-Helix*

The α-helix is the most frequently encountered secondary structure. It is a right handed helix with a pitch of 5.4 Å and 3.6 residues per turn.[9] It is stabilized by intrastrand hydrogen bonds between backbone NH and C=O of residues i and i+4. This results in an optimum N… O distance of 2.8 Å with the side chain projecting away from the helix and the hydrogen bonds oriented parallel to the helix axis. The typical main chain torsion angles are: $\varphi = -57^{o}$ and $\psi = -47^{o}$ (Figure 1.2A).

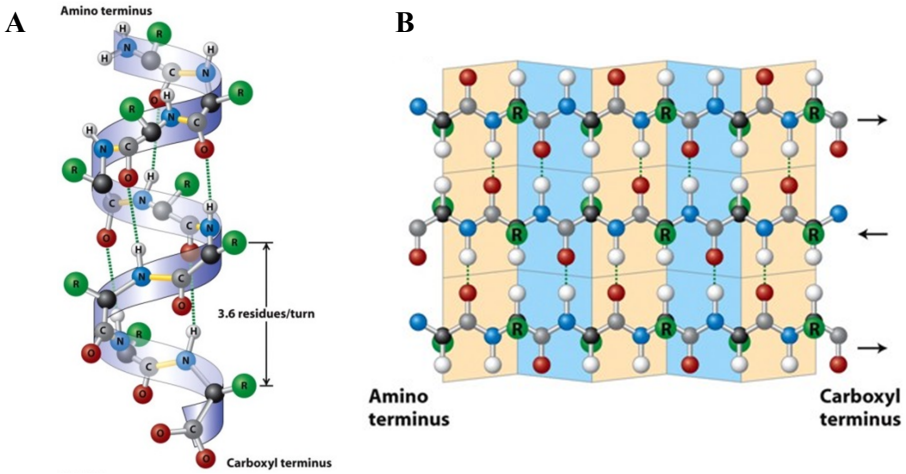


Figure 1.2: Schematic representation of secondary structures: α- helix (A) and β-sheet (B)[10]

1.1.2b. *β sheet*

The β sheet is an extended structure where the peptide backbone forms hydrogen bonds with those of the neighbouring polypeptide chains (interstrand) (Figure 1.2B). This is unlike the α-helix, where the hydrogen bonding occurs between residues of the same peptide segment (intrastrand). Depending on the orientation of the adjacent peptide strands involved in the β sheets, they can be of two types: (i) the antiparallel β sheet, where the neighbouring hydrogen bonded peptide chains run in opposite directions, (ii) the parallel β sheet, where the polypeptide chains are in the same direction. The latter is slightly more distorted as compared to the antiparallel β sheet and occurs less frequently. A series of β strands hydrogen bonded

together tends to form pleated sheets. In these, the side chains of adjacent amino acid residues in the peptide strands are oriented on opposite sides of the sheet, separated by a distance of 7.0 Å, corresponding to about two residue repeat distance. The β sheets are generally twisted and curled in the native structures of most proteins. In the Ramachandran plot, the β sheet conformations occupy a large region in the top left quadrant. The typical values of the main chain torsion angles are: $\varphi = -139^{o}$ and $\psi = +135^{o}$ for antiparallel β sheet and $\varphi = -119^{o}$ and $\psi = +113^{o}$ for parallel β sheet.[9]

1.1.2c *Turns*

Turns are regions in the peptide structure where the polypeptide chain reverses its direction (Figure 1.3). In these structural motifs, the C_α atoms of two residues separated by 1 to 5 peptide bonds are held close to each other, often with the help of hydrogen bonds between the residues.[11] Unlike the other secondary structures, turns do not have repeating backbone torsion angles.

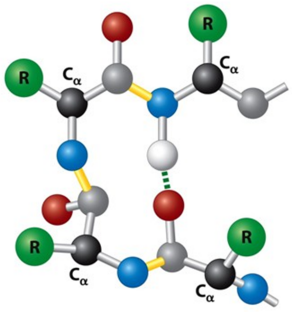


Figure 1.3: Structure of a β-turn[10]

The turns are classified based on the number of peptide bonds that separate the two end residues. An α-turn is formed between residues separated by four peptide bonds ($i \rightarrow i \pm 4$) and forms a single turn of an α-helix. The β-turn is formed when the residues separated by three peptide bonds ($i \rightarrow i \pm 3$) are held together by intrastrand hydrogen bond. Similarly, a γ-turn is formed between residues separated by two peptide bonds ($i \rightarrow i \pm 2$). δ-turn and π-turn

correspond to turns formed by peptides formed between residues that are four or five peptide bonds apart respectively.

1.1.2d *Polyproline Conformations: PPI and PPII*

Polyproline II (PP-II) is a common secondary structure that is present in both folded and unfolded proteins.[12] It is semi-extended left-handed helix and has three residues per turn with no intrastrand hydrogen bonds stabilizing the helix (Figure 1.4).[13] It is usually seen in peptides containing repeating proline residues that lack H-bond donor in its backbone, but it can be adopted by other non-proline residues as well. PP-II conformation is known to be involved in a variety of processes such as signal transduction, immune response and cell motility.[14] It is also a part of the native structure of many proteins. For instance, PP-II form is the conformation adopted by individual collagen polypeptide chains.[15] Three such PP-II left handed coils are wound around each other to form the stable collagen triplexes. The typical values of the main chain torsion angles in PP-II helix are: $\varphi = -65^{o}$ and $\psi = +145^{o}$.

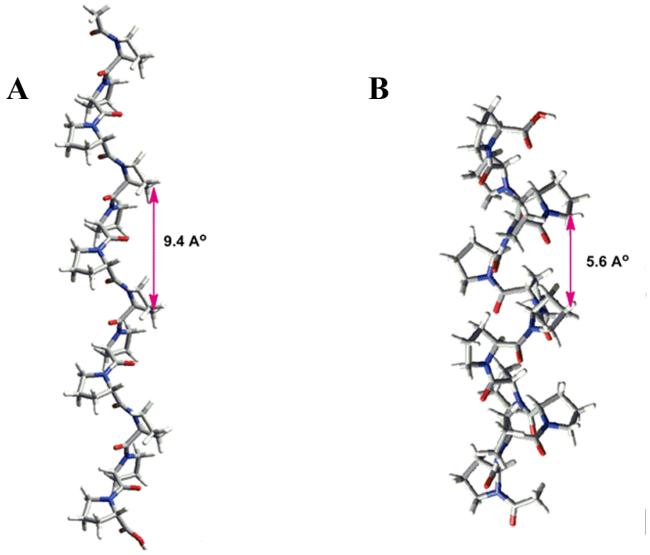


Figure 1.4: Structure of PP-II (A) and PP-I (B)[16]

Among the usual proteinogenic amino acids, proline is unique, as it has a sidechain that is cyclized on to the backbone nitrogen atom. The consequence of this is the restriction

of dihedral angle φ to ~ -65°. It also imposes restriction on the residue that precedes the proline.[17] These constraints play key role in determining the propensity of sequences to adopt specific secondary structures. For instance, occurrence of proline in an α- helix distorts it by introducing kinks. Proline is also known as "β-breaker".[18] However, conformational restriction on the residue preceding proline predisposes it to adopt β sheet conformation.[16] A homooligomer of proline is likely to adopt PP-II structure. In this extended form, the backbone carbonyls are exposed to the solvent and are readily available for H-bonding either with the solvent water molecules or other interacting proteins.[19] At the same time, the sidechain of proline offers a continuous stretch of hydrophobic surface around the helix. Thus, a PP-II helix provides both hydrogen bonding potential and offers an easily accessible hydrophobic surface.

Table 1.1: Comparison of structural features of PP-II and PP-I conformations

Parameter	**PPII conformation**	**PPI conformation**
Helix sense	Left handed	Right handed
Amide bond conformation	*trans*	*cis*
Nature of helix	Extended	More compact
Dihedral angles	ω=180°, φ = –75°, ψ = +145°	ω=0°, φ = –75°, ψ = +160°
Helical pitch	9.4 Å	5.6 Å
Number of residues per turn	3.0	3.3
Orientation of amide bond	Nearly perpendicular to the helix axis	Nearly parallel to the helix axis
Preferred solvent	Water	Aliphatic alcohols

The prolyl peptide bonds can exist in either *cis* or *trans* conformations. Peptidyl prolyl isomerase (PPIase) is a ubiquitous enzyme that catalyses this conversion and keeps the

proteins in their native conformation.[20] In PP-II helix, the peptide bonds are in *trans* conformation, which is the favoured form in aqueous solvents for polyproline peptides. In non-polar alcoholic solvents however, the polyproline peptides adopt an alternate conformation polyproline I (PP-I) form, which is a right handed helix with the amide bonds in *cis* conformation.[21] PP-I is more compact than the PP-II helix with 3.3 residues per turn.

Oligoprolines have found utility as molecular spacers in many synthetic constructions.[22] It is also used as a motif in self-assembling peptide designs either as a spacer[23] or as scaffold.[24] Several derivatives of polyproline oligomers have been reported in the past few decades. Among these, are many cell penetrating agents with membrane interacting cationic group guanidinium and different hydrophobic functional groups incorporated on a polyproline scaffold, either directly on the backbone of the peptide chain, or at the proline side-chains.[25-27]

1.1.3 4(*R/S*)-Substituted Polyproline

Conformational preference of the polyproline peptides are affected by the substitutions at C4 of the repeating proline residues. The nature of the substitution and its stereochemistry are known to influence the prolyl *cis-trans* isomerization and the backbone dihedral angles.[28] Studies on proline dipeptide models such as *N*-acetyl-*N*′-methylamides of 4(*R*/*S*)- hydroxy-L-proline, and 4(*R*/*S*)-fluoro-L-proline showed that while 4(*R*)-substitution of these electron withdrawing functional groups favoured *trans* amide bond and *exo* pyrrolidine ring pucker, 4(*S*)-substitution favoured *cis* amide bond conformation and an *endo* ring pucker.[29] In case of 4(*R/S*)-aminoproline derivatives, in addition to stereochemistry, protonation of the amino group is also known to affect the conformational properties of the peptide. Thus, 4(*R*/*S*)-aminoprolines have been used to achieve a pH dependent control over the stability of synthetic collagen triple helices.[30]

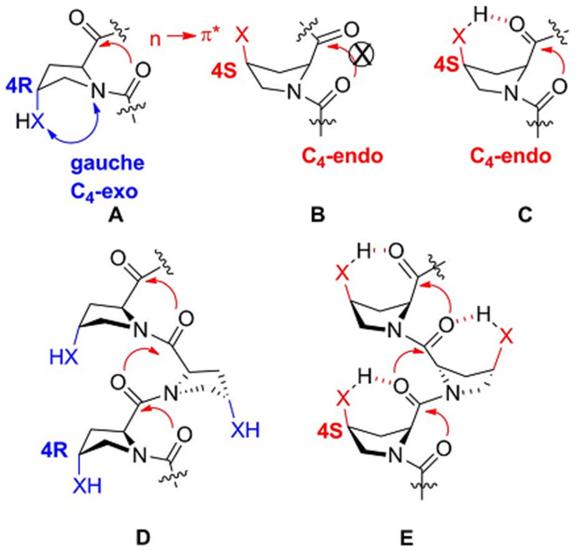


Figure 1.5: Factors affecting the conformation of 4(*R*/*S*)-substituted proline polypeptide[31]

In PP-II helices, stereo-electronic effects were shown to be dominant factors influencing its stability (Figure 1.5). Raines *et. al*.[28,32] suggested the role of backbone n → π* interaction in stabilizing PP-II helices by augmenting stereo-electronic effects that favors *trans* prolyl peptide bonds over *cis*. While this proved to be crucial to explain the stability of collagen triple helices, it was also found to be prevalent among different secondary structures in many proteins and model systems.[32] On one hand, an electron-withdrawing 4(*R*)-substitution in polyproline peptides favour *trans* peptide bond through a stronger n → π* interaction between O_{i-1} and C'_i. This also constrains the dihedral angles, ϕ and ψ to those required for the formation of PP-II helix. On the other hand, the same electron-withdrawing substituent in the 4(*S*) configuration obviates the n → π* interaction and does not contribute to the stability of PP-II structure.[28a]

1.2 Peptide Based Self-Assembly

In nature, several molecular machines, and supramolecular architectures are made out of proteins. Our efforts to emulate these nanoscale structures has led to a rapid increase in the interest in peptide based self-assemblies in the past few decades. Shorter than natural

proteins, peptides are easier to synthesize in relatively large amounts, and easier to handle as compared to many delicate proteins. Unlike large proteins which may have many domains with multiple secondary structural elements and various flexible regions such as loops and turns in their native structure, short peptides generally contain only one (or a few) conformation. This offers an added advantage of better predictability in terms of their conformational and self-assembling behaviour as compared to more complex proteins. Since they are made of the same building blocks as proteins, peptide based self-assembled structures offer the same functional diversity. Due to these reasons, peptide based self-assembly has yielded nanoscale materials of a large variety of morphologies and functions.[33]

As tools to build larger structures through the "bottom up" approach, peptides are useful because their building blocks, amino acids have been well-studied. Furthermore, the availability of a large repertoire of artificial building blocks enables peptides to be easily constructed through standard solid-phase peptide synthesis protocols. This enhances the functionalizing capacity in nanostructures built with peptides. Insights gained from investigations into protein folding and conformational properties of peptide chains therefore forms the foundation for the rational self-assembly with synthetic peptides. Peptide systems can be designed to assemble into materials with tailored properties for specific needs by rational design of the peptide sequence. In the same way, it is also possible to exploit the ability of certain amino acids to chemically respond to their environmental changes such as pH, ionic strength, presence of specific metals etc., for developing stimuli induced responsive nanostructures. Because it is possible to incorporate biologically relevant peptide sequences, into the design or as cargo, peptide based self-assembly can be useful in developing materials with many applications and fabricating devices in bioengineering and biotechnology.

1.2.1 Designing Peptides for Self-Assembly

In order to create supramolecular architectures, ability of simple peptide blocks acting as tectons must be made to hierarchically assemble through prescribed intermolecular associations mediated by various non-covalent, weak interactions. Rational design of self-assembling peptides mainly involves application of our understanding of the propensity for different amino acids and sequences to adopt specific secondary structures. The goal of such designs lies in the effective utilization of the rich functional group diversity of the amino acids in varying sequences, and the predictable orientation of sidechains. These depend on the conformation of the peptide chain to direct non-covalent interactions including electrostatic, hydrogen bonding, hydrophobic, aromatic pi-pi stacking and van der Waals interactions between specific atoms in the peptide backbone and side chains. Suitable designs lead to programming spontaneous assembly into specific patterns. Our inadequate understanding of protein folding notwithstanding, the progress in the area of peptide self-assembly has resulted in the generation of a large variety of peptide based materials with excellent control over their morphological features and with tunable functional properties.[33]

1.2.2 Interactions Involved in Peptide Self-Assembly

An ensemble of specific, but weak interactions hold self-assembled peptide structures together. Programmable interactions widely employed in peptide self-assembly include electrostatic, hydrophobic, and hydrogen bonding interactions. Other interactions such as π stacking and van der Waals interactions are also used to generate stable supramolecular assemblies.

1.2.2a *Ionic Interactions*

Ionic complementary peptides were designed to introduce differential charge

distribution patterns along the peptide chain by placing positively charged amino acids and negatively charged amino acids in appropriate positions in the β-sheet forming peptide sequence. Electrostatic interactions between the sidechains of these peptides lead to their organization into ordered supramolecular structures (Figure 1.6).

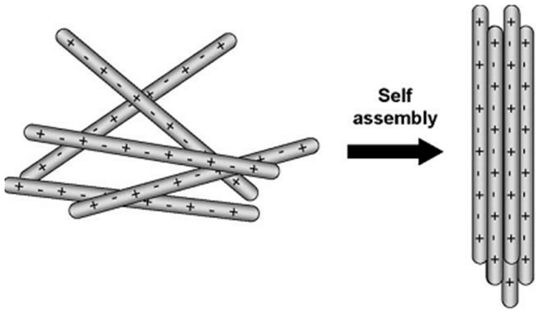


Figure 1.6: Schematic representation of self-assembly of peptides through ionic complementarity[34]

Interactions between peptide molecules can be controlled by pH and concentration of salt in the solution. A similar strategy was adopted to self-assemble collagen mimetic peptides into ordered nanosheets and nanofibers.[35]

1.2.2b *Hydrophobicity*

Many natural self-assembled structures such as cell membranes exhibit a balance between hydrophilic and hydrophobic properties. Use of hydrophobic amino acid residues in the peptides to drive self-assembly is a common strategy. In peptides that form β-sheet, designing the sequence to have alternating hydrophilic amino acids and hydrophobic amino acids produces β-sheet with two distinct surfaces, as the hydrophilic sidechains project on one face of the sheet, the hydrophobic sidechains form the other face. Increasing hydrophobicity in peptides is found to increase the driving force for their self-assembly. Zhang *et. al*.,[36] showed that increasing the hydrophobicity in self-assembling ionic complementary peptides, the critical aggregation concentration (CAC) for the peptide can be lowered. Increasing hydrophobicity was found to decrease the temperature required to trigger

the self-assembly. Lipidation of the peptides by conjugation of the peptides with one or more fatty acids is another common approach used to influence the self-assembling properties by altering the hydrophilicity-hydrophobicity balance in the peptide.[37]

1.2.2c *Other Non-covalent Interactions*

Among the weak interactions that are found to be involved in stabilizing supramolecular assemblies are hydrogen bonds, van der Waal forces and π stacking interactions. These non-covalent forces typically act collectively and provide stability to the structure. For instance, π-π interactions and hydrogen bonds are responsible for stabilization of structures formed by Fmoc containing dipeptides.[38]

1.2.3 Peptide Based Self-Assembling Systems

1.2.3a *Amphiphilic peptides*

Peptides with distinct hydrophilic and hydrophobic domains were designed for self-assembly. These amphiphilic molecules had repeating ionic complementary blocks positioned in ways that allowed them to assemble like lego bricks into a predetermined fashion and were hence called as "peptide lego".[39] The hydrophilic face of the peptides had repeating patterns of positive and negative charges. The positive charges were introduced by incorporation of Lysine (Lys, K) or Arginine (Arg, R) in the sequence. Similarly, the negative charge is introduced with aspartic acid (Asp, D) or glutamic acid (Glu, E). An example is the 16mer self-complementary peptide EAK16 $(Ala\text{-}Glu\text{-}Ala\text{-}Glu\text{-}Ala\text{-}Lys\text{-}Ala\text{-}Lys)_2$ derived from the natural the Z-DNA binding protein, Zuotin.[40] This adopts β-sheet conformation and self-assembles through association involving electrostatic interactions between the Lys and Glu residues and between the relatively hydrophobic faces comprising of alanine residues. The association of the peptide led to formation of nanofibers that were interwoven to form flat

membraneous architecture.[36]

1.2.3b *Lipopeptides*

Peptide amphiphiles constructed by conjugating one or more alkyl tails to a short peptide has been widely used as a molecular building block for fabrication of many peptide based self-assembled materials and devices. The peptide segment usually consists of a β-sheet forming sequence and acts as a polar head. The hydrophobic tail could be short or long (12-16 carbon) alkyl chains. The assembly of the peptides is driven by the hydrophobic interactions between the alkyl chains. The functionality and versatililty of these peptide based surfactants were demonstrated by Hartgerink *et. al*.[37] They developed a peptide amphiphile based system for biomineralization of hydroxyapatite (Figure 1.7).

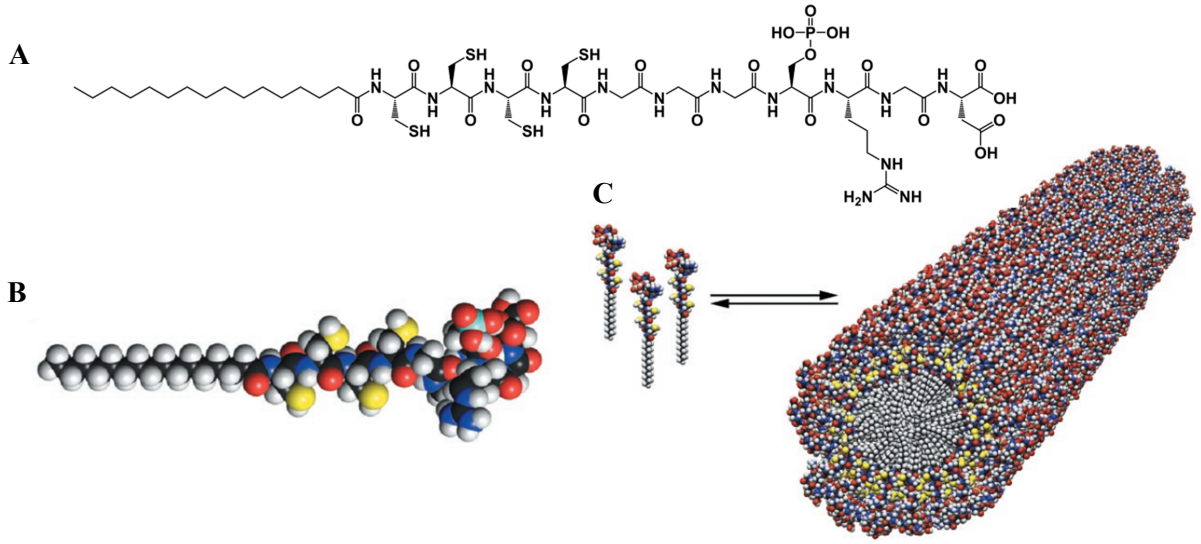


Figure 1.7: Peptide amphiphile based self-assembly. (A)Structure of the peptide amphiphile (B) Molecular model of the peptide surfactant monomer. (C) Assembly of the peptide amphiphile molecules into cylindrical micelles.[37]

The structure of the amphiphile had five components. The 16-carbon alkyl tail provided the necessary hydrophobicity to drive self-assembly into cylindrical micelles. To improve the stability of the structure, four cysteine residues were added. The disulphide bonds formed under oxidizing conditions lock the supramolecular assembly. A triglycine spacer provides flexibility to the structure. A phosphoserine was incorporated to promote

nucleation of hydroxyapatite at the surface of the peptide fibers. The C-terminus of the peptide contained RGD sequence, which is known to promote cell adhesion. The assembly or disassembly of the peptides was triggered by changing the pH of the solution. The lipopeptides were shown to provide a nanofibrous scaffold for biomineralization of hydroxyapatite. The composite formed by the peptide fibers and the mineral resembled natural collagen fibrils in bone.

1.2.3c *β-hairpin peptides*

A β-hairpin is a structural motif where two antiparallel β-strands are linked by a turn consisting of 2-4 residues (Figure 1.8). When the β-sheet forming sequence contains alternating hydrophilic and hydrophobic amino acid residues, these peptides in their β-hairpin form project alternating hydrophobic and hydrophilic faces. The facial and lateral assembly of these motifs led to fibers that occasionally crosslink, and form hydrogels.

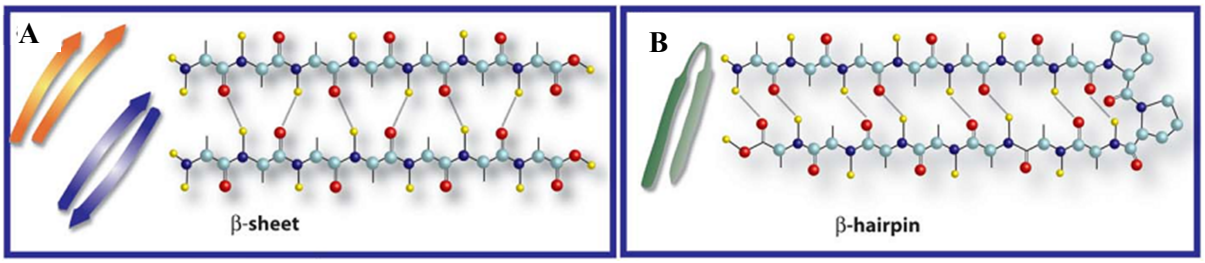


Figure 1.8: Structure of β-sheet and β-hairpin[41]

Lamm *et. al*.,[42] reported the self-assembly of the β-hairpin peptide MAX1 with a sequence $(VK)_4$-vPPT- $(KV)_4$. The two β-strand forming octamers $(VK)_4$ were separated by a tetrapeptide sequence that forms type II' turn aided by the two central prolyl residues. Valine was chosen as hydrophobic amino acid because of its propensity to form β-sheets. Lysine imparts solubility and allows control of the assembly with pH. At pH 9, the peptide forms stable hairpins as the neighbouring lysine residues are no longer protonated. Formation of β-hairpin produces two distinct faces. The hydrophobic faces are formed by the projecting valine side chains (Figure 1.9). Two β-hairpins associate with one another through

hydrophobic interactions to form bilayers. These later assemble laterally to form fibrils mediated by a network of intermolecular hydrogen bonds.[42]

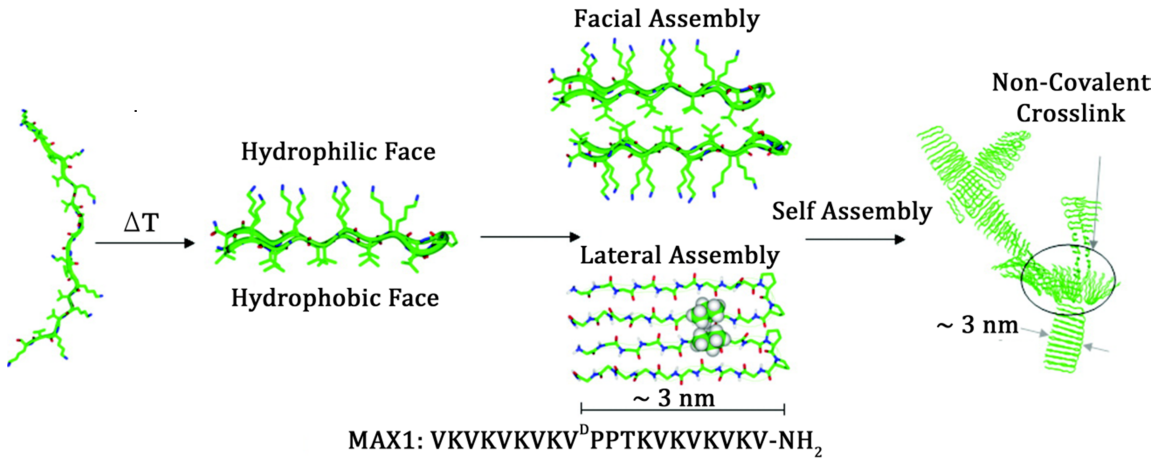


Figure 1.9: Self-assembly mechanism of MAX1 leading to hydrogel formation[42b]

1.2.3d *Coiled-coil peptides*

Coiled coils are another class of common structural motifs proteins that consists of two or more right-handed α-helices wound around each other mediated by interactions between the sidechains of the helices, positioned appropriately along the surface of the two helices (Figure 1.10). Coiled coil peptides typically contain a heptad repeat sequence, *abcdefg*. Placing a hydrophobic amino acid at *a* and *d* positions allows hydrophobic interactions between the α-helices.

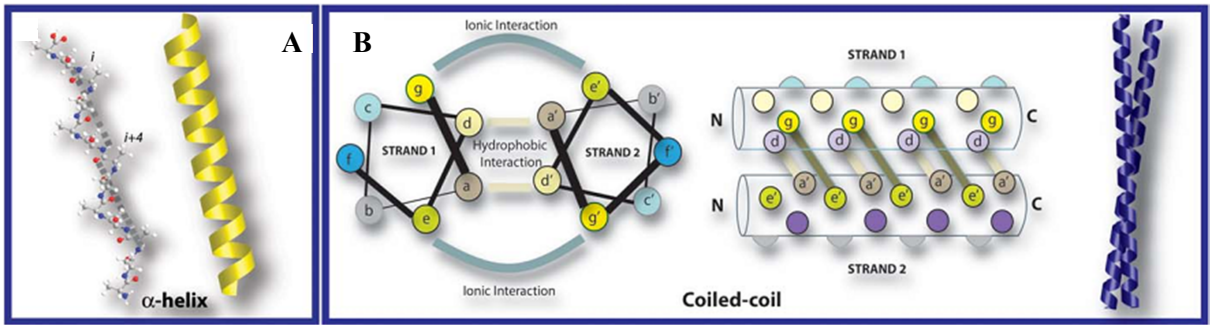


Figure 1.10: (A) Structure of parallel α-helix and (B) Schematic representation of coiled-coil[41]

Pandya *et. al.*,[43] showed that coiled coil peptides can be extended to form fibrillary

structures by introducing patterns of positive and negative charges, along the helical wheel, which acted as sticky ends and promoted association of coiled coils (Figure 1.11). They used isoleucine (Ile, I) and leucine (Leu, L) at positions *a* and *d* to ensure the formation of coiled-coils. At positions, *e* and *g*, they introduced glutamic acid (Glu, E), and lysine (Lys, K) in different combinations to produce a staggered dimer with sticky ends. This allowed peptides with complementary charge pattern to assemble into extended fibrils.

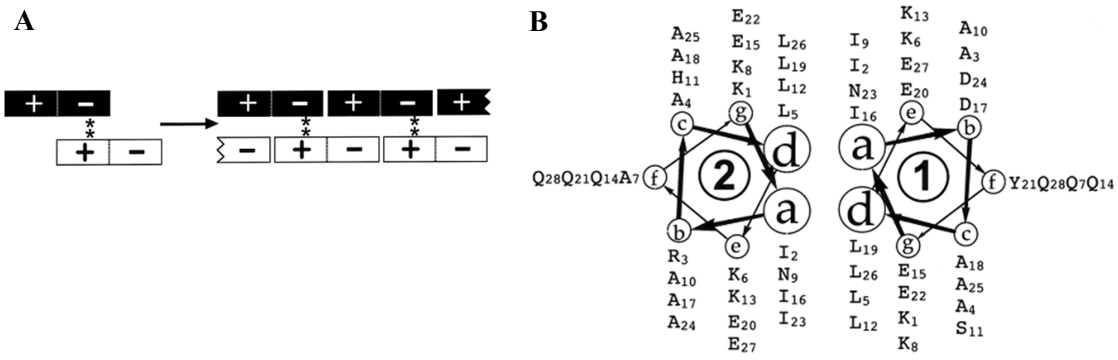


Figure 1.11: Design of the self-assembling fiber (SAF) peptides with sticky ends (A) and the sequence of the peptides shown helical wheel as heptad repeats (B)[43]

1.2.3e *Aromatic Peptide Systems*

Inspired by the amyloid fibres' self-assembly, Reches *et. al.*,[44] derived the core FF, diphenylalanine motif and showed that even the dipeptide alone was able to form regular supramolecular assemblies. Mediated by π stacking and hydrogen bonding interactions, these dipeptides formed nanotubes in solvent HFIP (Figure 1.12).

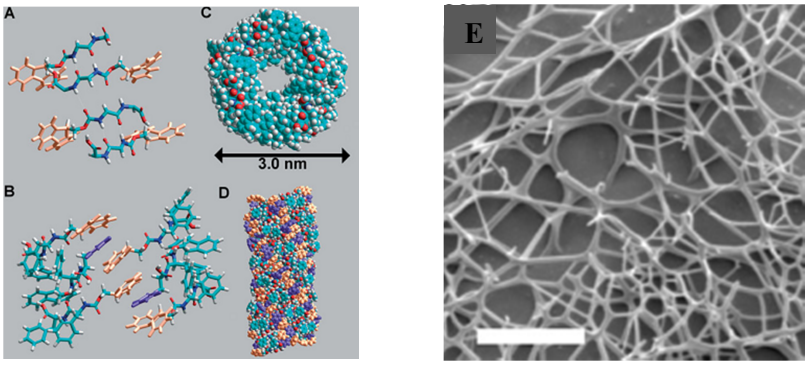


Figure 1.12: Molecular models illustrating self-assembly of Fmoc-FF dipeptides as stacks of a few molecules (A-B), the top view and side view of the overall architecture (C-D). (E) Cryo SEM images of bundles of fibres formed by Fmoc FF. Scale bar: 500 nm.[38]

1.2.3f *Cyclic Peptides*

A cyclic octapeptide [–(L-Gln-D-Ala-L-Glu-D-Ala)$_2$ –], containing alternating L and D amino acids were designed to induce tubular assembly.[45] The amide bonds of the cyclic peptides form intermolecular β-sheet like H-bonds allowing the peptide rings to stack on top of each other to produce hollow tubes. The diameter of the tube can be controlled by the number of amino acids in the cyclic peptide. The peptides with alternating hydrophilic and hydrophobic amino acids in its sequence lead to the tubes with hydrophilic interior and hydrophobic exterior. With hydrophobic exterior, the tubes could be engineered to incorporate themselves into membranes to form pores.

1.2.3g *Polyproline Peptides*

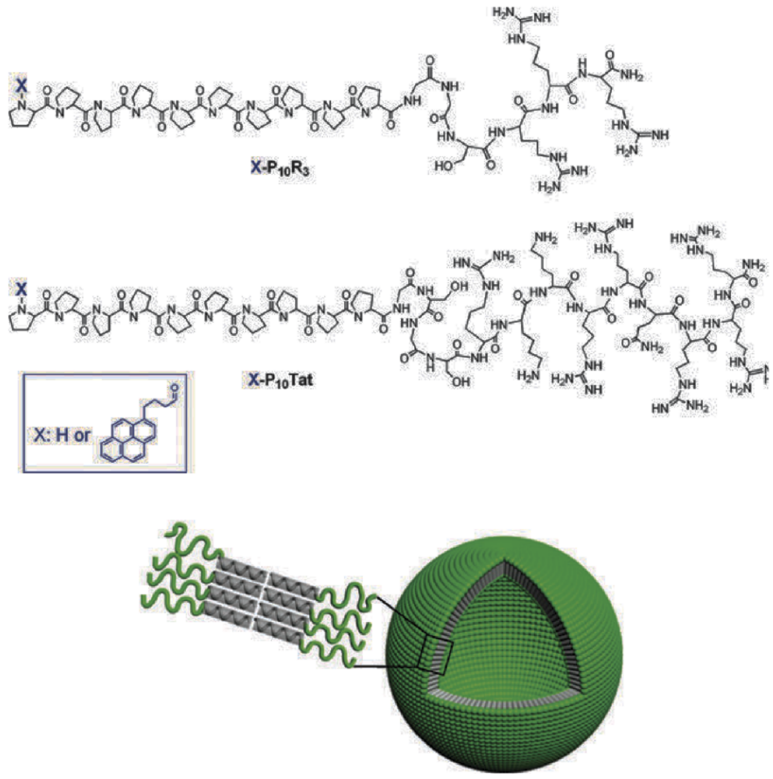


Figure 1.13: Self-assembly of PP-II containing rod-coil building blocks into nanocapsule.[23]

The constraints imposed by the cyclic sidechain results in the polyproline peptides (PP-II) to act as stiff helical rods. Three nonpolar methylene groups are aligned at the outer part of the rod after PPII helix formation. Utilizing this, Yoon *et. al*.,[23] constructed a rod-coil

by conjugating a polyproline oligomer to the cell penetrating peptide, TAT (Figure 1.13). The PP-II helix separated a slightly hydrophobic tail from the hydrophilic peptide coil, leading to the formation of self-assembled hollow nanocapsules.

Wennemers *et. al*.,[24] demonstrated that PP-II as a molecular scaffold for self-assembly can be valuable. They covalently conjugated perylene monoimide (PMI) to every third proline residue on an oligoproline scaffold. The peptide-chromophore conjugate was found to assemble into nanowires and nanotubes. By increasing the distance between the PMI functionalization sites on the polyproline scaffold, the peptide system assembled into a triaxial molecular weave.[46]

1.2.3h *Branched Peptides*

In branched peptides, one or more linear peptide segments branch off from one of the sidechains of the main chain. The amino acid used as branching unit is generally a lysine or one of its analogues. Branched peptides were developed as a means to improve the biological stability of the peptide for therapeutic applications. It was realized that branched peptides, in addition to exhibiting enhanced stability, were also more efficacious as vaccines with superior molecular recognition and antigenic properties than linear peptides due to their multivalent nature. From multivalent antigen peptides to drug delivery systems, the application value of branched peptides has expanded over the past few decades.

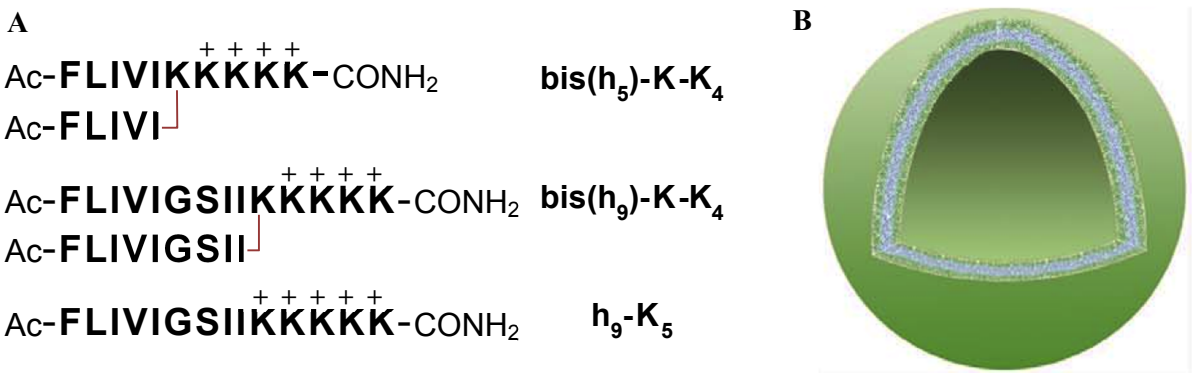


Figure 1.14: Self-assembly of branched amphiphilic peptides. (A) Sequence of the peptides (B) Representation of a nanocapsules formed by the peptide in water.[47]

Tublur *et. al*.,[47] demonstrated that branched peptides can be assembled into bilayer-delimited spheres (Figure 1.14). They designed an amphiphilic branched peptide bis(FLIVI)-K-K_4 and bis(FLIVIGSII)-K-K_4, containing one hydrophilic K_4 branch, and two hydrophobic branches, either a 5-mer or a 9 mer. A lysine residue was used as a branching point. These peptides were found to behave similar to phospholipids and also assembled into nanocapsules in water as the hydrophobic branches form intermolecular associations in the form of β-sheets.

1.3 Peptide Nucleic Acids

Peptide nucleic acid was designed and synthesized by Nielsen *et. al*.,[48] to be a mimic of oligonucleotides. It consists of repeating N-(2-aminoethyl) glycine units linked by amide bonds (Figure 1.15). The nucleobases are attached to the backbone via a methylenecarbonyl linker. It has a neutral, flexible pseudopeptide backbone instead of the oligonuleotide's negatively charged phosphodiester backbone. In design, PNA combines the structural features of peptides and nucleic acids.

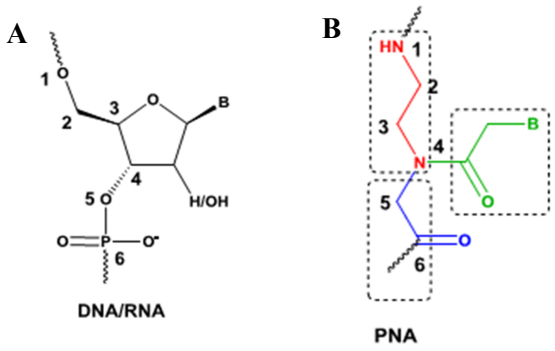


Figure 1.15: Comparison of structures of DNA/RNA (A) and PNA (B)

As a polyamide analogue of DNA, PNA hybridizes with its complementary DNA/RNA with higher affinity and specificity than DNA itself. Because of several favourable properties such as low mismatch tolerance, resistance to proteases and nucleases, and better stability, PNA has wide ranging applications in therapeutics, biosensors, and bioengineering.

1.3.1 Molecular Recognition in PNA

As in DNA/RNA, the Watson-Crick base pairing rules apply to PNA as well (Figure 1.16). A PNA-PNA duplex is a wide helix (28 Å diameter) with a large pitch (18 base pairs per turn). The base pairs are displaced away from helix. With DNA/RNA, PNA forms hybrids where the PNA strand binds to its complementary partner.

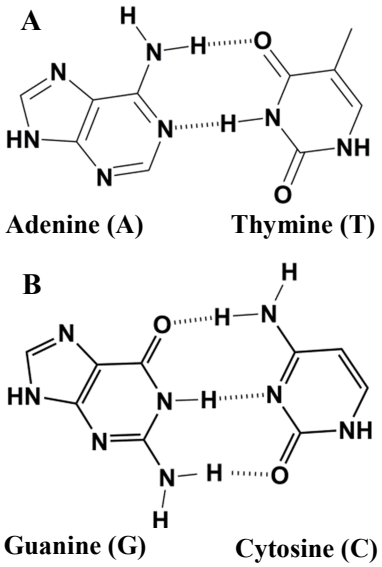


Figure 1.16: Watson-Crick Basepairing between adenine and thymine (A) and between guanine and cytosine (B).

PNA binds to complementary nucleic acids with higher specificity than DNA or RNA. Introduction of a single mismatch in PNA-DNA duplex causes a reduction in the T_m of 8-20^{o}C. However, in the corresponding DNA-DNA duplex, the extent of destabilization prompted by a single mismatch is about 10^{o}C. Unlike DNA-DNA duplexes, the stability of PNA-DNA duplexes and PNA-PNA duplexes are not significantly affected by the salt concentration due to its neutral backbone. Similar to DNA, PNA has also been found to form G-quadruplexes[49] and i-motif tetraplexes.[50] The hybrid quadruplexes formed by PNA with DNA/RNA exhibit high thermodynamic stability. These motifs expand the range of molecular recognition for PNA beyond duplex and triplexes.

1.3.2 PNA based Self-Assembly

As evidenced by the burgeoning field of DNA nanotechnology, the control of supramolecular assembly of a large number of molecules is possible with high degree of precision and predictability when the oligonucleotides are programmed using simple rules of Watson-Crick basepairing and duplex geometry. As PNA shares its informational blocks, the nucleobases with DNA, PNA can also be used in the same manner. With a peptide backbone, the PNA offers versatility, flexibility and structural complexity.

1.3.2a *PNA Amphiphiles*

Similar to peptides, PNA were also conjugated to alkyl chains to induce self-assembly in aqueous solvents. Schneider *et. al*., [51] prepared amphiphiles of 10 mer PNA and showed that it still retained its DNA hybridizing capacity. Stupp *et. al*.,[52] reported the self-assembly of peptide PNA conjugate into nanofibers. Ganesh *et. al*.,[53] showed that fluorinated chain in the PNA structure thus caused compaction of the assembled particles. PNA strands conjugated to a perfluoroalkyl chain formed particles that were smaller by 2-3 fold than the PNA amphiphiles conjugated to hydrocarbon tail.

1.3.2b *PNA-DNA Hybrid Tiles*

DNA double crossover (DX) molecules contain two double helical domains and two crossovers that link the two duplexes. They act as rigid tiles useful for two-dimensional assembly of DNA into different periodic patterns. Seeman *et. al*.,[54] incorporated PNA into the DX tiles to produce heteroduplex DX. Such a strategy allows PNAs to be used readily into the well-studied DNA nanostructures.

1.3.2c *di-PNAs*

Gazit *et. al*.,[55] showed that dimers of PNA containing guanines self-assembled into ordered architectures (Figure 1.17). Supramolecular organization of the di-PNAs was sustained by the usual Watson–Crick interactions between guanines and cytosines.[55] Several inter- and intra-molecular aromatic π-stacking interactions between neighbouring bases were also involved. The assemblies of PNA exhibited excitation-dependent emission over the entire visible spectrum. When GC di-PNAs assembly were deposited on a simple field-effect transistor (FET) device, in the gap between source and drain, and potential difference was applied across the device, the PNA assemblies produced electroluminescence at -5V and +5V.

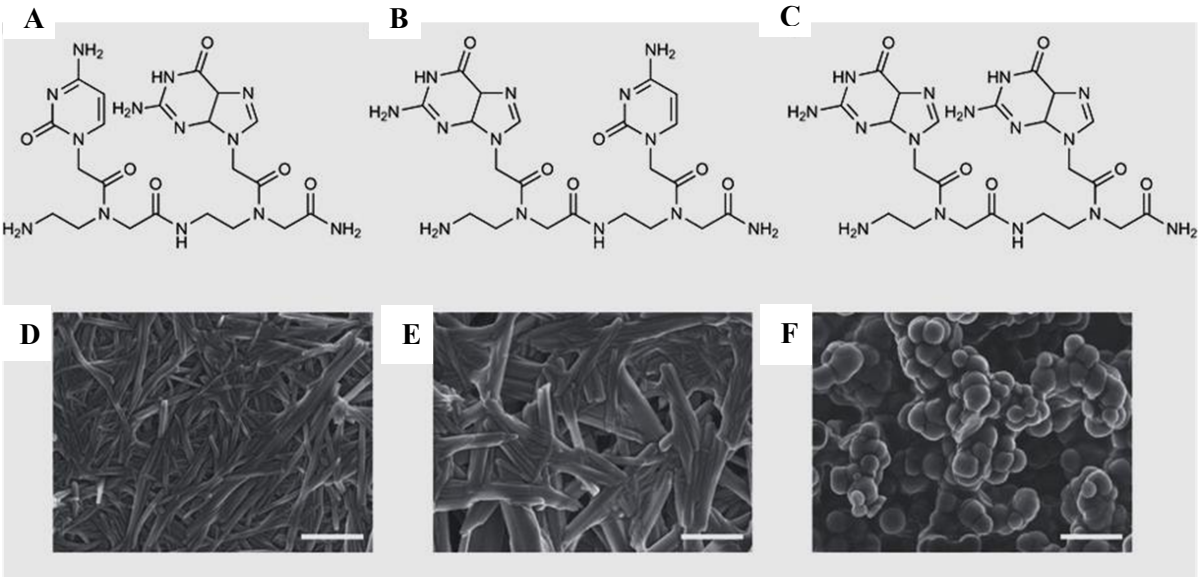


Figure 1.17: Structure of di-PNAs, CG (A), GC (B), and GG (C). FE-SEM images of morphologies formed by the di-PNAs CG (D), GC (E), and GG (F).[55]

These interesting optical properties of the diPNA assemblies have opened up new avenues for their application in organic optical devices.

1.4 Scope of the Thesis

Among the secondary structures adopted by peptides and proteins, polyproline II conformation (PP-II) has gathered interest due to the significant roles played by them in many biological processes such as molecular recognition and protein folding.[1] Oligoprolines with PP-II scaffold has been demonstrated to be a useful tool to template self-assembly.[2] Therefore manipulating the polyproline backbone to control their conformational behaviour assumes importance. Conformational preference of 4(*R*/*S*)-aminoprolyl polypeptides is influenced by the configuration at C4. 4(*S*)-aminoprolyl polypeptide, (4*S*)-amp_9 adopts β-sheet like conformation in TFE. This is unusual for a polyproline peptide as prolines are generally considered to be "β-breakers". Similar behaviour was observed in case of 4(*S*)-hydroxyprolyl polypeptides as well. Further, lipidated 4(*S*)-hydroxyprolyl polypeptides, (4*S*)-hyp_9 was found to also assemble into nanofibers in TFE, under the conditions where they exhibit β-structure.[7] A switch between intramolecular hydrogen bonding scheme to an intermolecular hydrogen bonding was proposed to explain this unusual stereo-specific conformational properties.

In this thesis, this conformational change is explored further. The effect of the cationic amino and guanidino substitutions on the conformational properties and supramolecular organization of peptides with polyproline backbone is studied systematically. This work also includes attempts made to utilize the rich conformational dynamics of 4(*R*/*S*)-aminoprolines to construct branched polyprolines and branched peptide nucleic acids to gain control over their self-assembly by using 4(*R*/*S*)-aminoprolines as a chiral branch point.

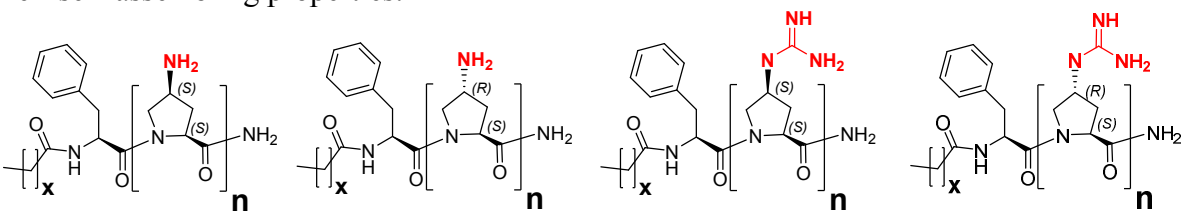
This thesis is comprised of studies on the stereo-dependent conformational changes in polyproline peptides and the effect of their conformational behaviour in different solvents on

their self-assembling properties. The thesis is divided into two sections. Section I deals with the linear peptides 4(*R*/*S*)-aminoprolyl polypeptides and their derivatives 4(*R*/*S*)-guanidinylprolyl polypeptides. Section II deals with branched peptides and peptide nucleic acids constructed with 4(*R*/*S*)-aminoproline as the branching core.

Section A: Linear Peptides

Chapter 2: Design and Synthesis of 4(*R/S*)-Amino and Guanidino Proline Based Peptides

This chapter describes the design and synthesis of 4(*R/S*)-aminoproline monomers, (4*S*)-*amp* and (4*R*)-*Amp* and the *synthesis of a series of linear peptides* - 4(*R/S*)-substituted aminoprolyl polypeptides, and guanidinylprolyl polypeptides, and their characterization (Figure 1.18). The peptides were prepared to probe the stereo-dependent conformational changes and to observe the effect of their conformational behaviour in different solvents on their self-assembling properties.



n = 3, 6, 9
x = 0, 10, 12, 14

n = 9; x = 0, 12

n = 9; x = 0, 12

n = 9; x = 0

Figure 1.18: Linear peptides used in this study

Chapter 3: Biophysical Studies of 4(*R/S*)-Amino and Guanidino Proline Based Peptides

This chapter deals with investigations into the conformational properties of C4(*S*)-NH_2 substituted aminoprolyl polypeptides, and guanidinylprolyl polypeptides in aqueous buffer and TFE to *elucidate the stereospecific conformational changes* caused by the substitutions at C4 position of proline sidechains in these peptides. The present work suggests

ways to alter and hence control the backbone conformation of polyproline peptides. With C4(*S*)-NH_2 substitution, the peptide can be tuned from a left handed PP-II helix to a ribbon-like β-sheet in TFE and in the presence of SDS micelles. With C4(*S*)-guanidine substitution however, the backbone conformation can be altered by conjugation with lipid chain at the N-terminus of the peptide.

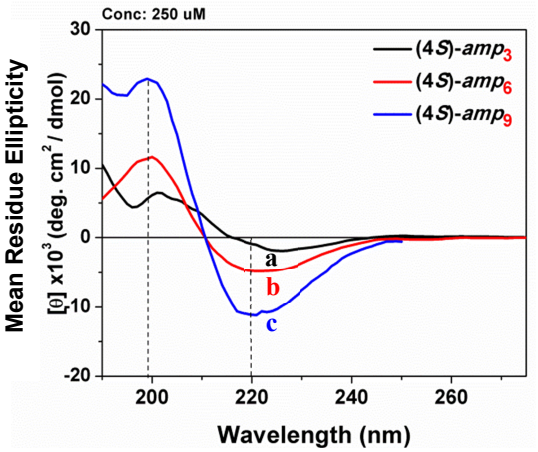


Figure 1.19: A) CD spectra of 250 μM solution of peptides (4*S*)-*amp*$_3$ (**P1**) (trace **a**), (4*S*)-*amp*$_6$ (**P2**) (trace **b**), (4*S*)-*amp*$_9$ (**P3**) (trace **c**) in TFE.

Chapter 4: Self-Assembly of 4(*R*/*S*)-Amino/Guanidino Proline Based Peptides

This chapter deals with *investigations into the self-assembling properties* of C4(*S*)-NH_2 substituted aminoprolyl polypeptides, and guanidnylprolyl polypeptides under different conditions, mainly using field emission scanning electron microscopy (FESEM) and atomic force microscopy (AFM) techniques.

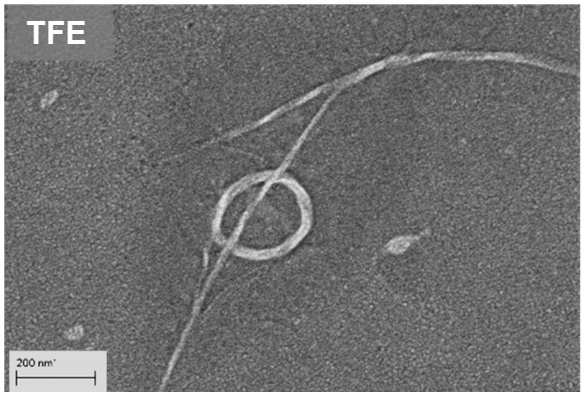


Figure 1.20: FE-SEM images of morphologies formed by peptide (4*S*)-*amp*$_9$ (**P3**) and in TFE

Chapter 5: Design, Synthesis, Biophysical Studies and Self-Assembly of Branched Polyproline Peptides

This chapter describes the synthesis of *branched polyproline peptides* with (4*S*)-*amp* and (4*R*)-*Amp* as the branching core-unit, and elucidates the effect of the stereochemistry of the core residue on their conformational and self-assembling properties in different solvents. The results suggested that a branched structure promotes self-assembly of the nanofibers as compared to linear topology, with the morphology dependent on the stereochemistry of the 4(*R*/*S*)-aminoproline at the branching point.

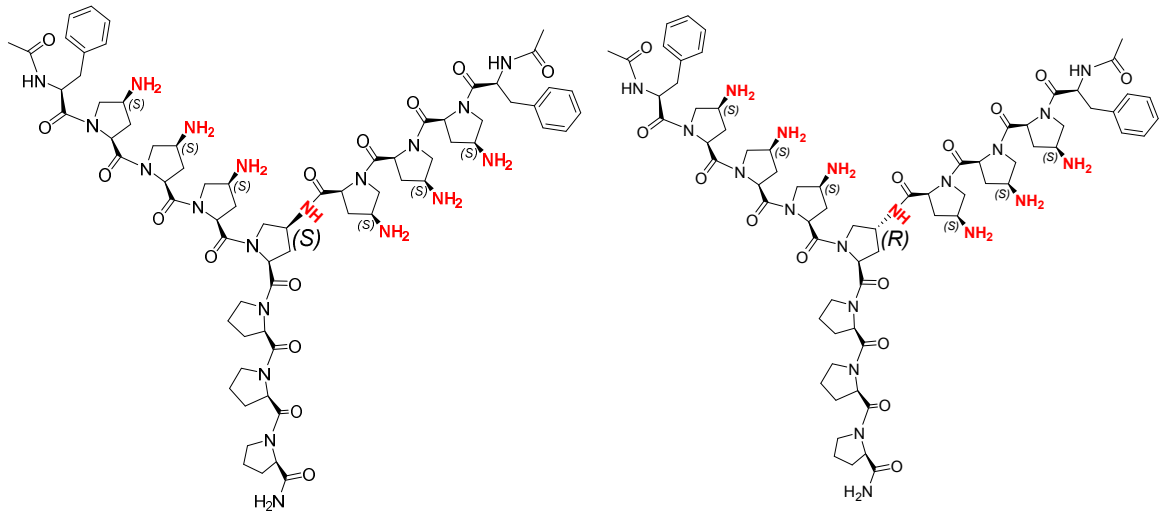


Figure 1.21: Branched peptides (**P12-P13**) with three branches

Chapter 6: Design, Synthesis, Biophysical Studies and Self-Assembly of Branched Peptide Nucleic Acids

This chapter describes the synthesis of *branched peptide nucleic acids* with (4*S*)-*amp* and (4*R*)-*Amp* as the branching core-unit, and illustrates how the *stereospecific conformational changes at the core might affect the morphology of their supramolecular assemblies*.

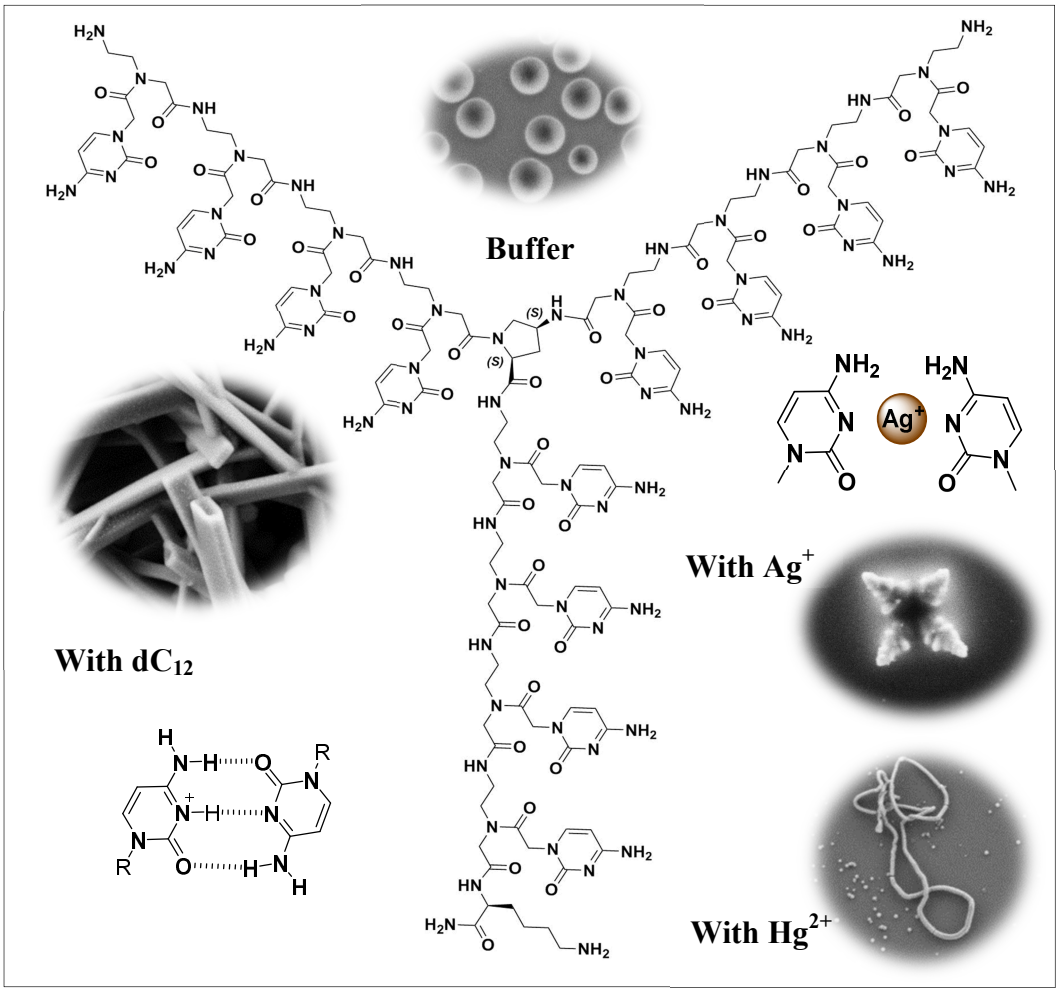


Figure 1.22: Branched PNA (4*S*)-*amp*$^{\lambda}$-$(C_4)_3$ (**P14**) and its supramolecular assemblies

Branched peptide nucleic acids PNAs (4*S*)-*amp*$^{\lambda}$-$(C_4)_3$ (**P14**) and (4*R*)-*Amp*$^{\lambda}$-$(C_4)_3$ (**P15**) were designed to have three PNA C_4 branches emerging from the chiral (4*S*)-*amp* or (4*R*)-*Amp* core These studies showed that a chiral control over the conformation and self-assembly could be achieved with these dendron like branched PNA enabled by the rich conformational dynamics of 4(*R*/*S*)-aminoproline. This novel motif that brings together the strengths of peptide backbone based peptide nanotechnology and sequence dependent nucleic acid nanotechnology, these chiral branched PNA proved to be highly promising as a tool for directed self-assembly and for construction of dynamic nanodevices as demonstrated by the diverse nanostructures like nanospheres, hollow capsules, nanostars, and nanotubes, formed by these molecules under various conditions.

1.5 Reference

1. Whitesides, G. M.; Mathias, J. P.; Seto, C. T. Molecular Self-Assembly and Nanochemistry: A Chemical Strategy for the Synthesis of Nanostructures. *Science* **1991**, *254*, 1312-1319.

2. Whitesides, G. M.; Grzybowski, B. Self-Assembly at All Scales. *Science* **2002**, *295*, 2418-2421.

3. a) Liu, Z.; Qiao, J.; Niu, Z.; Wang, Q. Natural Supramolecular Building Blocks: From Virus Coat Proteins to Viral Nanoparticles. *Chem. Soc. Rev.* **2012**, *41*, 6178–6194. b) Namba, K.; Stubbs, G. Structure of Tobacco Mosaic Virus at 3.6Å Resolution: Implications for Assembly. *Science* **1986**, *231*, 1401–1406.

4. Ow, S. Y.; Dunstan, D. E. Amyloid Fibres: A brief overview of amyloids and Alzheimer's disease. *Protein Sci*. **2014**, *10*, 1315–1331.

5. a) Minamino, T.; Imada, K.; Namba, K. Molecular Motors of the Bacterial Flagella. *Curr. Opin. Struct. Biol.* **2008**, *18*, 693-701. b) Evans, L. D. B.; Hughes, C.; Fraser, G. M. Building a Flagellum Outside the Bacterial Cell. *Trends Microbiol.* **2014**, *22*, 566-572.

6. Staley, J. P.; Woolford, J. L., Jr. Assembly of Ribosomes and Spliceosomes: Complex Ribonucleoprotein Machines. *Curr. Opin. Cell Biol.* **2009**, *21*, 109–118.

7. Nelson, D. L.; Cox, M. M. The Three-Dimensional Structure of Proteins. *Lehninger Principles of Biochemistry*, 4th Ed; W. H Freeman: New York, 2004; pp 116-156.

8. Anfinsen, C. B. Principles that Govern the Folding of Protein Chains. *Science* **1973,** *181* (4096), 223-230.

9. Voet, D.; W.; Voet, J. G. Three-Dimensional Structures of Proteins. *Biochemistry,* 4th Ed; Wiley & Sons: New York, 2011; pp 221-277.

10. Lodish, A.; Berk, A.; Kaiser, C. A.; Krieger, M.; Scott, M. P.; Bretscher, A.; Ploegh, H; Matsudaira, P. Protein Structure and Function. *Molecular Cell Biology*, 5th Ed; W. H. Freeman: New York, 2008; pp 63-110.

11. Rose, G. D.; Glerasch, L. M.; Smith, J. A. Turns in Peptides and Proteins. *Adv.*

Protein Chem. **1985**, *37*, 1-109.

12. Shi, Z.; Woody, R. W.; Kallenbach, N. R. Is polyproline II a major backbone conformation in unfolded proteins? *Adv. Protein Chem*. **2002**, *62*, 163-240. b) Shi, Z.; Chen, K.; Liu, Z.; Kallenbach, N. R. Conformation of the Backbone in Unfolded Proteins. *Chem. Rev.* **2006**, *106*, 1877−1897.

13. Cubellis, M. V.; Caillez, F.; Blundell, T. L.; Lovell, S. C. Properties of Polyproline II, a Secondary Structure Element Implicated in Protein–Protein Interactions. *Proteins: Struct., Funct., Bioinf.* **2005**, *58*, 880–892.

14. Adzhubei, A. A.; Sternberg, M. J. E. Left-handed Polyproline II Helices Commonly Occur in Globular Proteins. *J. Mol. Biol.* **1993**, *229*, 472-493. b) Esipova, N. G.; Tumanyan, V. G. Omnipresence of the Polyproline II Helix in Fibrous and Globular Proteins. *Curr. Opin. Struct. Biol.* **2017**, *42*, 41 –49.

15. Bella, J. Collagen structure: new tricks from a very old dog. *Biochem. J*. **2016**, *473*, 1001–1025.

16. Kuemin, M.; Schweizer, S.; Ochsenfeld, C.; Wennemers, H. Effects of Terminal Functional Groups on the Stability of the Polyproline II Structure: A Combined Experimental and Theoretical Study. *J. Am. Chem. Soc*. **2009**, *131*, 15474–15482.

17. a) Grathwohl, C.; Wuthrich, K. The X-Pro Peptide Bond as an NMR Probe for Conformational Studies of Flexible Linear Peptides. *Biopolymers* **1976**, *15*, 2025-2041. b) Reimer, U.; Scherer, G.; Drewello, M.; Kruber, S.; Schutkowski, M.; Fischer, G. Side-chain Effects on Peptidyl-Prolyl *cis*/*trans* Isomerization. *J. Mol. Biol*. **1998**, *279*, 449-460.

18. Chou, P. Y.; Fasman, G. D. Empirical Predictions of Protein Conformation. *Annu. ReV. Biochem*. **1978**, *17*, 251-276.

19. Metzler, D. E. Amino Acids, Peptides, and Proteins. *Biochemistry The Chemical Reactions of the Living Cell*, 2; Academic Press, 2003; pp 39-54.

20. Rostam, M. A.; Piva, T. J.; Rezaei, H. B.; Kamato, D.; Little, P. J.; Zheng, W.; Osman, N. Peptidyl-prolyl isomerases: functionality and potential therapeutic targets in cardiovascular disease. *Clin. Exp. Pharmacol. Physiol*. **2015**, *2*, 117-124.

21. Zhong, H.; Carlson, H. Conformational Studies of Polyprolines. *J. Chem. Theory Comput*. **2006**, *2*, 342-353.

22. Dobitz, S.; Aronoff, M. R.; Wennemers, H. Oligoprolines as molecular entities for controlling distance in biological and material sciences. *Acc.Chem. Res.* **2017**, *50* (10), 2420-2428.

23. Yoon, Y.; Lim, Y.; Lee, E.; Lee, M. Self-assembly of a peptide rod–coil: a polyproline rod and a cell-penetrating peptide Tat coil. *Chem. Commun*. **2008**, 1892-1894.

24. Lewandowska, U.;, Zajaczkowski, W.; Chen, L.; Bouillière, F.; Wang, D.; Koynov. K.; Pisula, W.; Müllen, K.; Wennemers, H. Hierarchical supramolecular assembly of sterically demanding π-systems by conjugation with oligoprolines. *Angew. Chem. Int. Ed.* **2014,** *53*(46), 12537-12541.

25. Sinfreu, J. F.; Giralt, E.; Castel, S.; Albericio, F.; Royo, M. Cell-Penetrating cis-γ-Amino-l-Proline-Derived Peptides. *J. Am. Chem. Soc*. **2005**, *127*(26), 9459–9468.

26. a) Crespo, L.; Sanclimens, G.; Montaner, B.; Tomás, R. P.; Royo, M.; Pons, M.; Albericio, F.; Giralt. E. Peptide Dendrimers Based on Polyproline Helices. *J. Am. Chem. Soc*. **2002**, *124*, 8876–8883. b) Pujals, S.; Giralt, E. Proline-rich, amphipathic cell-penetrating peptides. *Adv. Drug Delivery Rev.* **2008**, *60*, 473-484.

27. a) Fillon, Y. A.; Anderson, J. P.; Chmielewski, J. Cell penetrating agents based on a polyproline helix scaffold. *J. Am. Chem. Soc.* **2005**, *127*(33), 11798-11803. b) Nagel, Y. A.; Raschle, P. S.; Wennemers, H. Effect of Preorganized Charge-Display on the Cell-Penetrating Properties of Cationic Peptides. *Angew. Chem*. *Int. Ed.* **2017**, *129*(1), 128-132.

28. a) Shoulders, M. D.; Kotch, F. W.; Choudhary, A.; Guzei, I. A.; Raines, R. T. The Aberrance of the 4*S* Diastereomer of 4-Hydroxyproline. *J. Am. Chem. Soc.* **2010**, *132*, 10857-10865. b) Horng, J. C.; Raines, R. T. Stereoelectronic Effects on Polyproline Conformation. *Protein Sci.* **2006**, *15*, 74-83.

29. Song, I. K.; Kang, Y. K., Conformational Preference and *cis-trans* Isomerization of 4(*R*)-Substituted Proline Residues. *J. Phys.Chem. B* **2006**, *110*, 1915-1927.

30. Egli, J.; Siebler, C.; Maryasin, B.; Erdmann, R. S.; Bergande, C.; Ochsenfeld, C.;

Wennemers, H. pH-Responsive Aminoproline-Containing Collagen Triple Helices. *Chem. Eur. J.* **2017**, *23* (33), 7938-7944.

31. Bansode, N. D.; Madhanagopal, B.; Sonar, M. V.; Ganesh, K. N. Stereodependent and solvent specific formation of unusual β-structure through side chain-backbone H-bonding in C4(*S*)-(NH_2/OH/NHCHO)-L-prolyl polypeptides. *Peptide Science* **2017**, *108*(*1*), e22981.

32. Bartlett, G.; Choudhary, A.; Raines, R. T.; Woolfsonm D, N. n→π* Interactions in Proteins. *Nat. Chem. Biol.* **2010**, *6*(8), 615–620.

33. Tao, K.; Makam, P; Aizen, R.; Gazit, E. Self-assembling peptide semiconductors. *Science* **2017**, *358*, eaam9756. b) Basak, S.; Nanda, J.; Banerjee, A. Multi-stimuli responsive self-healing metallo-hydrogels: tuning of the gel recovery property. *Chem. Commun.* **2014,** *50*(18), 2356-2359. c) Self-assembling tripeptide based hydrogels and their use in removal of dyes from waste-water. Adhikari, B.; Palui, G.; Banerjee, A. *Soft Matter* **2009,** *5*, 3452-3460.

34. Gazit, E. Self-assembled peptide nanostructures: the design of molecular building blocks and their technological utilization. *Chem. Soc. Rev.* **2007,** *36*, 1263-1269.

35. Jiang, T.; Xu, C.; Liu, Y.; Liu, Z.; Wall, J. S.; Zuo, X.; Lian, T.; Salaita, R.; Ni, C.; Pochan, D.; Conticello, V. P. Structurally Defined Nanoscale Sheets from Self-Assembly of Collagen-Mimetic Peptides. *J. Am. Chem. Soc.* **2014**, *136*, 4300–4308.

36. Zhang, S.; Holmes, T.; Lockshin, C.; Rich, A. Spontaneous assembly of a self-complementary oligopeptide to form a stable macroscopic membrane. *P. Natl. Acad. Sci. USA* **1993,** *90*(8), 3334-3333.

37. Hartgerink, J. D.; Beniash, E.; Stupp, S. I. Self-assembly and mineralization of peptide-amphiphile nanofibers. *Science* **2001,** *294*, 1684-1688.

38. Smith, A. M.; Williams, R. J.; Tang, C.; Coppo, P.; Collins, R. F.; Turner, M. L.; Saiani, A.; Ulijn, R. V. Fmoc-Diphenylalanine self assembles to a hydrogel via a novel architecture based on pi-pi interlocked beta-sheets. *Adv. Mater.* **2008**, *20*, 37–41.

39. Zhao, X.; Zhang, S. Molecular designer self-assembling peptides. *Chem. Soc. Rev.* **2006**, 35, 1105–1110.

40. Zhang, S.; Lockshin, C.; Herbert, A.; Winter, E.; Rich, A. Zuotin, a putative Z-DNA

binding protein in Saccharomyces cerevisiae. *EMBO J*., **1992**, 11, 3787–3796.

41. Dasgupta, A.; Mondal, J, H.; Das, D. Peptide hydrogels. *RSC Advances,* **2013**, *3*, 9117.

42. Lamm, M. S.; Rajagopal, K.; Schneider, J. P.; Pochan, D. J. Laminated morphology of nontwisting β-sheet fibrils constructed via peptide self-assembly. *J. Am. Chem. Soc.* **2005,** *127,* 16692-16700. b) Rajagopal, K.; Lamm, M. S.; Butterick, L. A. H; Pochan, D. J. Schneider, J. P. Tuning the pH responsiveness of β-hairpin peptide folding, self-assembly, and hydrogel material formation. *Biomacromolecules* **2009**, *10*, 2619-2625.

43. Pandya, M. J.; Spooner, J. M.; Sunde, M.; Thorpe, J. R.; Woolfson, D. L. Sticky-End Assembly of a Designed Peptide Fiber Provides Insight into Protein Fibrillogenesis. *Biochemistry* **2000**, *39*, 8728–8734.

44. Reches, M.; Gazit. Casting Metal Nanowires Within Discrete Self-Assembled Peptide Nanotubes. *Science* **2003**, *300*, 625-627.

45. Ghadiri, M. R.; Granja, J. R.; Milligan, R. A.; McRee, D. E; Khazanovich, N. Self-assembling organic nanotubes based on a cyclic peptide architecture. *Nature* **1993**, *366*, 324-327.

46. Lewandowska, U.; Zajaczkowski, W.; Corra, S.; Tanabe, J.; Borrmann, R.; Benetti, E. M.; Stappert, S.; Watanabe, K.; Ochs, N. A. K.;Schaeublin, R.; Li, C.; Yashima, E.; Pisula, W.; Müllen, K.; Wennemers, H. A Triaxial Supramolecular Weave. *Nat. Chem*. **2017**, *9*, 1068–1072.

47. Gudlur, S.; Sukthankar, P.; Gao, J.; Avila, L. A.; Hiromasa, Y.; Chen, J.; Iwamoto, T.; Tomich, J. M. Peptide Nanovesicles Formed by the Self-Assembly of Branched Amphiphilic Peptides. *PLoS ONE* **2012**, *7*(9), e45374.

48. Egholm, M.; Buchardt, O.; Nielsen, P. E.; Berg, R. H. Peptide nucleic acids (PNA). Oligonucleotide analogs with an achiral peptide backbone. *J. Am. Chem. Soc*. **1992**, *114,* 1895–1897. b) Lundin, K. E.; Good, L.; Strömberg, R.; Gräslund, A.; Smith, C.I. Biological Activity and Biotechnological Aspects of Peptide Nucleic Acid. *Adv. Genet.* **2006**, *56,* 1-51.

49. Krishnan, Y.; Stephens, E.; Balasubramanian, S. A PNA_4 Quadruplex. *J. Am. Chem.*

Soc. **2004**, *126*, 5944–5945.

50. Sharma, N. K. & Ganesh, K. N. PNA C-C^+ i-motif: Superior Stability of PNA TC_8 Tetraplexes Compared to DNA TC_8 Tetraplexes at Low pH. *Chem. Commun.* **2005**, 4330–4332.

51. Vernille, J. P.; Kove, L. C.; Schneider, J. W. Peptide Nucleic Acid (PNA) Amphiphiles: Synthesis, Self-Assembly, and Duplex Stability. *Bioconjugate Chem.* **2004**, *15*, 1314–1321.

52. Guler, M. O.; Pokorski, J. K.; Appella, D. H.; Stupp, S. I. Enhanced oligonucleotide binding to self-assembled nanofibers. *Bioconjugate Chem.* **2005**, *16*, 501-503.

53. Ellipilli, S.; Vasudeva M. R.; Ganesh, K. N. Perfluoroalkylchain conjugation as a new tactic for enhancing cell permeability of peptide nucleic acids (PNAs) via reducing the nanoparticle size. *Chem. Commun.* **2016,** *52*(3), 521-524.

54. Lukeman, P. S.; Mittal, A. C.; Seeman, N. C. Two dimensional PNA/DNA arrays: estimating the helicity of unusual nucleic acid polymers. *Chem. Commun.* **2004**, *15*, 1694-1695.

55. Berger, O.; Adler-Abramovich, L.; Levy-Sakin, M.; Grunwald, A.; Liebes-Peer, Y.; Bachar, M.; Buzhansky, L.; Mossou, E.; Forsyth, V. T.; Schwartz, T.; Ebenstein, Y.; Frolow, F.; Shimon, L. J. W.; Patolsky, F.; Gazit, E. Light-emitting self-assembled peptide nucleic acids exhibit both stacking interactions and Watson-Crick base pairing. *Nat. Nanotechnol*. **2015**, *10*, 353-360.

Section A

Linear Peptides

Chapter 2

Design and Synthesis of 4(*R*/*S*)-Amino and Guanidino Proline Based Peptides

2.1 Introduction

Molecular self-assembly is a spontaneous process by which molecules of same or different kinds form well-defined, structured, and stable associations through non-covalent bonds under equilibrium conditions.[1] Structural compatibility and chemical complementarity between molecules underlay the process of their spontaneous assembly, and it is typically effectuated by a large number of weak non-covalent interactions such as hydrogen bonds, van der Waals interactions, and hydrophobic interactions. The result of this is the generation of complex structures which are composed of multiple copies of simpler constituent molecules. The large structures produced this way are often those that occupy the thermodynamic minima for the collection of molecules and atoms that constitute them.[1]

The process of molecular self-assembly is ubiquitous in nature. Nowhere is it better exemplified than in the living biological systems.[2] From the sequence-dependent association of deoxyribonucleotide/ ribonucleotide strands to form DNA or RNA duplexes respectively,[3] to the association of multimeric coat proteins into robust, hollow nucleic acid carriers in viruses,[4] molecular self-assembly lies at the core of innumerous biological structures. Dynamic assemblies such as those seen in bacterial flagellum,[5] mitotic spindles,[6] enzymes systems like pyruvate dehydrogenase complex,[7] transcriptional machinery – DNA polymerase,[8] translational machinery - ribosomes,[9] molecular motor proteins[10] such as dynein, and kinesin etc., are the archetypes that display the extraordinary level of sophistication achieved through millions of years of evolution at the use of various physical forces, the interplay of which crafts their chemical nature and hence the biological outcome of these self-assembled structures.

2.1.1. Biomolecular Self-Assembly

Biological self-assembly usually relies on the structural complementarity between the surfaces of macromolecules, [1] mediated by several weak non-covalent interactions and it is therefore heavily influenced by the solvent and the conditions in the microenvironment. It also provides a handle, through critical modulators, to control the behavior of these biomolecules, which eventually determines their functional state. The molecular recognition principles at work in these systems offer an excellent framework for us to build complex functional nanostructures that attempt to simulate nature's finesse.

Recognizing the molecular architectural motifs present in the biological systems is, therefore, an indispensable first step in our quest to synthetically mimic the exceptionally efficient nanomachines of nature. As evidenced by the various kinds of DNA nanostructures[11] fabricated using the simple base-pairing rules of complementarity, nucleic acids present an excellent case for the ability to program assembly of large macromolecules into complex structures with well-defined microscopic shape, form and stability.[12] However, nucleic acids are primarily restricted to information storage in cells and it is the proteins which are generally used in various life processes in all organisms. Several functional entities are composed of oligomers of proteins, where more than one polypeptide chains are associated with each other in a regular aggregate. Relatively simpler examples include insulin which exists as a hexamer[13] and hemoglobin which occurs as a tetramer.[14] Complex structures can also be found in plenty. For example, the capsid of Tobacco Mossaic Virus (TMV) is composed of 2130 copies of its coat protein, which self-assembles into a right handed helix to form a tubular structure of about 300 nm in length and a diameter of 18 nm to encase its RNA genome.[15]

2.1.2 Supramolecular Assembly with Peptides

Peptides are short, and do not have multiple structural components, so it is easy to predict their behavior and therefore it is simpler to study them than it is to study proteins, which are usually larger and more complex. Therefore, peptides can be useful models to understand how large proteins have been used as molecular motifs to construct nanoarchitectures in nature. Even though self-assembling peptides are short and simple, they retain the functional versatility of protein systems. It is possible to chemically synthesize them and they are also amenable to chemical modifications. They are also easy to produce in large scale through conventional solid phase peptide synthesis which expands the scope further for "designer peptides" with tunable properties.[16] This includes incorporation of chemical modifications that, in addition to modulating their supramolecular assembling properties, confer functional properties, facilitate cell penetration, or provide means for specific molecular recognition. Therefore, peptides hold the potential to be used as scaffolds for integrating multiple biological functions.[17]

Short peptides usually contain a single secondary structure and they have been routinely used to study sequence and environment triggered conformational transitions.[18] This allows us to investigate how a specific secondary structure motif influences the supramolecular assembly behavior of proteins. The outcome of such studies can be useful in understanding the molecular details of various pathologies involving aggregation of proteins: 1) aging related neurodegenerative disorders[19] such as Alzheimer's disease, and Parkinson's disease which occur due to aggregation of misfolded proteins,[20] 2) infectious diseases such as Creutzfeldt-Jakob's disease and Kuru caused by infectious misfolded proteins called prions,[21] 3) inherited genetic disorders such as Huntington's disease and Kennedy's disease (spinal and bulbar muscular atrophy) caused by polyglutamine expansion,[22] 4) aggregation of damaged, partially unfolded or

misfolded structural proteins such as the lens protein alpha-crystallins of the eyes causing cataract.[23] In all these cases, the aggregation behavior is pathological and is associated with changes in conformation of proteins.

Aggregation of the proteins is usually preceded by the conformational change of some regions of the proteins into β-sheets. Intermolecular interactions between the β-sheets causes them to stack into fibrils which later develop into plaques or form inclusion bodies either within the cell or in the extracellular space leading to disease conditions, which often include degeneration of the cells or tissue atrophy. Thus, understanding the structural factors that determine the secondary structural propensity of amino acids and sequences of amino acids in peptides and proteins holds the key to elucidating the processes of protein aggregation. This could also reveal ways to control them for better therapeutic management of these disorders. Conformation's deterministic control over the self-assembling properties of the peptides is also crucial for normal life processes under physiological conditions.

2.1.3 Polyproline Peptides and PP-II Conformation

Polyproline II (PP-II) is one of the common secondary structures in many proteins.[24] It is a left handed helix with 3-residues per turn. The repeating peptide chain torsion angles φ and ψ are around -75 ^{o} and +145^{o} respectively with all the amide bonds in *trans* (ω = 180^{o}) conformation.[25] PP-II is the preferred conformation of polyproline peptides in water, and so, they serve as good models to study this secondary structure under different conditions, especially in investigations that attempt to unravel the factors that stabilize this conformation in peptides.

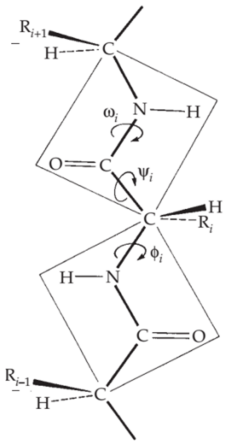


Figure 2.1: Structure of a polypeptide chain showing the peptide chain torsion angles.[27]

Unlike other secondary structures, PP-II and PP-I are not stabilized by intramolecular hydrogen bonds. Intrinsic stereo-electronic factors (gauche effect) and n(O) → π*(CO) interactions have also been attributed to the stability of PP-II conformation.[26] PP-II form is a semi-extended structure with its backbone heavily exposed to the solvent. Due to the lack of H bond donor in its backbone, the carbonyl groups are available for solvation. Backbone hydration has been shown to play an important role in stabilizing PP-II conformation, not only in polyprolines but also in peptides containing non-proline residues.[28a]

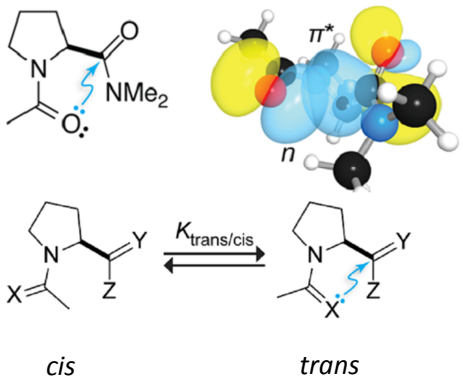


Figure 2.2: (A) n-π* interactions structure in N-acetylproline dimethyl amide.[26] (B) The *cis-trans* isomerism in prolyl peptide bond.

It is considered to be the structure adopted by proteins in unfolded state.[28b] Therefore, understanding the factors that facilitate the formation of PP-II conformation is imminent to unlock the molecular secrets of the protein folding problem.[29] It is also important because PP-II constitutes a major portion of several proteins in their folded state. In proteins that belong to the collagen superfamily, the triple helical regions exist in PP-II form which is essential for their structural integrity.[30] The repeating Pro-Hyp-Gly tripeptide motif found in collagen adopts a left-handed PPII structure. Three such left-handed helices intertwine around each other to form a right handed super helix. The stability of the collagen triple helix stems from the pre-organizing effects of various stereo-electronic factors[30b] and intermolecular hydrogen bonds between the PP-II strands.[30a]

Therefore, PP-II conformation is the fulcrum of collagen's structural constitution. It also plays an important functional role in many proteins. For example, tyrosine kinases containing PP-II region binding of which to SH3 domain of protein kinases is critical for effecting signal transduction.[31]

2.1.4 C4(*R*/*S*)-Substituted Prolyl Polypeptides

In the hands of chemists, polyproline peptide presents itself as an excellent canvas to edit the structure through rational design in order to study the interplay of various factors that affect the conformational stability and dynamics of the PP-II form. This can be done by introducing a new factor, reinforcing an existing one, or eliminating another and studying the effects of such modifications on the structures of the desired peptides.[32-37] Several investigations on polyproline peptides carried out with such an approach have focused primarily on the C4 position of the proline. Not only is this site amenable to easy chemical modifications, it also has a tremendous

influence on the backbone depending on the nature and stereochemistry of the substitution. Of particular interest are electron-withdrawing and hydrogen bonding substitutions such as NH_2 and OH groups[32-33] at C4, which have been shown to have significant effects on the backbone conformation.

In C4(*R*)-substituted polyprolyl peptides, the backbone n(O) → π*(CO) interaction has been shown to favour *trans* prolyl peptide bond which stabilizes the PPII helices.[26] Such an interaction has also been observed in unsubstituted polyproline peptides.[38] In case of C4(*S*)-NH_2 substituted prolyl peptides, the PP-II structure is stabilized by transannular H bonding in water.[26,35] In 2,2,2- trifluoroethanol (TFE), the peptide adopted β structure.[33a] The conformational change from PP-II to β was believed to be caused by a switch from the intrastrand H-bonding to interstrand H-bonding between the peptides.[33c]

2.2 Rationale

In view of the significance of PP-II conformation in biological systems, and the unusual conformational properties exhibited by the C4(*S*)-NH_2 substituted prolyl peptides, the present work attempts to further probe this phenomenon in order to extract basic principles behind the stability of PP-II structures which could help in understanding the origin of amino acid propensity for specific conformations.

2.2.1 Aminoprolyl Peptides

The solvent dependent conformational change observed in C4(*S*)-NH_2- prolyl peptides demonstrates the potential to tune the polyproline backbone to conformations beyond the conventional PP-II and PP-I. This may have significance in the use of these as dynamic scaffolds for self-assembling systems or in environment responsive structures. For this, it is necessary to

further explore the observed conformational change to identify agents and environmental conditions that modulate the conformation of the polyproline backbone.

The stability of PP-II structure in C4(*S*)-NH_2 prolyl peptides is influenced by the intra-residue H-bonding, and solvation of the backbone. In order to further probe the role of these on the change in conformational preference from PP-II to β-structure, following studies were designed. Since a shift from intramolecular to intermolecular H-bonding was postulated to be involved, studies on the effect of length on the conformational change could help understand the role of intermolecular H-bonding between the peptides.

SDS is an anionic surfactant and it is a membrane mimic.[39] It is used to study peptides which are expected to interact with membrane lipids. As conformationally dynamic cationic peptides, aminoprolyl peptides have the potential to be membrane active peptides, so understanding how they respond to membrane like environment could help in the design of cell penetrating peptides. It has also been shown that SDS induces conformational changes, similar to TFE.[40] Further, comparisons between the effect of SDS and TFE as modulators of peptide conformations is likely to help in understanding more about the factors that stabilize PP-II structure in water.

Conjugation of fatty acids to peptides affects the ability of the peptides to self-assemble into regular morphology by modulating the hydrophobic-hydrophilic balance of the molecule. Lipidation of peptides C4(*S*)-OH prolyl peptides, has resulted in the hierarchical self-assembly of antiparallel β-sheets of these peptides into long nanofibers in TFE.[33b] Therefore, similar self-assembling behaviour can be expected for C4(*S*)-NH_2 prolyl peptides. Even though the two peptides show similar conformational properties in TFE, they may still differ in the molecular

details due to the differences in the number of possible H-bonds, size, electron withdrawing strength between the two functional groups. All of these are likely to influence the extent of pyrrolidine ring pucker, strength of transannular H-bond, solvation of the backbone and other weak interactions that determine the structure of the molecule, their packing arrangement and hence the morphology. The observations and conclusions from this study could therefore contribute to laying out empirical principles of self-assembly for cationic peptides with polyproline backbone.

2.2.2 Guanidinylprolyl Polypeptides

When compared to amino group, guanidine function is strongly cationic at pH 7.0 and hence more electron withdrawing. 4(*R*/*S*)-Guanidinylprolyl polypeptides can therefore help elucidate the effect of size and charge of the 4(*S*) substitution on the polyproline backbone conformation.

As cationic peptides, guanidinylproline based peptides have been shown to be useful as cell penetrating peptides and DNA delivery agents.[41-42] With strongly cationic guanidine groups in the sidechain projecting from a rigid polyproline scaffold, these peptides present interesting possibilities of stereospecific interactions with anionic polymers of regular secondary structures like nucleic acids. This prompted the investigations into the interactions between guanidinylprolyl peptides and DNA. In the present work, in addition to drawing a comparison with aminoprolyl peptide on the solvent dependent conformation, interactions of these peptides with DNA oligonucleotides and their self-assembly are also studied. The effect of lipidation on these peptides, both on the conformation, and on the supramolecular assembly properties are investigated as well.

2.3 Objectives

The specific objectives of this section are the following:

- Synthesis of N(1)-t-Boc- and N^4-Fmoc-protected (2*S*,4*R*)- and (2*S*,4*S*)-4-aminoproline monomers.
- Synthesis of aminoprolyl peptides (4*S*)-amp_n and (4*R*)-Amp_n of different lengths (n= 3, 6, and 9) using the standard solid phase peptide synthesis protocol.
- Synthesis of guanidinylprolyl peptides (4*S*)-$gndp_9$ and (4*R*)-$Gndp_9$ by on-resin guanidinylation of the corresponding aminoprolyl peptides.
- Lipidation of different C4-substituted prolyl peptides by conjugation with lauric acid (C_{12}), myristic acid (C_{14}), and palmitic acid (C_{16}) at N-terminus.
- Investigations of the conformation of the aminoprolyl peptides in different solvents, temperature and in the presence of surfactants like SDS using circular dichroism spectroscopy.
- Fluorescence based ethidium bromide displacement assay and UV-Tm studies to check the stereo-dependent interaction of (4*S*)-$gndp_9$ and (4*R*)-$Gndp_9$with DNA.
- Study the effect of configuration at C4 on their self-assembly in water and TFE using field emission scanning electron microscopy (FESEM) and atomic force microscopy (AFM) to determine the how conformation dictates morphology.

2.4 Results and Discussion

Aminoprolyl polypeptides, (4*S*)-amp_n and (4*R*)-Amp_n were synthesized by solid phase peptide synthesis using t-Boc protocol by incorporating (2*S*,4*S*)-N(1)-t-Boc-N^4-Fmoc-4-

aminoproline and (2*S*,4*R*)-N(1)-t-Boc-N^4-Fmoc-4-aminoproline monomers respectively.[43] The peptides were synthesized as homo-oligomers of different lengths and at the end of the sequence, UV-absorbing amino acid phenylalanine was coupled to enable the estimation of the concentration of the peptide solutions. The peptides were suitably functionalized: N-terminus acetylation with acetic anhydride or lipidation with fatty acids and guanidinylation of the C4 amino substitution.

2.4.1 Synthesis of Monomers

The amino acid, 4-aminoproline has two stereo centers - C2 and C4 (Figure 2.3). It has two amino groups and to synthesize linear polyproline peptides, the two amino groups need to be differentially protected with two separate protecting groups (PG_1 and PG_2). PG_1 is the primary protecting group at N1, which is removed after every coupling step to allow the growth of the peptide chain. PG_2 is secondary protecting group at C4, which is used to render the sidechain amine inert during the synthesis of the peptide. It is removed at the end of the peptide synthesis either prior to cleaving the peptide from the resin or simultaneously with the cleavage from the resin. Here, the acid-sensitive t-Boc and the alkali-sensitive Fmoc groups were used as PG_1 and PG_2 respectively.

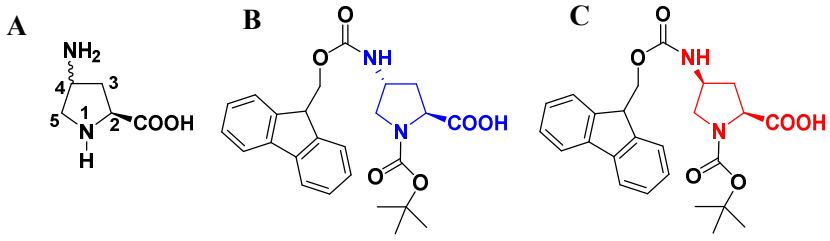


Figure 2.3: Orthogonally protected aminoproline monomers A) Unprotected aminoproline, B) (2*S*,4*R*)-N(1)-t-Boc-N^4-Fmoc- aminoproline **7**, and C) (2*S*,4*S*)- N(1)-t-Boc-N^4-Fmoc- aminoproline monomer **12.**

The orthogonal protection offered by these two common protecting groups enables synthesis of linear polyproline peptides. In order to synthesize the polyproline peptides using t-

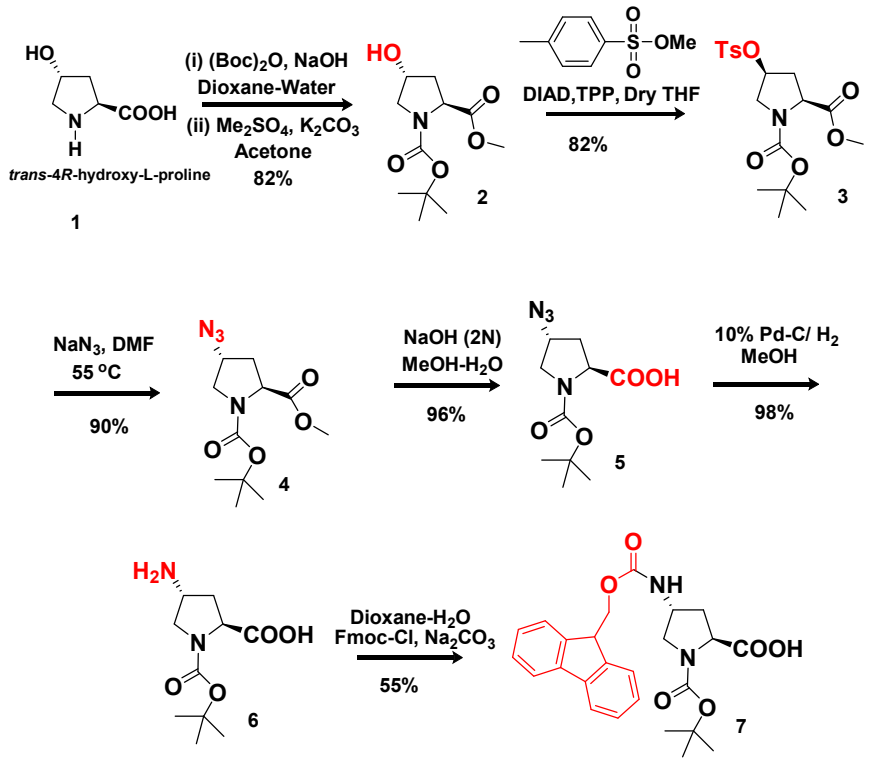
Boc strategy, monomers with N(1)–t-Boc and N4- Fmoc, were used (Figure 2.3). The use of orthogonal protecting groups also allows on-resin guanidinylation of the aminoprolyl peptides as reported by Nanda and Ganesh[41] in the case of guanidinylprolyl collagen peptides.

2.4.1a *Synthesis of (2S,4R)-4-Aminoproline Monomer*

Commercially available *trans*-4(*R*)-hydroxyproline **1** was used as precursor for the synthesis of 4(*R*/*S*) aminoproline monomers in 6 steps as reported in the literature[37] (Scheme 2.1). 4(*R*)-hydroxyproline **1** was treated with *bis*-*t*-butoxycarbonyl anhydride in presence of NaOH as base in water-dioxane mixture to give N(1)-t-Boc protected 4(*R*)-hydroxyproline, the carboxyl group of which was then protected as methyl ester **2** using dimethyl sulfate and potassium carbonate in anhydrous acetone. Characteristic peaks in the 1H NMR spectrum at δ 3.69 (-OCH_3) and δ 1.37 & 1.42 (*t*-Boc) was observed. The two sets of peaks observed for *t-Boc* indicated the presence of the *cis-trans* isomers for rotation about the -N(1)-CO- bond.

The synthesis of (2*S*,4*R*)-4-amino proline monomer was carried out from *trans*-4(*R*)-hydroxyproline methyl ester **2**. It was converted into 4*S*-O-tosylate **3** with DIAD/PPh_3 and methyl-*p*-toluenesulfonate (Mitsunobu condition), resulting in an inversion of configuration at C4 (1H NMR δ 7.30 – 7.87, aromatic protons). The reaction of 4(*S*)-tosylate **3** with NaN_3 in DMF at 60 °C resulted in inversion of stereochemistry again at C4, yielding (2*S*,4*R*)-N(1)-t-Boc-4-azidoprolinemethylester **4**. The peak at 2100 cm^{-1} observed in FTIR spectra confirmed the formation of 4-azide. Hydrolysis of the methyl ester group of compound **4** with aq. NaOH (2N) in methanol resulted in acid **5**. The 4(*R*)-azide group of compound **5** was reduced to the corresponding 4(*R*)-amine **6** by catalytic hydrogenation using 10% Pd-C. The C4-amine was

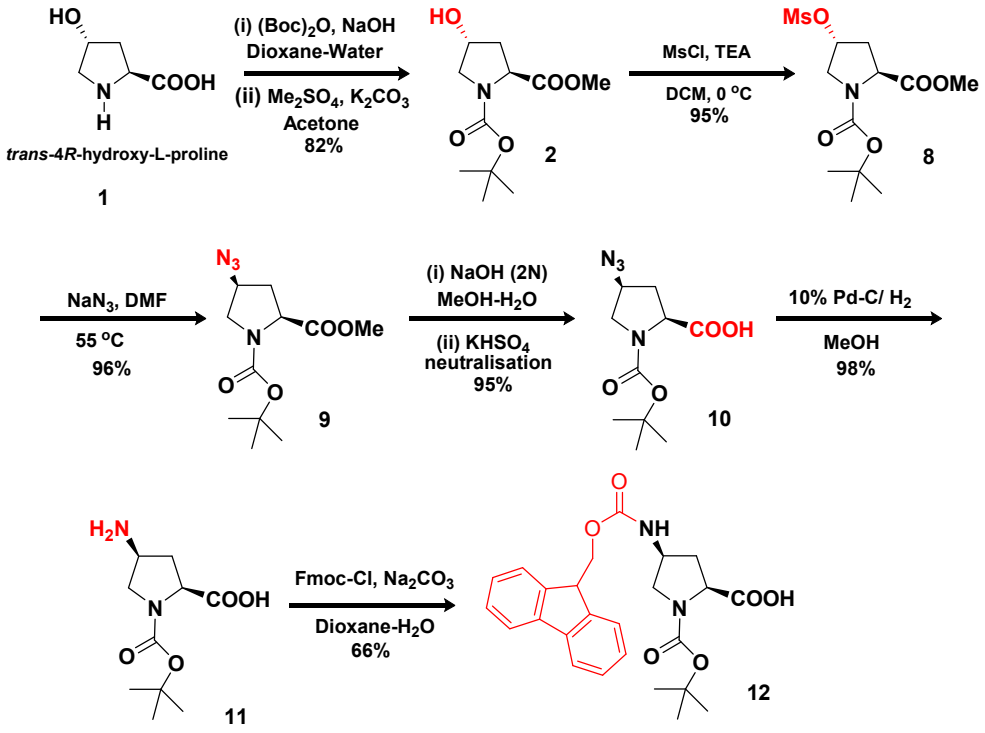
then protected with *Fmoc*, by reaction with 9-fluorenylmethyl chloroformate to obtain the fully protected 4*R*-aminoproline monomer **7**.



Scheme 2.1: Synthesis of (2*S*,4*R*)-4-aminoproline monomer

2.4.1b *Synthesis of (2S,4S)-4-aminoproline monomers*

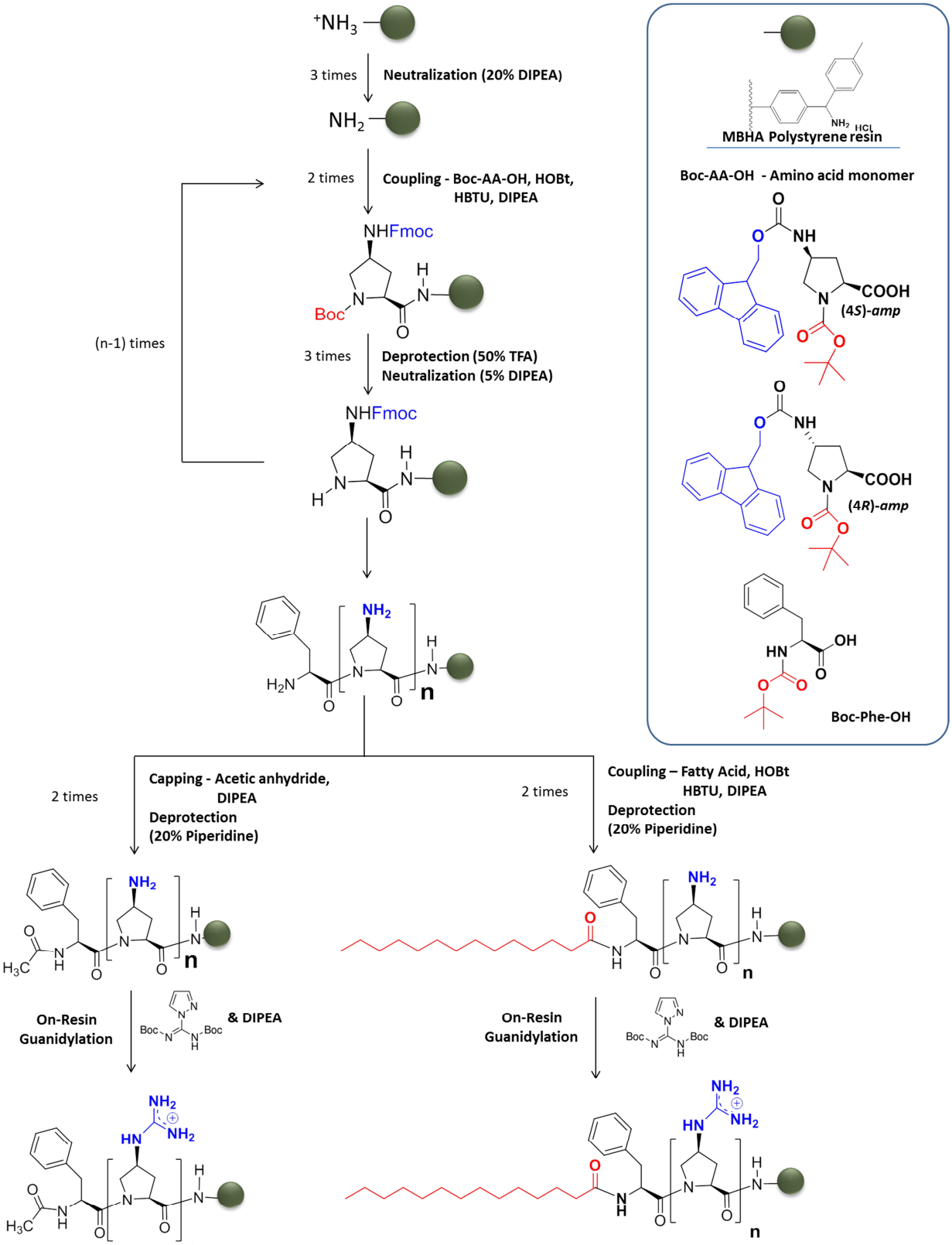
For the synthesis of (2*S*,4*S*)-4-amino proline monomer **12**, the 4(*R*)-OH group of the methyl ester **2** was treated with methanesulfonylchloride in DCM in the presence of Et_3N to obtain the corresponding 4(*R*)-mesyl derivative **8** (Scheme 2.2). Treatment of **8** with NaN_3 at 55^{o}C in DMF resulted in an S_N2 displacement of 4(*R*)-O-mesyl group to yield the 4(*S*)-azide **9**. The methyl ester of compound **9** was hydrolysed with aq. NaOH to yield (2*S*.4*S*)-azide acid **10**. Catalytic hydrogenation of the 4(*S*)-azide **10** yielded the corresponding 4(*S*)-amine **11**, which was treated with 9-fluorenylmethyl chloroformate in dioxane:water in the presence of Na_2CO_3 to yield the fully protected (2*S*,4*S*) 4-aminoproline monomer **12.**



Scheme 2.2: Synthesis of (2*S*,4*S*)-4-aminoproline monomer

2.4.2 Solid Phase Peptide Synthesis

The chemical synthesis of peptides is made relatively easy by solid-phase peptide synthesis (SPPS) developed by Merrifield in 1963.[44] In this versatile and elegant method, the C-terminal residue of the peptide chain is anchored to a polymer resin through a cleavable linker (Scheme 2.3). As the peptide is immobilized on the insoluble solid support, successive incorporation of amino acids to the growing chain leads to a C-terminus to N-terminus growth of peptides of defined sequence. The process involves the following steps: 1) removal of N(1) – protecting group at the leading end of the peptide, 2) washing the resin to remove impurities, excess reagents and by-products, 3) coupling of activated amino acid monomer and, 4) washing the resin.



Scheme 2.3: Solid phase synthesis of peptides using t-Boc chemistry

Polypeptides of any sequence and length can be synthesized by performing these steps with appropriate amino acids in repeating cycles. The amino acids with side chains containing reactive functional groups are protected by an orthogonal protecting group to ensure that the direction of synthesis is linear. After deprotection of the side-chains, cleaving the peptides from the resin yields the final peptide with C-terminal acid or amide.

2.4.2a *Synthesis of aminoprolyl polypeptides*

The 4(*R*/*S*)-aminoprolyl polypeptides were synthesized by manual solid-phase peptide synthesis on commercially available MBHA resin employing the standard t-Boc protocol (Scheme 2.3) using the orthogonally protected monomers (4*S*)-*amp* **7** and (4*R*)-*Amp* **12**, containing N(1)–t-Boc at the point of elongation and N^4- Fmoc at the side chain.

The loading capacity of the resin was reduced to 0.3 mmol/ g, by partial coupling of the first amino acid monomer and subsequent capping of the unreacted free amines with acetic anhydride. The resin bound t-Boc group was removed by treatment with 50% TFA/DCM. The deprotection step was followed by neutralization with 5% DIPEA/ DCM, which renders the free amine on the solid support ready for coupling to the next amino acid in the sequence. Prior to the coupling step, the free carboxyl group of the monomer was activated by treatment with HOBt, HBTU and DIPEA in DMF. This coupling mixture containing 3 equivalents each of the constituent was added to the resin beads and allowed to react under constant and gentle agitation. Here, HBTU acts as coupling reagent, HOBt as racemization suppressor and DIPEA as catalyst. The efficiency of coupling was qualitatively monitored using Chloranil test if the prolyl residues were at the leading end of the growing peptide chain. Ninhydrin based Kaiser's test was carried out when the N-terminus had primary amine. At every step, after the coupling, the positive

Kaiser's test or chloranil test indicated incomplete coupling, prompting repeating of the coupling step. After the coupling of the final prolyl monomer, phenylalanine was coupled to the resin.

For the synthesis of non-lipidated peptides, the terminal amino group after the final coupling was capped by treating it with acetic anhydride and DIPEA in DMF. The side chain protecting group, Fmoc was removed from all the amino proline residues with 20% piperidine /DMF.

2.4.2b *Synthesis of lipidated aminoprolyl polypeptides*

After the deprotection and neutralization steps following the coupling of the final amino acid, one of the desired fatty acids, lauric acid, myristic acid or palmitic acid was coupled to the amino group at the N-terminus. The coupling step was repeated to ensure complete reaction. The side chain protection was then removed from the aminoproline residues with 20% piperidine to get the final lipidated peptides **P4**-**P6**.

2.4.2c *Synthesis of guanidinylprolyl polypeptides*

The guanidinylation of aminoproline was performed on all the residues as the peptides still remained bound to the resin. The on-resin guanidinylation was carried out on the peptides with N,N'-bis-Boc-1H pyrazole-1-carboxamidine in DMF, after the capping of N-terminus or conjugation with fatty acid, and deprotection of the side-chain amine function.[41,43] This yielded the guanidinylated peptides without or with lipid chains at the N-terminus.

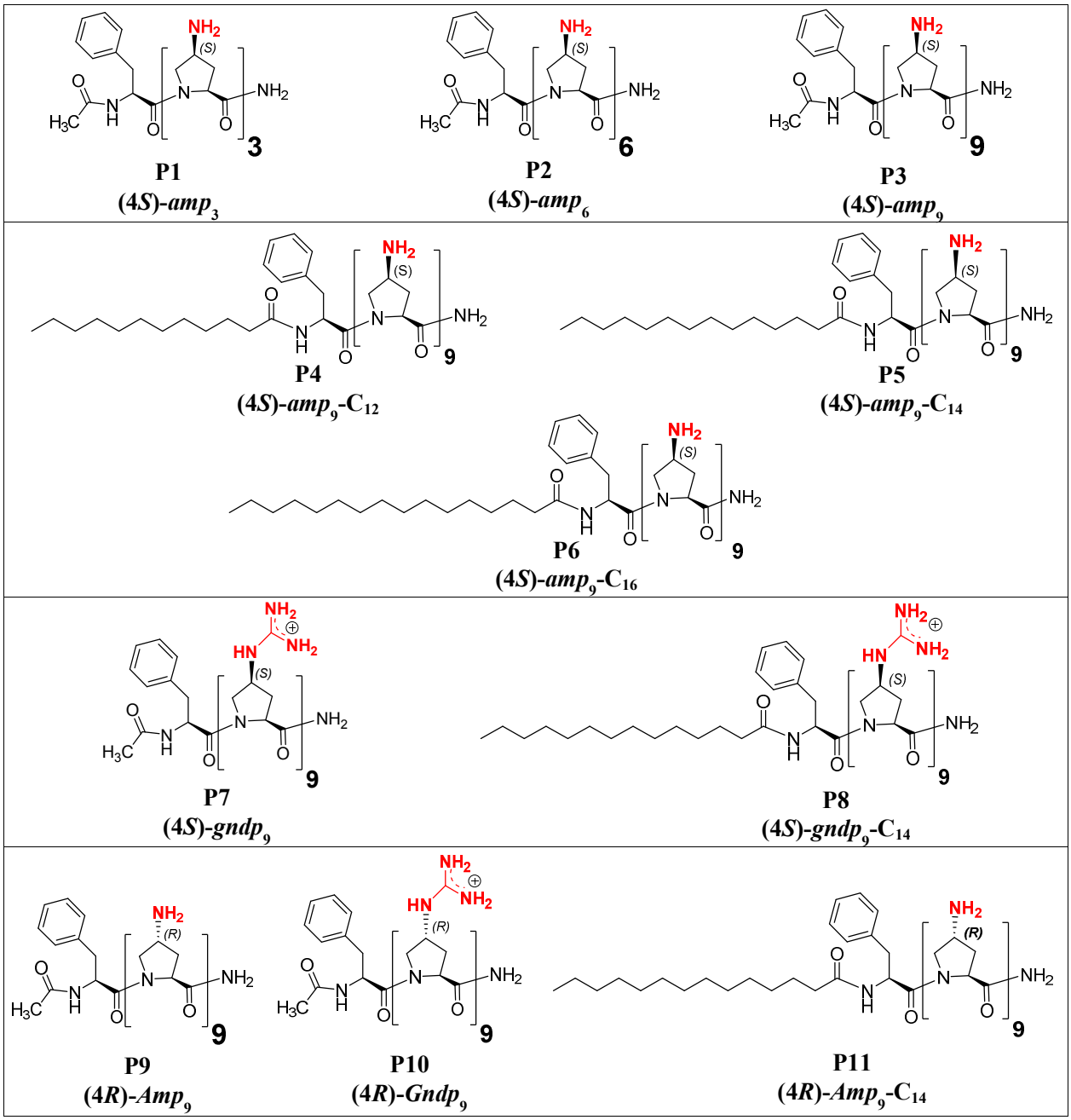


Figure 2.3: Peptides (**P1-P11**) used in the present study.

TABLE 2.1: HPLC retention time and MALDI-TOF mass spectral analysis of the peptides

	Peptide	HPLC RT (min)	Molecular Formula	Calculated Mass	Observed Mass
P1	Ac- Phe-**(*amp*)$_3$**-$CONH_2$ (4*S*)-*amp*$_3$	10.6	$C_{26}H_{38}N_8O_5$	565.29 ($M+Na^+$)	565.35 ($M+Na^+$)
P2	Ac- Phe-**(*amp*)$_6$**-$CONH_2$ (4*S*)-*amp*$_6$	11.0	$C_{41}H_{62}N_{14}O_8$	878.49	879.48 (M+1)
P3	Ac- Phe-**(*amp*)$_9$**-$CONH_2$ (4*S*)-*amp*$_9$	11.7	$C_{56}H_{86}N_{20}O_{11}$	1214.68	1215.77 (M+1)
P4	C_{12}- Phe-**(*amp*)$_9$**-$CONH_2$ (4*S*)-*amp*$_9$–C_{12}	15.8	$C_{66}H_{106}N_{20}O_{11}$	1354.84	1354.98
P5	C_{14}- Phe-**(*amp*)$_9$**-$CONH_2$ (4*S*)-*amp*$_9$–C_{14}	17.3	$C_{68}H_{110}N_{20}O_{11}$	1382.87	1383.98 (M+1)
P6	C_{16}- Phe-**(*amp*)$_9$**-$CONH_2$ (4*S*)-*amp*$_9$–C_{16}	18.4	$C_{70}H_{114}N_{20}O_{11}$	1410.90	1411.50 (M+1)
P7	Ac- Phe-**(*gndp*)$_9$**-$CONH_2$ (4*S*)-*gndp*$_9$	11.8	$C_{65}H_{104}N_{38}O_{11}$	1592.88	1594.10 (M+1)
P8	C_{14}- Phe-**(*gndp*)$_9$**-$CONH_2$ (4*S*)-*gndp*$_9$–C_{14}	12.9	$C_{77}H_{128}N_{38}O_{11}$	1761.06	1762.31 (M+1)
P9	Ac- Phe-**(*Amp*)$_9$**-$CONH_2$ (4*R*)-*Amp*$_9$	11.0	$C_{56}H_{86}N_{20}O_{11}$	1214.68	1215.92 (M+1)
P10	C_{14}- Phe-**(*Amp*)$_9$**-$CONH_2$ (4*R*)-*Amp*$_9$–C_{14}	13.9	$C_{68}H_{110}N_{20}O_{11}$	1382.87	1384.06 (M+1)
P11	Ac- Phe-**(*Gndp*)$_9$**-$CONH_2$ (4*R*)-*Gndp*$_9$	11.7	$C_{65}H_{104}N_{38}O_{11}$	1592.88	1593.92 (M+1)

2.4.2d *Cleavage of peptides from the resin*

After the N-terminal capping/ lipidation, and on-resin modifications on the immobilized peptides as per the requirement, the final peptides were cleaved from the MBHA linker as peptide carboxamides. In case of 4(*R*/*S*)-aminoprolyl polypeptides, the side chain N^4-Fmoc protecting group was removed by treatment with 20% piperidine in DMF. The peptide bound resin beads were taken in TFA containing TFMSA with thioanisole and 1, 2-ethanedithiol as scavengers. The insoluble residue polymer was filtered out and the filterate containing the peptide was treated with cold ether to precipitate the peptide. After washing the solid white precipitate with ether twice, the crude peptide was dissolved in distilled water and stored for biophysical studies.

2.4.3 Purification and Characterization of Peptides

After the peptides were cleaved from the solid support, they were purified by reverse phase high performance liquid chromatography (RP-HPLC) on a semi-preparative C18 column using a linear gradient of water in acetonitrile. The purity of the peptides was checked by injecting aliquots of the purified peptide on a C18 analytical column. The HPLC chromatograms of all the purified peptides (Figure 2.3) are shown in Appendix A.

The integrity of the synthesized peptides was confirmed by MALDI-TOF mass spectrometry using DHB as matrix. The calculated and observed molecular weights for all the peptides with their molecular formulae and HPLC retention time are in Table **2.1**. The MALDI-TOF mass spectra for all the synthesized peptides are shown in Appendix A.

2.5 Summary

The orthogonally protected monomers, (2*S*,4*R*)-N(1)-t-Boc-N^4-Fmoc-aminoproline **7** and (2*S*,4*S*)-N(1)-t-Boc-N^4-Fmoc-aminoproline **12** were synthesized for their incorporation into their corresponding homo-oligomeric peptides (4*S*)-amp_n (**P1-P3**) and (4*R*)-Amp_9 (**P9**) using the standard solid phase peptide synthesis protocol. The decamer (4*S*)-amp_9 (**P3**) was conjugated to fatty acids of different alkyl chain lengths - lauric acid (C_{12}), myristic acid (C_{14}), and palmitic acid (C_{16}) at the N-terminus to obtain the lipidated peptides **P4**, **P5** and **P6** respectively. On-resin guanidinylation of peptides **P3** and **P5** rendered the guanidinylprolyl polypeptides **P7** and **P8**. Similarly, aminoprolyl polypeptides **P9** and **P10,** and guanidinylprolyl polypeptide **P11** were prepared with (4*R*)-*Amp* monomer **12**. The peptides were cleaved from the polymer support and purified using RP-HPLC and characterized with MALDI-TOF. The peptides were prepared to probe the stereodependent conformational change and to observe its effect on the self-assembling properties of the peptides in different solvents as detailed in the subsequent chapters.

2.6 Experimental

This section describes the detailed synthetic procedures and spectral characterization of the rationally designed monomers.

2.6.1 General

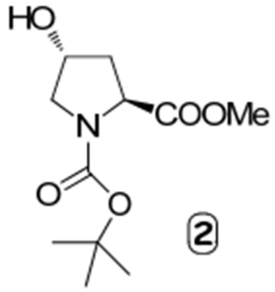
Materials and reagents were of the highest commercially available grade and used without further purification. Reactions were monitored by thin layer chromatography (TLC) carried out on precoated silica gel 60 F254 plates (E. Merck). TLCs were visualized under UV light, iodine and/or ninhydrin spray followed by heating upto 110^o C with heat gun. Silica gel 60-

120 and 100-200 mesh (Merck) was used for routine column chromatography. Elution was done with ethyl acetate/petroleum ether or dichloromethane/methanol mixture depending upon the compound polarity. Flash chromatography was done using 230-400 mesh silica. All solvents were distilled under an inert atmosphere with appropriate desiccant. Reactions in aqueous medium and workup processes were done using double distilled water. Unless otherwise noted, all reactions were carried out at room temperature. IR spectra were recorded on Bruker's Infrared Fourier Transform Spectrophotometer using chloroform and TFE, neat sample. ^{1}H and ^{13}C NMR spectra were recorded on Bruker AV 400 and JEOL AV 400 spectrometers. Chemical shifts are reported in ppm using TMS and $CDCl_3$ as a reference. Spectra were analyzed using ACD spectviewer software from ACD labs. NMR spectra of compounds show two sets of peaks arising from *cis-trans* isomerization of NCO bond. Mass spectra were obtained by ESI-MS technique on Waters-Acquity. Jasco J-815 (Japan) instrument was used for CD measurements. All graphs presented for CD spectra are drawn by Origin 8 software. Reagents for the buffer preparation such as NaCl, NaH_2PO_4, Na_2HPO_4, were obtained from Sigma and were of Molecular biology reagent grade. Double distilled water was demineralized using Millipore MilliQ deionizer and used for the preparation of buffers. pH was adjusted using NaOH and HCl.

Resins for solid phase peptide synthesis and Fmoc-protected amino acids were bought from Novabiochem and were used without further purification. The term "concentrated under reduced pressure" refers to the removal of solvents and other volatile materials using a rotary evaporator at water aspirator pressure (<20 Torr) while maintaining the water-bath temperature below 40 °C. Residual solvent was removed from samples at high vacuum (<0.1 Torr). The term "high vacuum" refers to vacuum achieved by a mechanical oil pump.

2.6.2 Synthesis of compounds 2-12

(2*S*, 4*R*)-N1-(t-butoxycarbonyl)-4-hydroxyproline methylester (2)



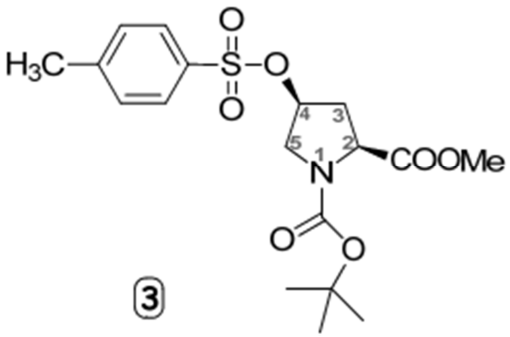
2

A solution of trans-4*R*-hydroxyproline (1 g, 7.6 mmol) in a solution of aq. NaOH (2N, 10 mL) and dioxane (10 mL) was cooled to 0^{o} C and Boc-anhydride (2 ml, 8.4 mmol) was added dropwise using addition funnel. The reaction mixture was stirred at 0 C for 1 h, and dioxane was removed under reduced pressure. The residue was extracted with diethyl ether (5 x 25 mL) to remove unreacted $(Boc)_2O$. The aqueous layer was then vigorously stirred by ethyl acetate under ice-cold condition and acidified with saturated $KHSO_4$ solution to pH 3. The ethyl acetate layer was separated and the aqueous layers were further extracted into ethyl acetate (3 x 20 mL). The organic layer were pooled and washed with water followed by brine, dried over anhydrous Na_2SO_4 and concentrated under vacuum. Removal of ethyl acetate under reduced pressure, gave a white solid which was recrystalized with EtOAc/Hexane. The white solid compound (1 g, 4.3 mmol) obtained in the above step was mixed with anhydrous K_2CO_3 (1.8 g, 13 mmol) and dissolved in anhydrous acetone (25 mL). The reaction mixture was stirred for 30 min at room temperature and dimethylsulphate (4.9 ml, 5.18 mmol) was added. Stirring was continued under reflux conditions for 5 h, when TLC confirmed maximum product formation. The solvent was evaporated under reduced pressure and resulting solid was dissolved in ethyl acetate (50 ml), washed with water (2 X 30 ml), followed by saturated brine solution and dried

over anhydrous Na_2SO_4. The ethyl acetate extract was concentrated under reduced pressure to a pale yellow solid which was then purified by silica gel chromatography, eluting with ethylacetate:hexane (1:1) to yield compound **2** as white crystalline solid. Yield 1.54 g, 82% over the two steps.

Mol. Formula	$C_{11}H_{19}NO_5$
mp	91.8 – 93.1 ^{o} C
Exact Mass	268.1160 $[M+Na]^+$
HR-MS *m/z*	268.1166 $[M+Na]^+$
^{1}H NMR (400 MHz, CDCl3)	**δH** (ppm) δ 4.48 – 4.31 (m, 2H), 3.69 (s, 3H), 3.54 (m, 2H), 2.25 (m, 1H), 2.07 – 1.96 (m, 1H), 1.39 (d, 9H).
^{13}C NMR (101 MHz, CDCl3)	**δC** (ppm) δ 173.8, 154.1, 80.5, 80.4, 70.1, 69.4, 58.0, 57.6, 54.7, 52.4, 52.2, 39.1, 38.5, 28.4, 28.3.

(2*S*,4*S*)-N1-(t-butoxycarbonyl)-4-(p-toluenesulfonyloxy)proline methylester (3)



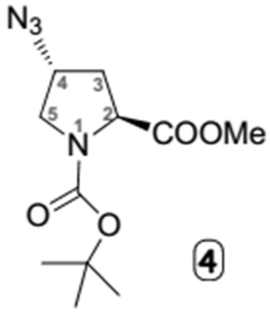
3

A mixture of compound **2,** (1 g, 4 mmol), PPh_3, (1.2 g, 4.5 mmol) and *p*toluenemethylsulfonate (6.8 ml, 4.5 mmol) was dissolved in dry THF (15 ml) cooled to 0 ^{o} C on ice bath, under nitrogen. After stirring for 30 min at ice-cold temperature, Diisopropylazodicarboxylate (DIAD) (8.8 ml, 4.47 mmol) was added slowly with syringe. The reaction mixture was brought to RT and stirred for another 8 hrs after which THF was removed

under vacuum. The resulting orange colored thick oil was dissolved in diethyl ether (60 mL). The resulting solution was kept overnight at room temperature and the white crystals were filtered and the residue was washed with petroleum ether followed by diethyl ether. The filtrate was concentrated under reduced pressure and column purified with silica gel, which gave compound **3** as white crystalline powder. Yield 1.56 g (82%)

Mol. Formula	$C_{18}H_{25}NO_7S$
mp	75.2 – 78.3 ^{o} C
Exact Mass	422.1249 $[M+Na]^+$
HR-MS *m/z*	422.1255 $[M+Na]^+$
^{1}H NMR (400 MHz, CDCl3)	**δH** (ppm) 7.87 – 7.60 (m, 2H), 7.30 (m, 2H), 5.18 – 4.78 (m, 1H), 4.33 (m, 1H), 3.86 – 3.37 (m, 5H), 2.59 – 2.13 (m, 5H), 1.37 (2s, 9H)
^{13}C NMR (101 MHz, CDCl3)	**δC** (ppm) 192.0, 173.3, 130.0, 127.8, 89.7, 28.4, 28.3, 21.7, 21.4.

(2*S*,4*R*)N1-(t-butyloxycabonyl)-4-azidoproline methylester (4)



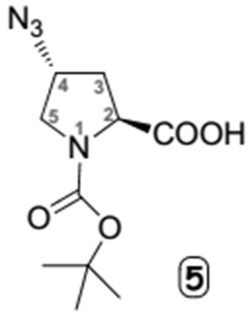
4

A solution of compound **3,** (1 g, 2.5 mmol) and NaN_3, (1.3 g, 20 mmol) in dry DMF (10 mL) was stirred at 55-60 ^{o} C for 12 hrs under nitrogen. When TLC indicated complete conversion of the starting material, DMF was removed under vacuum and the residue was

dissolved in water. The aqueous layer was extracted with ethyl acetate (3 x 25 mL). The combined organic layer was washed with water followed by brine, dried over anhydrous Na_2SO_4 and concentrated under vacuum. The crude product obtained was purified by silica gel chromatography (40% ethyl acetate/hexane elute) to afford compound **4** as colorless thick oil. Yield 0.65 g (90%).

Mol. Formula	$C_{11}H_{18}N_4O_4$
Exact Mass	293.1225 $[M+Na]^+$
HR-MS *m/z*	293.1233 $[M+Na]^+$
^{1}H NMR (400 MHz, CDCl3)	**δH** (ppm) 4.90 (m, 1H), 4.29 (m, 1H), 4.14 (m, 1H), 3.68 (s, 3H), 3.65 – 3.29 (m, 2H), 2.17 (m, 2H), 1.38 (2s, 9H).
^{13}C NMR (101 MHz, CDCl3)	**δC** (ppm) 173.0, 156.5, 153.4, 80.7, 69.8, 65.8, 59.2, 58.7, 57.7, 57.4, 52.2, 51.2, 36.3, 35.3, 28.3, 28.2, 21.9, 15.2.

(2*S*,4*R*)N1-(t-butyloxycabonyl)-4-azidoproline (5)

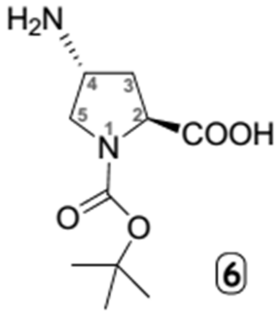


5

The methyl ester **4** (1 g, 3.7 mmol) was hydrolysed using aqueous NaOH (2N) in water-MeOH (1:1, 10 ml) mixture. The reaction mixture was stirred in RT for 2 hrs and methanol was removed under reduced pressure. The aqueous layer was acidified with saturated $KHSO_4$

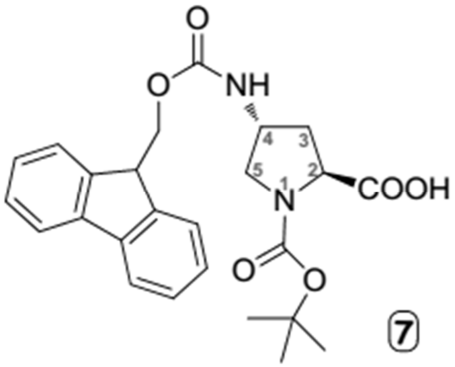
solution, extracted with ethyl acetate and dried over Na_2SO_4. The free acid **5** was obtained as a dark brown liquid upon concentration.

(2*S*,4*R*)N1-(t-butyloxycabonyl)-4-aminoproline (6)



Compound **5** (1 g, 3.9 mmol) was taken in methanol (10 mL) and to this was added 10% Pd-C (0.15 g). The mixture was subjected to hydrogenation Hydrogen bladder for 4 hrs. Pd-C suspension was removed by filtration through Celite and the filtrate was evaporated under reduced pressure to give reddish brown liquid. The (2*S*,4*R*)N1-(*t*-butoxycarbonyl)-4-aminoproline **6** thus obtained (0.88 g, 98% yield) was used without further purification.

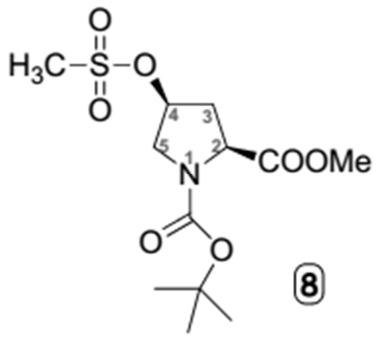
(2*S*,4*R*)-N1-(t-butoxycarbonyl)-4-(9-fluorenylmethyloxycarbonylamino) proline (7)



An aqueous solution (100 mL) of compound **6** (1 g, 4.3 mmol) was cooled to 0 ^{o} C and 10% aqueous Na_2CO_3 (20 mL) and dioxane (100 mL) were added. Fmoc-Cl (1.7 g, 6.5 mmol) dissolved in dioxane (10 mL) was added dropwise during 1 hr. The resulting mixture was stirred for 15 hrs at room temperature maintaining the pH of solution around 8.0. The reaction mixture was concentrated on a rotary evaporator to remove dioxane and to the resulting slurry 50 mL of water was added. The mixture was extracted with diethyl ether (5 x 50 mL) to remove unreacted Fmoc-Cl. The aqueous layer was then vigorously stirred by ethyl acetate under ice-cold condition, and acidified with saturated $KHSO_4$ solution to pH 3. The ethyl acetate layer was separated and the aqueous layer was further extracted into fresh ethyl acetate (3 x 50 mL), the organic layers were pooled and washed with water followed by brine, dried over anhydrous Na_2SO_4 and concentrated under vacuum. The crude material was purified by silica gel chromatography (80% ethyl acetate/hexane elute) afford compound **7** as white solid. Yield 1.28 g (55%).

Mol. Formula	$C_{25}H_{28}N_2O_6$
mp	Decomposes around 183 – 189 ^{o} C
Exact Mass	475.1844 $[M+Na]^+$
HR-MS *m/z*	475.1845 $[M+Na]^+$
^{1}H NMR (400 MHz, DMSO-D6)	**δH** (ppm) 7.89 (d, 2H), 7.68 (m, 2H), 7.62 (m, 1H), 7.41 (t, 2H), 7.33 (t, 2H), 4.38 – 4.29 (m, 2H), 4.24 – 4.14 (m, 2H), 4.10 – 3.99 (m, 1H), 3.60 – 3.44 (m, 1H), 3.16 (m, 1H), 2.21 – 1.95 (m, 2H), 1.36 (2s, 9H).
^{13}C NMR (101 MHz, CDCl3)	**δC** (ppm) 177.9, 175.1, 156.3, 155.5, 154.6, 143.7, 141.3, 127.9, 127.2, 125.2, 125.1, 120.1, 79.9, 68.4, 67.3, 66.0, 64.8, 58.7, 53.7, 50.1, 47.2, 47.1, 34.8, 28.5, 15.3.

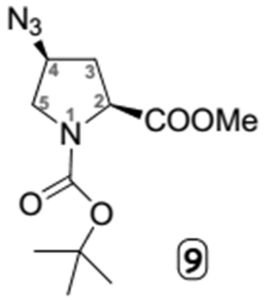
(2*S*,4*R*)N-(t-butyloxycabonyl)-4-O-mesyl proline methylester (8)



The solution of methylester **2** (1 g, 4.1 mmol) and triethylamine 1.7 mL (12.2 mmol) in 20 mL of dry dichloromethane was cooled to 0 ^{o} C on ice bath under Argon. While stirring (4.7 mL, 6.1 mmol) methanesulfonyl chloride was added in one shot. Stirring was continued over a period of 3 hrs at 0 ^{o} C. The reaction mixture was then washed with water, followed by saturated brine solution. The organic layer was dried over anhydrous Na_2SO_4 and concentrated under vacuum. The crude material was purified by silica gel chromatography (30% ethyl acetate/hexane) which afforded mesylated compound **8** as a white solid. Yield 1.26 g (95%)

Mol. Formula	$C_{12}H_{21}NO_7S$
mp	83 – 86.4 ^{o} C
Exact Mass	346.0936 $[M+Na]^+$
HR-MS *m/z*	346.0939 $[M+Na]^+$
^{1}H NMR (400 MHz, CDCl3)	**δH** (ppm) 1.42 & 1.47 (2s, 9H), 2.17-2.30 (m, 1H), 2.5-2.71 (m, 1H), 3.04 (s,3H), 3.71-3.87 (m, 5H), 4.32-4.48 (m, 1H), 5.24-5.3 (m, 1H)
^{13}C NMR (101 MHz, CDCl3)	**δC** (ppm) 172.8, 153.4, 81.0, 78.2, 78.0, 57.5, 57.2, 52.6, 52.4, 52.3, 38.8, 37.6, 36.4, 28.4, 28.3.

(2*S*,4*S*)N1-(t-butyloxycabonyl)-4-azidoproline methylester (9)

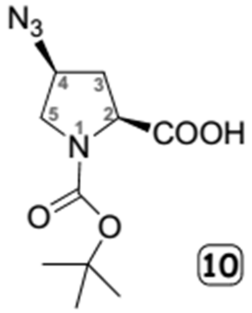


9

(*2S,4S*)-azido compound **9** (0.75 g, 90%) was synthesized from (1 g, 3.1 mmol) the mesylate **8** accordingly as mentioned earlier for compound **4.** Yield 96%.

Mol. Formula	$C_{11}H_{18}N_4O_4$
Exact Mass	293.1225 $[M+Na]^+$
HR-MS *m/z*	293.1227 $[M+Na]^+$
^{1}H NMR (400 MHz, CDCl3)	**δH** (ppm) 4.34 (m, 1H), 4.17 – 4.05 (m, 1H), 3.79 – 3.60 (m, 4H), 3.44 (m, 1H), 2.54 – 2.35 (m, 1H), 2.13 (m, 1H), 1.45 – 1.37 (m, 9H)
^{13}C NMR (101 MHz, CDCl3)	**δC** (ppm) 172.3, 172.0, 154.0, 153.5, 80.6, 59.3, 58.3, 57.8, 57.4, 52.5, 52.4, 51.3, 50.9, 36.1, 35.2, 28.4, 28.3.

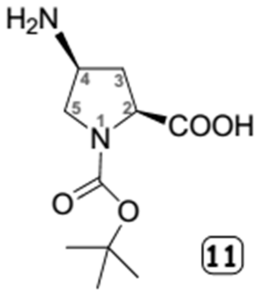
(2*S*,4*S*)N1-(t-butyloxycabonyl)-4-azidoproline (10)



10

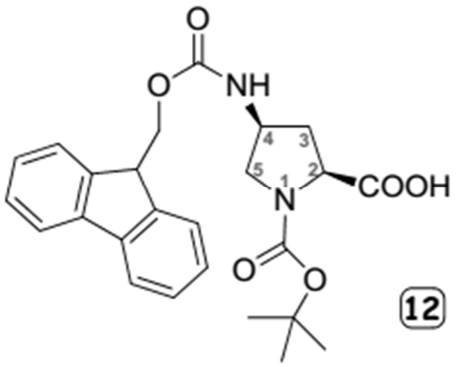
This acid was hydrolysed from its corresponding methyl ester **9** by aq. NaOH (2N) in Water/MeOH. The product was obtained as brown liquid in 98% yield following previously mentioned procedure in case of compound **5**. Yield 95%.

(2*S*,4*S*)N1-(t-butyloxycabonyl)-4-aminoproline (11)



(*2S,4S*)-amino compound **11** (0.87 g, 97.8%) was synthesized from the analogous azide **10** accordingly by PdC/H_2 reduction as mentioned earlier for compound **6.**

(2*S*,4*S*)N1-(t-butoxycarbonyl)-4-(fluorenylmethyloxycarbonylamino) proline (12)



The compound **12** was prepared from the free amine **11** using the similar procedure as the one described for the compound (2*S*,4*R*)-**7** as foamy white solid with yield 1.14g (66%).

Mol. Formula $C_{25}H_{28}N_2O_6$

mp 148.6 – 153.6 ^{o} C

Exact Mass	453.2025 $[M+H]^+$
HR-MS *m/z*	453.2032 $[M+H]^+$
^{1}H NMR (400 MHz, METHANOL-D3)	**δH** (ppm) 7.74 (d, 2H), 7.58 (d, 2H), 7.34 (t, 2H), 7.26 (t, 2H), 4.29 (d, 2H), 4.15 (m, 3H), 3.73 (m, 1H), 3.19 (m, 1H), 2.64 – 2.45 (m, 1H), 1.93 – 1.79 (m, 1H), 1.40 (2s, 9H).
^{13}C NMR (101 MHz, CDCl3)	**δC** 174.0, 157.2, 156.0, 143.9, 141.3, 127.8, 127.2, 125.3, 120.1, 82.9, 67.2, 66.0, 58.7, 54.0, 50.7, 47.2, 33.2, 28.4, 15.3.

2.6.3 Solid phase synthesis

2.6.3a *Synthesis of peptides*

Peptides were synthesized manually using a sintered (G2) reaction vessel equipped with a Teflon stopcock. All the materials used were of peptide synthesis grade (Novabiochem) and was used without further purification. Analytical grade DMF was purchased from (Merck, India) and stored over 4Å molecular sieves for 2 days before using for peptide synthesis. Similarly DCM was distilled over CaH_2 and stored over 4 Å molecular sieves. Coupling reactions were carried out using *in situ* active ester method, by HBTU as coupling reagent, HOBt as recemization suppresser and DIPEA as catalyst.

Resin functionalization

Commercially available MBHA (4-methyl benzhydrylamine) resin (Novabiochem, 100-200 mesh) the hydrochloride salt was neutralized prior to amino acid coupling and the following steps were done for the synthesis (100 mg scale). The resin was washed and swollen in dry DCM for at least 1 hr. The DCM was drained and 50% solution of DIPEA in DCM was added (3 x 3ml; 10 min each) followed by thorough

washing with DCM. Further, washing and swelling with dry DMF for 1 hr was followed by immediate coupling of the 1st amino acid desired in the C-terminus of the peptide.

Synthesis protocol

Boc–strategy was used for synthesis on MBHA resin for acid-labile protecting groups.

- DCM wash (4 x 5 mL)
- 50% TFA in DCM (2 X 5 mL; 10 min each) for deprotection of Boc group
- 5% DIPEA in DCM (3 X 5 mL; 5 min each) for neutralization of TFA salt
- DCM, MeOH wash (3 x 3 mL each)
- Kaiser's/Chloranil test
- DCM, DMF wash (3 x 3 mL each)
- Coupling reaction (3 eq. each of aminoacid, DIPEA, HOBt and HBTU in 10eq. volume of DMF and NMP mixture)
- Kaiser's/Chloranil test

These cycles were repeated for every amino acid. The coupling and deprotection reactions were monitored by a combination of Kaiser's (ninhydrin) test and chloronil test. In case of negative test after coupling, re-coupling was performed with the same amino acid. It was followed by capping of the unreacted amino groups using Ac_2O, DIPEA & DMF (1:1:1), in case coupling does not go to completion even after re-coupling.

Kaiser's test

Kaiser's test was used to monitor the t-Boc/Fmoc deprotection and coupling in the solid phase peptide synthesis using three solutions. Solution A: Ninhydrin (5.0 g) dissolved in ethanol (100 mL) Solution B: Phenol (80.0 mg) dissolved in ethanol (20 mL) Solution C: KCN (2 mL, 0.001 M aqueous solution) added to 98 mL pyridine

- Few beads of resin to be tested were taken in a test tube and washed 3 times with ethanol.
- 3-4 drops of each of the three solutions described above were added to it
- The test tube was heated to 120 °C for 4-6 min
- The successful deprotection was indicated by blue resin beads while colourless beads indicated the completion of coupling step.

Chloranil test

A few beads of resin were taken in a glass test tube (5 ml capacity) and were washed with methanol followed by toluene. To this, three drops of saturated chloranil solution in toluene and 200 µL of acetone were added. The mixture was shaken for 2-3 minutes. Blue or green color is observed on the resin beads if free amines are present.

2.6.3b *On-resin guanidylation of peptides*

On-resin guanidylation was carried out on peptide **P3**, **P6**, and **P9.** The Fmoc-protection on the side chains of the peptides were deprotected using 20% piperidine/DMF treatment. N',N'-bis-Boc-1 H-pyrazole-1-carboxamidine (5 eq. for each amino group on peptide chain) with equivalent amount of DIPEA in minimum volume of DMF were added to the on-resin peptides and 4 hrs of reaction time was allowed. This step was repeated thrice till Kaiser's test confirmed

complete conversion. The peptides were later cleaved from their corresponding resin to obtain peptide.

2.6.3c *Peptide cleavage from resin*

Finally after the last coupling the resin was washed with DMF (5 x 5 mL), DCM (5 x 5 mL), then with toluene (5 x 5 mL) and methanol (5 x 5 mL) then flushed with N2-gas for 3 mins. The resin along with the sintered flask was dried in vacuum desiccator over KOH and P_2O_5 for 6 hrs.

The resin MBHA (10 mg) with peptides attached to it was stirred with TFA (200 µL) and deionized water (10 µL) in an ice bath for 10 min. TFMSA (16 µL) was added slowly with vigorous shaking to dissipate the heat generated. The reaction mixture was stirred for 1.5 hrs at room temperature. The resin was removed by filtration under reduced pressure and washed with TFA (3 x 1 mL). The combined filtrate was concentrated, the product was precipitated with cold dry ether and the peptide was isolated by centrifugation (5 times at 5000 rpm) as white powder. Peptides which had Fmoc-protection in side groups were removed by 20% piperidine/DMF treatment and dried properly before cleavage.

2.6.4 High performance liquid chromatography (HPLC)

Peptides were purified by reverse phase-HPLC on Agilent Technologies 1260 Infinity equipped with Photodiode array detector (PDA). Semi-preparative RP-C18 columns (250x10 mm, 10 μm) was used for peptides. The solvent system comprised of MeCN:Water (5:95) with 0.1% TFA for solution A and for solution B MeCN: Water (50:50), 0.1% TFA. A gradient of 0-100% at a flow rate of 3 mL/min was used to elute the peptide and the eluant was monitored at

220 nm. The peak corresponding to the peptide was collected and the fractions were frozen. Subsequently these peptides were concentrated by using speed vacuum. The purity of the final peptides were further analyzed on the Phenomenex Analytical RP-C18 (250 x 4 mm, 5 μm) column by using a gradient flow of 0 to 100% B in 30 min at a flow rate of 1 mL/min. The absorbance of the eluant was monitored at its corresponding wavelength and the purity was obtained from the integrator output. The purities of the hence purified peptides were found to be more than 95%. Overall yields of the peptides are given in table 2.2

Table 2.2: Overall yields of the peptides used in the present study

	Peptide	**Overall Yield (%)**
P1	(4*S*)-amp_3	22
P2	(4*S*)-amp_6	31
P3	(4*S*)-amp_9	31
P4	(4*S*)-amp_9–C_{12}	17
P5	(4*S*)-amp_9 –C_{14}	27
P6	(4*S*)-amp_9–C_{16}	23
P7	(4*S*)-$gndp_9$	25
P8	(4*S*)-$gndp_9$–C_{14}	13
P9	(4*R*)-Amp_9	16
P10	(4*R*)-Amp_9–C_{14}	6
P11	(4*R*)-$Gndp_9$	5

2.6.5 MALDI-TOF characterization

MALDI-TOF mass spectra were obtained on either Voyager-Elite instrument (Perspective Biosystems Inc., Farmingham, MA) equipped with delayed extraction or on

Voyager-De-STR (Applied Biosystems) instrument. 2,5-Dihydroxy benzoic acid (DHB) and α-cyano-4- hydroxycinnamic acid (CHCA) both were used as matrix for peptides of which DHB was found to give satisfactory results. A saturated matrix solution was prepared with typical dilution solvent (50:50:0.1 Water: MeCN: TFA) and spotted on the metal plate along with the oligomers. The metal plate was loaded to the instrument and the analyte ions are then accelerated by an applied high voltage (15-25 kV) in reflector mode, separated in a fieldfree flight tube and detected as an electrical signal at the end of the flight tube.

2.7 References

1. Whitesides, G. M.; Mathias, J. P.; Seto, C. T. Molecular Self-Assembly and Nanochemistry: A Chemical Strategy for the Synthesis of Nanostructures. *Science* **1991**, *254*, 1312-1319.

2. Whitesides, G. M.; Grzybowski, B. Self-Assembly at All Scales. *Science* **2002**, *295*, 2418-2421.

3. Watson, J. D.; Crick, F. H. C. Molecular Structure of Nucleic Acids. *Nature* **1953**, *171*, 737-738.

4. Liu, Z.; Qiao, J.; Niu, Z.; Wang, Q. Natural Supramolecular Building Blocks: From Virus Coat Proteins to Viral Nanoparticles. *Chem. Soc. Rev.* **2012**, *41*, 6178–6194.

5. a) Minamino, T.; Imada, K.; Namba, K. Molecular Motors of the Bacterial Flagella. *Curr. Opin. Struct. Biol.* **2008**, *18*, 693-701. b) Evans, L. D. B.; Hughes, C.; Fraser, G. M. Building a Flagellum Outside the Bacterial Cell. *Trends Microbiol.* **2014**, *22*, 566-572.

6. Karsenti, E.; Vernos, I. The Mitotic Spindle: A Self-Made Machine. *Science* **2001**, *294*, 543-547.

7. Bates, D. L.; Danson, M. J.; Hale, G.; Hooper, E. A.; Perham, R. N. Self-assembly and Catalytic Activity of the Pyruvate Dehydrogenase Multienzyme Complex of Escherichia coli. *Nature* **1977**, *268*, 313–316.

8. Sun, J.; Shi, Y.; Georgescu, R. E.; Yuan, Z.; Chait, B. T.; Li, H.; O'Donnell, M. E. The Architecture of a Eukaryotic Replisome. *Nat. Struct. Mol. Biol.* **2015**, *22*, 976–982.

9. Staley, J. P.; Woolford, J. L., Jr. Assembly of Ribosomes and Spliceosomes: Complex Ribonucleoprotein Machines. *Curr. Opin. Cell Biol.* **2009**, *21*, 109–118.

10. Hess, H. Self-assembly Driven by Molecular Motors. *Soft Matter*, **2006**, *2*, 669–677.

11. a) Chen, J.; Seeman, N. C. Synthesis from DNA of a Molecule with the Connectivity of a Cube. *Nature* **1991**, *350*, 631-633. b) Rothemund, P. W. K. Folding DNA to create nanoscale shapes and patterns. *Nature* **2006,** *440*, 297–302.

12. a) Han, D.; Pal, S.; Nangreave, J.; Deng, Z.; Liu, Y.; Yan, H. DNA Origami with Complex Curvatures in Three-Dimensional Space. *Science* **2011**, *332*, 342-346. b) Wagenbauer, K. F.; Christian Sigl, C.; Dietz, H. Gigadalton-scale shape-programmable DNA assemblies. *Nature* **2017**, *552*, 78–83.

13. Dodson, D. D.; Dodson, E. J.; Turkenburg, J. P.; Bing, X. Molecular Recognition in Insulin Assembly. *Biochem. Soc. Trans.* **1993**, *3*, 609-14.

14. Bunn, H. F. Subunit Assembly of Hemoglobin: An Important Determinant of Hematologic Phenotype. *Blood* **1987**, *69*, 1-6.

15. Namba, K.; Stubbs, G. Structure of Tobacco Mosaic Virus at 3.6Å Resolution: Implications for Assembly. *Science* **1986**, 231, 1401–1406.

16. Zhao, X.; Zhang, S. Molecular Designer Self-Assembling Peptides. *Chem. Soc. Rev.* **2006**, *35*, 1105-1110.

17. Hendricks, M. P.; Sato, K.; Palmer, L. C.; Stupp, S. I. Supramolecular Assembly of Peptide Amphiphiles. *Acc. Chem. Res.* **2017**, *50*, 2440−2448.

18. a) De la Paz, M. L.; Goldie, K.; Zurdo, J.; Lacroix, E.; Dobson, C. M.; Hoenger, A.; Serrano, L. *De novo* Designed Peptide-Based Amyloid Fibrils. *Proc. Natl. Acad. Sci. U. S. A.* **2002**, *99*, 16052-16057. b) Oas, T.G.; Kim, P. S. A Peptide Model for Protein Folding. *Nature* **1988**, *336*, 42–48.

19. Murphy R. M. Peptide Aggregation in Neurodegenerative Disease. *Annu. Rev. Biomed. Eng.* **2002**, *4*, 155–174.

20. Irvine, G. B.; El-Agnaf, O. M.; Shankar, G. M.; Walsh, D. M. Protein Aggregation in the Brain: The Molecular Basis for Alzheimer's and Parkinson's Diseases. *Mol. Med.* **2008**, *14*, 451–464.

21. Cobb, N. J.; Surewicz, W. K. Prion Diseases and Their Biochemical Mechanisms. *Biochemistry* **2009**, *48*, 2574–2585.

22. Zoghbi, H. Y.; Orr, H. T. Glutamine Repeats and Neurodegeneration. *Annu. Rev. Neurosci.* **2000**, *23*, 217–247.

23. Moreau, K. L.; King, J. A. Protein Misfolding and Aggregation in Cataract Disease and Prospects for Prevention. *Trends Mol. Med*. **2012**, *18*, 273-282.

24. a) Adzhubei, A. A.; Sternberg, M. J. E. Left-handed Polyproline II Helices Commonly Occur in Globular Proteins. *J. Mol. Biol*. **1993**, *229*, 472-493. b) Esipova, N. G.; Tumanyan, V. G. Omnipresence of the Polyproline II Helix in Fibrous and Globular Proteins. *Curr. Opin. Struct. Biol.* **2017**, *42*, 41 –49.

25. Cubellis, M. V.; Caillez, F.; Blundell, T. L.; Lovell, S. C. Properties of Polyproline II, a Secondary Structure Element Implicated in Protein–Protein Interactions. *Proteins: Struct., Funct., Bioinf.* **2005**, *58*, 880–892.

26. Horng, J. C.; Raines, R. T. Stereoelectronic Effects on Polyproline Conformation. *Protein Sci.* **2006**, *15*, 74-83.

27. Metzler, D. E. Amino Acids, Peptides, and Proteins. *Biochemistry The Chemical Reactions of the Living Cell*, 2; Academic Press, 2003; pp 39-54.

28. a) Meral, D.; Toal, S.; Schweitzer-Stenner, R.; Urbanc, B. Water-Centered Interpretation of Intrinsic pPII Propensities of Amino Acid Residues: In Vitro-Driven Molecular Dynamics Study. *J. Phys. Chem. B* **2015**, *119*, 13237 −13251. b) Shi, Z.; Chen, K.; Liu, Z.; Kallenbach. N. R. Conformation of the Backbone in Unfolded Proteins. *Chem. Rev*. **2006**, *106*, 1877−1897.

29. a) Tiffany, M. L.; Krimm, S. New Chain Conformations of Poly(glutamic acid) and Polylysine. *Biopolymers* **1968**, *6*, 1379–1382. b) Krimm, S.; Tiffany, M. L. The Circular Dichroism Spectrum and Structure of Unordered Polypeptides and Proteins. *Israel J. Chem.* **1974**, *12*, 189–200. c) Tiffany, M. L.; Krimm, S. Circular Dichroism of the "Random" Polypeptide Chain. *Biopolymers*, **1969**, *8*, 347–359.

30. a) Brodsky, B.; Thiagarajan, G.; Madhan, B.; Kar, K. Triple-Helical Peptides: An Approach to Collagen Conformation, Stability, and Self-association. *Biopolymers* **2008**, *89*, 345-353. b) Shoulders, M. D.; Raines, R. T. Collagen Structure and Stability. *Ann. Rev. Biochem.* **2009**, *78*, 929-958.

31. Musacchio, A.; Saraste, M.; Wilmanns, M. High-Resolution Crystal Structures of Tyrosine Kinase SH3 Domains Complexed with Proline-Rich Peptides. *Nat. Struct. Mol. Biol.* **1994**, *1*, 546–551.

32. a) Babu, I. R.; Ganesh, K. N. Enhanced Triple Helix Stability of Collagen Peptides with 4*R*-Aminoprolyl (Amp) Residues: Relative Roles of Electrostatic and Hydrogen Bonding Effects. *J. Am. Chem. Soc*. **2001**, *123*, 2079–2080. b) Umashankara, M.; Ramesh Babu, I.; Ganesh, K. N. Two prolines with a difference: contrasting stereoelectronic effects of 4*R*/*S*-aminoproline on triplex stability in collagen peptides [Pro(X)-Pro(Y)-Gly]n. *Chem. Commun. (Cambridge, U. K.)* **2003,** 2606–2607.

33. a) Sonar, M. V.; Ganesh, K. N. Water-induced switching of β-structure to polyproline II conformation in the 4*S*-aminoproline polypeptide via H-bond rearrangement. *Org. Lett.* **2010***, 12*, 5390–5393. b) Bansode, N. D.; Sonar, M. V.; Ganesh, K. N. A nanofiber assembly directed by the non-classical antiparallel β-structure from 4S-(OH) proline polypeptide. *Chem. Commun*. **2016,** *52*, 4884-4887. c) Bansode, N. D.; Madhanagopal, B.; Sonar, M. V.; Ganesh, K. N. Stereodependent and solvent specific formation of unusual β-structure through side chain-backbone H-bonding in C4(*S*)-(NH_2/OH/NHCHO)-L-prolyl polypeptides. *Biopolymers* **2017**, *108*, e22981.

34. Umashankara, M.; Sonar, M. V.; Bansode, N. D.; Ganesh, K. N. Orchestration of Structural, Stereoelectronic, and Hydrogen-Bonding Effects in Stabilizing Triplexes from Engineered Chimeric Collagen Peptides (ProX-ProY-Gly)$_6$ Incorporating 4(*R*/*S*)-Aminoproline. *J. Org. Chem.* **2015,** *80*, 8552-8560.

35. Shoulders, M. D.; Kotch, F. W.; Choudhary, A.; Guzei, I. A.; Raines, R. T. The Aberrance of the 4*S* Diastereomer of 4-Hydroxyproline. *J. Am. Chem. Soc.* **2010**, *132*, 10857-10865.

36. Kumin, M.; Sonntag, L.; Wennemers, H. Azidoproline Containing Helices: Stabilization of the Polyproline II Structure by a Functionalizable Group. *J. Am. Chem. Soc*. **2007**, *129*, 466-467.

37. Thomas, K. M.; Naduthambi, D.; Tririya, G.; Zondlo, N. J. Proline Editing: A Divergent Strategy for the Synthesis of Conformationally Diverse Peptides. *Org. Lett*. **2005**, *7,* 2397-2400.

38. Wilhelm, P.; Lewandowski, B.; Trapp, N.; Wennemers, H. A Crystal Structure of an Oligoproline PPII-Helix, at last. *J. Am. Chem. Soc.* **2014**, *136*, 15829-15832.

39. Tulumello, D. V.; Deber, C. M. SDS Micelles as a Membrane-Mimetic Environment for Transmembrane Segments. *Biochemistry*, **2009**, *48*, 12096–12103.

40. Liu, Z.; Chen, K.; Ng, A.; Shi, Z.; Woody, R. W.; Kallenbach, N. R. Solvent Dependence of PII Conformation in Model Alanine Peptides. *J. Am. Chem. Soc.* **2004**, *126*, 15141–15150.

41. Nanda, M.; Ganesh, K. N. 4(*R*/*S*)-Guanidinylprolyl Collagen Peptides: On-Resin Synthesis, Complexation with Plasmid DNA, and the Role of Peptides in Enhancement of Transfection. *J. Org. Chem.* **2012**, *77*, 4131–4135.

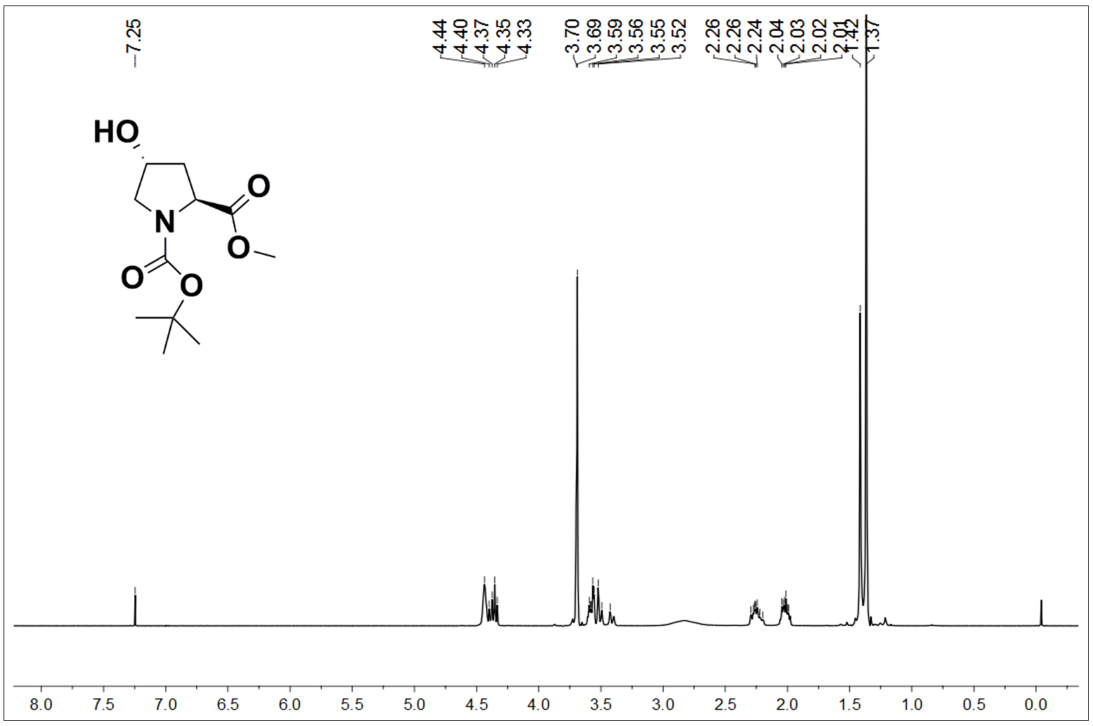
42. Nagel, Y. A.; Raschle, P. S.; Wennemers, H. Effect of Preorganized Charge Display on the Cell Penetrating Properties of Cationic Peptides. *Angew. Chem. Int. Ed.* **2017**, *56*, 122–126.

43. Nanda M. Synthesis and Comparative Biophysical Studies of Peptides Derived From 3- and 4-Substituted Prolines. PhD Thesis, University of Pune, April 2011.

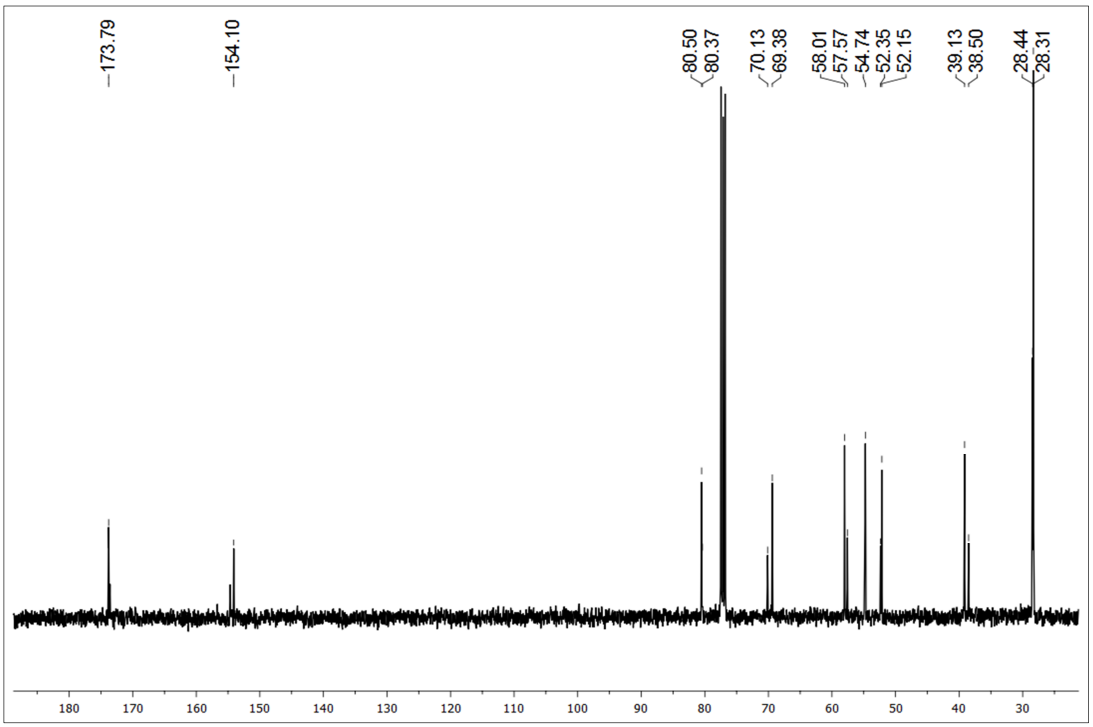
44. Merrifield, R. B. Solid Phase Peptide Synthesis. I. The Synthesis of a Tetrapeptide *J. Am. Chem. Soc.* **1963**, *85*, 2149- 2154.

2.8 Appendix A: Characterization Data of Synthesized Compounds and Peptides

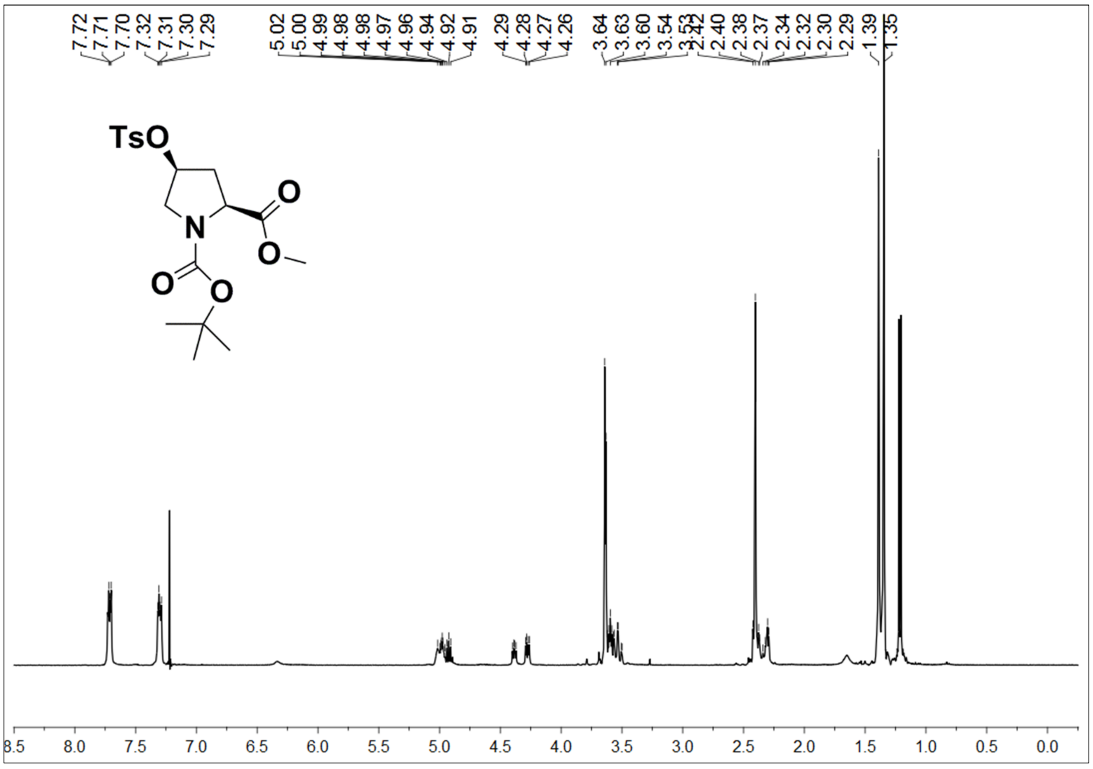
^{1}H NMR of Compound **2**



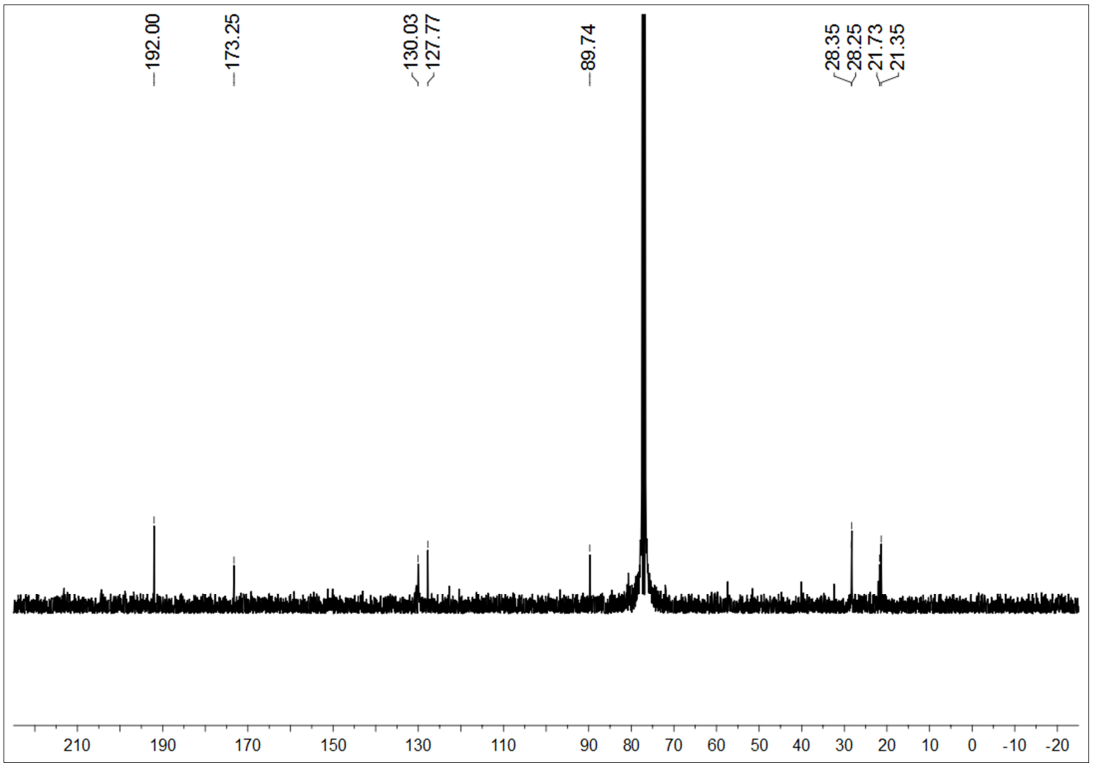
^{13}C NMR of Compound **2**



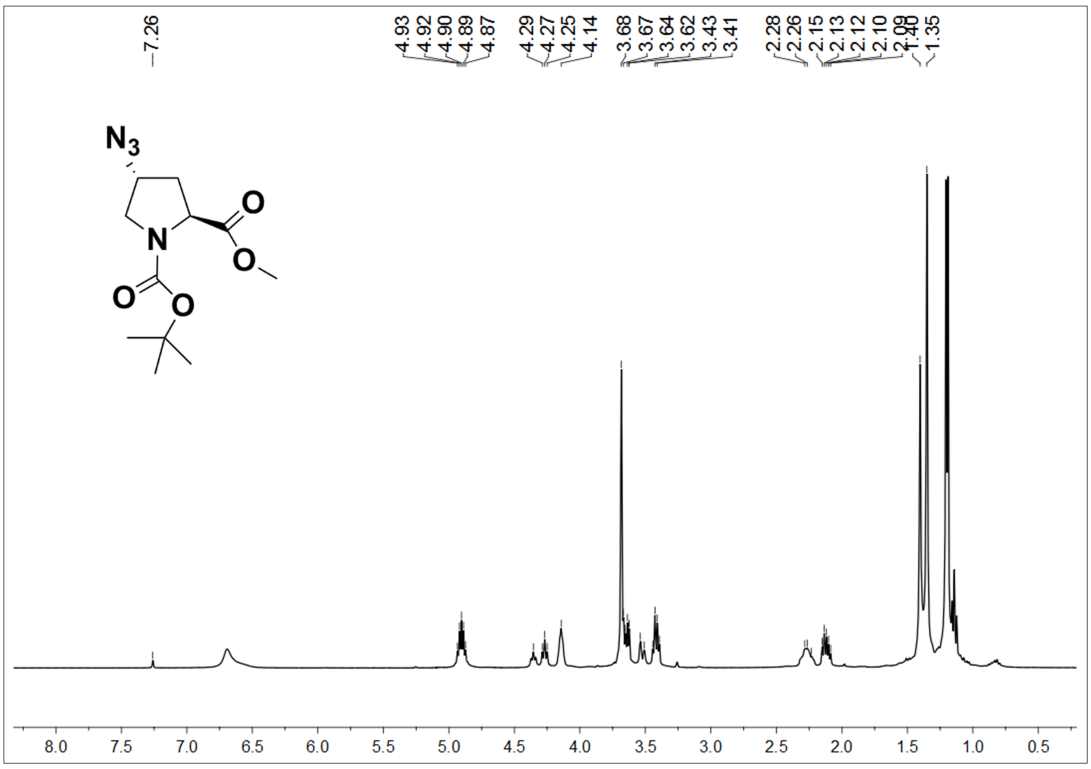
^{1}H NMR of Compound **3**



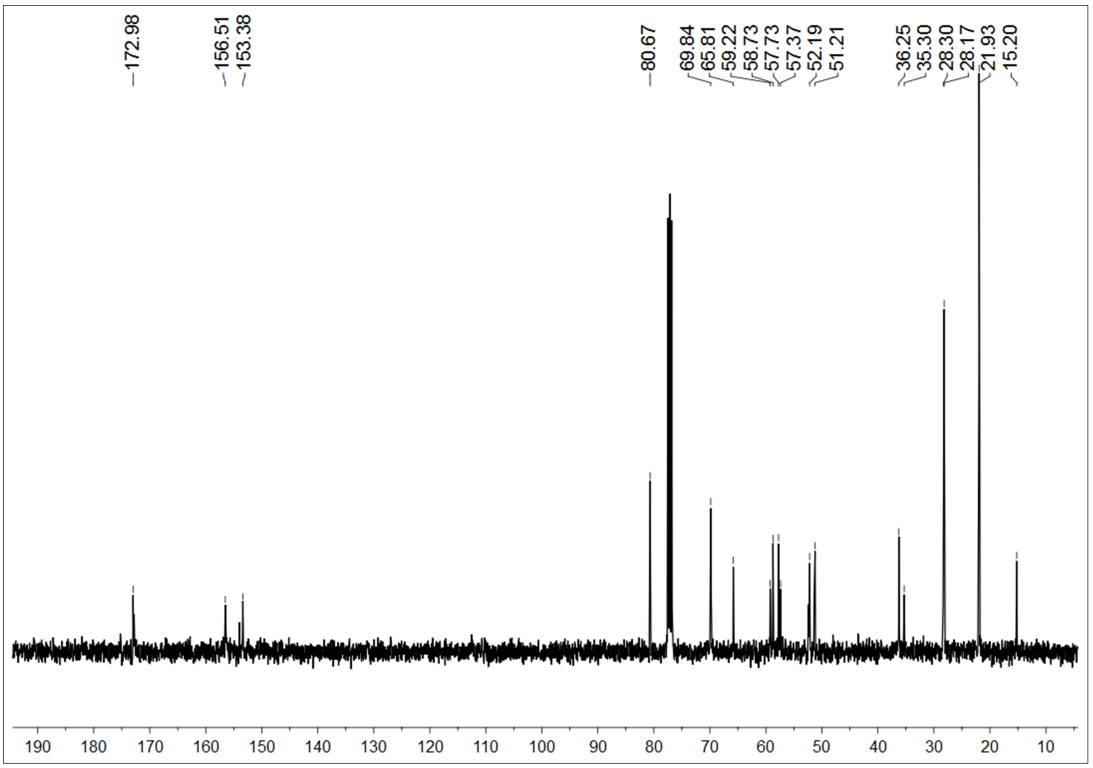
^{13}C NMR of Compound **3**



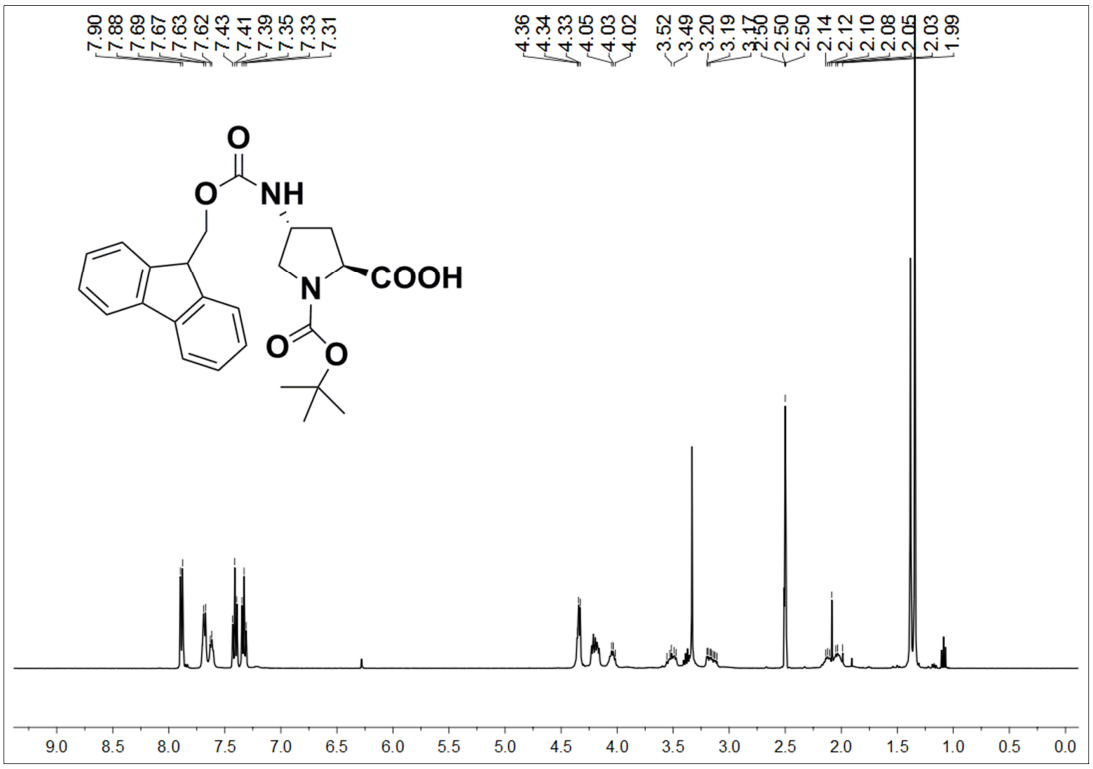
^{1}H NMR of Compound **4**



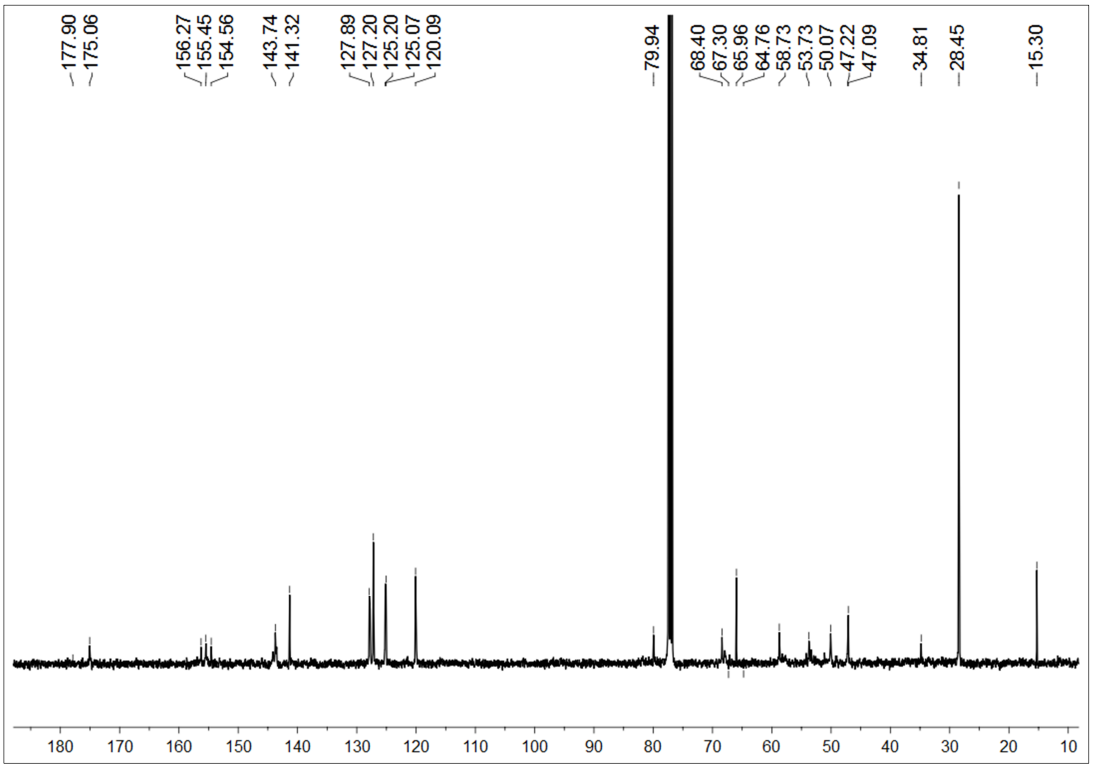
^{13}C NMR of Compound **4**



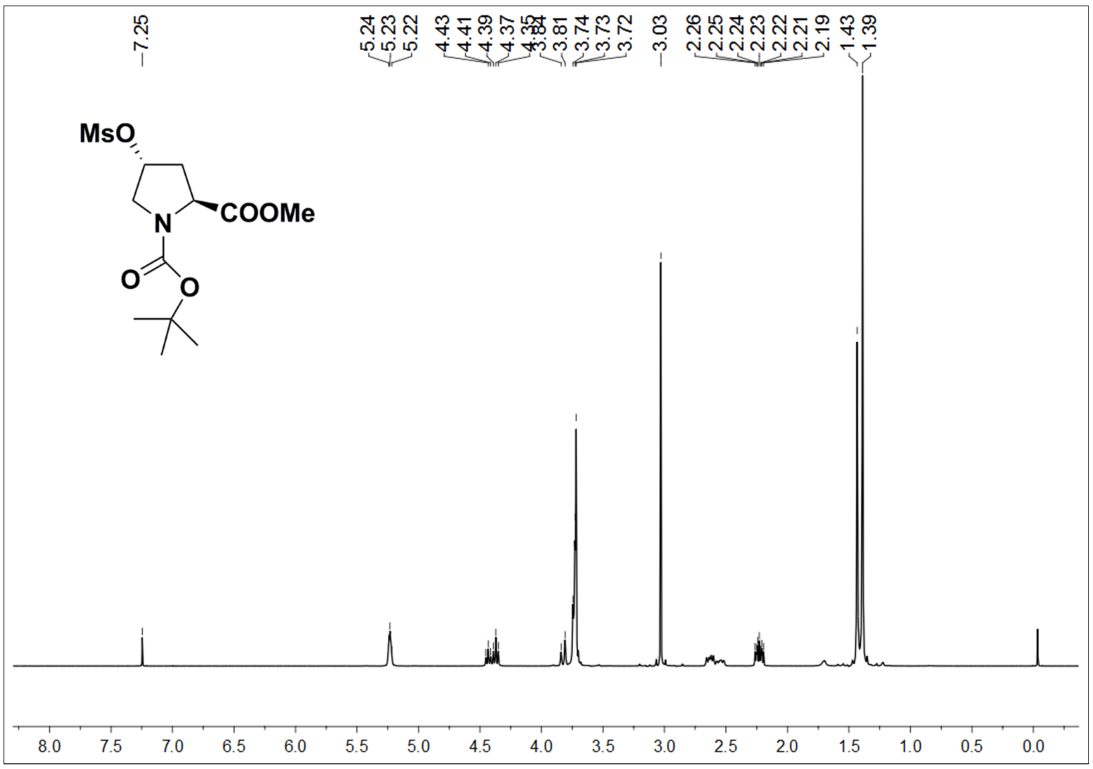
^{1}H NMR of Compound **7**



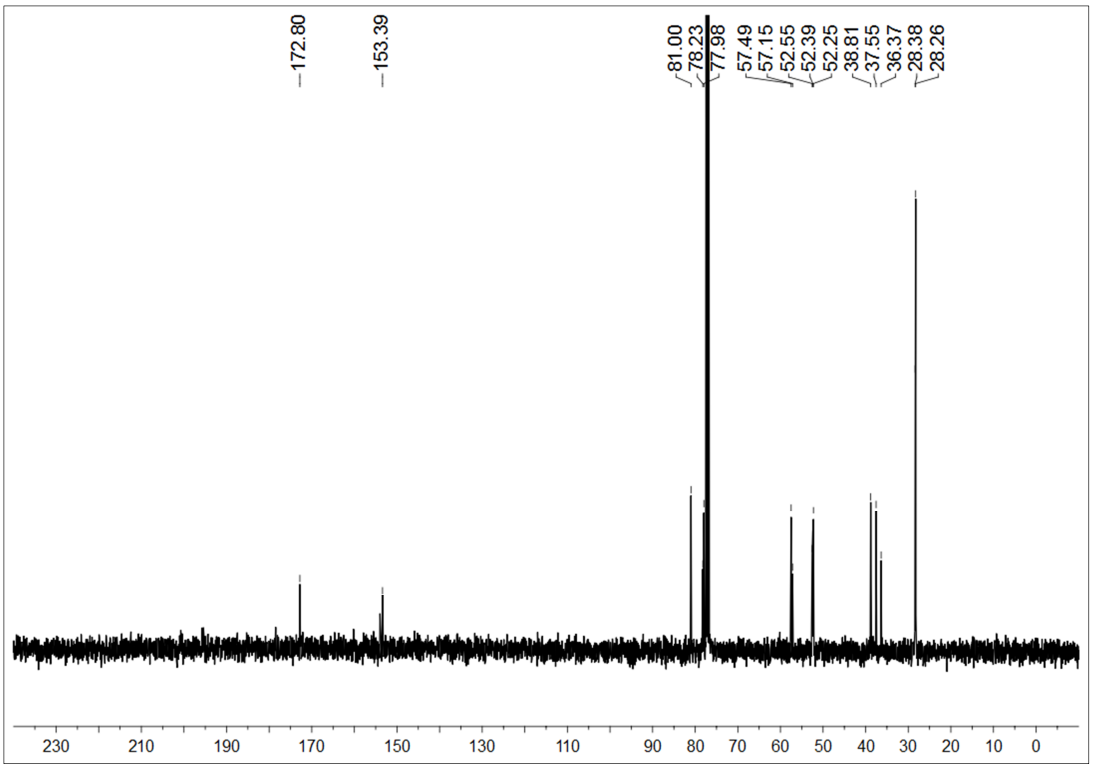
^{13}C NMR of Compound **7**



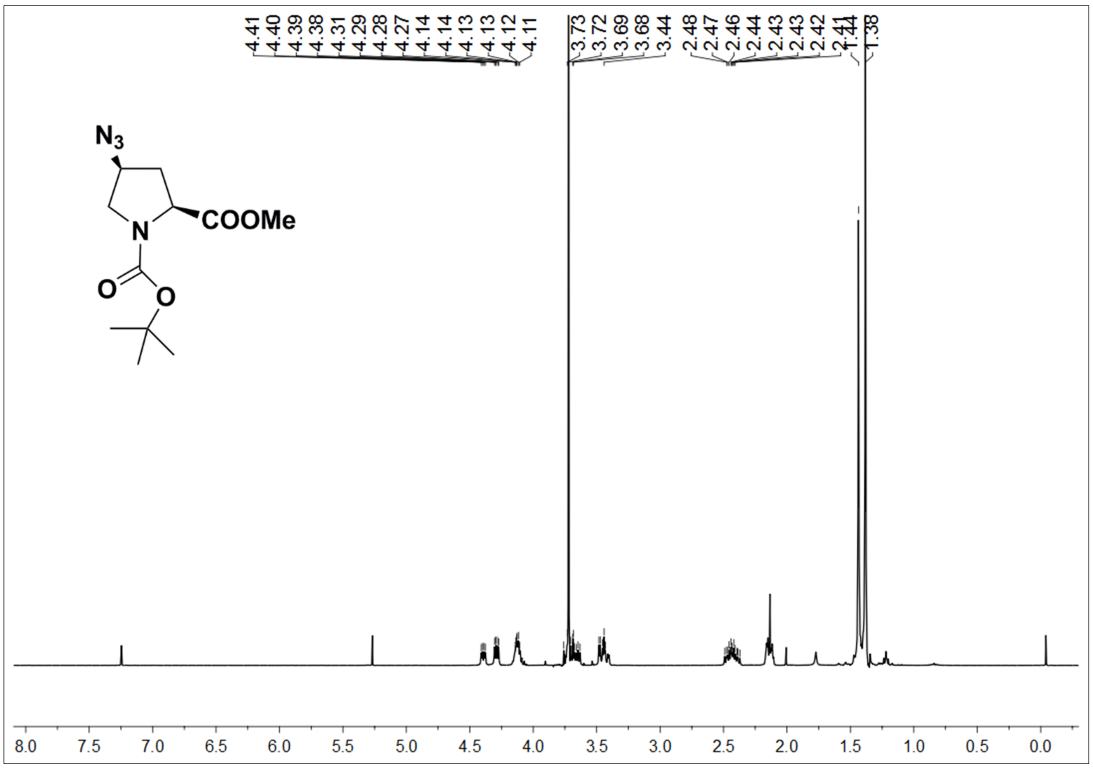
^{1}H NMR of Compound **8**



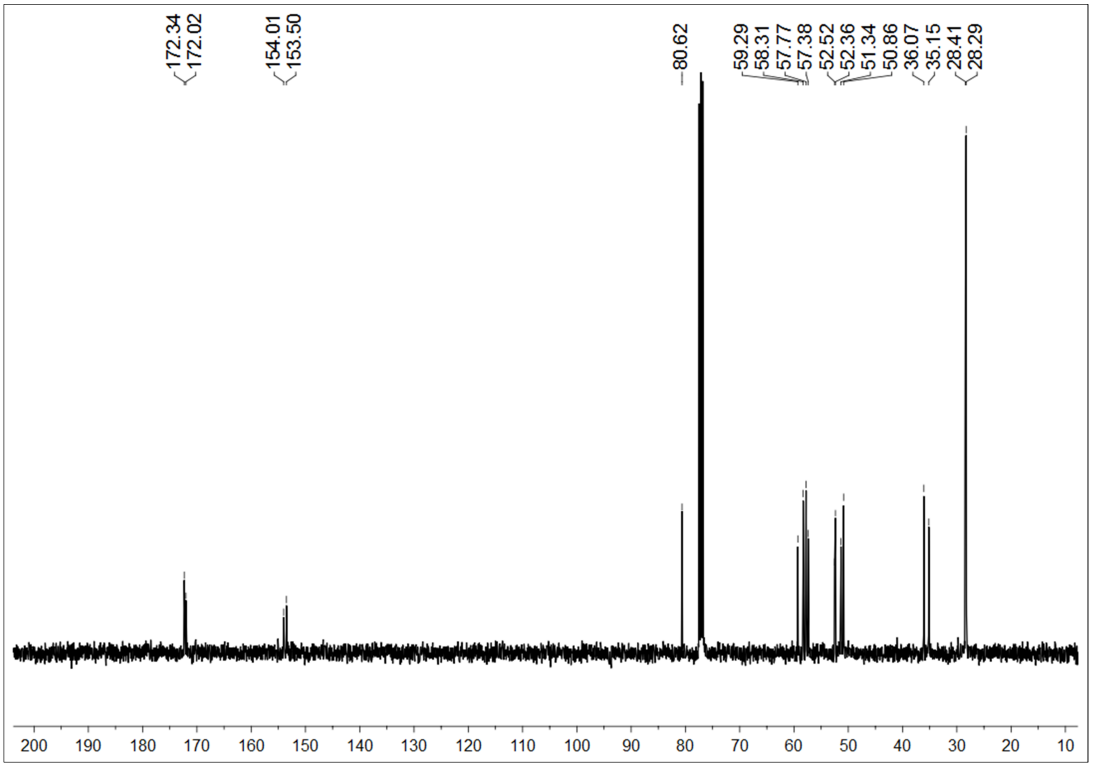
^{13}C NMR of Compound **8**



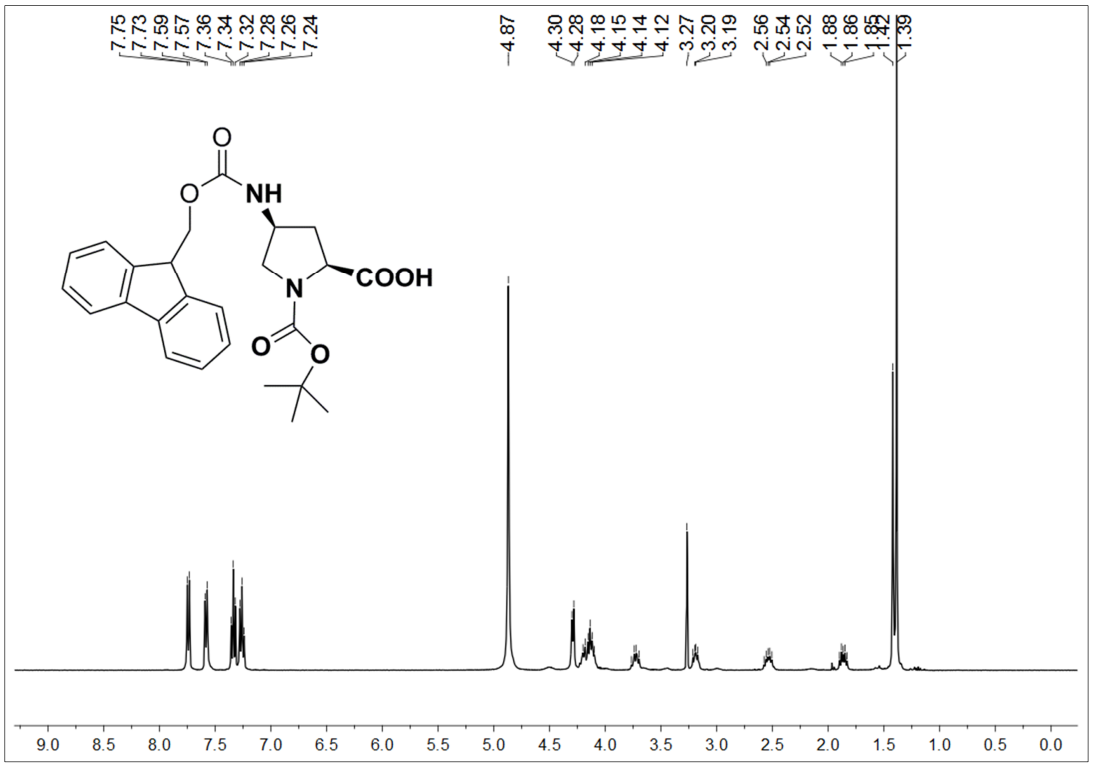
^{1}H NMR of Compound **9**



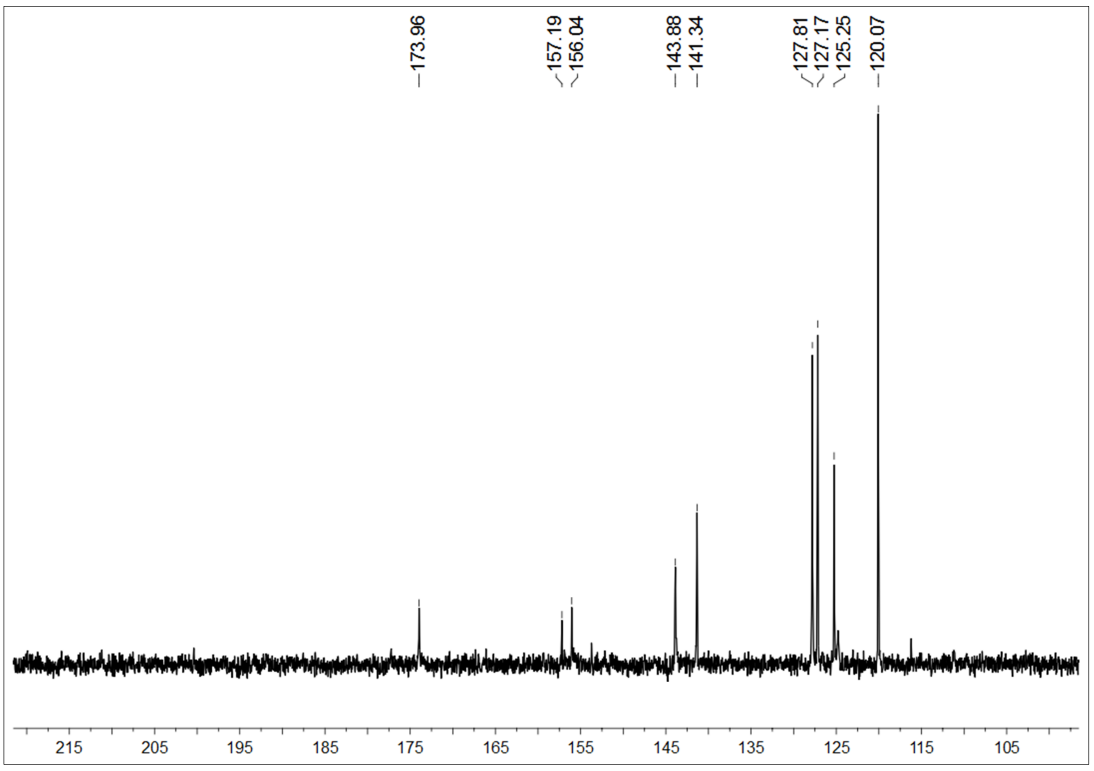
^{13}C NMR of Compound **9**



^{1}H NMR of Compound **12**

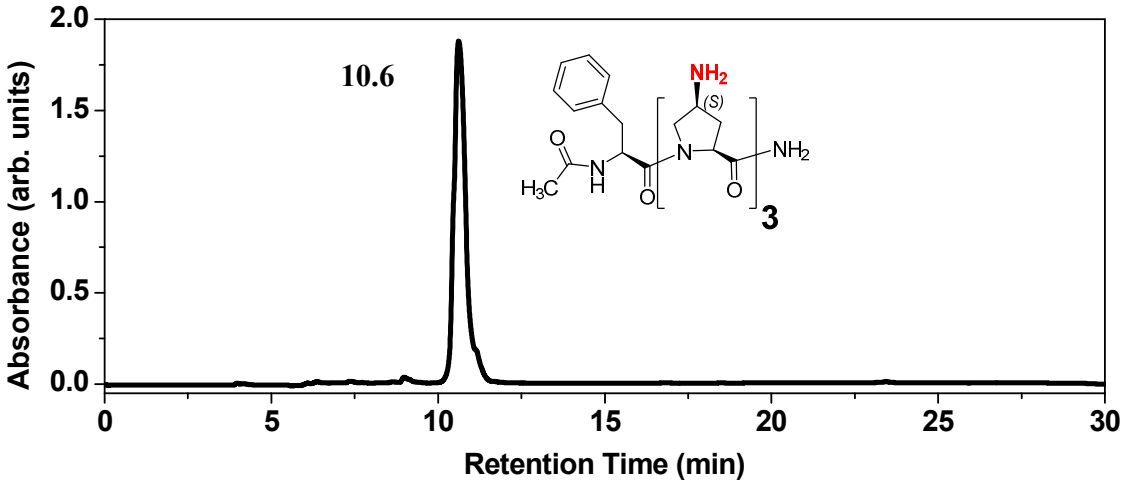


^{13}C NMR of Compound **12**

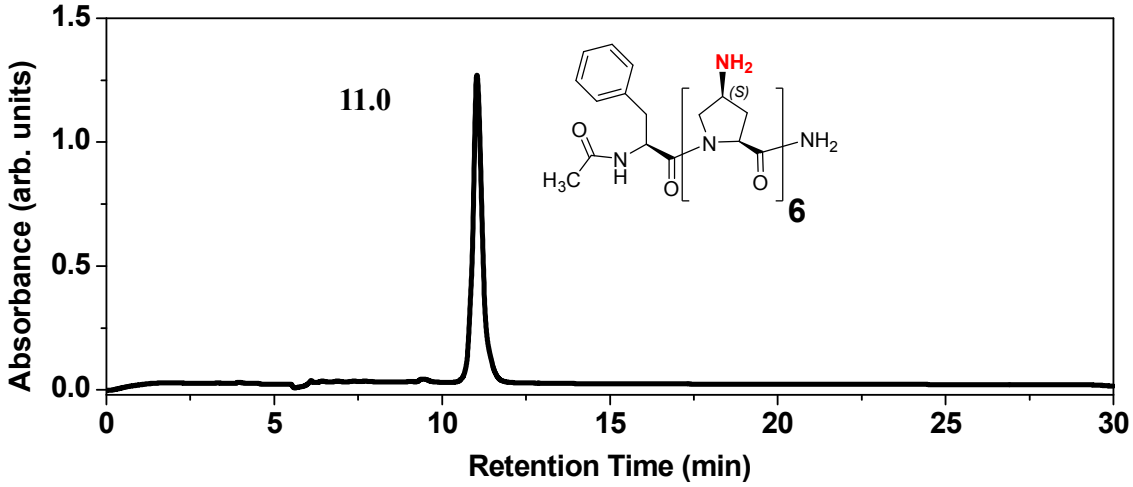


HPLC chromatograms of peptides

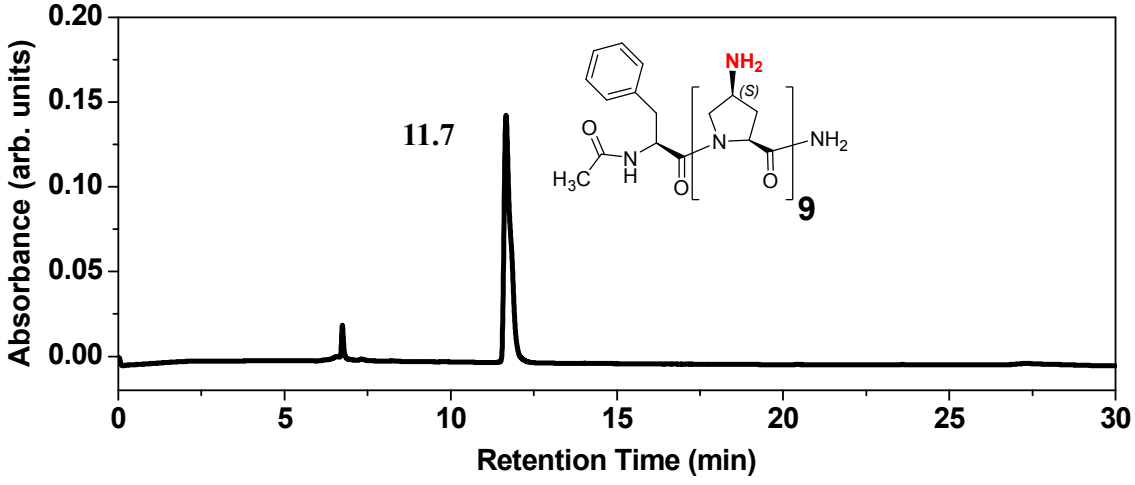
HPLC chromatogram of peptide **P1**



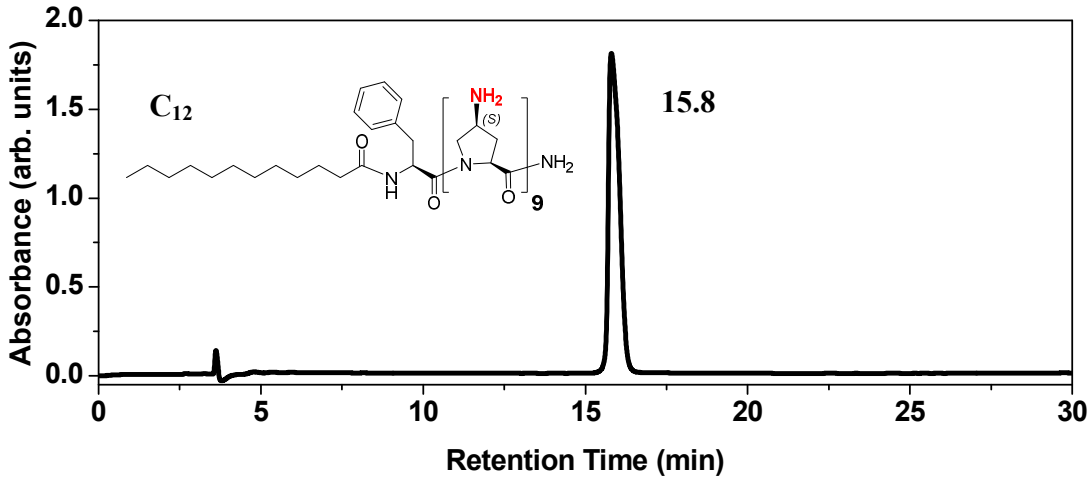
HPLC chromatogram of peptide **P2**



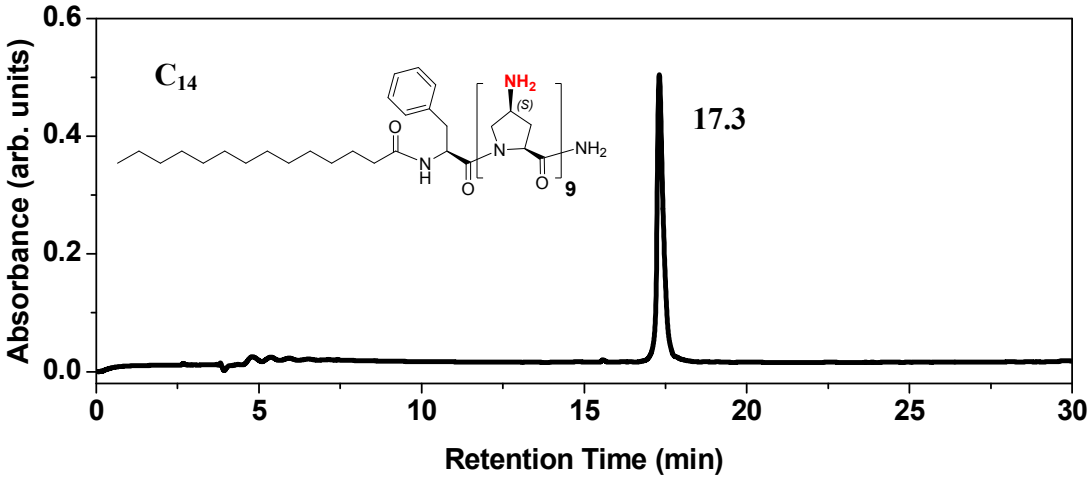
HPLC chromatogram of peptide **P3**



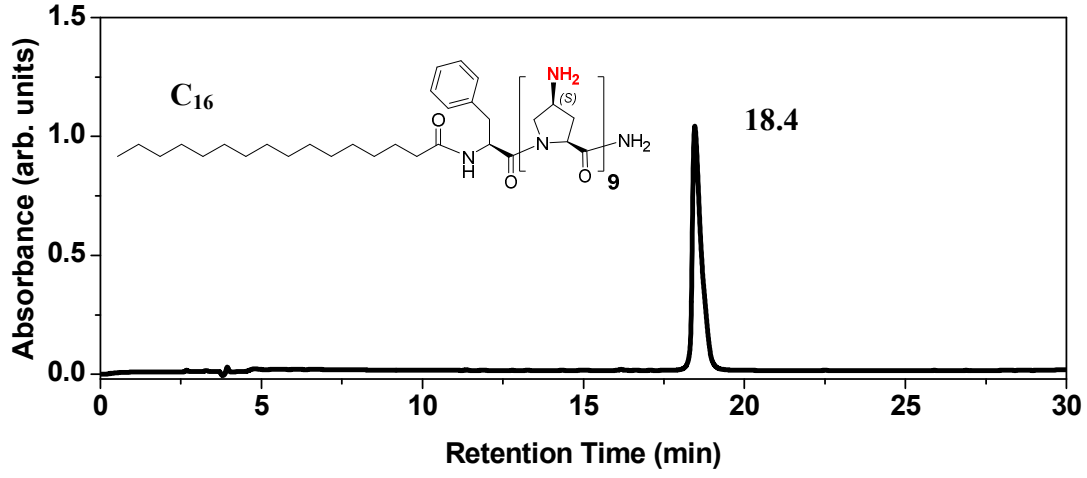
HPLC chromatogram of peptide **P4**



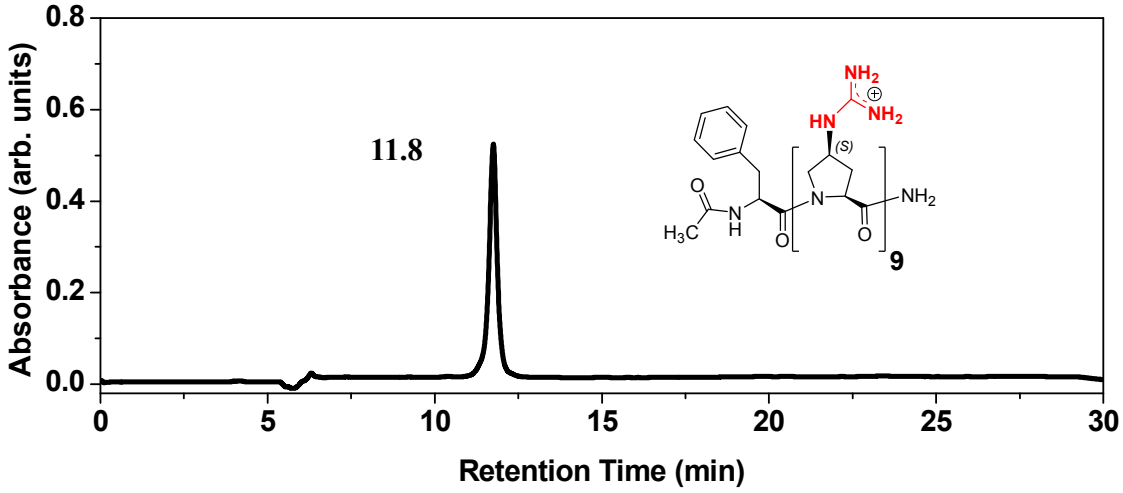
HPLC chromatogram of peptide **P5**



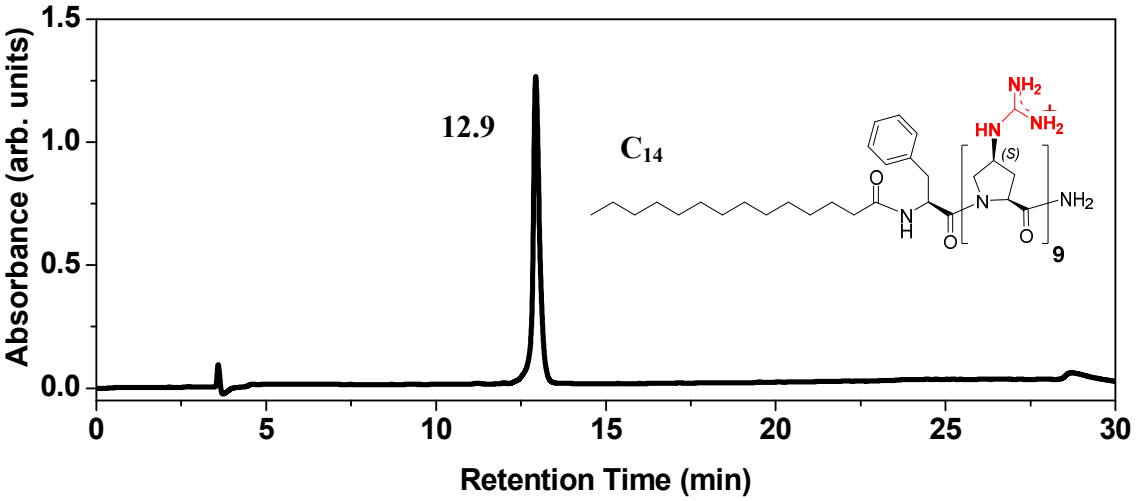
HPLC chromatogram of peptide **P6**



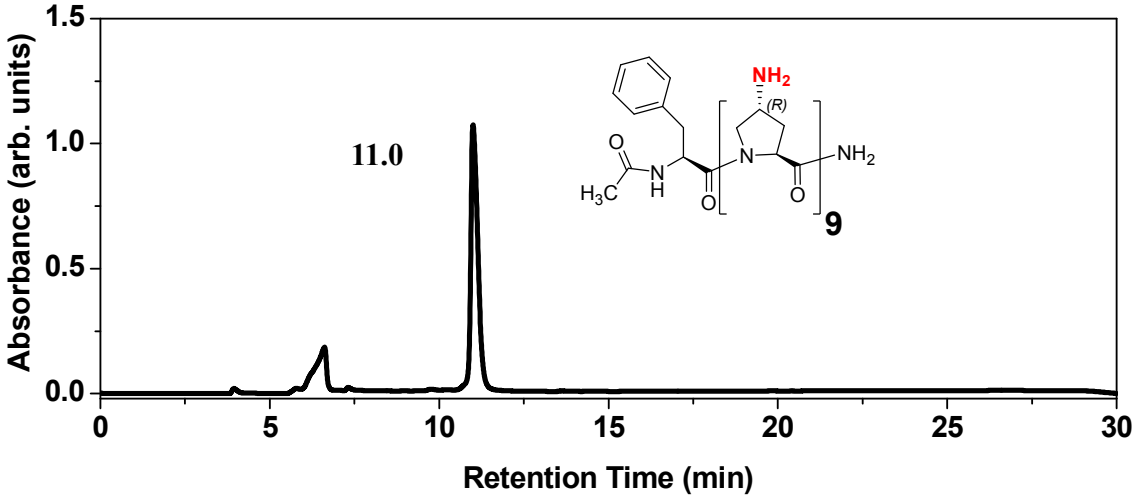
HPLC chromatogram of peptide **P7**



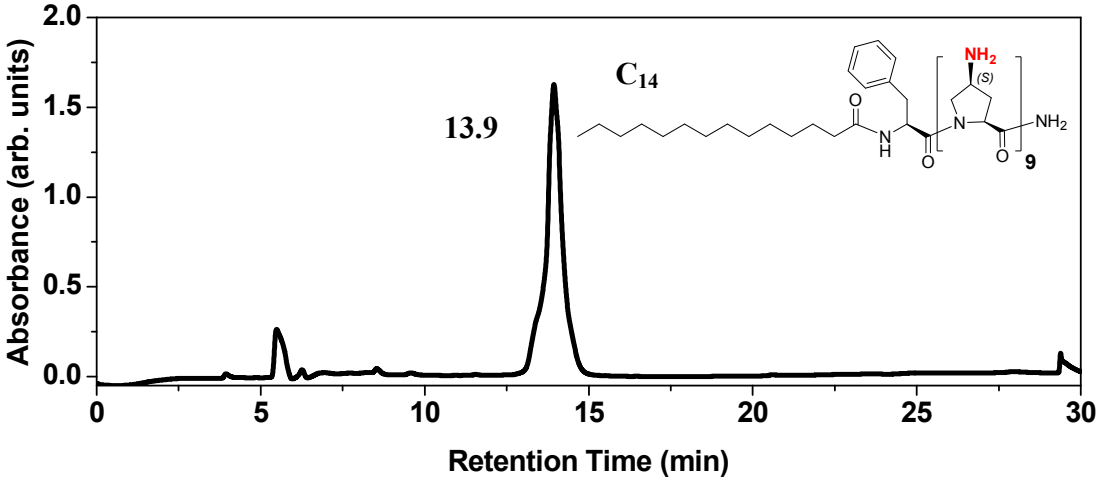
HPLC chromatogram of peptide **P8**



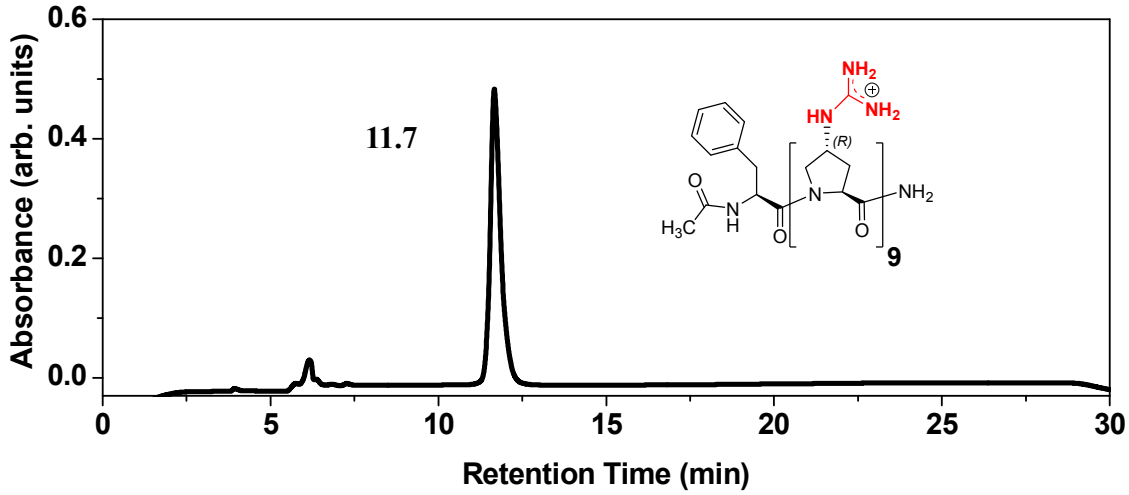
HPLC chromatogram of peptide **P9**



HPLC chromatogram of peptide **P10**

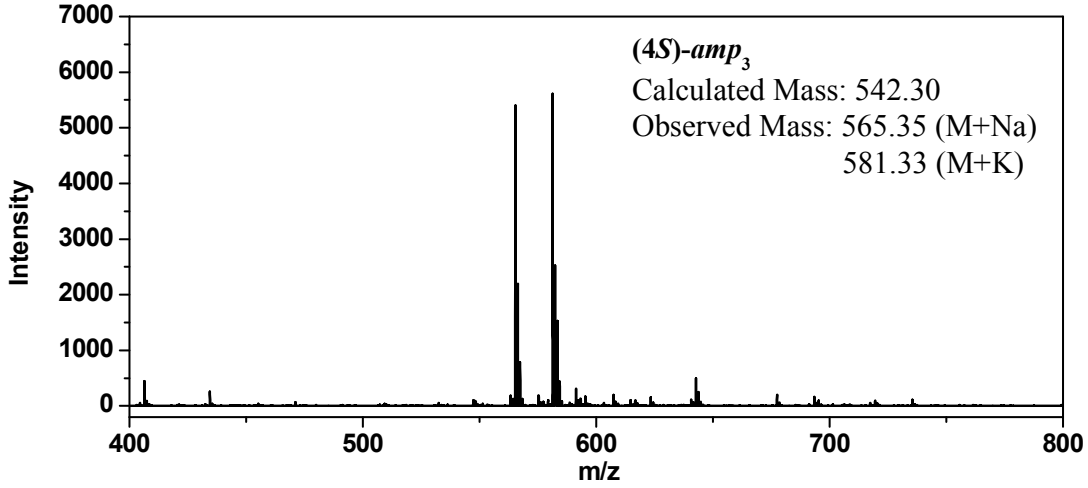


HPLC chromatogram of peptide **P11**

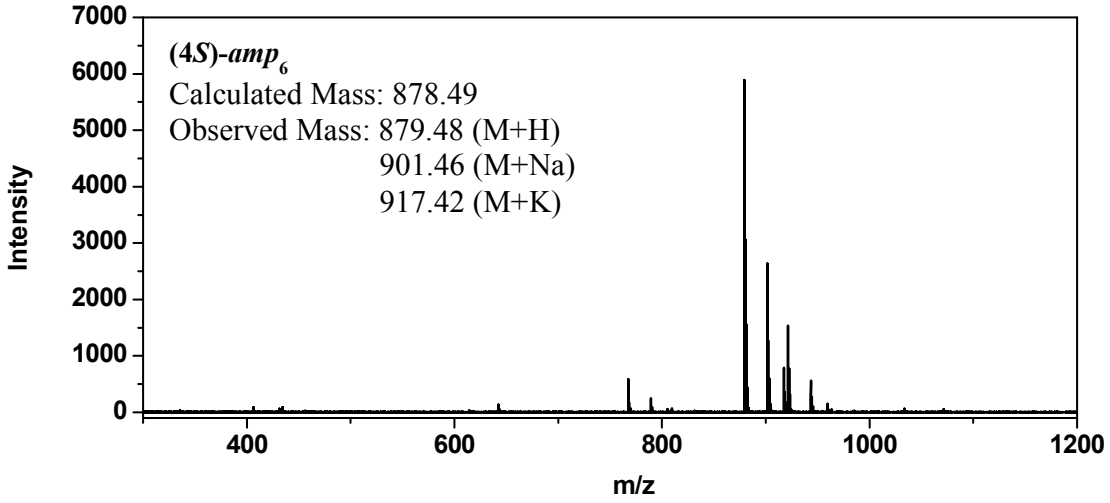


MALDI-TOF Spectra of Peptides

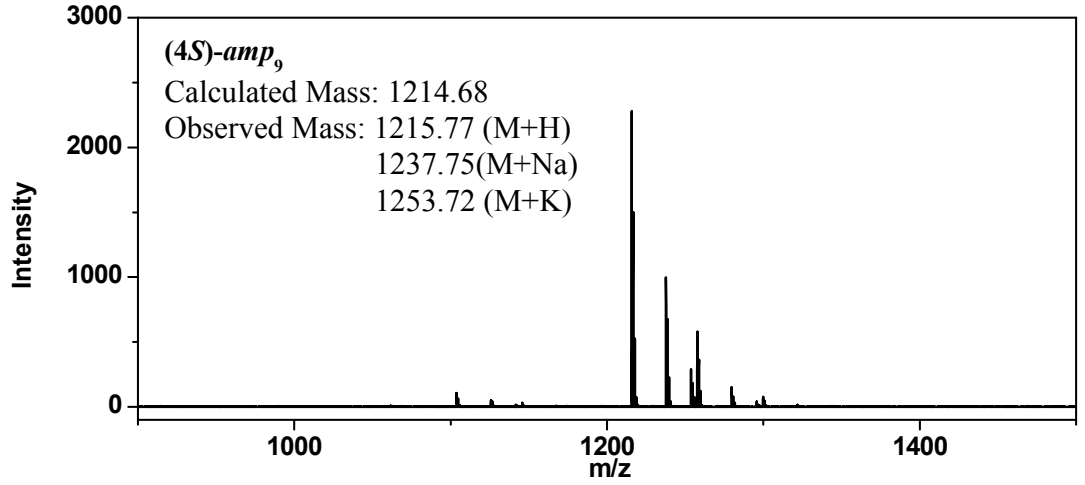
MALDI-TOF Spectrum of Peptide **P1**



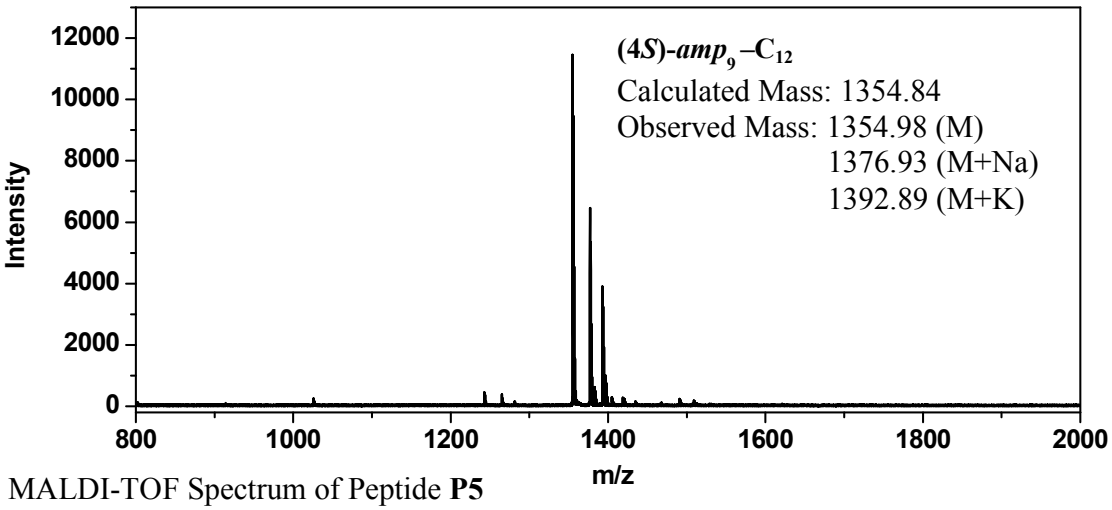
MALDI-TOF Spectrum of Peptide **P2**



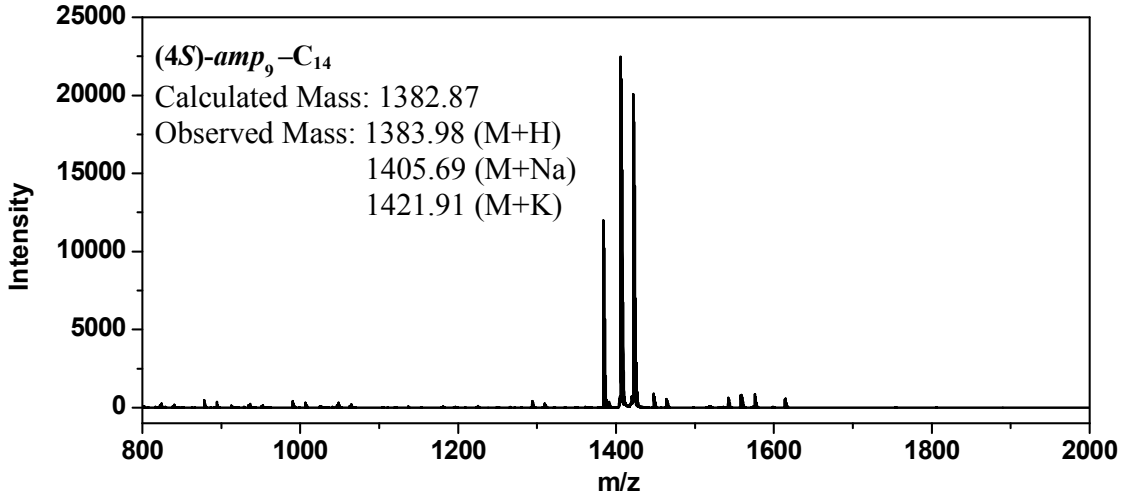
MALDI-TOF Spectrum of Peptide **P3**



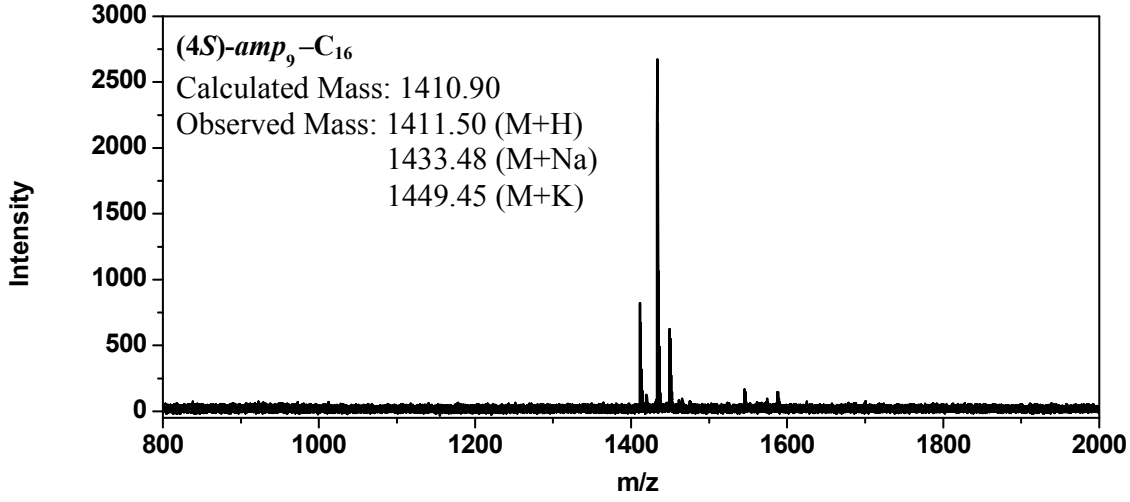
MALDI-TOF Spectrum of Peptide **P4**



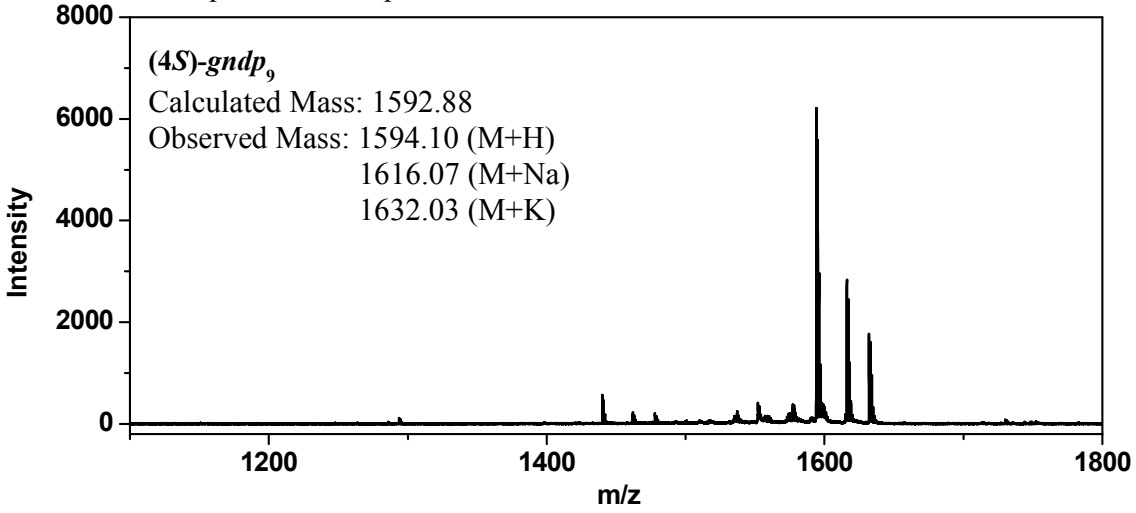
MALDI-TOF Spectrum of Peptide **P5**



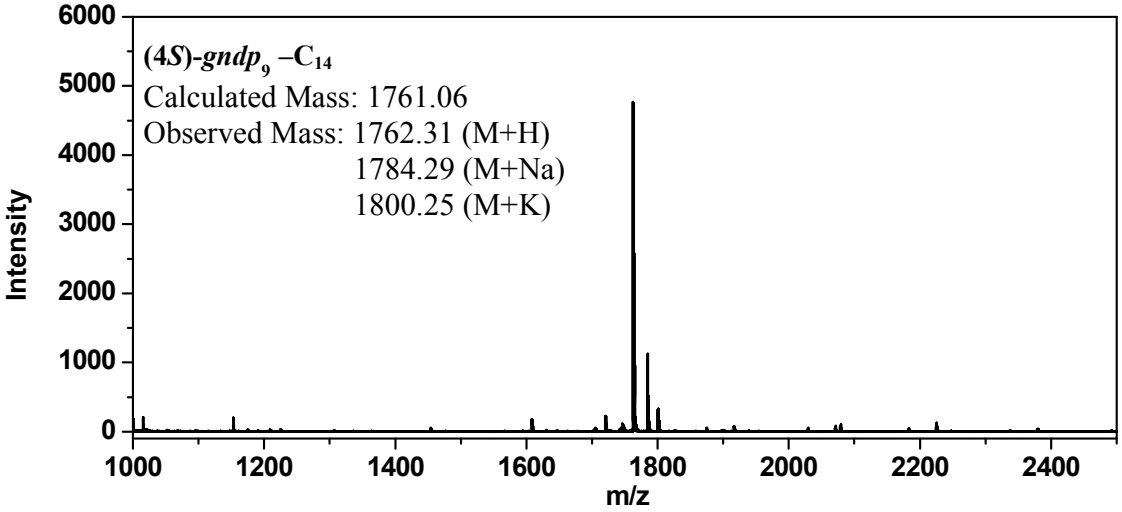
MALDI-TOF Spectrum of Peptide **P6**



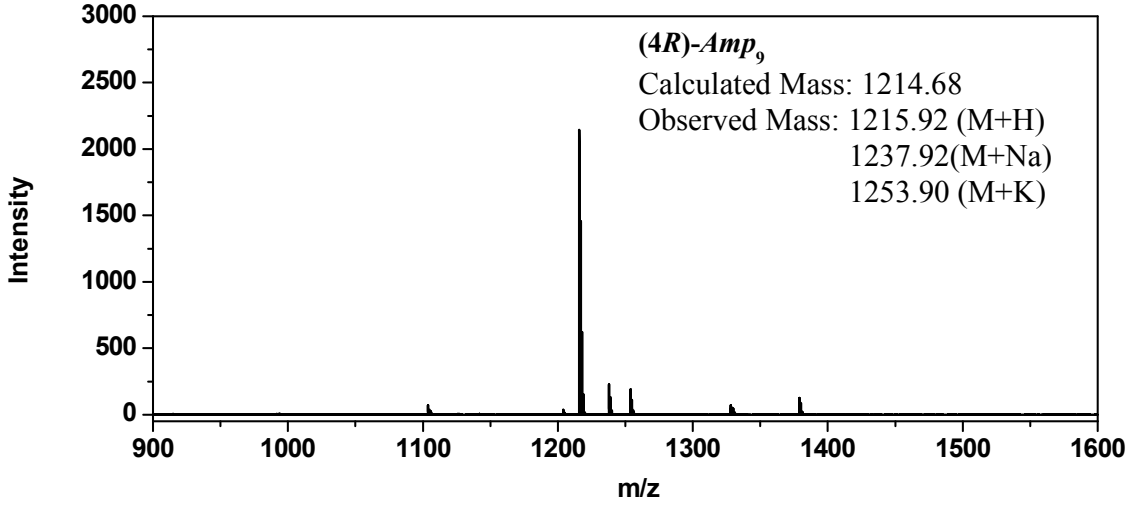
MALDI-TOF Spectrum of Peptide **P7**



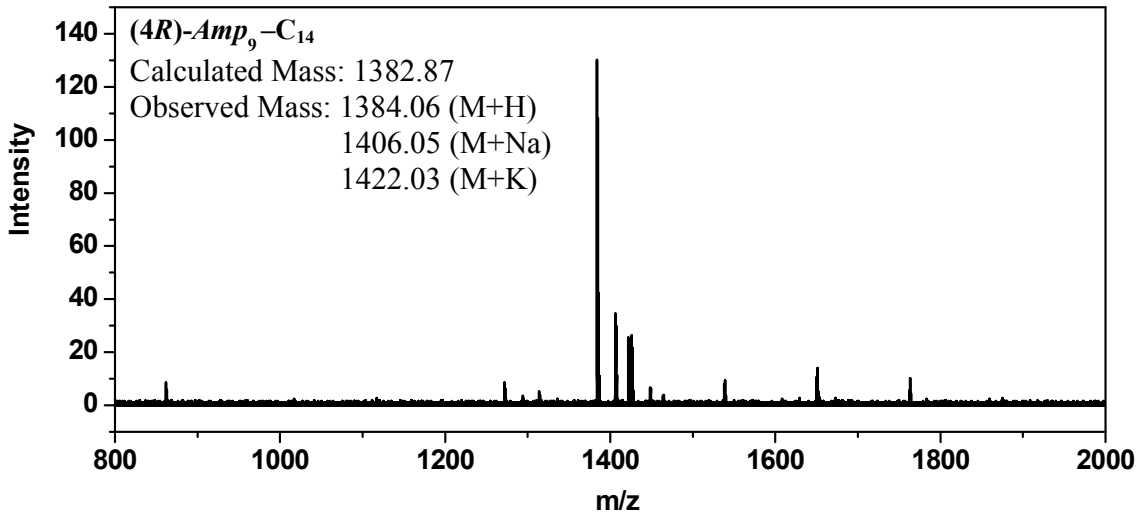
MALDI-TOF Spectrum of Peptide **P8**



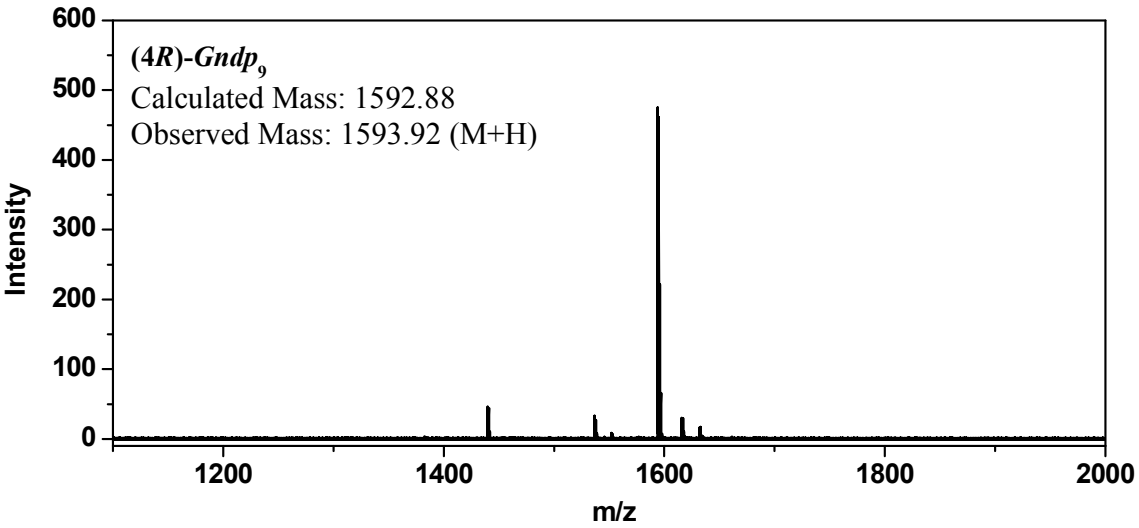
MALDI-TOF Spectrum of Peptide **P9**



MALDI-TOF Spectrum of Peptide **P10**



MALDI-TOF Spectrum of Peptide **P11**



Chapter 3

Biophysical Studies of 4(*R*/*S*)-Amino and Guanidino Proline Based Peptides

3.1 Introduction

In biomolecules, structure and function are inextricably linked to one another. Understanding the relationship between the two is one of the major goals, which would eventually lead to rational design of synthetic analogues of biomacromolecules with customized functional properties through engineered self-assembling abilities. For dynamic molecules like peptides, the conformational preference adopted by them depends not only on their chemical constitution, but also on various external factors such as solvent,[1-5] strength and composition of ions in the solution,[6] temperature, interactions with supramolecular structures like lipid membranes[7] and other biomolecules like polysaccharides,[8] and nucleic acids.[9] Utilization of any peptide motif for various purposes such as development of functional materials or design of therapeutic drugs therefore warrants a thorough investigation into its conformational properties and how it is affected by various conditions and external agents.

3.2 Objectives

The homo-oligomeric peptides with repeating residues of (4*S*)-*amp* tend to confer unusual conformational properties depending on the solvent.[10-12] Specifically, the shift in the conformational preference of these peptides from the typical PP-II structure to β conformation was studied further in this chapter. In order to control this phenomenon and utilize it, it is imperative to understand the intrinsic properties of the substitution and the polyproline backbone that facilitate this transition. It can also be useful to identify external agents that act as modulators of the conformation of the peptide by interacting with the substitution of the peptide backbone to gain better control over the process.

In this chapter, conformational properties of C4(*S*)-NH_2 substituted aminoprolyl polypeptides (**P1**-**P6**), and guanidinylprolyl polypeptides (**P7**-**P8**) were studied using CD spectroscopy and compared with their C4(*R*)-substituted counterparts to elucidate stereospecific effects on the secondary structure adopted by the polyproline peptides.

The specific objectives of this chapter include the following:

- Study the effect of peptide length on the propensity of the C4(*S*)-NH_2 substituted aminoprolyl polypeptides to adopt different conformations in different solvents.
- Examine the effect of temperature and micellar environments on the conformation of the peptides.
- Investigate the effects of lipidation on the solvent dependent conformational properties of the aminoprolyl polypeptides.
- Interrogate the conformational preference of the guanidinylprolyl polypeptides (**P7**-**P8**) and lipidated guanidinylprolyl polypeptide **P11** in different solvents and conditions.
- Study the interaction between cationic guanidinylprolyl polypeptides with polyanionic single stranded and double stranded DNA.

3.3 Results and Discussion

3.3.1 Aminoprolyl Polypeptides

In an attempt to gain insight into how substitutions at C4 position of repeating proline residues in polyproline peptides affect their conformational preference, the CD spectral properties of the aminoprolyl polypeptides, **P1**-**P6** were monitored under different conditions. The effects of peptide length, temperature, solvents, and different conditions such as micellar

environments (CTAB, SDS, and oil-in-water microemulsions) on the conformation of the peptides are studied.

3.3.1a *Effect of Length on (4S)-amp$_n$*

Circular dichroism spectra were recorded for peptides (4*S*)-*amp*$_n$ **P1**–**P3** containing three, six and nine residues of (4*S*)-*amp* in aqueous buffer (10 mM phosphate buffer containing 10 mM NaCl) and 2,2,2-Trifluoroethanol (TFE). The results show that all the peptides gave CD spectra with a positive band at 220 - 225 nm corresponding to n→π* transition, and a negative band around 200 - 205 nm corresponding to π→π* transition in the peptide bonds (Figure 3.1A, C), the signature characteristic of left-handed PP-II conformation.

In TFE, the shorter peptides (4*S*)-*amp*$_3$ (**P1**) and (4*S*)-*amp*$_6$ (**P2**), which contain 3 and 6 residues of (4*S*)-*amp* respectively also show β-sheet like CD spectra with a negative band around 220 nm and a positive band around 200 nm (Figure 3.1) similar to that exhibited by the longer peptide (4*S*)-*amp*$_9$ (**P3**). The magnitude of PP-II and β-sheet content in appropriate solvents was found to be significantly affected by the peptide length, as evident from the comparison of the mean residue ellipticity (MRE) of the peptides (Figure 3.2A).

In buffer, the mean residue ellipticity (MRE) of the positive band at 222 nm used as an indicator of PP-II content,[13] decreased 3.8 fold with a shift in the position of the band from 222 nm to 227 nm to the longer wavelengths as peptide length increases from 3 to 9 residues (Figure 3.2C). In TFE, the MRE magnitude of the –ve band at ~220 nm showed a significant 7.8-fold increase when the number of aminoprolines was increased from 3 to 9.

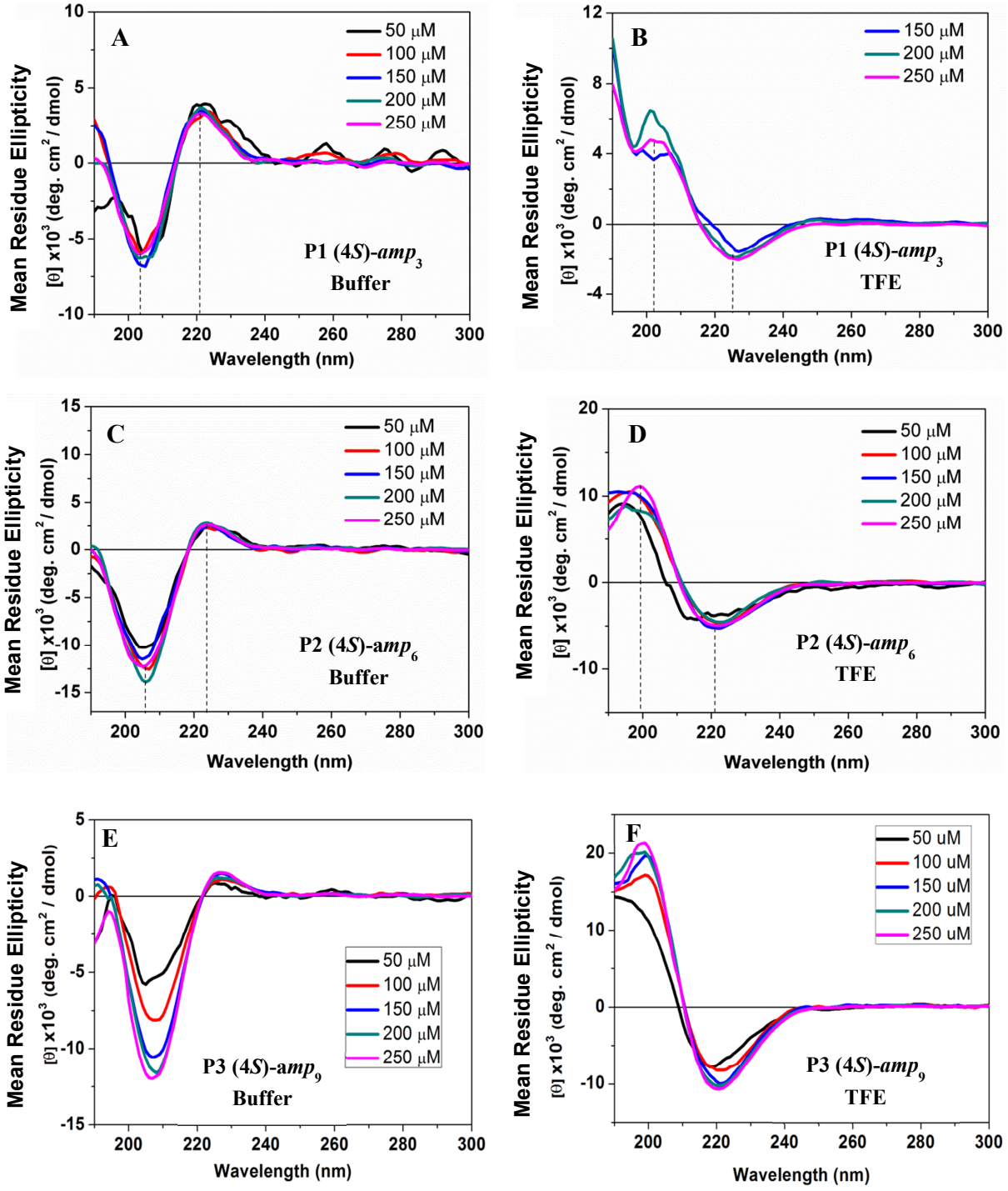


Figure 3.1: Concentration dependent CD spectra of peptides: **P1**, (4*S*)-amp_3 in 10 mM phosphate buffer (pH 7.0) with 10 mM NaCl (A) and in TFE; (B), peptide **P2,** (4*S*)-amp_6 in phosphate buffer (C) and in TFE (D), and peptide **P3,** (4*S*)-amp_9 in phosphate buffer (E) and in TFE (F).

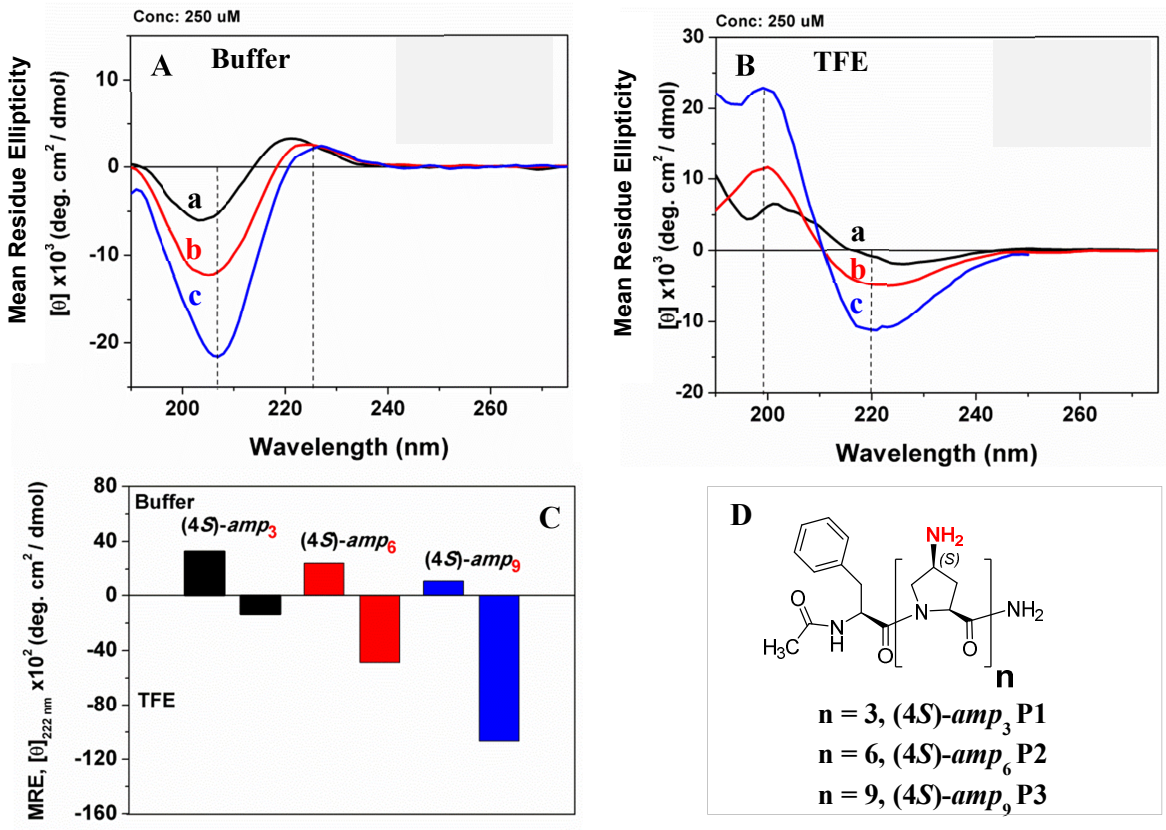


Figure 3.2: Effect of peptide length on the conformation for the peptides. CD spectra of 250 µM solution of peptides (4*S*)-*amp*$_3$ (**P1**) (trace **a**), (4*S*)-*amp*$_6$ (**P2**) (trace **b**), (4*S*)-*amp*$_9$ (**P3**) (trace **c**) in 10 mM phosphate buffer, pH 7.0 with 10 mM NaCl (A) and in TFE (B). C) Comparison of the magnitude of mean residue ellipticity (MRE) of the peptides at 222 nm in buffer and TFE. D) Peptides used in this study.

The +ve CD band at 220 – 230 nm, corresponds to PP-II and a –ve band around 210 - 220 nm indicates beta sheet.[14] The increase in the intensities of CD signals from n→π* transitions at 220 nm is accompanied by a concomitant increase in the CD signals at 200 nm arising from π→π* transitions. This suggests the co-operative increase in the propensity of the peptides to adopt β-like conformations in TFE, as the number of residues of (4*S*)-*amp* increase from 3 to 9. A decrease in the PP-II content was apparent from the CD spectra of the peptides in buffer, the peptide still shows typical signature of the PP-II structure in the presence of water (Figure 3.2C).

3.3.1b *Effect of Temperature*

The thermal stability of the β-sheet like conformation adopted the aminoprolyl polypeptide, (4*S*)-*amp*$_9$ (**P3**) in TFE was studied using temperature dependent CD spectroscopy. The circular dichroism spectrum of a TFE solution of the peptide (200 μM) was recorded at a range of temperatures from -5°C to 65°C (Figure 3.3C). The change in the CD signal at the characteristic positive and negative bands at 220 nm and 195 nm respectively were monitored. This was compared with those obtained from similar experiments carried out with shorter peptides (4*S*)-*amp*$_3$ (**P1**) and (4*S*)-*amp*$_6$ (**P2**) (Figure 3.3A, B).

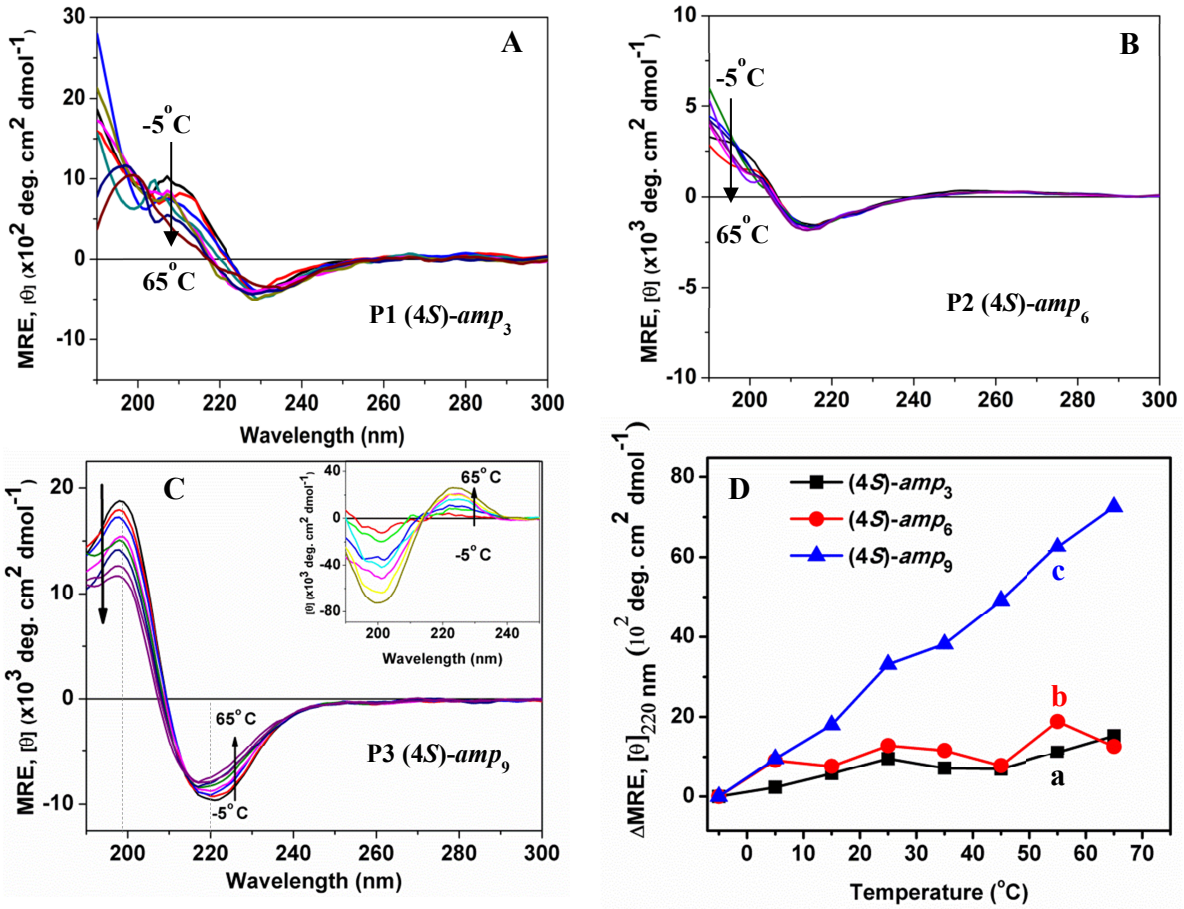


Figure 3.3: Temperature dependent CD spectra of 250 μM solution of the peptides (4*S*)-*amp*$_3$ (**P1**) (A), (4*S*)-*amp*$_6$ (**P2**) (B), and (4*S*)-*amp*$_9$ (**P3**) (C) in TFE. Inset in (C) is differential CD spectra showing formation of PP-II. D) Change in the magnitude of MRE at 220 nm with temperature for peptides (4*S*)-*amp*$_3$ (**P1**) (trace **a,** ■), (4*S*)-*amp*$_6$ (**P2**) (trace **b,** ●), (4*S*)-*amp*$_9$ (**P3**) (trace **c** ▲).

Peptide (4*S*)-amp_9 (**P3**) showed a temperature dependent decrease in the magnitudes of both the +ve band at 198 nm, and the –ve band at 220 nm as the temperature of the solution was gradually increased from an initial temperature of -5^oC to a final temperature of 65^oC. An isodichroic point at 212 nm was observed, which indicated the occurrence of a transition between two conformational states. Differential CD spectra profiles calculated by subtracting the CD spectra measured at every temperature (t) from that recorded at the initial temperature -5 ^oC (t_0) is shown as inset in Figure 3.3C.

This revealed an emergence of PP-II like CD signature with increasing temperature indicating a thermal induced shift of β conformation to PP-II form in the TFE solution. A linear decrease in the intensities of the two characteristic bands of β structure was seen across the temperature range for peptide (4*S*)-amp_9 (**P3**) (Figure 3.3D). In case of peptides (4*S*)-amp_3 (**P1**) and (4*S*)-amp_6 (**P2**), the apparent change in the CD signature with temperature was minimal or negligible (Figure 3.3D). These observations point to the significant role of length of the peptides in inducing intermolecular interactions between the peptides to stabilize β-like conformation.

3.3.1c *Effect of Solvents*

Polyproline peptides generally adopt either PP-II or PP-I structures depending on the solvent. In aqueous solvents, polyproline peptides prefer left handed PP-II helix and in alcoholic solvents, they adopt a right handed PP-I helix.[15] In case of C4(*S*)-NH_2 substituted aminoprolyl polypeptides, solvent sensitivity found was however, between the PP-II helix (in water) and β-like structure (in TFE), and not PP-I form. In order to identify solvents other than TFE that could alter the conformational preference of aminoprolyl polypeptides, CD spectra of solutions

(100 μM) of peptides (4*S*)-*amp*$_3$ (**P1**) and (4*S*)-*amp*$_9$ (**P3**) were recorded in a variety of solvents, namely, water, methanol, ethanol, propanol, isopropanol, acetonitrile and TFE (Figure 3.4).

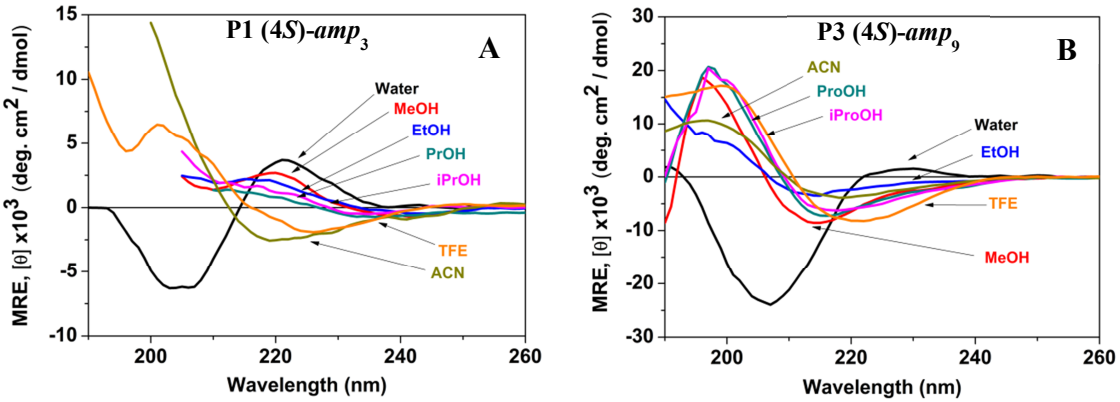


Figure 3.4: Effect of solvent on conformation of peptides **P1** (4*S*)-*amp*$_3$ (A) and **P3** (4*S*)-*amp*$_9$ (B)

The results of this study showed that while in water, both the peptides (4*S*)-*amp*$_3$ (**P1**) and (4*S*)-*amp*$_9$ (**P3**) adopted PP-II form, in other solvents, the PP-II is progressively destabilized as indicated by the decreasing magnitude of the positive 225 nm band. The shorter peptide **P1** with three aminoproline residues adopted β structure only in TFE and ACN. However, the longer peptide **P3** with nine residues of aminoproline preferred β-like conformation in all solvents other than water.

3.3.1d *SDS Induced PP-II to β Conformational Change*

Sodium dodecyl sulphate (SDS) is a common anionic surfactant with a critical micellar concentration of 8.2 mM at 25 ^{o}C in water.[16] SDS is commonly used as a detergent and its micelles act as simple membrane model.[17] The effect of SDS on the conformation of (4*S*)-*amp*$_9$ (**P3**) was therefore studied to check whether a membrane-like environment stimulates a conformational change in the cationic polyprolyl peptides, similar to the one induced by TFE. Circular dichroism spectra of an aqueous solution of the peptide (4*S*)-*amp*$_9$ (**P3,** 100 μM) in

variable concentrations of SDS (0.1 μM to 0.1 M) was recorded (Figure 3.5). The changes in the spectral signatures corresponding to characteristic conformational changes were monitored. The conformation of the peptide **P3** was found to be influenced by the concentration of SDS. At concentrations below 1 mM, the conformation of the peptide showed hardly any change in water (Figure 3.5A, trace a-e).

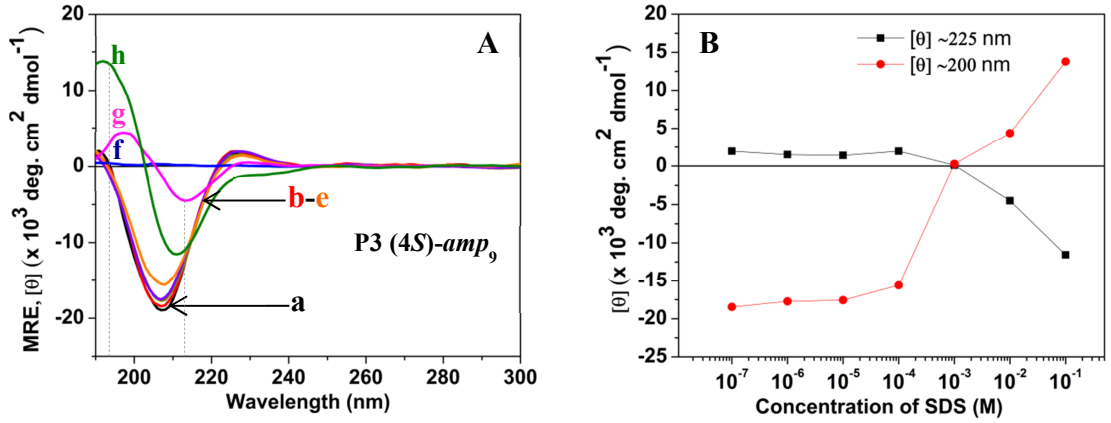


Figure 3.5: SDS induced conformational changes in peptide (4*S*)-*amp*$_9$ (**P3**). A) CD spectra of the peptide **P3** (100 μM) in the presence of different concentrations of SDS: 0 M (trace **a**); 0.1 μM SDS (trace **b**); 1.0 μM SDS (trace **c**); 10 μM SDS (trace **d**); 100 μM SDS (trace **e**); 1 mM SDS (trace **f**); 10 mM SDS (trace **g**); 100 mM SDS (trace **h**). B) Change in magnitude of CD bands at 225 nm (black squares) and 200 nm (red circles) with concentration of SDS.

Interestingly, at 1 mM, the CD signals of the peptide completely obliterated (Figure 3.5A trace f) and at higher concentrations, the peptide showed a β-sheet like CD signature (Figure 3.5A trace g), similar to the conformational transition induced by TFE. At 10 mM SDS, the positive n→π* transitions band at 220-225 nm associated with PPII content blue-shifted to about 5 nm along with an inversion of the cotton effect, leading to a negative band at 212 nm, suggesting the formation of β structure. A concomitant rise in the magnitude of the CD signal at 195 nm resulting in a positive band, characteristic of π→π* transitions of β structure was also observed. Increasing the concentration of SDS to 10 mM, the magnitude of the CD bands intensified further with shift of the bands to lower wavelengths and appearance of a broad

shoulder around 230 nm. The conformational transition was found to take place around the cmc of SDS, (8.2 mM) (Figure 3.5B), indicating the importance of micelle formation leading to β structure.

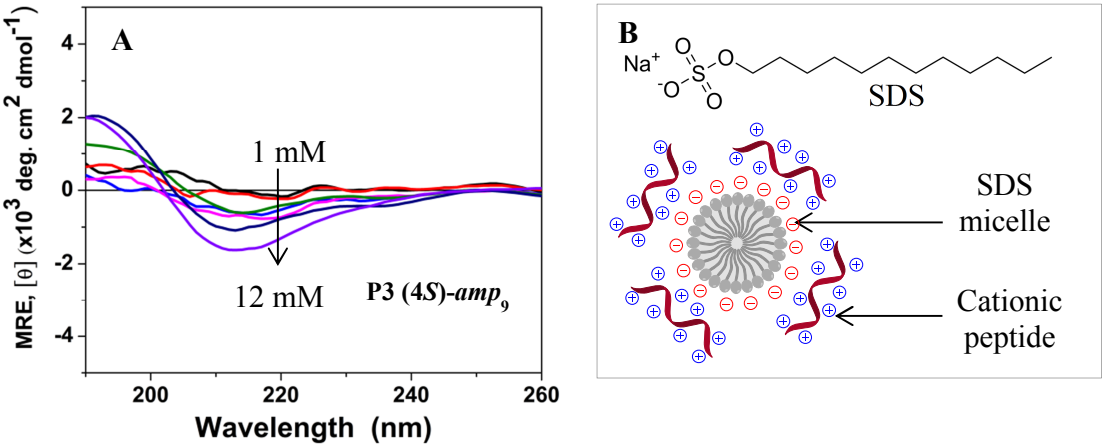


Figure 3.6: Conformational change observed around cmc of SDS. A) CD spectra of the peptide **P3** (100 μM) with increasing concentrations of SDS from 1 mM to 12 mM. B) Schematic depiction of interaction of SDS micelles with peptide.

The CD spectra of peptide **P3** was monitored in narrower range of the concentration of SDS from 1 mM to 12 mM. The peptide **P3** (100 μM) in water was titrated against 100 mM SDS solution. Figure 3.6A shows the CD spectra of the peptide solution with incremental (4 μL) addition of the aqueous SDS (0.1 M). As the concentration of the surfactant was increased beyond the cmc, a broad negative band emerged around ~215 nm from a featureless and nearly flat circular dichroic spectrum and a clear β-sheet like spectra was obtained at 10 - 12 mM concentration of SDS. From these results, it is apparent that SDS in the micellar form, is able to shift the conformation of **P3** from PP-II to β-like structure. At concentrations below cmc, only the PP-II form of the peptide is seen. This suggests that the changes observed in the peptide conformation around and above cmc of the detergent, is a direct result of interaction of the detergent with the peptide molecules.

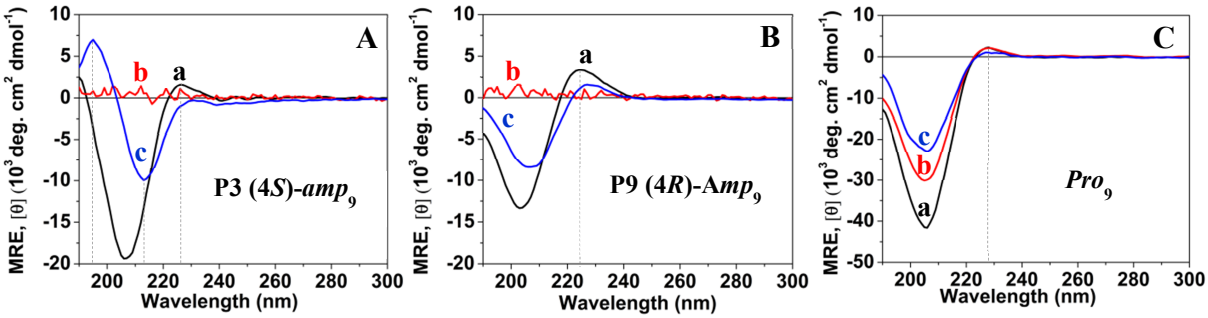


Figure 3.7: Effect of substituent on the conformational change induced by SDS. CD spectra of the 100 µM peptide (4*S*)-amp_9 (**P3**) (A), (4*R*)-Amp_9 (**P9**) (B), Pro_9 (C) without SDS (trace **a**), 1 mM SDS (trace **b**) and 10 mM SDS (trace **c**).

In order to explore the interaction between SDS and peptides further, similar experiment was carried out with (4*R*)-Amp_9 (**P9**) and the results show that the peptide **P9** also exhibited a loss of CD signal at 1 mM surfactant concentration (Figure 3.7). However, at higher concentration (10 mM) above cmc, the peptide (4*R*)-Amp_9 (**P9**) still adopted PP-II conformation and not β-like structure seen with the 4(*S*)- amp_9 (**P3**). The intensity of the positive band at 225 nm was found to lower in the presence of SDS as compared to that in its absence (Figure 3.7B). Unsubstituted polyprolines, on the other hand showed negligible change in the conformation upon addition of SDS (Figure 3.7C) and no loss of CD signals at 1 mM was observed unlike that seen with (4*S*)-amp_9 (**P3**) and (4*R*)-Amp_9 (**P9**).

From these experiments, it is clear that peptide conformation alteration with anionic SDS is effective with cationic (amino) substitution at C4 position of prolines. Below cmc of SDS, when the electrostatic interactions between the cationic peptides (4*S*)-amp_9 (**P3**) or (4*R*)-Amp_9 (**P9**) and the anionic surfactant molecules resulted in a loss of CD signals below cmc, may be a result of aggregation driven hydrophobic collapse of the peptide induced by monomeric detergent molecules, as seen with similar polycationic peptides in the literature.[18] Above its cmc, where SDS forms thermodynamically stable micelles, the hydrophilic peptides reside at the

interface. The peptide-micelle interaction seems to be stereodependent since C4(*S*)-NH_2 substitution favours the β conformation, and C4(*R*)-NH_2 still conferred PP-II conformation. A membrane-like SDS micellar environment promotes the stereodependent conformational change in aminoprolyl polypeptide with (4*S*)-amp_9 (**P3**) assuming β-sheet like form even in aqueous detergent media.

To identify the specific role of SDS in inducing observed conformational change in peptide (4*S*)- amp_9, the conformational studies on the peptide was done in the presence of other related surfactants.

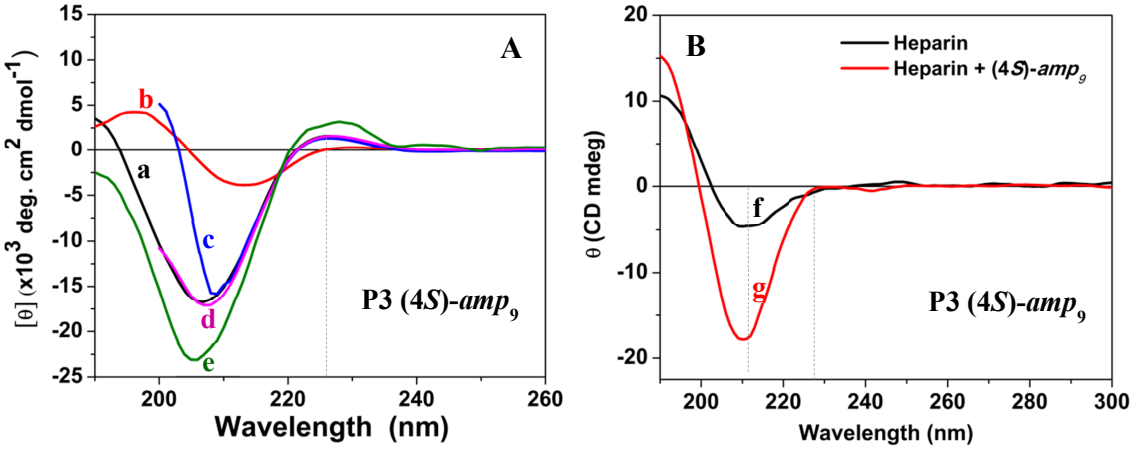
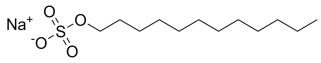
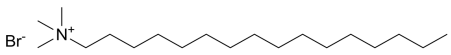
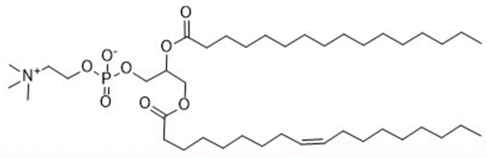
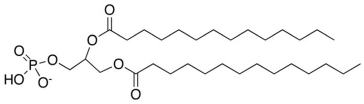


Figure 3.8: Effect of surfactants (A) and anionic polymer heparin (B) on conformation of peptide **P3** (4*S*)-amp_9 . A) CD spectra of 100 μM peptide **P3** (4*S*)-amp_9 in water without any surfactant (trace **a**) and in the presence of SDS (trace **b**); CTAB (trace **c**); PC, phosphatidyl choline (trace **d**); POPA, poshphatidic acid (trace **e**). B) CD spectra of heparin (trace **f**) and a mixture of heparin and peptide **P3** (4*S*)-amp_9 (trace **g**).

SDS has a negatively charged sulphate group as its polar head group and an alkyl chain of 12 carbon length. Surfactants that are different from SDS in their head group and the lipid chain were examined for the effect on PP-II content of the peptide (4*S*)-amp_9 (**P3**). This was done to elucidate the structural requirements for an agent to induce the PP-II to β conformational change in the aminoprolyl polypeptides. The surfactants chosen are listed in table 3.1 and

included (i) CTAB, which carries a quarternary ammonium group and a single alkyl chain, (ii) phosphatidic acid with a phosphate head group and two alkyl chains, and (iii) phosphatidyl choline, a zwitter ionic lipid with a phosphate and choline groups along with two alkyl chains. All surfactants were used at a concentration above their respective cmc. With all the above surfactants studied, the peptide adopts stable PP-II conformation as evident from the positive band at 227 nm. While POPA produced a marginal increase in the magnitude of the positive and negative bands, the other surfactants did not alter the features of the peptide's CD spectra.

Table 3.1 Influence of surfactants on structure of peptide **P3**.

Trace	Surfactant	Remarks	Observation
a	Only peptide, (4*S*)-*amp*$_9$ (**P3**)	Cationic peptide	PP-II
b	(4*S*)-*amp*$_9$ (**P3**) + SDS 	Negatively charged, Sulphate head group A single alkyl chain.	β
c	(4*S*)-*amp*$_9$ (**P3**)+ CTAB 	Positively charged Quaternary ammonium A single alkyl chain.	PP-II
d	(4*S*)-*amp*$_9$ (**P3**)+ PC 	Neutral zwitter ionic lipid Phosphate and choline in head group. Two alkyl chains.	PP-II
e	(4*S*)-*amp*$_9$ (**P3**)+ POPA 	Negatively charged lipid Phosphate head group. Two alkyl chains.	PP-II
f	(4*S*)-*amp*$_9$ (**P3**)+ Heparin	Anionic polysaccharide Sulphate	Random

In all these cases, the peptide (4*S*)-*amp*$_9$ (**P3**) retained its PP-II form suggesting that for the conformation altering effects, all the structural characteristics of SDS are essential. Since an ensemble of structural properties is required for inducing the conformational change, the interaction of SDS with cationic aminoprolyl polypeptides is likely to have a complex and multidimensional origin. A negatively charged head group and single hydrocarbon chain maintains the right hydrophilic/hydrophobic balance in SDS. The latter aspect seems to be crucial since PC and POPA with double chains did not exhibit β-form.

In addition to these surfactants, heparin, an anionic surfactant rich in sulphate groups was also used to ascertain the role of large densities of negatively charged groups as found in SDS micelles (Figure 3.8B). In the presence of heparin, the peptide showed no positive band at 227 nm. However, the CD spectrum of the mixture was dominated by the two bands observed with only heparin, which seemed to intensify on addition of the peptide. With a negative band at 210 nm and no positive band at 227 nm, it is likely that heparin caused destabilization of the PP-II helix leading to random conformation. Since the spectral bands of both the polymer and the peptide overlap, it is difficult to discern the effect of the peptide on the secondary structure of heparin. The loss of positive band at 227 nm suggests that heparin had a destructive effect on this conformation.

In TFE, peptide (4*S*)-*amp*$_9$ (**P3**) adopts β conformation but shifts to PP-II on addition of small aliquots of water.[10] Since aqueous SDS promotes β conformation, it would be interesting to study the cumulative effect of both SDS and TFE. Hence, the peptide **P3** (100 μM) was taken in TFE and titrated with aliquots of aq. SDS (1M). Figure 3.9 shows the result of such a CD titration experiment.

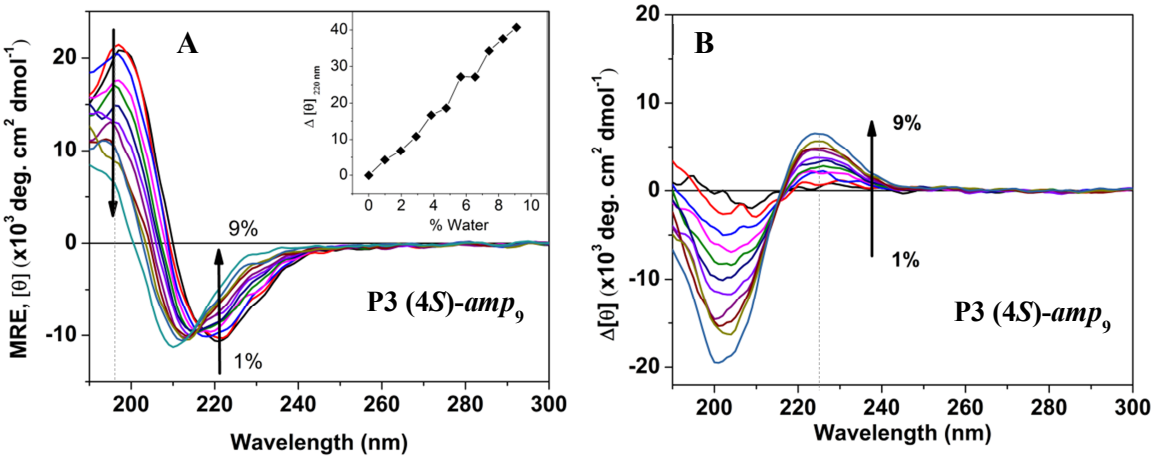


Figure 3.9: Effect of aqueous SDS on the conformation of peptide **P3** in TFE. A) CD titration of aqueous SDS into TFE solution of peptide **P3** (4*S*)-amp_9. Inset: Change in the magnitude of negative band at 220 nm with increasing volume percentage of water. B) Differential CD spectra showing the formation of PP-II conformation.

As aliquots (0.5 µL) of the aqueous solution of SDS was added to the peptide solution in TFE, the negative band at 220 nm decreased in magnitude (Figure 3.9A), accompanied by a fall in the intensity of the positive band at 195 nm and emergence of a negative band at 210 nm. Differential CD spectra were computed by subtracting every spectrum obtained after addition of incremental volumes of SDS solution from the initial spectra of the peptide **P3** in TFE (Figure 3.9B). This showed the transformation of β-structure to PP-II helix with the addition of aqueous SDS solution. The observance of isodichroic point at 215 nm supports such a conformational change from β in TFE to PP-II with addition of SDS. Thus, the ability of water to drive the conformational change towards PP-II greatly outweighs the ability of SDS to destabilize PP-II structure or form β-structure from this peptide.

3.3.1e *Conformation of (4S)-amp$_9$ in Water-in-oil Microemulsion*

In order to examine if a crowded environment relevant in the context of biological systems like cellular organelles,[19] would induce the conformational change in peptide (4*S*)-*amp*$_9$ (**P3**), CD spectra of the peptide **P3** was recorded in AOT/Heptane water-in-oil microemulsion system (Figure 3.10). In the reverse micelles formed by AOT in water/heptane, the peptide **P3** did not show negative CD band at 220 nm, characteristic of β-sheet. A weak negative band at 200-205 nm suggested random conformation, which was also seen with myristoylated peptide (4*S*)-*amp*$_9$ -C$_{14}$ (**P5**).

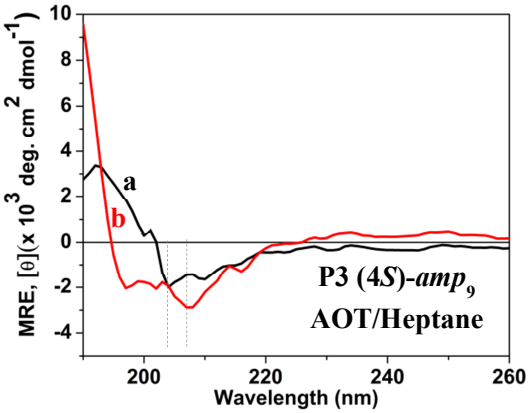


Figure 3.10: CD spectra of peptides **P3** (4*S*)-*amp*$_9$ (trace **a**) and **P5** (4*S*)-*amp*$_9$ -C$_{14}$ (trace **b**) in AOT/Heptane water-oil microemulsion.

3.3.1f *Effect of Lipidation on Conformation of 4(R/S)-Aminoprolyl Polypeptides*

A balance between the hydrophobic and hydrophilic properties of molecules is crucial for supramolecular assembly in aqueous medium. With the rationale of improving the self-assembling properties of the 4(*R*/*S*)-aminoprolyl polypeptides, they were conjugated to fatty acids of different alkyl chain lengths (N=12 to 16) to yield amphiphilic polyproline peptides. Peptide (4*S*)-*amp*$_9$ (**P3**) was coupled to lauric acid (C$_{12}$), myristic acid (C$_{14}$) and palmitic acid (C$_{16}$) at its N-terminus on the solid phase resin to obtain fatty acid conjugated peptides, (4*S*)-

amp$_9$-C$_{12}$ (**P4**), (4*S*)-*amp*$_9$-C$_{14}$ (**P5**), and (4*S*)-*amp*$_9$-C$_{16}$ (**P6**) respectively. The conformational properties of these peptides were studied using CD spectroscopy.

The conjugation of fatty acids to the peptide (4*S*)-*amp*$_9$, did not alter its conformational properties, either in buffer or in TFE (Figure 3.11). In phosphate buffer, all the peptides showed a positive band at 222-225 nm and a negative band at 205 – 210 nm, which was typical of PP-II form.

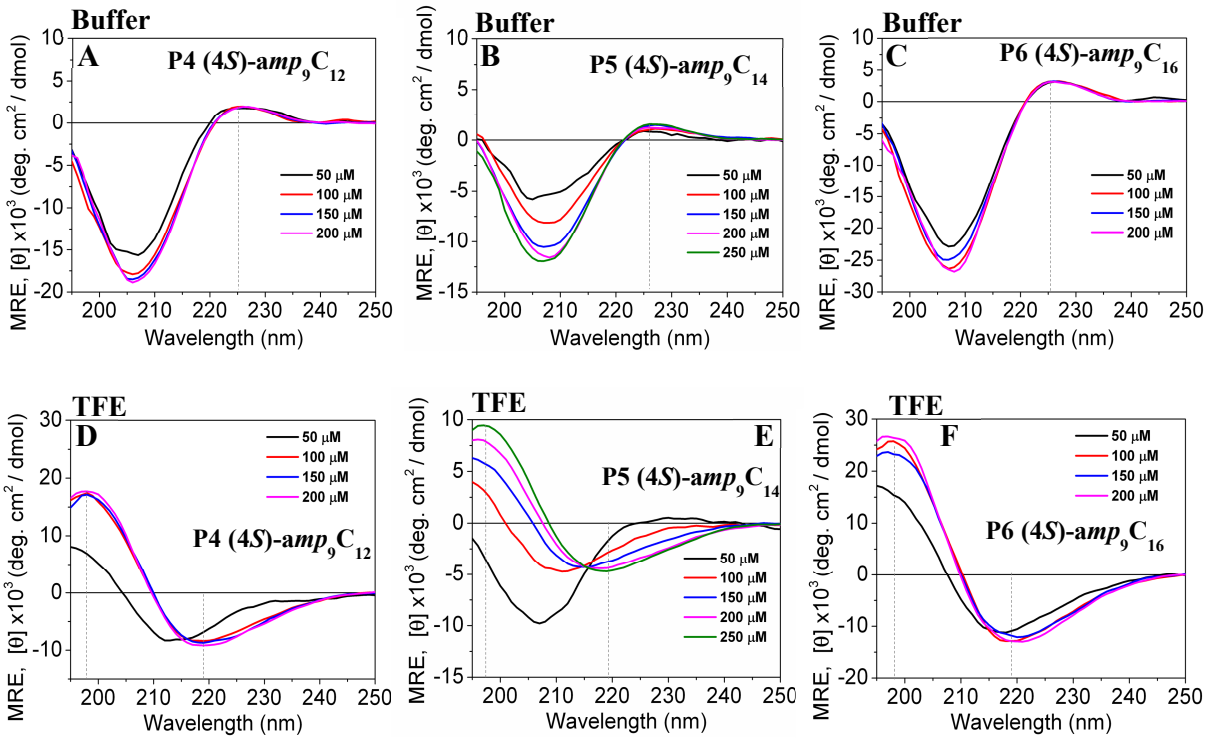


Figure 3.11: CD spectra of peptides (4*S*)-*amp*$_9$-C$_{12}$ (**P4**) in buffer (A) and in TFE (D); (4*S*)-*amp*$_9$-C$_{14}$, (**P5**) in buffer (B) and in TFE (E); (4*S*)-*amp*$_9$-C$_{16}$ (**P6**) in buffer (C) and in TFE (F).

In TFE, all the peptides showed a CD signature characteristic of β structure, similar to the one observed in non-lipidated (4*S*)-*amp*$_9$ (**P3**). They showed a negative band at ~218 nm and a positive band at ~198 nm. At 50 µM, the negative band at 218 nm was nearly absent in (4*S*)-*amp*$_9$-C$_{12}$ (**P4**) and (4*S*)-*amp*$_9$-C$_{14}$ (**P5**) but with increasing concentrations, the magnitude of the

negative band increased along with a gradual shift in the position of the band towards longer wavelengths, resting finally with a CD band at 218 nm at concentrations 200 μM and 250 μM. This was accompanied by the emergence of positive band at 198 nm at 100 μM and the enhancement of its intensity with increasing concentrations.

Lipidation of aminoproline peptides was aimed at promoting β sheet like structural arrangement through additional interchain hydrophobic interactions. The CD studies reveal that in buffer conjugation of fatty acyl tails to the peptides does not overcome the forces that stabilize PP-II structure of the peptides in water. In TFE, the peptides readily formed β sheets suggesting the higher hydrophobicity of TFE compared to water was not competent to disrupt the interchain associations. As evident from the spectra, increasing the concentrations (above 50 μM), facilitated the formation of β-sheet like conformation among these peptides, especially in (4*S*)-amp_9-C_{14} (**P5**).

3.3.2 Guanidinylprolyl polypeptides

3.3.2a *pK_a of Guanidinylprolyl polypeptides*

As compared to amines, the guanidine groups are more cationic with a pK_a around 12, which results in them being mostly positively charged, even at neutral pH. In order to check if the presence of highly cationic multiple guanidine groups on a rigid polyproline backbone alters their relative pK_as, pH titration was carried out to determine the average pK_a of guanidine substitutions on peptides, (4*S*)-$gndp_9$ (**P7**) and (4*R*)-$Gndp_9$ (**P11**). A solution of the peptide was titrated with incremental additions of aliquots of aq. NaOH and pH change was monitored after each step. The pH vs [NaOH] plot showed an equivalence point at pH 7 for peptide (4*S*)-$gndp_9$ (**P7**) (Figure 3.12A) and pH 6.5 for (4*R*)-$Gndp_9$ (**P11**) (Figure 3.12B).

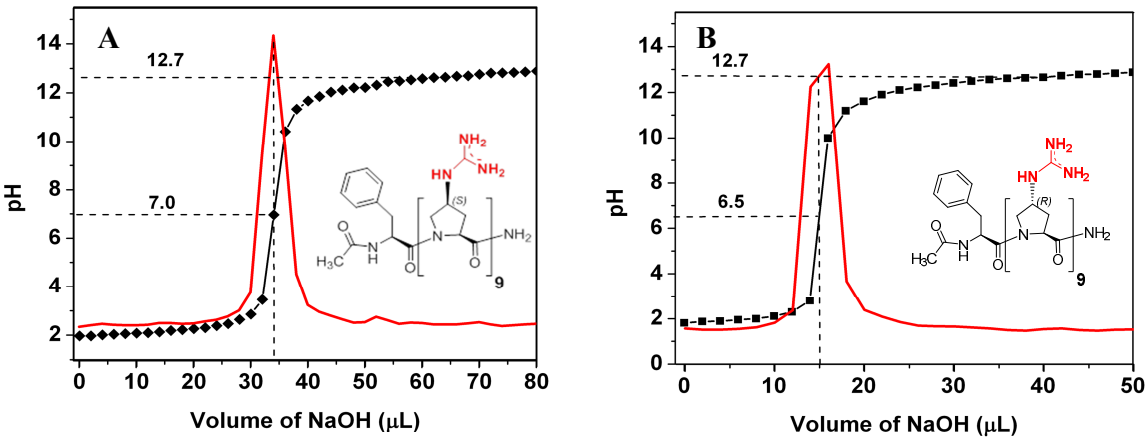


Figure 3.12: pH titration of polyguanidinylprolyl peptides with 1 N NaOH. A) **P7** (4*S*)-*gndp*$_9$, 75 μM; B) **P11** (4*R*)-*Gndp*$_9$, concentration 35 μM.

From these plots, the pK_a of guanidines in both these peptides were found to be 12.7, irrespective of 4(*R*)/4(*S*). This was unlike aminoprolyl polypeptides where the (4*R*)-*Amp*$_9$ showed a slightly higher pK_a as compared to (4*S*)-*amp*$_9$.[20] This suggested that in polyproline peptides, physico-chemical properties of guanidine moieties did not significantly depend on the stereochemistry at C4 of the proline residues.

3.3.2b *Conformational Studies of 4(R/S)-Guanidinylprolyl Polypeptides*

The stereoelectronic effects and hydrogen bonding properties of the C4(*R*/*S*)-NH_2 substitutions was implicated in the solvent dependent conformational change observed in the 4(*R*/*S*)-aminoprolyl polypeptides. As compared to the 4-amino group, 4-guanidino group is was more electron-withdrawing and a better hydrogen-bonding function. With a pK_a > 12, it stays positively charged at pH ~ 7.0. In order to study the effect of highly cationic guanidine group on the conformation of the polyproline peptides, (4*S*)-*gndp*$_9$ (**P7**) and (4*R*)-*Gndp*$_9$ (**P11**) were synthesized. The comparative CD spectra of these peptides were recorded in phosphate buffer (10 mM) containing NaCl (10 mM), and in TFE.

The peptide (4*S*)-*gndp*$_9$ (**P7**) showed spectra that is typical of PP-II structure in both aqueous buffer, and TFE (Figure 3.13).

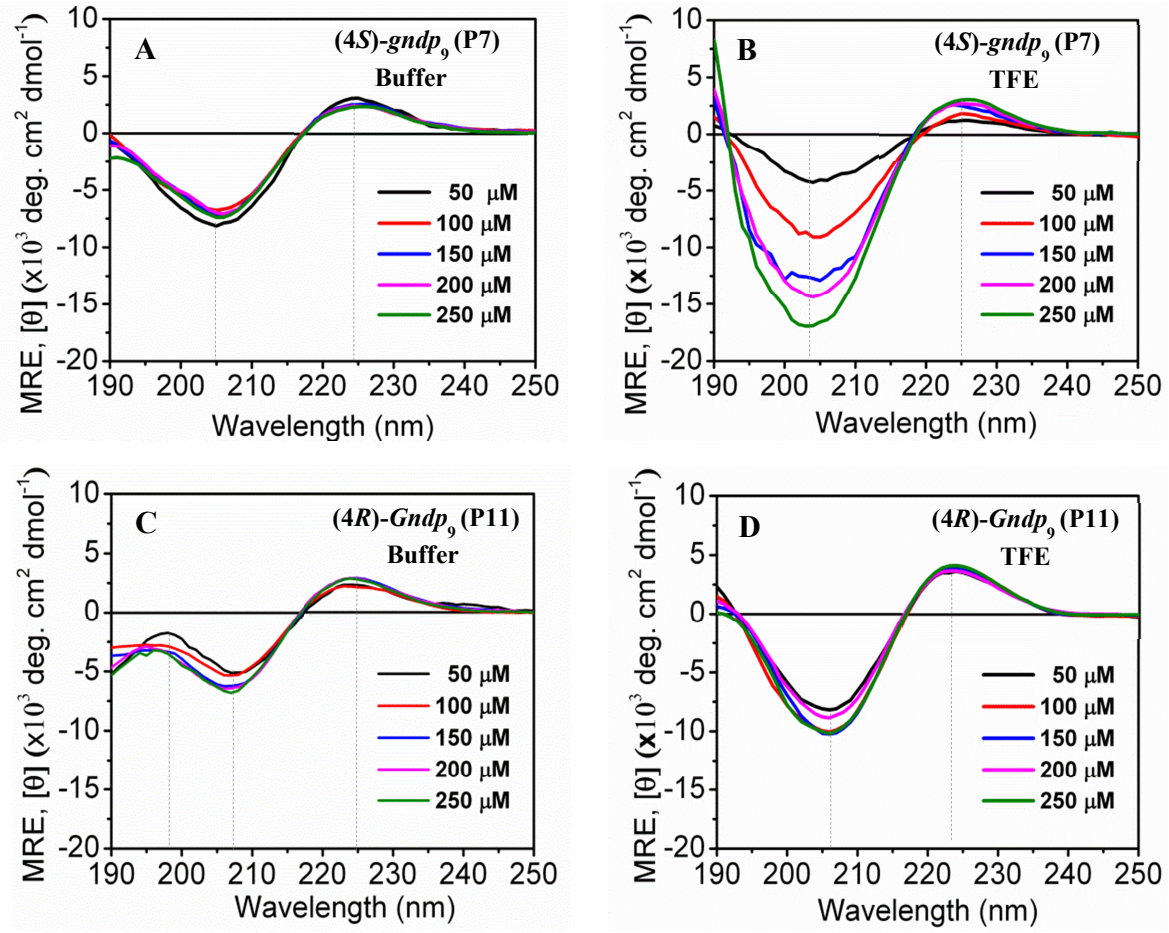


Figure 3.13: CD spectra of peptides (4*S*)-*gndp*$_9$ (**P7**) in buffer (A) and in TFE (B); (4*R*)-*Gndp*$_9$, (**P11**) in buffer (C) and in TFE (D).

In buffer (Figure 3.13A), the positive n→π* band at 225 nm was more intense as compared to the aminoprolyl polypeptides. The negative π →π* band was found to be centered at 205 nm. In TFE (Figure 3.13B), the peptide retained its PP-II form. The positions of the two bands were the same as observed in buffer. However, there was a significant change in the MRE intensity of the two bands with increase in the concentration of the peptide. Both the positive band at 225 nm and the negative band at 205 nm intensified with increasing concentrations. This

trend was absent in buffer, where the molar ellipticity spectra was almost identical over the concentration range of 50 μM to 250 μM. The peptide (4*R*)-*Gndp*$_9$ (**P11**) also showed a PP-II conformation in their CD spectra in both buffer and TFE. Although, the positive band at ~ 225 nm was not unusual, the negative band showed a red-shift to 207 nm. Both in buffer and in TFE, the peptide (4*R*)-*Gndp*$_9$ (**P11**) showed no change in their mean residue ellipticity with concentration of the peptide.

Unlike 4(*S*)-aminoprolyl polypeptides, the corresponding guanidine derivatives did not show a solvent-dependent conformational change, regardless of the stereochemistry of the substitution at C4 position. The absence of conformational change in guanidylprolyl peptides suggests that substituents sterically bulkier than NH_2 do not facilitate a stabilization of β structure. Strong electrostatic repulsion between the cationic sidechains of the strands could also abrogate the formation of β conformation in these peptides.

3.3.2c *Effect of Lipidation on Conformation of 4-Guanidinylprolyl Polypeptides*

The guanidinylprolyl polypeptides (4*S*)-*gndp*$_9$ (**P7**) was conjugated to fatty acids at its N termini to produce amphiphilic peptide (4*S*)-*gndp*$_9$-C_{14} (**P8**). With several guanidine groups in their polar heads, these peptide amphiphiles are likely to be highly charged and have an altered hydrophilic-hydrophobic balance as compared to those peptides composed of 4-aminoproline residues, while having the same polyproline structural scaffold. Therefore, these peptides may be expected to show different conformational and self-assembling properties.

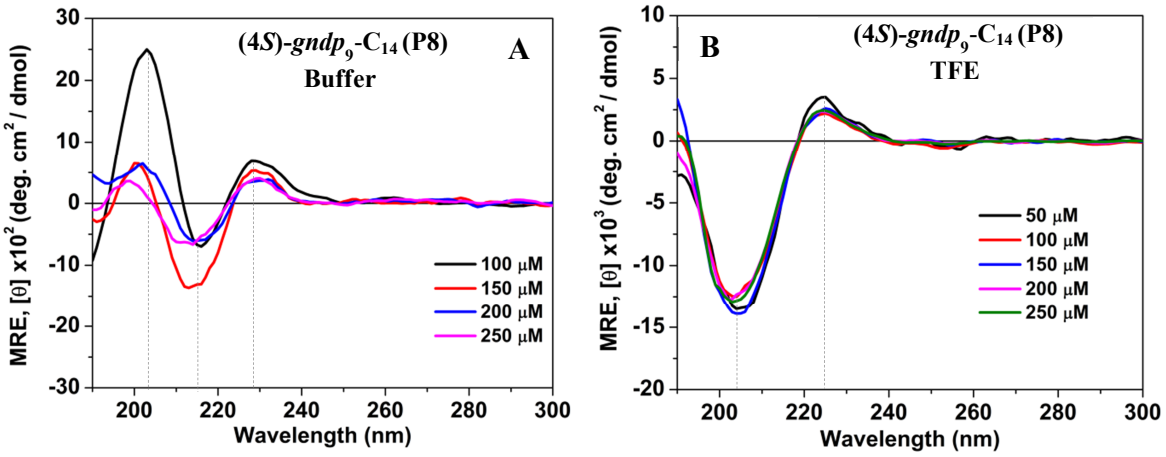


Figure 3.14: CD spectra of peptide (4*S*)-*gndp*$_9$-C$_{14}$ (**P8**) in 10 mM phosphate buffer (pH 7.0) with 10 mM NaCl (A) and in TFE (B)

The CD spectrum of the peptide **P8** was recorded in phosphate buffered saline and in TFE to study their conformational properties. In TFE, the lipidated peptide **P8** showed a prominent positive band at 225 nm and a more intense negative band at 204 nm, which were characteristics of PP-II form (Figure 3.14B). There was no change in the spectra with the concentration of the peptide over the range of 50 μM – 250 μM. However, in phosphate buffered saline, the effect of lipidation was apparent in the CD spectra. Two positive bands at 205 nm, and 230 nm, and a negative band at 215 nm were observed. The appearance of a positive band at 205 nm is an indication of minor departure of the conformation from a typical PP-II structure (Figure 3.14A). A time-resolved CD studies showed that the peptide existed in PP-II form soon after preparation of the solution in the buffer. The conformational change was observed over a period of 30 minutes during which the band at 205 nm increased in intensity and the negative band at 215 nm decreases in its intensity ((Figure 3.14B). A positive band at 205 nm in hydrophobic peptides was attributed to formation of intermolecular associations in solution.[21]

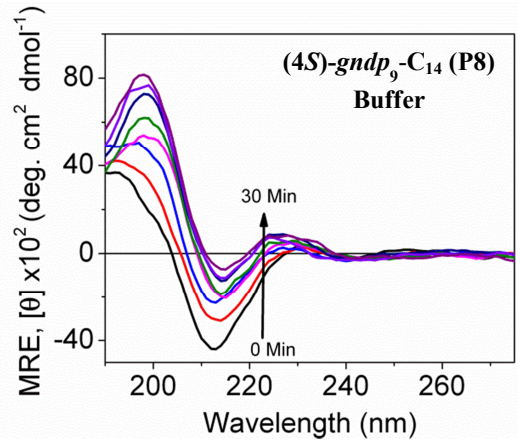


Figure 3.15: Time dependent CD spectra of 100 μM of peptides **P8** (4*S*)-*gndp*$_9$-C$_{14}$ in 10 mM phosphate buffer (pH 7.0) with 10 mM NaCl.

Hydrophobic interactions between amino acid residues and their interactions with surrounding water molecules are known to cause "salt-in" or "salt-out" of proteins depending on the presence of different salts.[22] In order to probe the role of counter-ions in the observed conformational change in lipidated guanidiylprolyl polypeptide (4*S*)-*gndp*$_9$-C$_{14}$ (**P8**), CD spectra of the peptide was recorded in solutions containing different salts.

In water, and in the absence of salts, the peptide (4*S*)-*gndp*$_9$-C$_{14}$ (**P8**) showed a strong positive band at ~225 nm and a deep negative band at 205 nm, characteristic of PP-II conformation. Same spectral features were observed in the presence of sodium acetate, sodium chloride, or sodium perchlorate (Figure 3.16). However, in the presence of sulphate and phosphate counter ions, the CD signature deviated from the typical PP-II spectrum with the appearance of a positive band at 195 nm and a weak negative band between 205 nm to 215 nm. The positive band at 222 nm was stunted as compared to the spectra observed in water in the presence of other counterions studied.

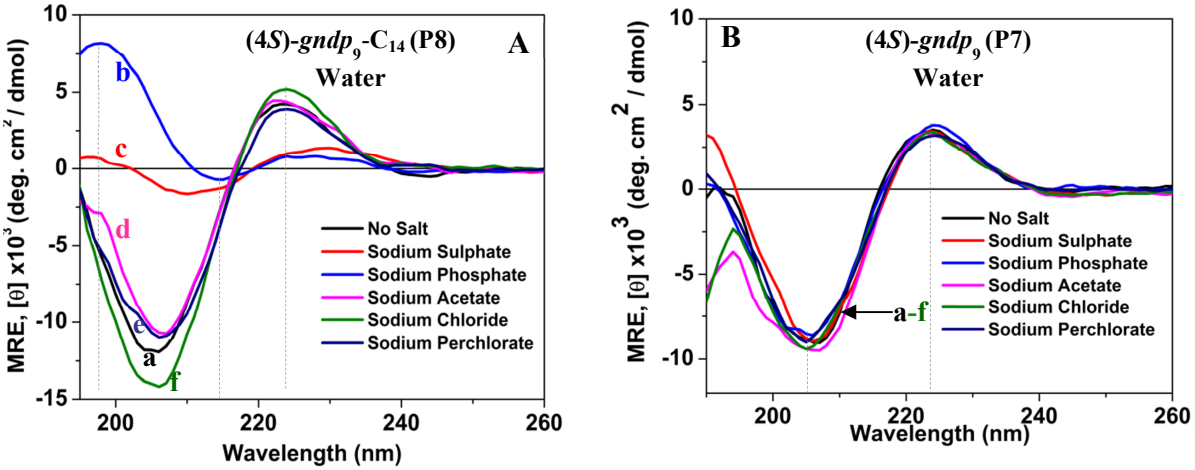


Figure 3.16: Effect of counter ions on the conformation on guanidinylprolyl polypeptides. CD spectra of 100 μM of lipidated peptide **P8** (4*S*)-*gndp*$_9$-C_{14} (A) and non-lipidated peptide **P7** (4*S*)-*gndp*$_9$ (B) in water containing no salt (trace **a**), sodium phosphates (trace **b**), sodium sulphate (trace **c**), sodium acetate (trace **d**), sodium chloride (trace **e**) and sodium perchlorate (trace **f**).

Unlike the lipidated peptide, the non-lipidated peptide (4*S*)-*gndp*$_9$ (**P7**) showed no change in the CD spectra with changes in the counter ions present in the solution (Figure 3.15B). The observed sensitivity to anionic "hydrophilic" phosphate and sulphate counterions was therefore a consequence of lipid chains of the peptide. This study underlines the role of counterions in influencing the conformation of these cationic polyguanidinyl prolyl peptides when they are lipidated. These observations can be explained by plausible conformational changes induced by a process of aggregation of the peptides driven by hydrophobic interactions between the lipid chains.[20] Since formation of any ordered aggregation requires the electrostatic repulsion between the head groups be shielded, the role of counterions become significant in these systems. As evidenced here, phosphates and sulphates apparently screen the positive charges of guanidinium groups and help in association of peptides, while other anions such as acetate, chloride and perchlorates ("hydrophobic"counterions) provide inadequate screening of the charges between neighboring peptides. Upon formation of such associations, the changes in the hydration of the peptide head group might result in loss of their conformational preference for PP-II structure.

3.3.2d *Interaction of Guanidinylprolyl Polypeptides with DNA*

The guanidinylprolyl polypeptides are strongly cationic in nature and would therefore have strong affinity for anionic polymers such as DNA. In these peptides, the guanidine moieties are held on a rigid polyproline scaffold,[23] which is characterized by a left handed helix with 3 residues per turn. This results in the homooligomeric peptides presenting their cationic groups separated by a periodic distance, controlled by helical pitch of the polyproline scaffold so that they can interact with phosphates of DNA.[24] To see whether stereochemistry of the C4 substitution influence the interaction of the 4(*R*/*S*)-guanidinylprolyl polypeptides with short single and double stranded DNA, binding of polypeptides (4*S*)-$gndp_9$ (**P7**) and (4*R*)-$Gndp_9$ (**P11**) with homo-oligomers dA_{12}, dG_{12}, dC_{12} and dT_{12} were studied using CD spectroscopy, temperature dependent UV-absorption spectroscopy and fluorescence based ethidium bromide displacement assay.

*CD studies of interactions between **P7** and **P11** with ssDNA*

The circular dichroism spectra of oligonucleotides is sensitive to structural perturbations resulting from binding of cationic DNA condensing agents.[25] The CD spectra of an aqueous solution of these oligonucleotides (4 μM) in phosphate buffer (10 mM, pH 7.0) and NaCl (10 mM) were recorded. Aliquots of the guanidinylprolyl polypeptide **P7** or **P11** were added and changes to the spectral signature of the single stranded DNA were monitored. As shown in the Figure 3.17, the peptides (4*S*)-$gndp_9$ (**P7**) did not show any appreciable change in the CD spectra of the oligonucleotides dA_{12}, dT_{12} and dG_{12} when the [guanidine]/[phosphate] in the mixture was maintained at 1.

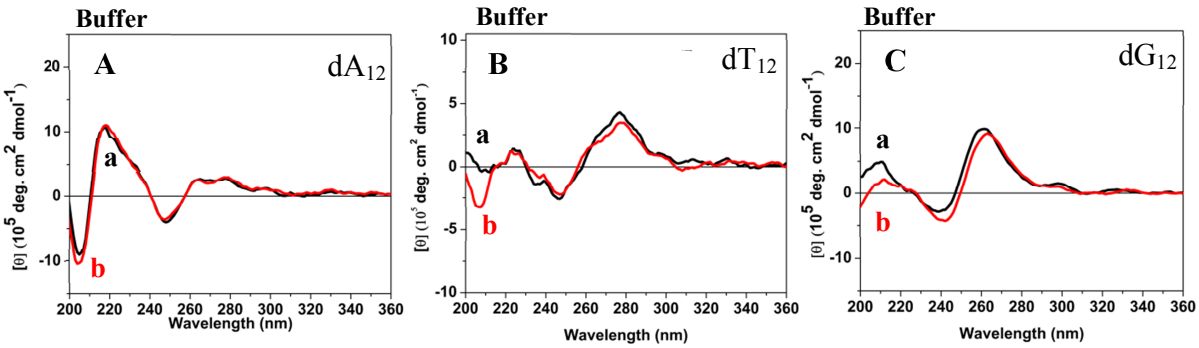


Figure 3.17: Interaction of single stranded oligonucleotides with peptide (4*S*)-*gndp*$_9$ (**P7**). CD spectra of ssDNA dA_{12} (A), dT_{12} (B), and dG_{12} (C) without the peptide (trace **a**) and with peptide (4*S*)-*gndp*$_9$ (**P7**) at equal concentration guanidine and phosphate (trace **b**).

While there were no change in the CD spectra of dA_{12}, dG_{12} and dT_{12}, in the presence of peptide, with dC_{12} however, the guanidinylprolyl polypeptide (4*S*)-*gndp*$_9$ (**P7**) produced significant concentration dependent changes in the CD spectrum of the oligonucleotide (Figure 3.18). dC_{12} showed a strong positive band at 288 nm and a weak negative band at 266 nm. On addition of the peptide **P7**, the band at 288 nm diminished (Figure 3.18A) and a band at 295 nm strongly emerged to become distinct as the concentration of the guanidine peptide increased close to 5 equivalents. To check whether the interaction with dC_{12} was affected by the configuration at C4, the same experiment was conducted with (4*R*)-*Gndp*$_9$ (**P11**) (Figure 3.18B).

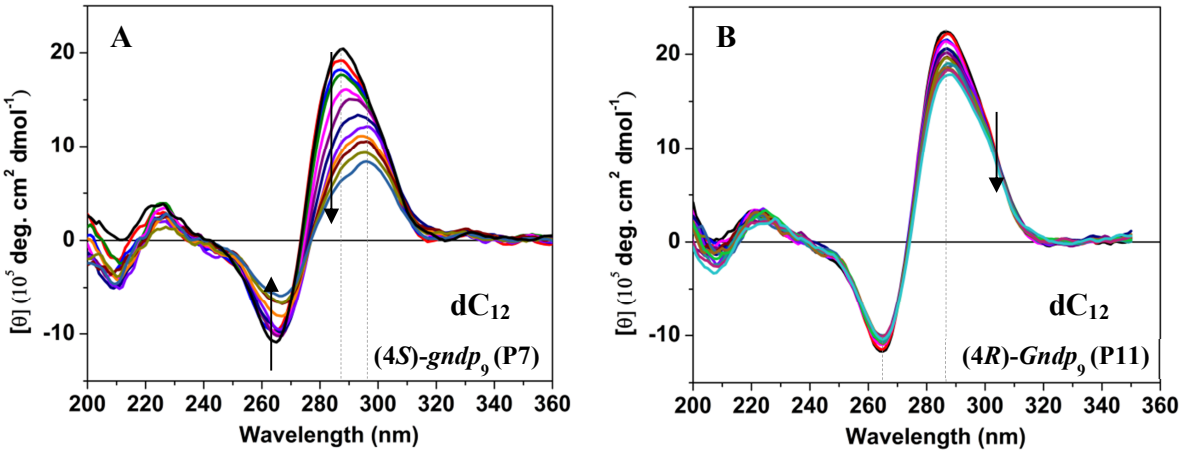


Figure 3.18: Comparison of structure perturbation effect of (4*S*)-*gndp*$_9$ (**P7**) (A) and (4*R*)-*Gndp*$_9$ (**P11**) (B) on single stranded oligonucleotide dC_{12}.

Even though (4*R*)-*Gndp*$_9$ (**P11**) produced a decrease in the intensity of the peptide, the effect was not as well pronounced as the case was with (4*S*)-*gndp*$_9$ (**P7**).

*CD studies of interactions between **P7** and **P11** with dsDNA*

From the results of the figure 3.18, it was apparent that the stereochemistry of the guanidine substitution influences the way or the extent to which the guanidinylprolyl polypeptides with the (4*S*)-*gndp*$_9$ (**P7**) was able to selectively perturb the structure of oligocytosine. In order to check if this selectivity is restricted to ssDNA or manifests to double stranded DNA as well, CD studies were carried out with duplexes of d(G_{12}.C_{12}) and d(A_{12}.T_{12}) (Figure 3.19).

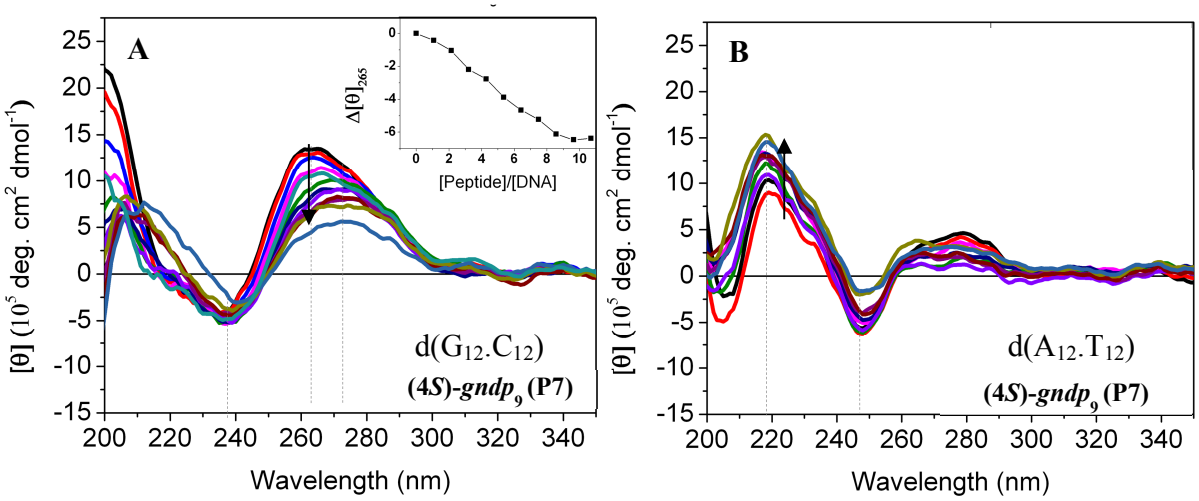


Figure 3.19: Comparison of structure perturbation effect of (4*S*)-*gndp*$_9$ (**P7**) on duplexes d(G_{12}.C_{12}) (A), and d(A_{12}.T_{12}) (B). Insets show change in molar ellipticity at 265 nm (A) and 218 nm (B) with concentration ratio of peptide to DNA.

The peptide (4*S*)-*gndp*$_9$ (**P7**) was titrated against the duplexes d(G_{12}.C_{12}) and d(A_{12}.T_{12}) in 10 mM phosphate buffered saline and their CD spectra were recorded to examine the effect of interaction of the peptide on the conformation of the oligonucleotides and their stability. The

CG-rich duplex, d(G_{12}.C_{12}) showed a shallow negative band at 240 nm and a strong positive band at 265 nm (Figure 3.19A). Addition of aliquots of the peptides resulted in the fall of the positive band at 265 nm in a concentration dependent manner. This was also accompanied by the broadening of the band and a shift in its position towards longer wavelengths. The band at 240 nm however, did not show any change in its intensity or its position. The fall in the magnitude of the positive band at 265 nm was found to be almost linear over a range of [peptide]/[DNA] molar concentration ratio of 0 to 10.

The CD spectra of duplex, d(A_{12}.T_{12}) showed strong positive band at 220 nm, a shallow negative band at 250 nm, and a weak and broad positive band at 280 nm (Figure 3.19B). With the AT-rich duplex, the peptide did not show any characteristic concentration dependent change in the CD spectra of the oligonucleotide. The comparison of the CD plots revealed a sequence dependent effect of the peptide on the conformation of DNA in case of peptide (4*S*)-*gndp*$_9$ (**P7**).

UV-Thermal Melting studies with dsDNA

Interaction of the peptide with the DNA oligonucleotides affects its thermal stability,[26] which can be followed with temperature dependent UV absorption spectroscopy. Absorbance at 260 nm of the hybridized duplexes was followed as the temperature of the solution was raised from 17 ^{o}C to 90 ^{o}C. As the duplexes undergo thermal denaturation, an increase in the absorbance was observed with a hyperchromicity of about 30%. The transition from duplex to single stranded state is typically sigmoidal and the midpoint of the sigmoidal transition represents the melting temperature (Tm) of the duplex. This corresponds to the temperature at which one-half of the molecules exist in duplex form and the remaining half exists as single strands. Tm is a measure of the stability of the duplex.

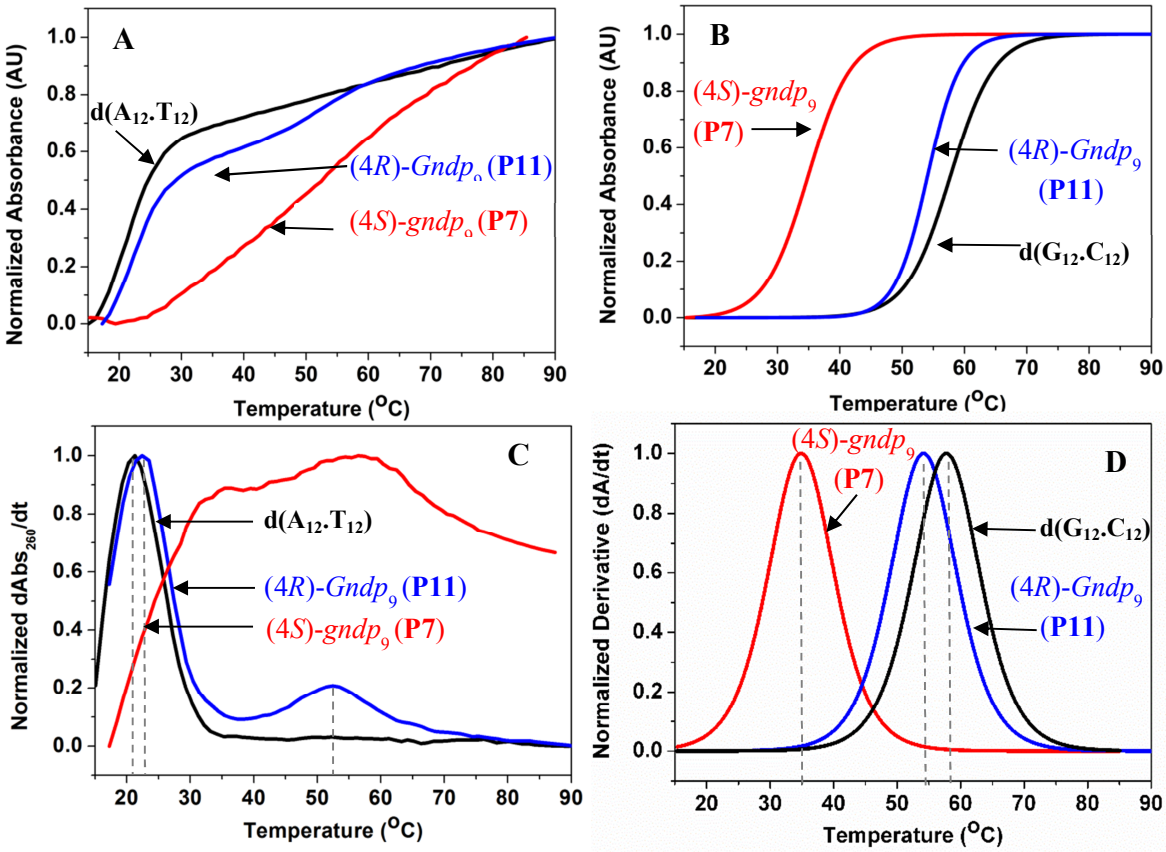


Figure 3.20: UV-Thermal melting curves of peptide complex with DNA d(A_{12}.T_{12}) (A) and d(G_{12}.C_{12}) (B) and their respective derivative curves (C) and (D). Duplexes without any peptide (trace **black**), DNA with peptide (4*R*)-*Gndp*$_9$ (**P11**) (trace **blue**), DNA with peptide (4*S*)-*gndp*$_9$ (**P7**) (trace **red**).

A 4 μM solution of the AT-rich duplex, d(A_{12}.T_{12}) in phosphate buffer (10 mM, pH 7.0) containing NaCl (10 mM), was found to have a melting temperature (T_m) of about 20 °C (Figure 3.20A). In the presence of the peptide (4*S*)-*gndp*$_9$ (**P7**), the T_m of the duplex d(A_{12}.T_{12}) shifted to higher temperatures to 54 °C. This indicates that the peptide **P7** stabilizes AT-rich duplexes. However, it was found to deviate slightly from the sigmoidal transition. **P11** (4*R*)-*Gndp*$_9$ also had a stabilizing effect on the dsDNA. The peptide was also found to produce two distinct transitions indicating that the binding of the peptide to the duplex might involve stabilization of both duplexes and triplexes formed by polyadenines and polythymines.

The CG-rich duplex, d(G_{12}.C_{12}), under the same conditions as above, showed a T_m of 58 ^oC. When an equimolar concentration of (4*S*)-*gndp*$_9$ (**P7**) was added to the solution, the melting transition decreased to 35 ^oC (Figure 3.20B). This indicates severe destabilization of the duplex d(G_{12}.C_{12}) by the peptide. The peptide (4*R*)-*Gndp*$_9$ (**P11**) also had a similar destabilizing effect on the duplex DNA, however the extent of it was considerably less as the reduction in T_m was only 5 ^oC.

Ethidium bromide displacement assay

The interaction of the (4*S*)-*gndp*$_9$ (**P7**) peptide with CG-rich and AT-rich duplexes was further probed using fluorescence spectroscopy by ethidium bromide displacement assay.[27] Ethidium bromide intercalates between the base-pairs of duplex DNA and shows an enhancement of its fluorescence emission. Binding of the cationic peptide to the dsDNA causes a displacement of the intercalator resulting in a reduction in the fluorescence emission. Normalized emission intensity was plotted against molar ratio of the peptide to DNA. It revealed distinct fluorescence quenching profiles for binding of peptide (4*S*)-*gndp*$_9$ **(P7)** to CG rich DNA duplex, d(G_{12}.C_{12}) and AT-rich DNA duplex, d(A_{12}.T_{12}) (Figure 3.21A). With AT-duplex, the fall in fluorescence was steeper than with GC duplex. At around 3:1 molar ratio of peptide to dsDNA, nearly 50% quenching was achieved for AT duplex, whereas only 15% quenching was attained for GC duplex. This revealed a differential affinity of (4*S*)-*gndp*$_9$ **(P7)** peptides to GC and AT duplex. More specifically, a higher affinity for AT duplex was observed as compared to GC duplexes.

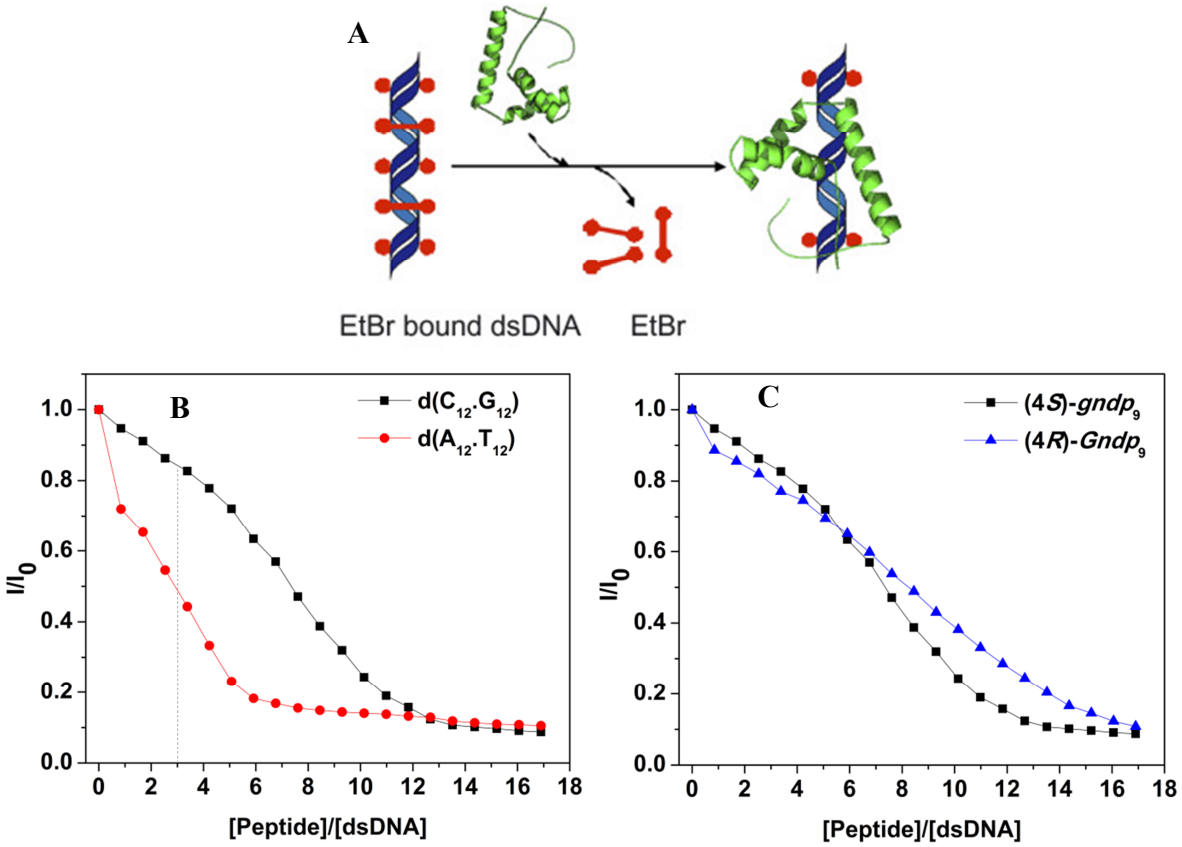


Figure 3.21: A) Schematic ethidium bromide displacement assay.[27b] B) Fluorescene emission decay by peptide (4*S*)-*gndp*$_9$ (**P7**) on duplexes d(G_{12}.C_{12}) (black square) and d(A_{12}.T_{12}) (red circle). C) Comparison of fluorescence emission decay caused by peptide (4*S*)-*gndp*$_9$ (**P7**) and (4*R*)-*Gndp*$_9$ (**P11**) with d(G_{12}.C_{12}) (blue triangle).

The peptide **P11** (4*R*)-*Gndp*$_9$ was also able to displace ethidium bromide from GC duplexes. However, a comparison of the quenching profiles of (4*S*)-*gndp*$_9$ (**P7**) and (4*R*)-*Gndp*$_9$ (**P11**) showed that the nature of interaction between the peptides and the double helical DNA was dependent on the stereochemistry of the guanidine substitutions at C4 position of the repeating 4(*R*/*S*) guanidinyl prolyl residues on a polyproline scaffold (Figure 3.21B).

These observations suggest that guanidinylprolyl polypeptides can effectively bind to oligonucleotides, as expected for a cationic peptide. The differences in the CD spectral changes,

UV-Tm studies and ethidium bromide displacement profiles indicate that the peptides distinguish between oligonucleotides of CG base pairs and those with AT base pairs.

3.4 Summary

Introduction of hydrogen-bonding and electron withdrawing functional groups such as NH_2, and OH at C4 position had been shown to cause stereodependent changes to the conformational preference of the backbone.

- 4(*S*)-Aminoprolyl polypeptides show CD spectra that are typical of a β-sheet in TFE, but in aqueous buffer it adopts PP-II form. This solvent dependent conformational transition was absent in 4(*R*)-Aminoprolyl polypeptides.
- The propensity of the aminoprolyl polypeptides to form β-like conformation was found to increase with the length of the homo-oligomeric peptide (4*S*)-amp_n.
- Temperature dependent CD studies supported the involvement of interchain hydrogen bonding between peptide (4*S*)-amp_9.
- The 4(*R*/*S*)-aminoprolyl polypeptides were found to have stereodependent interactions with SDS micelles. In an aqueous solution of SDS, the conformational behavior of both (4*S*)-amp_9 and (4*R*)-Amp_9 similar below the cmc of SDS showing non-specific electrostatic interaction. Above cmc of SDS, (4*S*)-amp_9 adopted a β-like conformation, while (4*R*)-Amp_9 exhibited PP-II like CD spectra.
- Although guanidinylprolyl polypeptides were found to lack the ability to change their conformation in TFE, lipidation of the peptide was shown to destabilize the PP-II form in the presence of hydrophilic salts such as sodium sulphate and sodium phosphate. Thus,

the present work suggests ways to alter and hence control the backbone conformation of polyproline peptides.

- With C4(*S*)-NH_2 substitution, the peptide can be tuned from a left handed PP-II helix to a ribbon-like β-sheet in TFE and in the presence of SDS micelles. With C4(*S*)-guanidine substitution however, the backbone conformation can be altered by conjugation with lipid chain at the N-terminus of the peptide.
- Since polyprolines have been used as molecular rulers,[29] means to control the peptide backbone either by addition of external agents or by structural modifications could be useful to design nanodevices that respond to stimuli or to rationally guide self-assembly of molecules using a scaffold.
- As cationic peptides, guanidinylprolyl polypeptides could be useful as cell penetrating peptides or as DNA transfection agents, as was shown to be the case for guanidinoprolyl collagenous peptides reported from this lab.[30] The ability of the guanidinylprolyl polypeptides to selectively bind to oligocytosines and CG rich regions of DNA, revealed by the studies in this chapter further augments their potential.
- It also presents a scope for improving the utility of peptides based on polyproline scaffolds in these applications by controlling the conformational dynamics of the peptide backbone.

3.5 Experimental

The DNA and RNA oligonucleotides were obtained commercially from IDT (integrated DNA technologies). All other chemicals were of analytical grade.

3.5.1 Circular dichroism (CD) spectroscopy

CD spectrometric study was carried out on JASCO J-815 spectropolarimeter using cylindrical, jacketed quartz cell (10 mm path length), which was connected to Julabo-UC25 water circulator. For reproducible data, each set of spectra were measured using at least three individually prepared solutions. CD spectra were recorded using a spectral bandwidth of 1.0 nm at 25 °C with a time constant of 1 s and a step resolution of 1 nm. All the spectra were corrected for respective buffer condition and are typically averaged over 3-6 scans. A quartz cell with a path length of 1 mm was used with solutions containing approximately 0.25 mL (50 to 250 μM).

All peptides had same peptide concentration (50-250 μM) for CD measurements done in Na-phosphate buffer (pH 7.0). The data processing and curve fitting were performed using Origin 8.0 software. All spectra were collected at 25^{o} C with a 1 nm resolution and a scan rate of 50 nm/min. Spectra are the averages of 3-6 scans.

4.5.2 Fluorescence Spectroscopy

Fluorescence measurements were recorded ethidium bromide displacement assay for peptide **P7** and **P10** using Horiba Jobin Yvon Fluorolog 3 spectrophotometer. The samples for fluorescence spectra were prepared by mixing calculated amounts of polyproline peptides in sodium phosphate buffer (pH 7.0, 10 mM). The prepared samples were used to record fluorescence

spectra in a quartz cell (Hellma, path length 1.0 cm) at ambient temperature. The concentration of the DNA duplexes were 2 μM. The concentration of ethidium bromide was fixed at 13 μM.

4.5.3 UV-Tm measurements

UV-melting experiments were carried out on Varian Cary 300 UVspectrophotometer equipped with a Peltier temperature programmer and Julabo water circulator. The samples for Tm measurements were prepared at 2 μM concentration of each DNA strand (500 μL of 10 mM phosphate buffer, pH 7.2 and 10 mM NaCl), were mixed together in stoichiometric amounts of 1:1 and annealed at 90 oC for 3 min and cooled to room temperature over 8 hours. The peptide of appropriate concentrations from mixed and incubated at room temperature for 1 hour and the measurements were carried out. The samples were transferred to quartz cell, sealed with Teflon stopper and the optical density (OD) was recorded at 260 nm with a rate of 1.0^{o} C/min temperature increment from 16^{o} C to 85^{o} C. The normalized absorbance at 260 nm was plotted as a function of the temperature and the *Tm* was determined from the first derivative plots with respect to temperature and is accurate to ± 0.5^{o} C. The data were processed using Origin 8.0.

3.6 References

1. Liu, Z.; Chen, K.; Ng, A.; Shi, Z.; Woody, R. W.; Kallenbach, N. R. Solvent Dependence of PII Conformation in Model Alanine Peptides. *J. Am. Chem. Soc.* **2004**, *126*, 15141-15150.

2. Drozdov, A. N.; Grossfield, A.; Pappu, R. V. Role of Solvent in Determining Conformational Preferences of Alanine Dipeptide in Water. *J. Am. Chem. Soc.* **2004**, *126*, 2574-2581.

3. Prabhu, N.; Sharp, K. Protein−Solvent Interactions. *Chem. Rev.* **2006**, *106*, 1616−1623.

4. Li, W.; Qin, M.; Tie, Z.; Wang, Wei. Effects of Solvents on the Intrinsic Propensity of Peptide Backbone Conformations. *Phys Rev E* **2011**, *84*, 041933.

5. Sessions, R. B.; Thomas, G. L.; Parker, M. J. Water as a Conformational Editor in Protein Folding. *J. Mol. Biol.* **2004,** *343*, 1125–1133.

6. a) Raghuraman, H.; Chattopadhyay, A. Effect of Ionic Strength on Folding and Aggregation of the Hemolytic Peptide Melittin in Solution. *Biopolymers* **2006**, *83*, 111–121. b) Kriz, Z; Klusak, J; Kristofikova, Z; Koca, J. How Ionic Strength Affects the Conformational Behavior of Human and Rat Beta Amyloids – A Computational Study. *PLoS ONE* **2013**, 8, e62914.

7. a)Lee, C.; Sun, Y.; Huang, H. W. Membrane-Mediated Peptide Conformation Change from *α*-Monomers to *β*-Aggregates. *Biophysical Journal* **2010,** *98*, 2236–2245.b) Lear, J. D.; DeGrad, W. F. Membrane Binding and Conformational Properties of Peptides Representing the NH, Terminus of Influenza HA-2. *J. Biol. Chem.* **1987**, *262*, 6500-6505.

8. Jin, L.; Abrahams, J. P.; Skinner, R.; Petitou, M.; Pike, R. N.; Carrell, R. W. The Anticoagulant Activation of Antithrombin by Heparin. *Proc. Natl. Acad. Sci. U. S. A.* **1997**, *94*, 14683–14688.

9. a) Andrabi, M.; Mizuguchi, K.; Ahmad, S. Conformational Changes in DNA-Binding Proteins: Relationships with Precomplex Features and Contributions to Specificity and Stability. *Proteins* **2014**, *82*, 841-57. b) Johnson, N. P.; Lindstrom, J.; Baase, W. A.; Hippel, P. H. Double-Stranded DNA Templates can Induce α-helical Conformation in Peptides Containing Lysine and Alanine: Functional Implications for Leucine Zipper and Helix-loop-helix Transcription Factors. *Proc. Natl. Acad. Sci. USA* **1994**, *91*, 4840-4844.

10. Sonar, M. V.; Ganesh, K. N. Water-induced switching of β-structure to polyproline II conformation in the 4*S*-aminoproline polypeptide via H-bond rearrangement. *Org. Lett.* **2010***, 12*, 5390–5393.

11. Bansode, N. D.; Sonar, M. V.; Ganesh, K. N. A nanofiber assembly directed by the non-classical antiparallel β-structure from 4*S*-(OH) proline polypeptide. *Chem. Commun*. **2016**, *52*, 4884-4887.

12. Bansode, N. D.; Madhanagopal, B.; Sonar, M. V.; Ganesh, K. N. Stereodependent and solvent specific formation of unusual β-structure through side chain-backbone H-bonding in C4(*S*)-(NH_2/OH/NHCHO)-L-prolyl polypeptides. *Biopolymers* **2017**,*108*, e22981.

13. a) Woody, R. W. Circular Dichroism Spectrum of Peptides in the Poly(Pro)II Conformation. *J. Am. Chem. Soc.* **2009**, *131*, 8234–8245.b) Rabanal, F.; Ludevid, M. D.; Pons, M.; Giralt, E. CD the of Proline-Rich Polypeptides: Application to the Study of Repetitive Domain of Maize Glutelin-2. *Biopolymers* **1993**, *33*, 1019-1028. Bovey FA, Hood FP. Circular dichroism spectrum of poly-L-proline. *Biopolymers* **1967**, *5,* 325–326.

14. Greenfield, N.; Fasman, G. D. Computed Circular Dichroism Spectra for the Evaluation of Protein Conformation. *Biochemistry* **1969,** *8*, 4108–4116.

15. a) Zhong, H.; Carlson, H. A. Conformational Studies of Polyprolines *J. Chem. Theory Comput.* **2006**, *2,* 342-353. b) Cubellis, M. V.; Caillez, F.; Blundell, T. L.; Lovell, S. C. Properties of Polyproline II, a Secondary Structure Element Implicated in Protein–Protein Interactions. *Proteins: Struct., Funct., Bioinf.* **2005**, *58*, 880–892.

16. Rosen, M. J. Surfactants and Interfacial Phenomena, 3rd ed.; Wiley: Hoboken , NJ, 2004.

17. Tulumello, D. V.; Deber, C. M. SDS Micelles as a Membrane-Mimetic Environment for Transmembrane Segments. *Biochemistry*, 2009, *48*, 12096–12103.

18. Hong, Z.; Damodaran, K.; Asher, S. A. Sodium Dodecyl Sulfate Monomers Induce XAO Peptide Polyproline II to α- Helix Transition. *J. Phys. Chem. B* **2014**, *118*, 10565 −10575.

19. Walde, P.; Giuliani, A. M.; Boicelli, C. A.; Luisi, P. L. Phospholipid-Based Reverse Micelles. *Chem Phys Lipids.* **1990,** *53*, 265-288.

20. Sonar, M. V. Synthesis and Structural Studies of 4(*R*/ *S*)-Aminoproline Polypeptide and Collagen Mimetics. PhD Thesis, University of Pune, Nov 2011.

21. Crisma, M.; Fasman, G. D.; Balaram, H.; Balaram, P. Peptide Model for β-turns. *Int. J. Peptide Protein Res.* **1984**, *23*, 411-419.

22. Zhang, Y.; Cremer, P. S. Chemistry of Hofmeister Anions and Osmolytes. *Annu. Rev. Phys. Chem.* **2010,** *61*, 63–83.

23. Kumin, M.; Sonntag, L.; Wennemers, H. Azidoproline Containing Helices: Stabilization of the Polyproline II Structure by a Functionalizable Group. *J. Am. Chem. Soc.* **2007**, *129*, 466-467. B) Dobitz, S.; Aronoff, M. R.; Wennemers, H. Oligoprolines as Molecular Entities for Controlling Distance in Biological and Material Sciences. *Acc. Chem. Res.* **2017**, *50*, 2420-2428.

24. a) Nagel, Y. A.; Raschle, P. S.; Wennemers, H. Effect of Preorganized Charge-Display on the Cell-Penetrating Properties of Cationic Peptides. *Angew. Chem. Intl. Ed.* **2016**, *56*, 122-126.

b) Fillon, Y. A.; Anderson, J. P.; Chmielewski, J. Cell Penetrating Agents Based on a Polyproline Helix Scaffold. *J. Am. Chem. Soc.* **2005**, *127*, 11798-11803.

25. Akao, T.; Fukumoto, T.; Ihara, H.; Ito, A. Conformational Change in DNA Induced by Cationic Bilayer Membranes. *FEBS Lett.* **1996**, *391*, 215-218.

26. Mergny, J.; Lacroiz, L. Analysis of Thermal Melting Curves. *Oligonucleotides* **2003**, *13*, 515–537.

27. Woods, C. R.; Ishii, T.; Wu, B.; Bair, K.W.; Boger, D. L. Hairpin versus extended DNA binding of a substituted β-alanine linked polyamide. *J. Am. Chem. Soc.* **2002**, *124*, 2148-2152. b) Ham, Y.; Tse, W. C.; Boger, D. L. High-Resolution assessment of protein DNA binding affinity and selectivity utilizing a fluorescent intercalator displacement (FID) assay. *Bioorganic Med. Chem. Lett.* **2003**, *13*, 3805–3807.

28. Chiang, Y.; Lin, Y.; Horng, J. Stereoelectronic Effects on the Transition Barrier of Polyproline Conformational Interconversion. *Protein Sci.* **2009,** *18*, 1967—1977.

29. Schuler, B.; Lipman, E. A.; Steinbach, P. J.; Kumke, M.; Eaton, W. A. Polyproline and the "Spectroscopic Ruler" Revisited with Single-Molecule Fluorescence. *Proc. Natl. Acad. Sci. U. S. A.* **2005**, *102,* 2754-2759.

30. Nanda, M.; Ganesh, K. N. 4(*R*/*S*)-Guanidinylprolyl Collagen Peptides: On-Resin Synthesis, Complexation with Plasmid DNA, and the Role of Peptides in Enhancement of Transfection. *J. Org. Chem.* **2012**, *77*, 4131–4135.

Chapter 4

Self-Assembly Studies of 4(*R*/*S*)-Amino and Guanidino Proline Based Peptides

4.1 Introduction

Supramolecular assemblies of peptides have various properties that make them suitable for many technological applications including drug delivery,[1] electronics[2] and tissue regeneration.[3] The rich diversity of chemical functional groups available in the repertoire of building blocks consisting of both natural and synthetic amino acids allows for construction of nanostructures of a variety of morphologies with features and functionalities that could be tuned by rational design of the primary sequence of the peptide. The self-assembling peptides have been used to generate structures such as sphere,[4] fibrils,[5] sheets,[6] hollow vesicles,[7] nanotubes[8] and networks[9] etc. The frontier of the landscape of peptide based supramolecular assemblies continues to expand as the molecular details of morphogenesis involved in these processes emerge.[10]

The rational design of peptides to assemble into a defined morphology involves controlling various factors such as intermolecular hydrogen bonding between the peptide chains, hydrophobic effects, electrostatic, van der Waals and dipole-dipole interactions, imparted by both the side-chains and the peptide backbone.[11] Since the fundamental secondary structure of the peptides affects the multitude of these forces that act between the participating molecules, understanding the propensity of aminoacids to adopt one of the regular secondary structures is, therefore, quintessential in designing the peptides for self-assembly. Positioning aminoacids bearing hydrophobic (Val, Leu, Ile, Phe, Tyr, and Trp) or a charged sidechain (Glu, Asp, Lys, and Arg) at appropriate places in a primary sequence that adopts a particular secondary structure such as α-helix, β-sheet or PP-II helix, the amphipathicity of the resulting peptide could be tailored.[12]

Since β-structure involves intermolecular hydrogen bond between peptide strands, it is widely used in the self-assembling peptide motifs. By varying the pattern of charges and

hydrophobic nature of sidechains in the sequences, peptides have been designed to assemble into extended β- sheets.[13-14] The hydrophobic-hydrophilic balance in the monomeric peptides has been manipulated to effect self-assembly by incorporation of hydrophobic amino acid residues at specific positions in the sequence.[15]

Naturally occurring fibrillar plaques of amyloids have also been extensively studied to understand how β- sheets can be stacked together to produce stable fibrillar nanostructures. [16] In these plaques, the β-strands are stacked into nanofibers where the individual strands of the peptide lie perpendicular to the fiber axis. This gives rise to characteristic cross- β pattern in fibre diffraction studies. This pattern consists of two rings: one corresponding to an interplanar distance of 4.74 Å and another corresponding to 10-11 Å. Such an organization is mainly stabilized by hydrogen bonding interactions between the backbone amides of the peptides in plane. The β- sheet conformation is found to be necessary for fibrillogenesis in Aβ1–42 peptides. The process of fibrillogenesis proceeds through formation of protofilaments that are typically stacks of β- sheets measuring about 25-30 Å. Several protofilaments assemble together to form fibrils of 60-80 Å. For fibrillar morphology, β-hairpins have been used to promote self-organization of the β-strands into sheets. Such designs have led to fabrication of peptide based hydrogels.[17]

PP-II form is a left handed helix with 3 residues per turn. It has been used as a scaffold to position charged hydrophilic groups and hydrophobic groups at specific positions along the helix. Maize γ-zein protein consists of an amphiphilic proline rich sequence $(VHLPPP)_8$. This was modified by Giralt *et.al.*,[18] to produce an amphiphilic peptide $(ZXZPPP)_n$, where Z represents different hydrophobic aminoacid residues and X represents one of the three cationic amino acids, His, Lys and Arg. Through this design, they constructed peptides that carry three

facets – one cationic and two hydrophobic. These peptides were also found to assemble into fibrous morphologies. PP-II form is the characteristic feature of the abundant structural protein, collagen. Attempting to mimic the structural characteristics of natural collagen for various applications including tissue regeneration,[19] several design strategies have been adopted to produce morphologically well-defined hierarchical self-assembly of collagen mimetic peptides. These include (i) the use of metal ions to generate cage-like hollow structures by collageneous peptides bearing metal binding ligands,[20] (ii) use of electrostatic interactions between negatively and positively charged amino acid residues. Employing this strategy, a variety of morphologies such as nanofibers,[21] hydrogels,[22] and nanosheets[23] had been created by placing different amino acids in strategic positions along the peptide chains to induce favorable intermolecular salt bridges.

PP-II helix was used as a principal component in the design of peptide amphiphile based nanovesicles used for drug delivery. Lee *et.al*.,[24] used the PP-II form of polyproline as stiff "rod-coils" to separate a cell penetrating hydrophilic Tat peptide or oligoarginine and a hydrophobic alkyl tail. It was shown to be useful as a carrier for intracellular drug delivery, owing to its hollow hydrophilic interior and cationic exterior surface.

Polyproline peptides are amenable to modifications. 4-Substituted polyproline peptides provide an excellent opportunity to control spatial arrangement of different functional groups while keeping the backbone PP-II conformation of the backbone intact.[25] Such a scaffold has been used to organize perylenemonoimide moieites along the PP-II backbone at regular spatial intervals.[26] These peptides have been shown to assemble into fibres or into an exquisite molecular weave.[27]

In the context of the present study, peptide amphiphiles constructed by conjugation of fatty acids such as lauric acid, myristic acid and palmitic acid to hydroxyprolyl polypeptides containing C4(*S*)-hydroxy proline residues were found to assemble into long nanofibers in TFE.[28] In water however, they show irregular morphologies. The solvent dependent self-assembling nature of the peptides stems from their solvent-dependent conformational property, with the peptides adopting the β-sheet like structure only in TFE.

4.2 Objectives

The solvent and stereo-dependent conformational properties of aminoprolyl polypeptides were found to be similar to those of hydroxyprolyl polypeptides. However, the nature of the substituent at C4 position (OH/NH_2) was expected to influence the mode and the extent of intermolecular interactions necessary for the peptides to self-assemble. These two analogues of peptides offer a unique opportunity to study the effect of fine structural changes in the conformation caused by the differences of the chemical and electronic properties of the 4-substituents on the self-assembly of the peptides, while the backbone remains in the same overall secondary structure. In addition to these two substitutions, guanidinylprolyl polypeptide showed changes in conformation on lipidation at the N-terminus, which prompted investigations into their self-assembling behavior as well.

In this chapter, self-assembling properties of C4(*S*)-NH_2 substituted aminoprolyl polypeptides (**P1**-**P6**), and guanidnylprolyl polypeptides (**P7**-**P8**) were studied by imaging the morphology formed by these peptides under different conditions.

The specific objectives of this chapter include the following:

- Study the effect of solvent, peptide length and concentration on the morphology of the self-assembled structures formed by C4(*S*)-NH_2 substituted aminoprolyl polypeptides.
- Observe the changes in the morphology to elucidate the mechanism of formation of nanostructures.
- Examine the role of lipidation on the morphology of the 4-aminoprolyl polypeptides (**P4-P6**).
- Investigate the self-assembling properties of the non-lipidated 4-guanidinylprolyl polypeptide (**P7** and **P11**) and lipidated 4-guanidinylprolyl polypeptide **P8** in different solvents and conditions.

4.3 Results and Discussion

4.3.1 Aminoprolyl Polypeptides

The conformational studies of the peptide (4*S*)-amp_9 (**P3**) indicate that in TFE, 4-aminoprolyl polypeptides form β-sheet like conformation (β-structure), stabilized by intermolecular interactions. In order to examine the self-assembling properties of these peptides, the morphology of the particles and supramolecular organizations formed by the peptides were studied using field emission scanning electron microscopy (FESEM), atomic force microscopy (AFM) and dynamic light scattering (DLS). Figure 4.1 shows the peptides used in this investigation.

The samples for FE-SEM analysis were prepared by dissolving the peptide in the appropriate solvent and incubating the peptide solution for a period of 12 hours at room temperature.

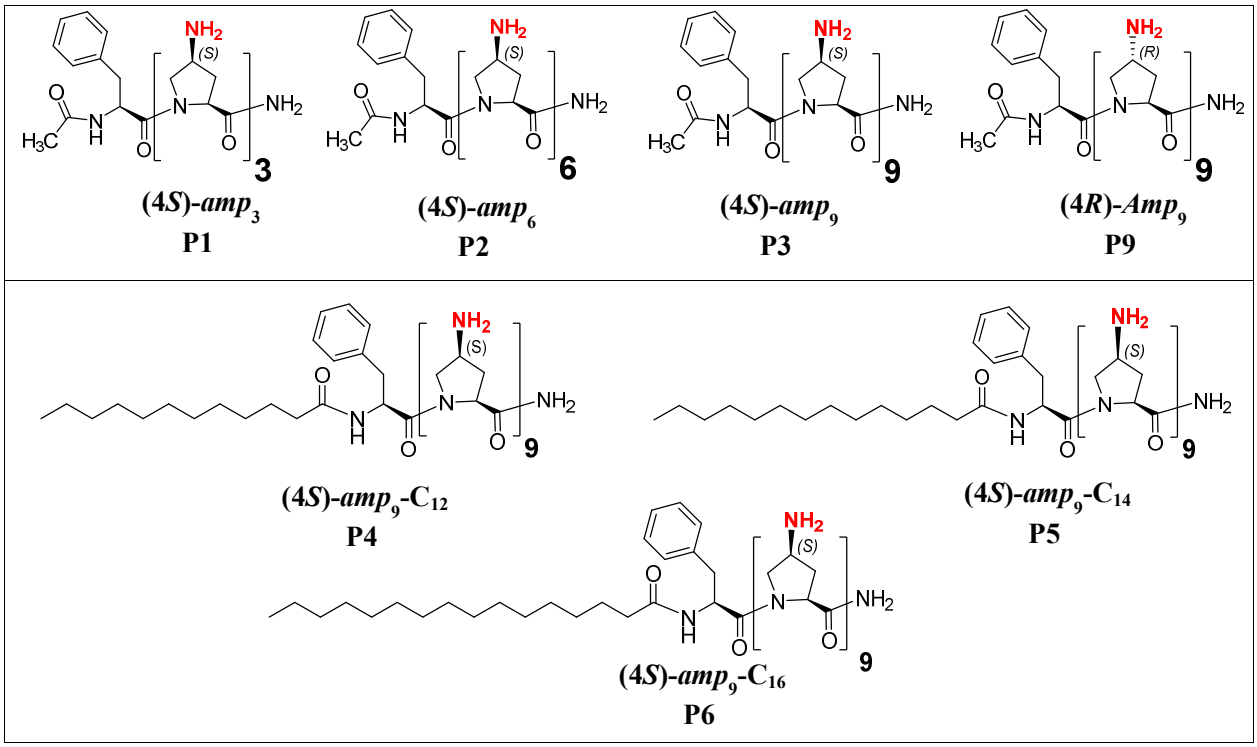


Figure 4.1: Structure of 4(*R*/*S*)-Aminoprolyl polypeptides **P1-P6 and P9**

An aliquot (2 µL) of the peptide solution was taken and dropped on the polished surface of a clean silicon wafer. The solvent was allowed to evaporate from the peptide solution under ambient conditions for about 12 hours and was subsequently dried under high-vacuum for about 4 hours. The dried peptide film on the surface of the silicon wafer was sputter-coated with gold before imaging. For AFM analysis, the samples were prepared the same way, except that the substrate used for drop-casting the peptide solution was either silicon wafer or freshly cleaved mica. The dried film of peptide was imaged without any sputter coating as was done for SEM studies.

4.3.1a *Solvent Dependent Self-assembly of (4S)-amp$_9$ (P3)*

The peptide (4*S*)-*amp*$_9$ (**P3**) shows distinct conformations in water and TFE. In water, the peptide adopts PP-II, and in TFE, it shows β-sheet like conformation. Anticipating this solvent dependent conformational property to reflect on the self-assembling properties of the peptides,

the morphology of the structures formed by the peptides taken in water and TFE was examined under FE-SEM (Figure 4.2).

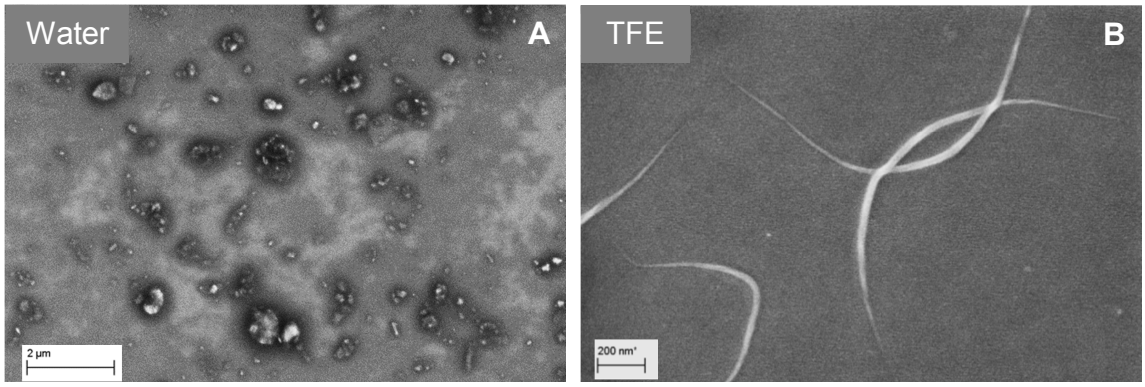


Figure 4.2: FE-SEM images of morphologies formed by peptide (4*S*)-*amp*$_9$ (**P3**) in water (A) and in TFE (B).

In water, 200 µM solution of the peptide was found to show no regular structures (Figure 4.2A). Only aggregates of random shapes and form were observed. When the peptide was taken in TFE, it was found to self-assemble into fibrous structures (Figure 4.2B). The individual nanofibers were found to be about 20 nm in diameter in the middle. The mass of the fibres was found to be at its maximum at the middle and it progressively tapered down to the two extremities. The nanofibers also had a gentle left handed twist (Figure 4.3). The helical pitch was around 80 nm for fibrils with a diameter of 15-20 nm. The helical twist, measured by the angle formed by the screw edge to the longitudinal axis was about 37^o.The individual fibrils were found to assemble into larger fibres of up to 60 nm in width and several micrometers in length. Akin to protofilaments of amyloid fibres, these fibrils intertwine around each other to form longer and thicker fibres and bundles of fibres (Figure 4.3B). Not only is the helical handedness of the smaller fibrils was retained during this hierarchical assembly, it also appeared to be more strongly pronounced.

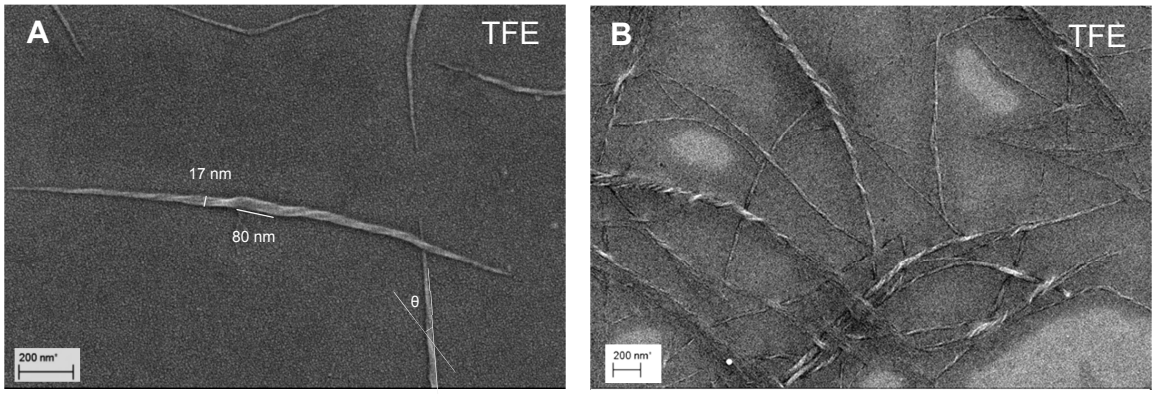


Figure 4.3: FE-SEM images of morphologies formed by peptide (4*S*)-*amp*$_9$ (**P3**) in TFE showing individual fibre (A) and bundles of fibres(B) with left handed twists.

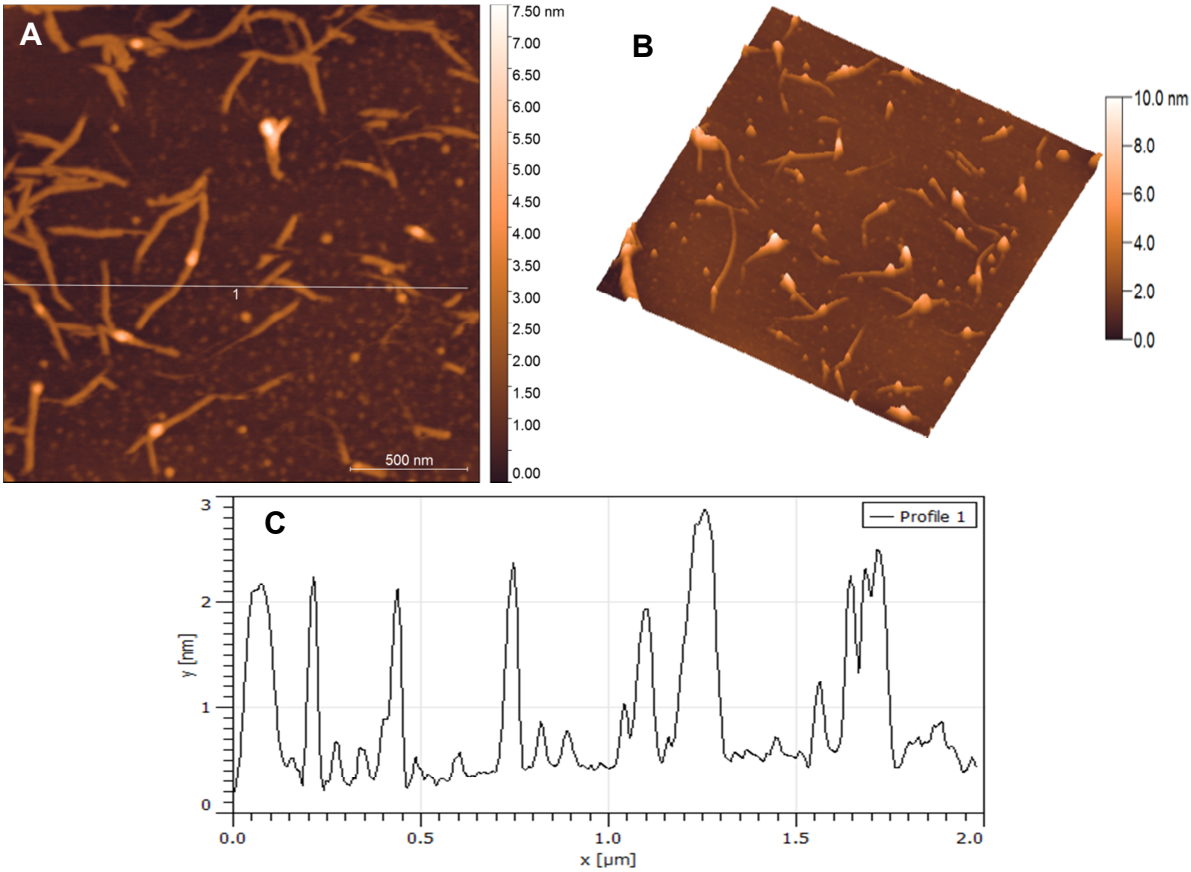


Figure 4.4: AFM images of nanofibres formed by peptide (4*S*)-*amp*$_9$ (**P3**) in TFE. (A) A cluster of nanofibers. (B) 3D view of the fibres at a different region. (C) Line profile extracted from (A) showing height of individual fibre.

The fibres were also characterized with AFM by drop casting the TFE solution of the peptide (4*S*)-amp_9 (**P3**) on a freshly cleaved mica surface. The morphology obtained was similar to the one found in SEM analysis (Figure 4.4). Clusters of nanofibrils of height about 2-3 nm were observed, which indicates that the fibrils are composed of linear stacks of the polypeptides (Figure 4.4C). The AFM micrographs also revealed that some of the fibres have particles bound on them, which was apparent in the 3D view (Figure 4.4B).

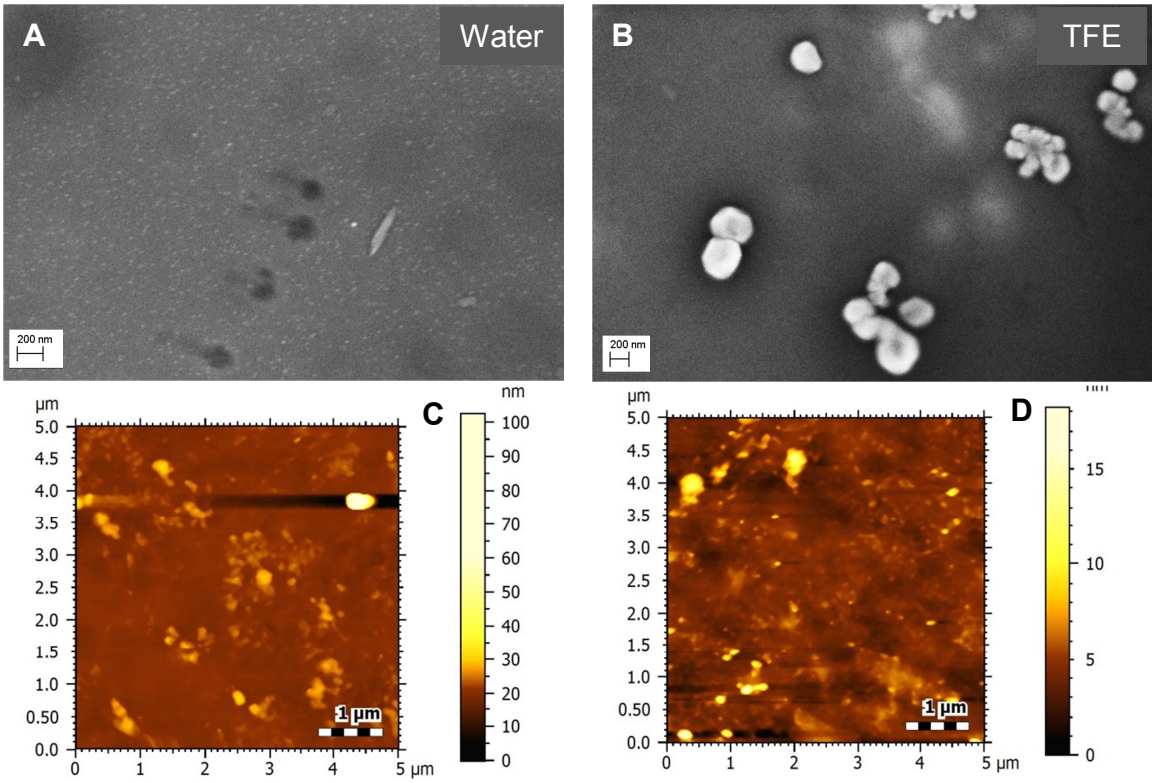


Figure 4.5: FE-SEM images of morphologies formed by peptide (4*R*)-Amp_9 (**P9**) in water (A) and in TFE (B) and the AFM images of morphologies formed by the peptide in water (C) and (D).

The peptide (4*R*)-Amp_9 (**P9**), which showed no conformational change with solvent and adopted PP-II form in both water and TFE, was found to show no such self-assembling properties. They formed irregular particles with random shapes in both water and TFE (Figure 4.5). This underlines the role of secondary structure of the peptide in determining the morphology of the supramolecular assemblies in these peptides.

4.3.1b *Effect of concentration on morphology in TFE*

In order to check the effect of concentration of the peptide (4*S*)-*amp*$_9$ (**P3**) on the morphology of their assemblies, TFE solutions of different concentrations (2 μM, 50 μM, 100 μM, 150 μM, 200 μM and 2 mM) were studied (Figure 4.6).

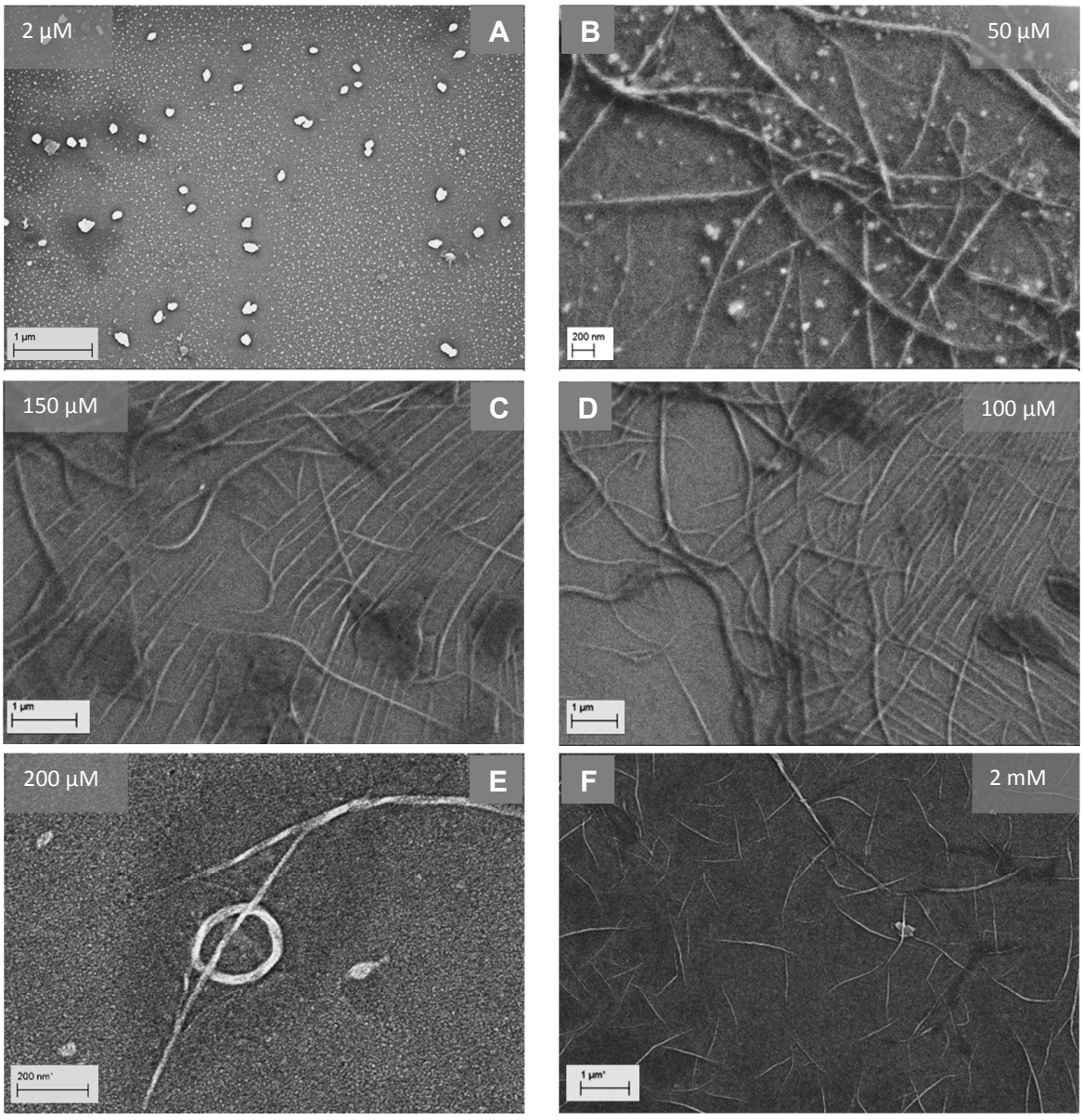


Figure 4.6: FE-SEM images of morphologies formed by peptide (4*S*)-*amp*$_9$ (**P3**) in TFE at different concentrations: 2 μM (A); 50 μM (B); 100 μM (C); 150 μM (D); 200 μM (E); 2 mM (F) imaged after an incubation period of 12 hours..

At a low concentration of 2 mM, the peptide was unable to assemble into nanofibers. Instead, they were found to form spherical or elongated structures of less than 100 nm in width. At the concentration of 50 μM, both fibres and spherical particles were found. With concentrations increasing from 100 μM to 200 μM, presence of nanofibres become more prominent. At 2 mM, fibrils were well separated and were often found to be isolated and of uniform length (Figure 4.6F). The images reveal progressively increased intensity of self-assembling process, with increase in concentration.

4.3.1c *Time Dependent Change in Morphology of (4S)-amp*$_9$

The growth of the nanofibers of peptide (4*S*)-*amp*$_9$ (**P3**) was studied by monitoring the changes in the morphology of the peptide under FE-SEM at different time intervals from the time of preparation of the solution. A solution of 200 μM concentration of the peptide was prepared in TFE. The solution was left to stand undisturbed at room temperature. Aliquots of 2 μL were drawn from the peptide solution at time points 1 hour, 6 hours and 12 hours of preparing the solution, and it was drop-cast on silicon wafers and dried for a period of at least 16 hours as mentioned above.

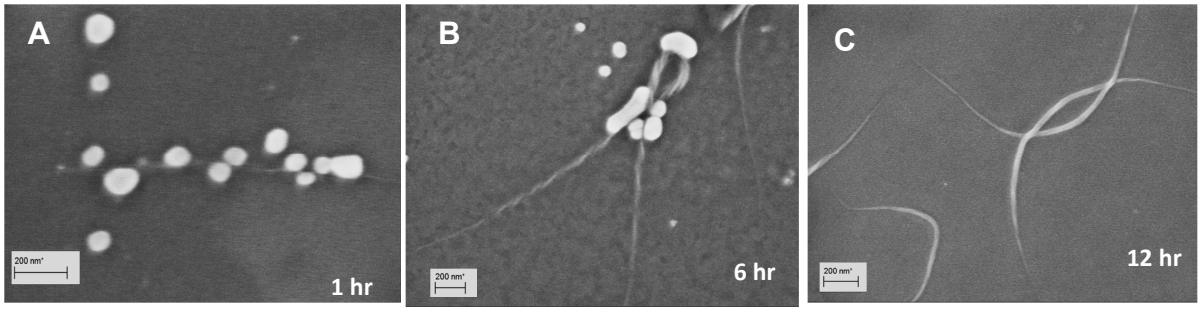


Figure 4.7: Growth of nanofibres. FE-SEM images of morphologies formed by peptide (4*S*)-*amp*$_9$ (**P3**) in TFE at different incubation time: 1 hr (A); 6 hr (B); 12 hr (C). Concentration of the peptide was 200 μM

After incubation of only 1 hour, peptide had formed only particles of 20-100 nm in size (Figure 4.7A). Most of these were spherical and some were irregular in shape. In some cases, the particles seemed to be aligned along thin fibrous structures. Within 6 hours, nanofibers had formed along such an axis. However, they still had some spherical particles bound on them. The 12 hours sample showed fully formed nanofibers (Figure 4.7C).

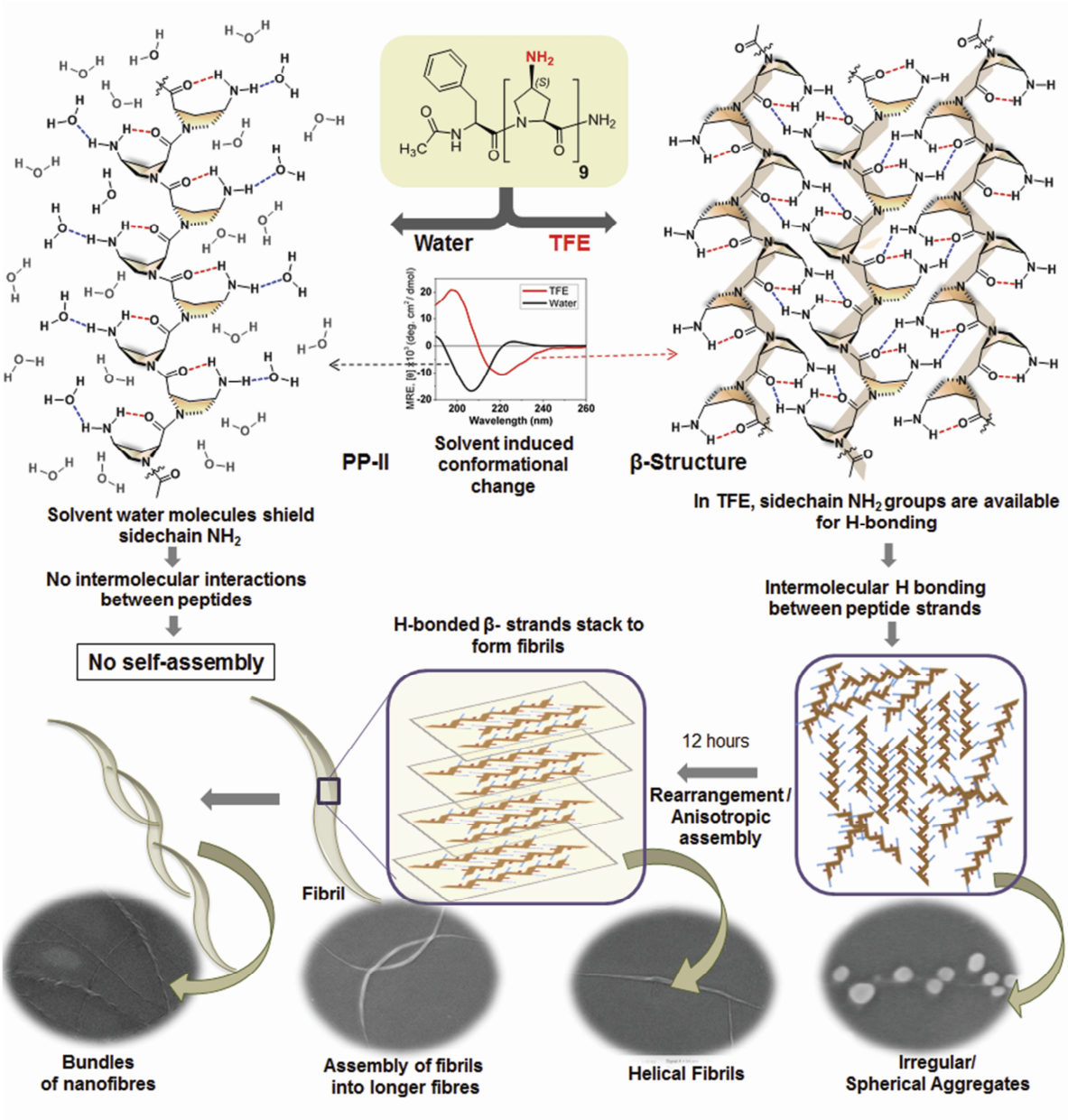


Figure 4.8: Schematic representation of self-assembly (4*S*)-*amp*$_9$ (**P3**)

The time-dependent SEM imaging studies showed that the peptide (4*S*)-amp_9 (**P3**) undergoes a morphological transformation involving the mass transfer from irregular aggregates to ordered helical nanofibers over a period of 12 hours (Figure 4.8). The nanofibers at that stage was already helical, indicating that the development of helical twists of the fibres were synchronous with fibers spinning out of the spherical particles, rather than developing it later.

Although TFE is generally found to stabilize α-helix in peptides, in the case of (4*S*)-amp_9 (**P3**), it is found to promote β-structure and facilitate the self-assembly of the peptides into nanofibers. The plausible role of TFE in the conformational change and self-assembly of (4*S*)-amp_9 (**P3**) is shown in Figure 4.8. In aqueous solutions, the sidechain NH_2 of peptide (4*S*)-amp_9 (**P3**), is likely to be solvated with water molecules. This prevents any substantial intermolecular H-bonding interactions between the peptide strands which would favour PP-II form. In a dehydrating solvent such as TFE, sidechain NH_2 groups might be available for intermolecular H-bonding with backbone CO of other peptide chains. This facilitates the peptides to adopt β-like structure.

4.3.1d *Effect of Peptide Length on Morphology of (4S)-*amp_n

Since the conformational studies of the peptide (4*S*)-amp_n showed an increasing propensity for β-sheet structure with increasing peptide length (as shown in Chapter 3), the morphology of the shorter peptides (4*S*)-amp_3 (**P1**), and (4*S*)-amp_6 (**P2**) with three and six residues of (4*S*)-*amp* respectively, were compared with the nanofibers of (4*S*)-amp_9 (**P3**).

In water, the peptides (4*S*)-amp_3 (**P1**) and (4*S*)-amp_6 (**P2**) were found to have no regular structures (Figure 4.9). In TFE, the peptide (4*S*)-amp_3 (**P1**) formed ellipsoidal particles of about 200 nm in size. (4*S*)-amp_6 (**P2**) showed spherical-to-irregular shaped particles both in water and

in TFE. These indicate that for the formation of extended fibrous aggregates, lengths of 3 and 6 residues are insufficient and that a minimum of nonamer is required for the peptide to produce stable intermolecular interactions necessary to generate nanofibers.

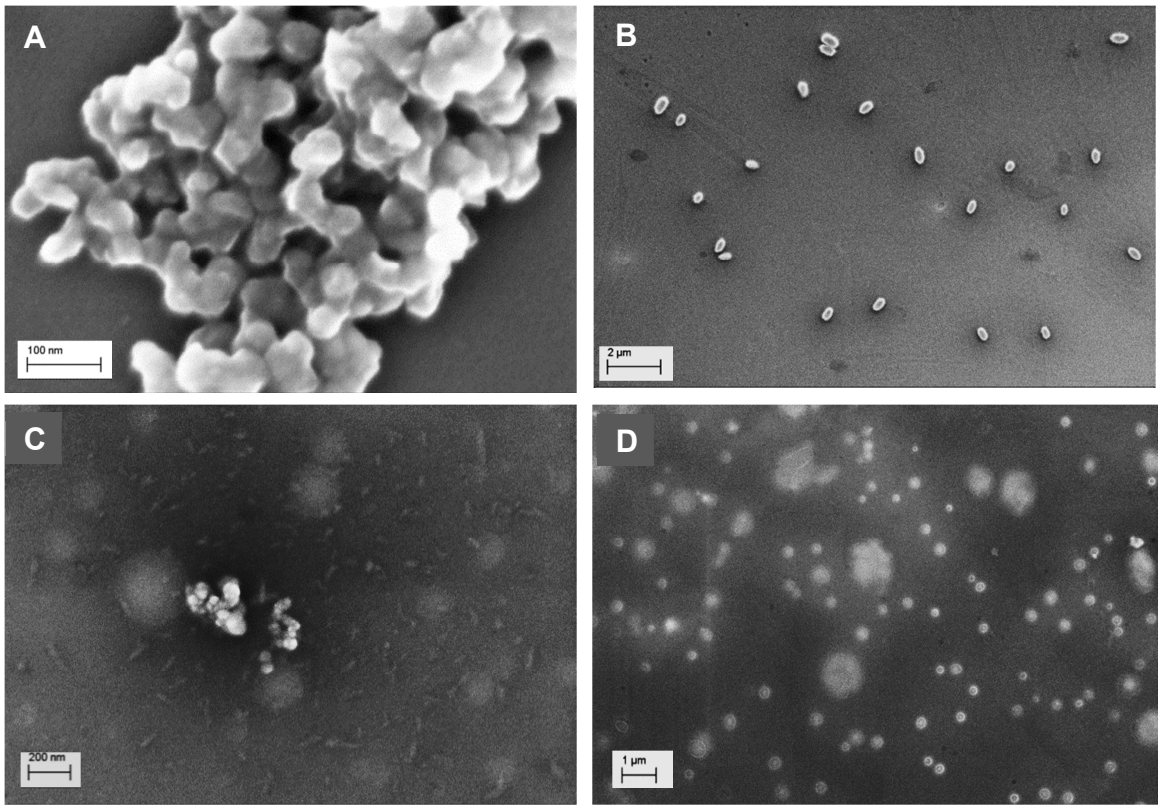


Figure 4.9: FE-SEM images of morphologies formed by peptides (4*S*)-amp_3 (**P1**) in water (A) and in TFE (B), and peptide (4*S*)-amp_6 (**P2**) in water (C) and in TFE (D).

The TFE solutions of these peptides were also subjected to dynamic light scattering to track the formation of aggregates. The size distribution profiles of the peptides (4*S*)-amp_3 (**P1**), and (4*S*)-amp_6 (**P2**) centered around 3 nm with the former producing a slightly narrower distribution as compared to the latter (Figure 4.10). The peptide (4*S*)-amp_9 (**P3**) on the other hand, showed a narrow distribution of particles around 500 nm. These also indicate that the peptides of lengths 3 and 6 do not form nanofibers and only at a length of 9 residues, the peptides self-assemble into fibrillar structures. The length of the peptide chain was therefore found to be

an important factor in determining the morphology of the assemblies formed by the aminoprolyl polypeptides of (4*S*)-*amp*$_n$. Even though the conformation of all the three peptides in the study adopted β-sheet like conformation in CD, the requirement for a length of nine residues established the role of intermolecular interactions for the formation of stable fibrillar supramolecular architectures.

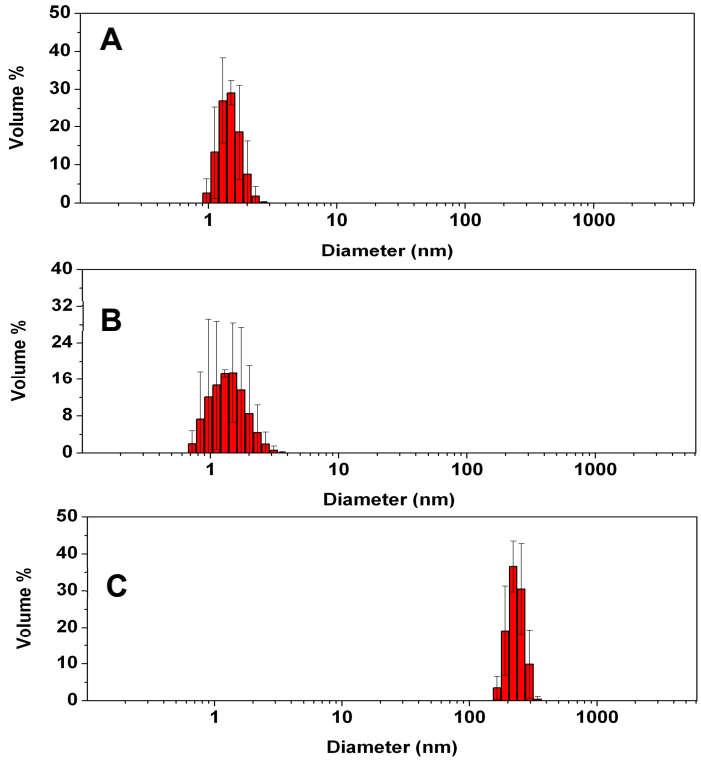


Figure 4.10: DLS size distribution in TFE measured for peptides (4*S*)-*amp*$_3$(**P1**) (A); (4*S*)-*amp*$_6$(**P2**) (B); (4*S*)-*amp*$_9$(**P3**) (C).

4.3.1e *Effect of Lipidation on Aminoprolyl Polypeptides*

Hydrophobic-hydrophilic balance is critical for self-assembly of molecules. In case of peptides, conjugation of fatty acids is one of the widely used strategies to fine-tune amphiphilicity and to control self-assembly of the peptides.[28,29] To improve the supramolecular assembly of the cationic peptides (4*S*)-*amp*$_9$ (**P3**), fatty acids with different alkyl chains (C_{12}, C_{14},

C_{16}) were coupled at the N-terminus. Dried films of these peptides were prepared with water and TFE as solvents as described above and studied under FE-SEM (Figure 4.11).

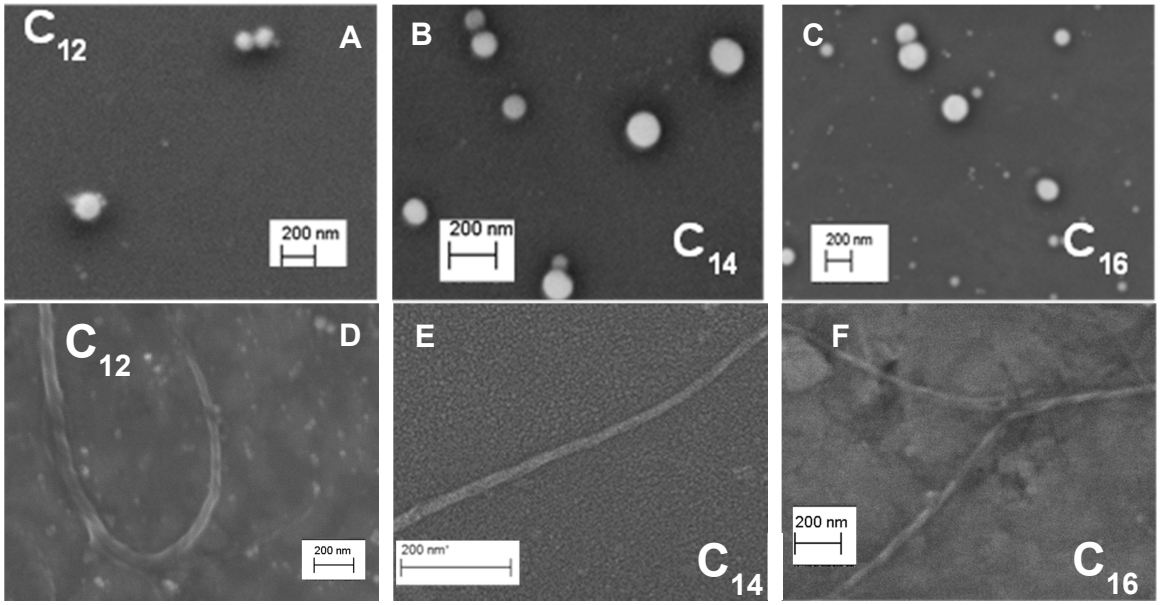


Figure 4.11: FESEM images of peptides (4*S*)-*amp*$_9$–C_{12} (**P4**) in water (A) and TFE (D); (4*S*)-*amp*$_9$–C_{14} (**P5**) in water (B) and TFE (E); (4*S*)-*amp*$_9$–C_{16} (**P6**) in water (C) and TFE (F).

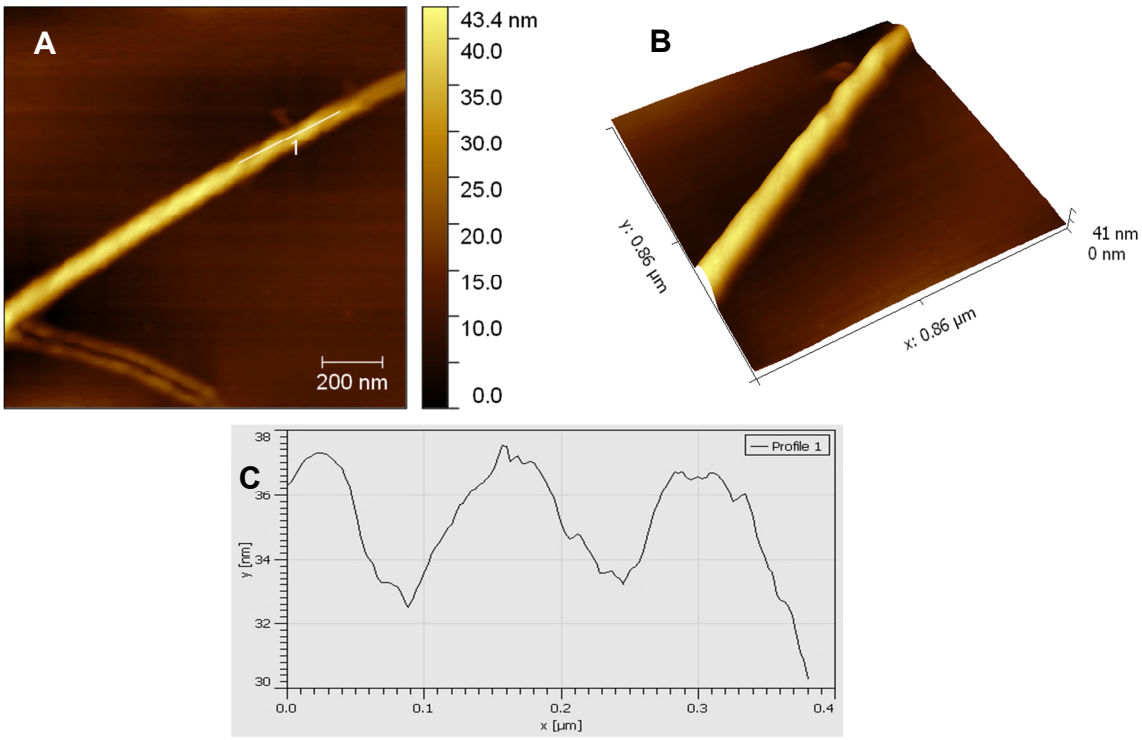


Figure 4.12: AFM Images of peptides (4*S*)-*amp*$_9$–C_{14} (**P5**) in TFE (A). 3D view of the same fibre showing grooves (B). Line profile showing the depth of the groove across the fibres (C).

In water, all three lipidated peptides showed well-formed spherical particles. The size of the particles was around 50 nm to 200 nm in diameter. In TFE, the peptides showed nanofibres as seen with the non-lipidated peptides. These fibres were also found to have a left handed helical twist. The nanofibers of myristoylated peptide (4*S*)-*amp*$_9$–C_{14} (**P5**) were characterized by AFM (Figure 4.12). The fibrillar bundles were found to have a height of about 30 nm. The grooves were shallow and had a depth of about 3 nm (Figure 4.12). Thus, lipidation did not produce any significant change to the self-assembling property of the peptide.

4.3.1f *Thioflavin T Fluorescent Assay of Nanofibres of (4S)-amp*$_9$ *(**P3**)*

Thioflavin T (ThT) is a fluorescent dye, which is known to show an enhanced fluorescent emission on binding to peptide aggregates. It has been widely used to stain cross-β aggregates of amyloid fibres. [30]

In TFE, the peptide (4*S*)-*amp*$_9$ (**P3**) adopts β sheet-like conformation, as evident from the CD studies, and assembles into nanofibres with a left-handed helical twist.[31] The fibrils wind around each other to form larger bundles of many microns in length. Since these characteristics of 4(*S*)-aminoprolyl polypeptide are similar to those of many of the well-known amyloid fibres such as the antiparallel cross-β arrangement of Aβ-peptides,[32] these peptides were assayed with Thioflavin T to ascertain whether the 4(*S*)-aminoprolyl polypeptides also are able to produce an enhancement of fluorescent emission of the dye.

A solution of the peptide (4*S*)-*amp*$_9$ (**P3**) in TFE or 10 mM phosphate buffered saline was incubated with the dye ThT for 1 hour under ambient conditions and the fluorescence emission spectra (excitation at 420 nm or 440 nm) of the peptide solutions were recorded and compared with the fluorescence emission of the dye without the peptide in the respective solvents. In buffer, where the peptide showed PP-II conformation and formed no regular structure as

observed in FE-SEM, the intensity of fluorescence emission was almost negligible. The excitation spectra for the sample also showed no characteristic peak (Figure 4.13A). However, in TFE, the peptide assemblies were able to produce an almost 8-fold enhancement in fluorescence emission as compared to the one recorded in buffer (Figure 4.13B).

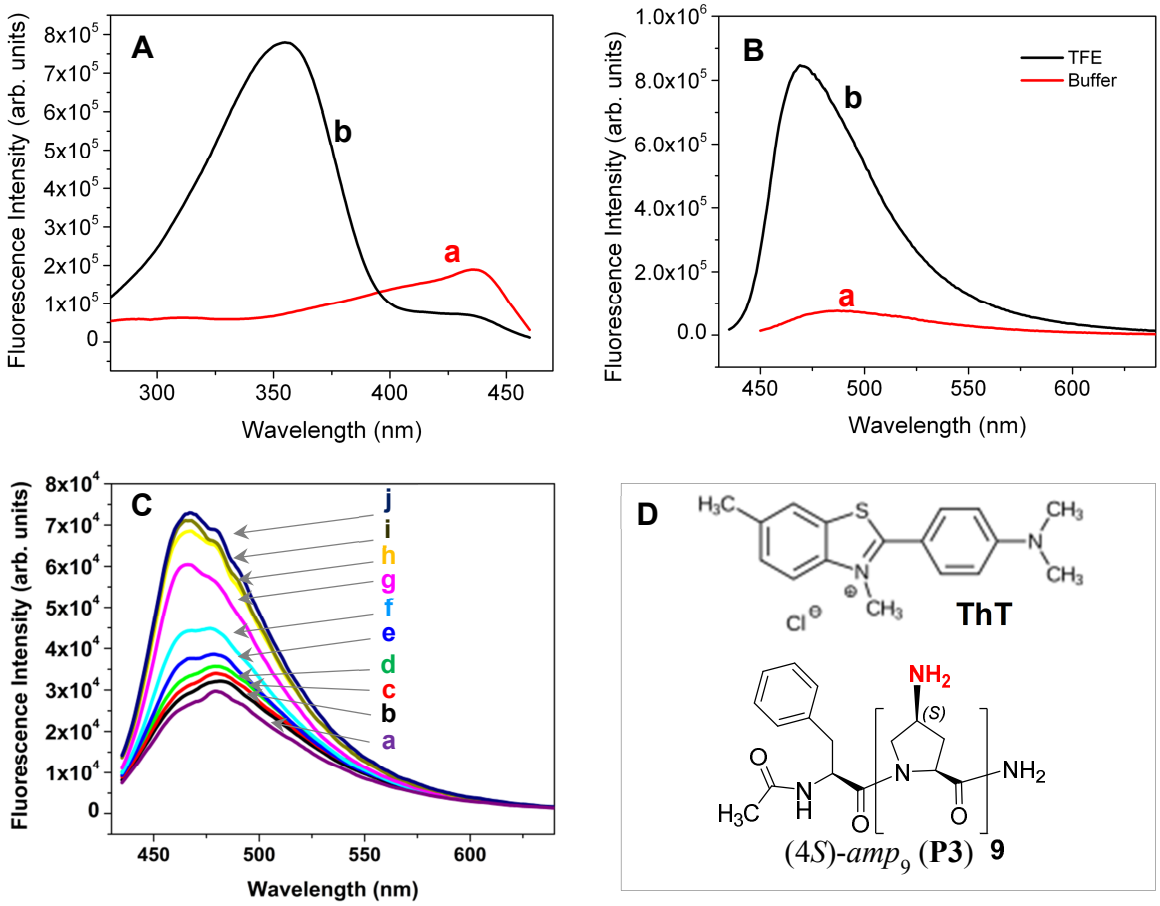


Figure 4.13: Thioflavin-T assay of peptide (4*S*)-*amp*$_9$ **(P3).** (A) Excitation spectra of ThT in the presence of peptide (4*S*)-*amp*$_9$ **(P3)** in buffer (trace **a**) and in TFE (trace **b**). (B) Emission spectra of ThT in the presence of peptide **P3** in buffer (trace **a**) and in TFE (trace **b**). (C) Enhancement of fluorescence of ThT in TFE with increasing concentration of peptides: 0 µM (trace **a**); 2 µM (trace **b**); 4 µM (trace **c**); 6 µM (trace **d**); 8 µM (trace **e**); 10 µM (trace **f**); 50 µM (trace **g**); 100 µM (trace **h**);150 µM (trace **i**); 200 µM (trace **j**). (D) Molecular structure of compounds used in this study.

The excitation spectra also showed a sharp band at 350 nm and suppression of the weak band at 420 nm. These are characteristics of the dye binding to the peptide assemblies.[30] The

intensity of the fluorescence emission of the dye was found to increase when the concentration of the peptide was increased from 2 μM to 200 μM (Figure 4.13C). These results suggest that the packing of the molecules in the assemblies forming the fibres are likely to be similar to the ones found in amyloid fibres.

4.3.2 Guanidinylprolyl Polypeptides

The gunidino peptides (4*S*)-*gndp*$_9$ (**P7**) and (4*R*)-*Gndp*$_9$ (**P11**) were designed to be highly cationic, since such peptides may have applications in DNA transfection as membrane perturbing agents and as cell penetrating peptides or antimicrobial peptides. A superior self-assembling property can be beneficial for the peptides in the context of these applications. Figure 4.14 shows the guanidinyl prolyl polypeptides used in this investigation.

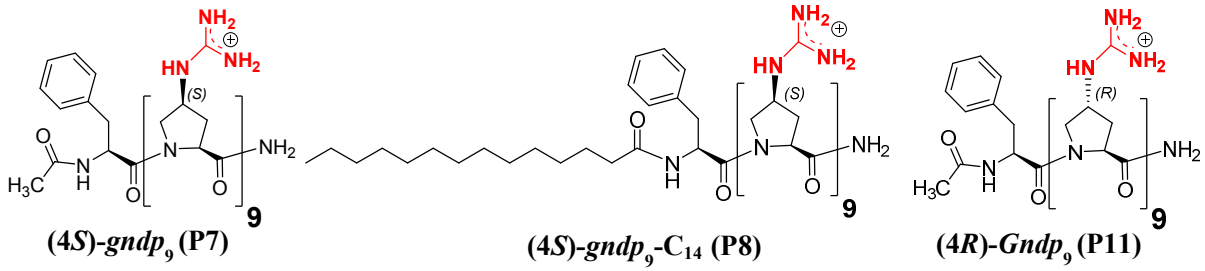


Figure 4.14: Structure of 4(*R*/*S*)-Guanidinylprolyl polypeptides **P7-P8 and P11**

4.3.2a *Self-assembly of 4-Guanidinylprolyl Polypeptides*

In an aqueous solution of 200 μM of the 4-guanidinylprolyl Polypeptides, only irregular aggregates were observed in the SEM micrographs. The same was the case in TFE solution of the peptide as well. The peptides (4*S*)-*gndp*$_9$ **(P7)** did not show any regular morphology in water or TFE (Figure 4.15). When the peptide (4*R*)-Gndp$_9$ (**P11**) was examined under the FESEM, at a of concentration 200 μM, similar morphologies were seen in both water and TFE. These were irrergular to spherical shaped particles of about 50 nm in size and they found to be clustered together as large aggregates (Figure 4.15 C-D).

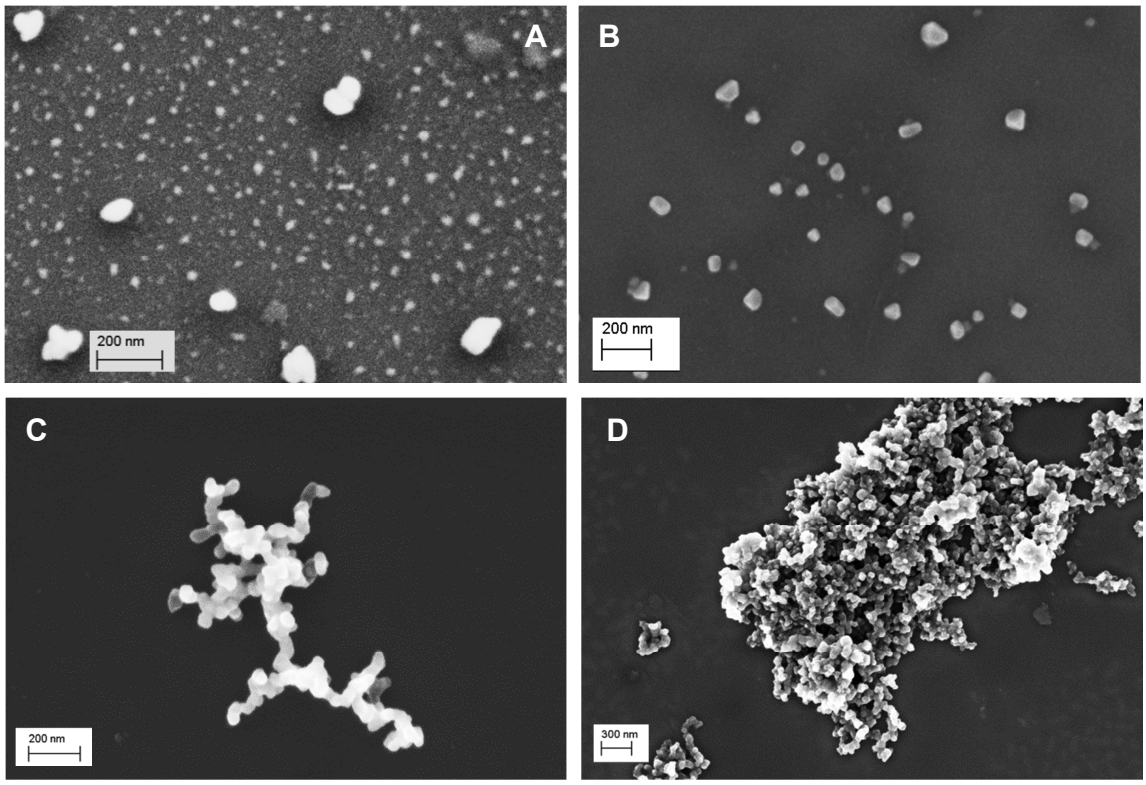


Figure 4.15: FESEM images of peptides(4*S*)-$gndp_9$ (**P7)** in water (A), and in TFE (B) and of peptide (4*R*)-$Gndp_9$ (**P11**) in water (C), and in TFE (D)

In case of guanidinylprolyl polypeptides, there was no change in the morphology of the particles both in size and in shape with the nature of the solvent used to make the solution. It needs to be noted that these peptides adopted PP-II form in both buffer and TFE as seen in their circular dichroism spectra (Chapter 3).

4.3.2b *Effect of Lipidation on Morphology of Guanidinylprolyl Polypeptides*

N-terminal lipidation of guanidinylprolyl polypeptide (4*S*)-$gndp_9$ (**P7**) produced changes in the secondary structures of the peptide as seen in CD studies (Section 3.3.2c in Chapter 3). Since introduction of hydrophobic alkyl chain usually promotes self-assembly of the peptides, morphology formed by the lipidated peptide (4*S*)-$gndp_9$–C_{14} (**P8**) in water and TFE were studied using FESEM and AFM.

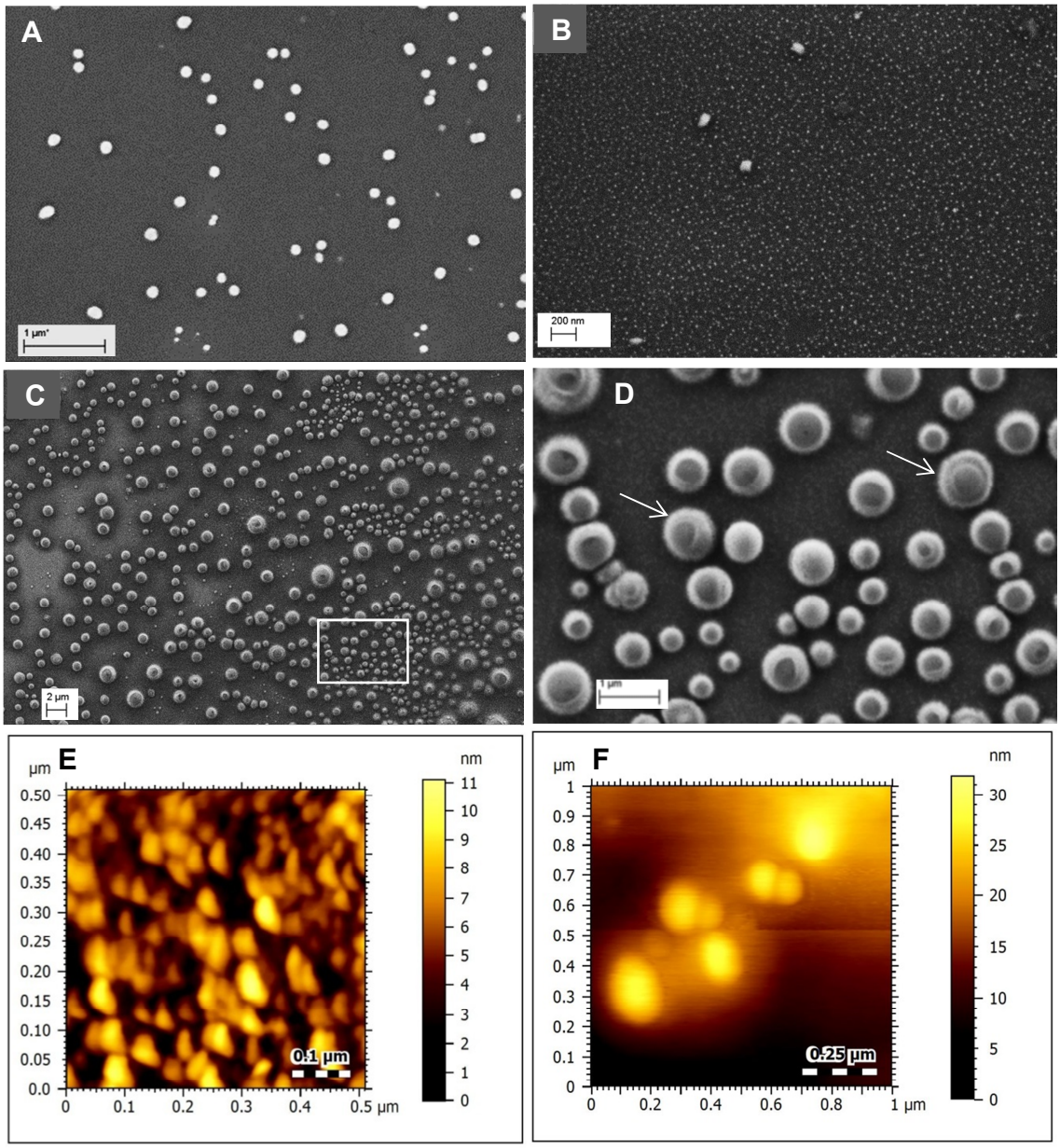


Figure 4.16: FESEM images of peptides (4*S*)-*gndp*$_9$–C_{14} (**P8**) in water (A), in TFE (B), in 10 mM phoshphate buffer containing 10 mM NaCl (C). D) Magnified region of the area marked by white rectangle in (C). AFM images of a cluster of spheres of (4*S*)-*gndp*$_9$–C_{14} (**P8**) in 10 mM phoshphate buffer containing 10 mM NaCl (E), and a few isolated spheres under the same condition (F).

The peptide showed changes in the conformation depending on the counterion present in the solution. Therefore, the morphologies in water were compared with those formed in 10 mM

phosphate buffer. In water, the peptide amphiphiles at a concentration of 500 μM formed spherical particles of about 50 nm in diameter (Figure 4.16). In TFE, no discernible morphology was observed and aggregates smaller than 20 nm were found scattered on the silicon substrate.

In 10 mM phosphate buffer, the peptide showed similarly shaped spherical particles. These spheres were about 50 nm to 400 nm in diameter. The SEM micrographs suggest that the particles had a layered architecture. The distinct layers of the peptide material were apparent upon closer examination of the particles (Figure 4.16D). AFM images obtained from these samples also showed spherical morphology (Figure 4.16E-F).

4.4 Summary

In nature, proline rich regions are used to prevent fibrillation of proteins. Introduction of a stretch of polyprolines in protein was found to reduce the tendency of the protein to form β sheets and thereby reduce the chances of their aggregation into amyloidogenic fibrils.[32] Interestingly, while unsubstituted polyprolines adopt the PP-II form which prevents fibrillation, the present work shows that C4(*S*)-NH_2 substitution in TFE can instead produce nanofibers similar to those formed by misfolded amyloid proteins.[16]

The morphological features of nanofibers formed by peptide (4*S*)-amp_9 (**P3**) were studied using FE-SEM and AFM to derive information about its dimensions and their growth behavior.

- The peptide was found to have superior self-assembling properties only in TFE. The peptide (4*S*)-amp_9 (**P3**) assembled spherical particles which transformed into helical fibres with left handed twist in 12 hours. The fibrils formed were about 2 – 3 nm in height and showed a gentle left-handed helical twist.

- These fibrils intertwined to form larger left handed helical fibres and bundles of about 30 nm to 60 nm in diameter.
- The formation of mature fibres was observed only when the peptide had at least 9 residues of 4(*S*)-aminoproline units suggesting the involvement of interchain hydrogen-bonding interactions in stabilizing the extended structures formed by the peptides in TFE.[33]

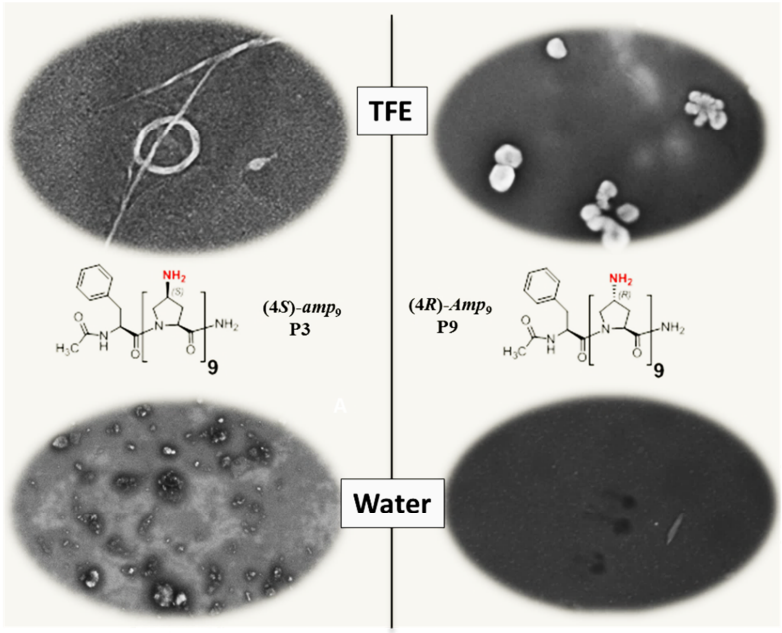


Figure 4.17: Stereo-dependent self-assembly 4(*R*/*S*)-aminoproline polypeptides in water and TFE.

- N-terminal lipidation of the aminoprolyl polypeptide (4*S*)-amp_9 (**P3**) did not alter the morphological properties of the peptide in TFE.
- Guanidinylprolyl polypeptides (4*S*)-$gndp_9$ (**P7**) and (4*R*)-$Gndp_9$ (**P11**) did not show solvent dependent conformational change and adopted PP-II in both water and TFE.
- The myristoylated peptide (4*S*)-$gndp_9$–C_{14} (**P8**) produced spherical particles with multilayered structures. As cationic peptides, the tendency of the peptides to form spherical particles could make them promising candidate as carriers of drugs and other cargo for drug delivery applications.

4.5 Experimental

4.5.1 Field Emission Scanning Electron Microscopy (FESEM)

Appropriate volumes of the peptides were taken into microfuge tube from stock solution and water was evaporated by using speed vac. Desired solvent was added to it and solution was vortexed for 1 min and centrifuged. 2 μL of supernatant solution was then drop casted on clean silicon vapor. Samples were allowed to dry at room temperature in vacuum desiccators and then coated with gold. Scanning electron microscopic imaging was performed using ZEISS ULTRA PLUS electron microscope.

4.5.2 Atomic Force Microscopy (AFM)

Atomic force microscopy (AFM) characterizations are done using a NanoWizard II (JPK instruments, Germany). Samples for AFM were prepared the same way as was done for FE-SEM analysis. The solutions were drop-cast either on Si wafer or freshly cleaved mica surface.

4.5.3 Fluorescence Spectroscopy

Thioflavin T binding assay for peptides **P3** were carried out by recording fluorescence emission spectra with Fluorolog-3 fluorimeter (Jobin Yvon Inc. Edison, NJ). A freshly prepared solution of ThT was added to the peptide (100uM) taken in either TFE or phosphate buffer (5mM, pH 7.2) to a final concentration of ThT of 13uM. The solution was allowed to stand for 1 hour. Following incubation with the peptide, the emission spectra of the dye was recorded by exciting at 420 nm for TFE solution, and 440 nm for buffer solution with 1nm slit widths.

4.5.4. Dynamic Light Scattering

The particle size distributions was studied by dynamic light scattering (DLS), using a Nano ZS-90 apparatus utilizing a 633 nm red laser (at 90° angle) from Malvern instruments. Samples were

prepared in appropriate solvent and left to stand for 1 hour prior to measurements. Three measurements were carried out for each sample. All the measurements were recorded at 25^{o} C. Each measurement consisted of 8 runs with data collected for 30 seconds in each run.

4.6 Reference

1. Nagai, Y.; Unsworth, L. D.; Koutsopoulos, S.; Zhang, S. Slow Release of Molecules in Self-Assembling Peptide Nanofiber Scaffold. *J. Controlled Release* **2006**, 115, 18– 25.

2. Amit, M.; Appel, S.; Cohen, R.; Cheng, G.;Hamley, I. W.;Ashkenasy, N. Hybrid Proton and Electron Transport in Peptide Fibrils. *Adv. Funct. Mater.* **2014**, *24*, 5873–5880.

3. a) Davis, M. E.; Motion, J. P. M.; Narmoneva, D.A.; Takahashi, T.; Hakuno, D.; Kamm, R. D.; Zhang, S.; Lee, R.T. Injectable Self-Assembling Peptide Nanofibers Create Intramyocardial Microenvironments for Endothelial Cells. *Circulation* **2005**, *111*, 442-450. b) Koutsopoulos, S.; Zhang, S. Long-Term Three-Dimensional Neural Tissue Cultures in Functionalized Self-Assembling Peptide Hydrogels, Matrigel, and Collagen I. *Acta Biomater.* **2013**, *9*, 5162–5169. c) Kisiday, J.; Jin, M.; Kurz, B.; Hung, H.; Semino, C.; Zhang, S.; Grodzinsky, A.J. Self-Assembling Peptide Hydrogel Fosters Chondrocyte Extracellular Matrix Production and Cell Division: Implications for Cartilage Tissue Repair. *Proc. Natl. Acad. Sci. U.S.A.* **2002**, 99, 9996–10001.

4. Mumcuoglu, D.; Ekiz, M. S.; Gunay, G.; Tekinay, T.; Tekinay, A. B.; Guler, M. O. Cellular Internalization of Therapeutic Oligonucleotides by Peptide Amphiphile Nanofibers and Nanospheres. *ACS Appl. Mater. Interfaces* **2016**, *8*, 11280−11287.

5. Zhang, P.; Cheetham, A. G.; Lin, Y.; Cui, H. Self-Assembled Tat Nanofibers as Effective Drug Carrier and Transporter. *ACS Nano* **2013**, *7*, 5965–5977.

6. Moon, K. S.; Lee, E.; Lim, Y.; Lee, M. Bioactive molecular Sheets from Self-assembly of Polymerizable Peptides. *Chem. Commun.* **2008**, 4001–4003.

7. Chung, E. K.; Lee, E.; Lim, Y.; Lee, M. Cyclic Peptide Facial Amphiphile Preprogrammed to Self-Assemble into Bioactive Peptide Capsules. *Chem. – Eur. J.* **2010**, *16*, 5305–5309.

8. Reches, M.; Gazit, E. Casting Metal Nanowires within Discrete Self-Assembled Peptide Nanotubes. *Science* **2003**, *300*, 625−627.

9. Hule, R. A.; Nagarkar, R. P.; Hammouda, B.; Schneider, J. P.; Pochan, D. J. Dependence of Self-Assembled Peptide Hydrogel Network Structure on Local Fibril Nanostructure. *Macromolecules* **2009**, *42*, 7137–7145.

10. Hendricks, M. P.; Sato, K.; Palmer, L. C.;Stupp. S. I. Supramolecular Assembly of Peptide Amphiphiles. *Acc. Chem. Res.* **2017**, *50*, 2440−2448.

11. Cui, H.; Cheetham, A. G.; Pashuck, E. T.; Stupp, S. I. Amino Acid Sequence in Constitutionally Isomeric Tetrapeptide Amphiphiles Dictates Architecture of One-Dimensional Nanostructures. *J. Am. Chem. Soc.* **2014**, *136*, 12461−12468.

12. Fernandez-Carneado, J.; Kogan, M. J.; Pujals, S.; Giralt, E. Amphipathic Peptides and Drug Delivery.*Biopolymers* **2004**, *76*, 196 –203.

13. Gazit, E. Self-assembled peptide nanostructures: the design of molecular building blocks and their technological utilization. *Chem. Soc. Rev*. **2007**, *36*, 1263-1269.

14. Zhao, X.; Zhang, S. Molecular designer self-assembling peptides. *Chem. Soc. Rev.* **2006**, 35, 1105–1110.

15. Hartgerink, J. D.; Beniash, E.; Stupp, S. I. Self-assembly and mineralization of peptide-amphiphile nanofibers. *Science* **2001**, *294*, 1684-1688.

16. Serpell, L. C. Alzheimer's amyloid fibrils: structure and assembly. *BBA-Mol. Cell Res*. **2000**, *1502*, 16-30.

17. Lamm, M. S.; Rajagopal, K.; Schneider, J. P.; Pochan, D. J. Laminated morphology of nontwisting β-sheet fibrils constructed via peptide self-assembly. *J. Am. Chem. Soc*. **2005**, *127*, 16692-16700. b) Rajagopal, K.; Lamm, M. S.; Butterick, L. A. H; Pochan, D. J. Schneider, J. P. Tuning the pH responsiveness of β-hairpin peptide folding, self-assembly,and hydrogel material formation. *Biomacromolecules* **2009**, *10*, 2619-2625.

18. Kogan, M. J.; Dalcol, I.; Gorostiza, P.; LoÂpez-Iglesias, C.; Pons, M.; Sanz, F.; Ludevid, D.; Giralt, E. Self-assembly of the Amphipathic Helix $(VHLPPP)_8$. A Mechanism for Zein Protein Body Formation. *J. Mol. Biol.* **2001**, *312*, 907-913.

19. Strauss, K.;Chmielewski, J. Advances in the Design and Higher-Order Assembly of Collagen Mimetic Peptides for Regenerative Medicine. *Curr. Opin. Biotechnol.* **2017**, *46*, 34–41.

20. Gleaton, J.;Chmielewski, J. Thermally Controlled Collagen Peptide Cages for Biopolymer Delivery. *ACS Biomater. Sci. Eng.* **2015**, *1*, 1002–1008.

21. Rele, S.; Song, Y.;Apkarian, R. P.; Qu, Z.;Conticello, V. P.;Chaiko, E. L. D-periodic collagen-mimetic microfibers. *J. Am. Chem. Soc.* **2007**, *129*, 14780–14787.

22. O'Leary, L. E. R.;Fallas, J. A.;Bakota, E. L.; Kang, M. K.;Hartgerink, J. D. Multi-hierarchical self-assembly of a collagen mimetic peptide from triple helix to nanofibre and hydrogel. *Nat. Chem.* **2011**, *3*, 821–828.

23. Jiang, T.; Xu, C.; Liu, Y.; Liu, Z.; Wall, J. S.;Zuo, X.;Lian, T.; Salaita, K.; Ni, C.;Pochan, D. J.;Conticello, V. P. Structurally Defined Nano-scale Sheets from Self-Assembly of Collagen-Mimetic Peptides. *J. Am. Chem. Soc.* **2014**, *136*, 4300–4308.

24. Yoon, Y.; Lim, Y.; Lee, E.; Lee, M.Self-assembly of a peptide rod–coil: a polyproline rod and a cell-penetrating peptide Tat coil. *Chem. Commun.* **2008**, 1892-1894.

25. a) Kumin, M.; Sonntag, L.; Wennemers, H. Azidoproline Containing Helices: Stabilization of the Polyproline II Structure by a Functionalizable Group. *J. Am. Chem. Soc.***2007**, *129*, 466-467. b) Dobitz, S.; Aronoff, M. R.; Wennemers, H. Oligoprolines as Molecular Entities for Controlling Distance in Biological and Material Sciences. *Acc. Chem. Res.* **2017**, *50*, 2420-2428.

26. Lewandowska, U.;Zajaczkowski, W.; Chen, L.;Bouillière, F.; Wang, D.; Koynov, K.;Pisula, W.;Müllen, K.;Wennemers, H. Hierarchical Supramolecular Assembly of Sterically Demanding π-Systems by Conjugation with Oligoprolines. *Angew. Chem. Int. Ed.* **2014**, *53*, 12537 – 12541.

27. Lewandowska, U.; Zajaczkowski, W.; Corra, S.; Tanabe, J.; Borrmann, R.; Benetti, E. M.; Stappert, S.; Watanabe, K.; Ochs, N. A. K.;Schaeublin, R.; Li, C.; Yashima, E.; Pisula, W.; Müllen, K.; Wennemers, H. A Triaxial Supramolecular Weave. *Nat. Chem*. **2017**, *9*, 1068–1072.

28. Bansode, N. D.; Sonar, M. V.; Ganesh, K. N. A nanofiber assembly directed by the non-classical antiparallel β-structure from 4*S*-(OH) proline polypeptide. *Chem. Commun*. **2016**, *52*, 4884-4887.

29. Cui, H.; Webber, M. J.; Stupp, S. I. Self-Assembly of Peptide Amphiphiles: From Molecules to Nanostructures to Biomaterials *Biopolymers* **2010**, *94*, 1–18.

30. a) Wolfe, L. S.; Calabrese, M. F.; Nath, A.; Blaho, D. V.; Miranker, A. D.; Xiong, Y.Protein-Induced PhotophysicalChanges to the Amyloid Indicator Dye Thioflavin T. *Proc. Natl. Acad. Sci. USA* **2010**, *107*, 16863-16868.; b) Sabate, R.; Rodriguez-Santiago, L.; Sodupe, M.; Saupe, S. J.; Ventura, S. Thioflavin-T Excimer Formation Upon Interaction with Amyloid Fibers. *Chem. Commun.* **2013**, *49*, 5745-5747.

31. a) Volpatti, L. R.; Vendruscolo, M.; Dobson, C. M.; Knowles, T. P. J. A Clear View of Polymorphism Twist and Chirality in Amyloid Fibril Formation. *ACS Nano* **2013**, *7*, 10443–10448. b) Nelson, R.; Sawaya, M. R.; Balbirnie, M.; Madsen, A. Q; Riekel, R.; Grothe, R.; Eisenberg, D. Structure of Cross-β Spine of Amyloid Like Fibrils. *Nature* **2005**, *435*, 773-778.

32. Darnell, G.; Orgel, J. P.; Pahl, R.; Meredith, S. C. Flanking Polyproline Sequences Inhibit β -sheet Structure in Polyglutamine Segments by Inducing PPII-like Helix Structure. *J Mol Biol.* **2007**, *374*, 688-704.

33. Bansode, N. D.; Madhanagopal, B.; Sonar, M. V.; Ganesh, K. N. Stereodependent and solvent specific formation of unusual β-structure through side chain-backbone H-bonding in C4(*S*)-(NH_2/OH/NHCHO)-L-prolyl polypeptides. *Biopolymers* **2017**, *108*, e22981.

Section B

Branched Peptides

Chapter 5

Design, Synthesis, Biophysical Studies and Self Assembly of Branched Polyproline Peptides

5.1 Introduction

Branching topology is a recurrent phenomenon in nature. From branches in shoots and roots of trees to the network of capillaries branching out of arterioles and venules in higher animals, there are numerous instances in the biological systems where a dendritic architecture is employed for optimal use of space for the purposes such as harvesting and distributing resources and nutrients. At the molecular level, proteins like immunoglobulins,[1] proteoglycans such as syndecans,[2] and supramolecular organizations of extracellular proteins like collagen[3] utilize this topology for various structural and functional reasons. Naturally occurring branched-peptides in which the backbone itself shows a branching pattern are relatively uncommon since proteins are synthesized as linear polymers by ribosomes. One example could be found on the cell walls of bacteria such as *Staphylococcus aureus* where, adjacent linear tetrapeptides are crosslinked by pentaglycine segment to produce a structurally rigid peptidoglycan layer, reinforced with the branching peptide architecture.[4]

While these large and complex natural nanostructures provide ample inspiration, the synthetic challenges involved in mimicking them at such a scale are enormous and even daunting at times. However, emulating them is easier with short peptides with natural and unusual amino acids. Unrestricted by the constraints associated with the biological systems, chemical approaches enable construction of branched peptidogenic nanostructural motifs with good control over their structural, chemical, biophysical and self-assembling properties. Thus, synthetic branched peptides and peptide based dendrimers have gathered significant interest in the past few decades and have been explored for various applications.[5] They are mainly used as multiple antigen peptides[6] for their superior molecular recognition and immunogenic properties as antimicrobial peptides[7] because they provide a promising alternative to antibiotics, especially

against antibiotic resistant strains; as antitumoral therapeutics[8] and as gene/drug delivery agents[9] due to their drug loading efficiency and cell penetrating properties.

In the previous chapter, linear 4-aminoprolyl polypeptides and their lipid conjugates were shown to possess solvent dependent PP-II or β structure propensity. In this chapter, the synthesis, conformational and self-assembling properties of branched polyproline peptides, constructed with (4*S*)-*amp* and (4*R*)-*Amp* residues as the core-branching unit were explored.

5.2 Rationale and Objectives

4(*R*/*S*)-Aminoproline is an amino acid endowed with three functional groups - primary amine (N1), a secondary amine (N^4) and a carboxylic acid (C2) (Figure 5.1). This makes the molecule suitable for use as a branching point to grow linear peptides from three directions to lead to branched peptides.[10]

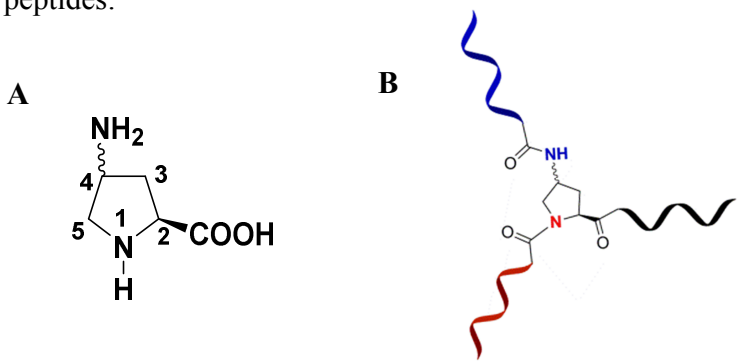


Figure 5.1: (A) Structure of 4(R/S)-aminoproline core. (B) Schematic representation of a branched peptide with 4-aminoprolyl residue as branching point.

With two asymmetric carbons at C4 and C2, it is a chiral molecule with 4 possible diasteromers – (2*S*,4*S*)–*amp*, (2*S*,4*R*)–*Amp*, (2*R*,4*S*)–*amp*, and (2*R*,4*R*)–*Amp*. When used as a branch point, it presents a useful system to study the effect of chirality on the way the three peptide arms are oriented and investigate how this influences the way these trivalent molecules organize themselves to form supramolecular structures of different morphological properties. Here, through the choice of configuration at C4 position of the aminoproline core, that is, by

using either (4*S*)-*amp* or (4*R*)-*Amp*, a chiral control over the conformation of the molecule was expected to be achieved. The influence of chirality of the core on the conformation and morphology of supramolecular assemblies of these branched molecules were therefore studied (Figure 5.1).

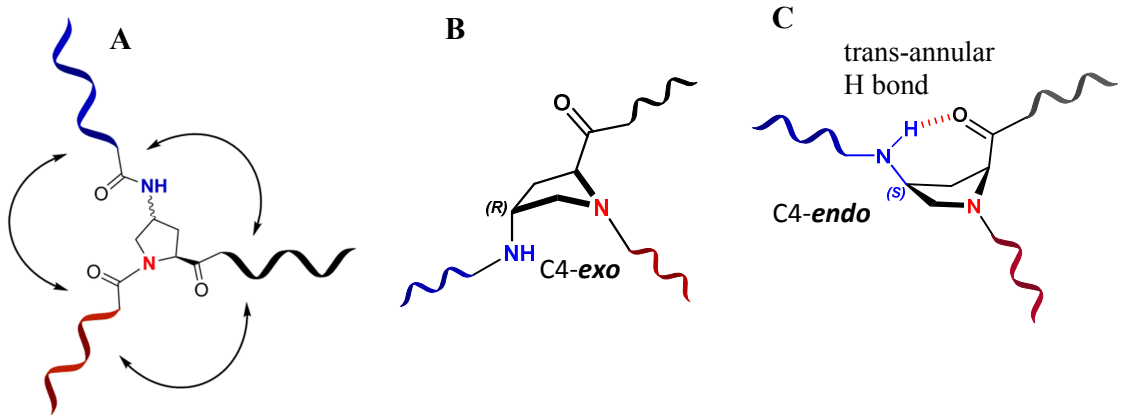


Figure 5.2: Schematic representation of the branched peptides with 4(R/S)-aminoproline core (A). Variable relative orientation of the peptide arms controlled by the 4-aminoprolyl core with pyrrolidine ring pucker C4 *exo* and (B) C4 *endo.*

A unique feature with the use of aminoproline was that the orientation of the peptide arms would be dependent upon the pyrrolidine ring pucker, which was influenced by the stereoelectronic factors discussed earlier and by the possibility of trans-annular hydrogen bonding in the case of (4*S*)-*amp*[11] (Figure 5.2). Thus, configuration at C4 could exert a strong influence on the orientation of the branching peptide arms because of the hydrogen bonding pattern at the core and C4-endo ring pucker.

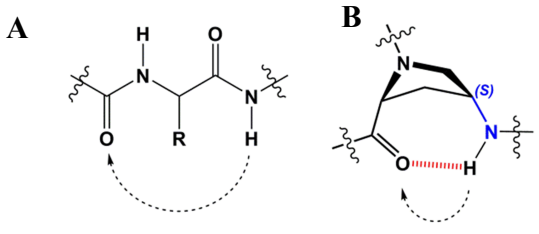


Figure 5.3: (A) A peptide backbone showing 7- membered γ –turn like H bond pattern. (B) C4-endo puckered (4*S*)-*amp* forming 7- membered H bond, a γ –turn mimic.

When an intra-residue H bond forms between C2 carbonyl and N^4 amine, it mimics the hydrogen bonding pattern of γ-turns[12] in peptides and proteins (Figure 5.3). (4*S*)-*amp* has been recognized as a γ-turn mimic.[13] Therefore, one could expect the branched peptides constructed with (4*S*)-*amp* as branching core to have two of its arms held in place by a γ-turn like form. (4*R*)-*Amp*, on the other hand, due to its inability to form such a trans-annular hydrogen bond could be expected to have diverse orientations as the "proline hinge" would be more flexible. Rather than water, these differences are likely to be more influential in a non-aqueous solvent such as TFE, where the backbone is not hydrated and so there would be no water molecules to compete, thus favoring the intramolecular hydrogen bonding.

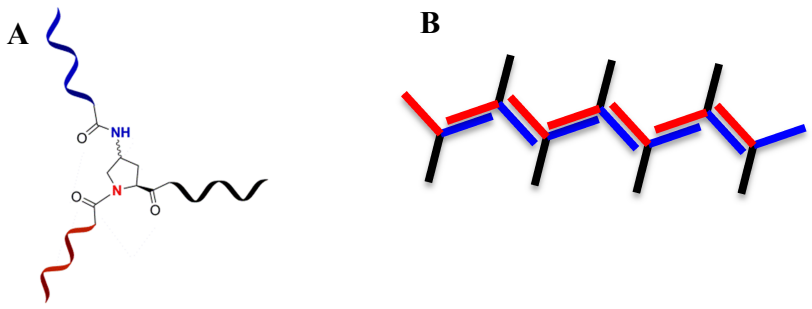


Figure 5.4: Schematic representation of 3-arm branched peptides forming supramolecular structures via intermolecular interactions between aminoprolyl segments Y and Z arms.

Any intermolecular interactions like the ones expected to occur between the aminoproline residues on the linear C4(*S*)-NH_2 substituted aminoprolyl polypeptides is unlikely to be involved at the core of the branching peptide as it was demonstrated that an amide at C4 prefers PP-II form in both TFE and water.[14] However, the (4*S*)-*amp* on the arms of the peptide are free to form extended higher order structures,[14,15] unless restricted by the geometry around the core (Figure 5.4). Therefore, envisaging stereo-controlled and solvent dependent assembly of complex architectures, the branched peptides with the following design were synthesized and compared with their linear counterparts.

In the design of the molecule, the first arm (X) was chosen to be unsubstituted polyproline to avoid synthetic complications that could arise from the orthogonal protecting groups. As compared to the aminoproline arms Y and Z, the polyproline arm is relatively non-polar. This could be expected to confer an amphiphilic character to the peptide.

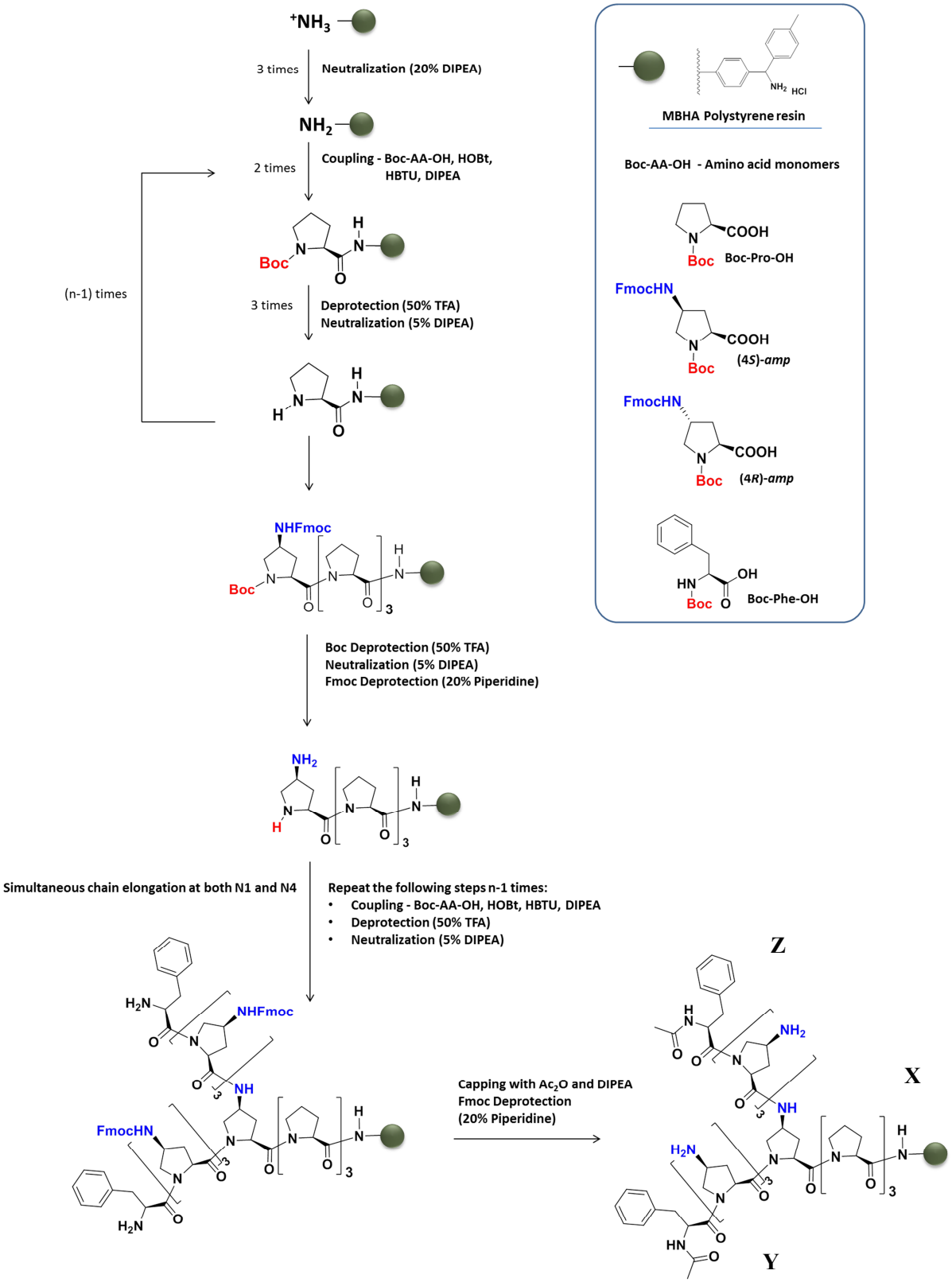
The specific objectives of the project include the following:

- Synthesis of branched polyproline peptides with (4*S*)-*amp* and (4*R*)-*Amp* as branching core. It has one trimeric polyprolyl arm (X = Pro_3) attached to the core aminoproline at C2, one trimeric aminoprolyl segment (Z = amp_3) attached at N^4 and another trimeric aminoprolyl segment attached at N(1) of the core (Y = amp_3).
- Study the effect of the configuration at C4 of the aminoproline core on the conformation of the molecule in aqueous phosphate buffer and in TFE.
- Investigate the effect of self-assembly of the branched molecules in different solvents to elucidate the role of branching topology on the self-assembling properties of the aminoproline peptides.

5.3 Results and Discussion

5.3.1 Synthesis of Branched Peptides

Branched polyprolyl peptides with (4*R*)-*Amp* and (4*S*)-*amp* as branching core were synthesized by solid phase peptide synthesis protocol as shown in Scheme 5.1. For the synthesis of branched polyprolyl peptides, orthogonally protected monomers: (2*S*,4*R*)-N(1)-t-Boc-N^4-Fmoc-aminoproline **7** and (2*S*,4*S*)-N(1)-t-Boc-N^4-Fmoc-aminoproline monomer **12** were synthesized as described in Chapter 2 (Scheme 2.1 and 2.2). MBHA resin was used for the synthesis of the peptides and a modified t-Boc strategy was adopted.

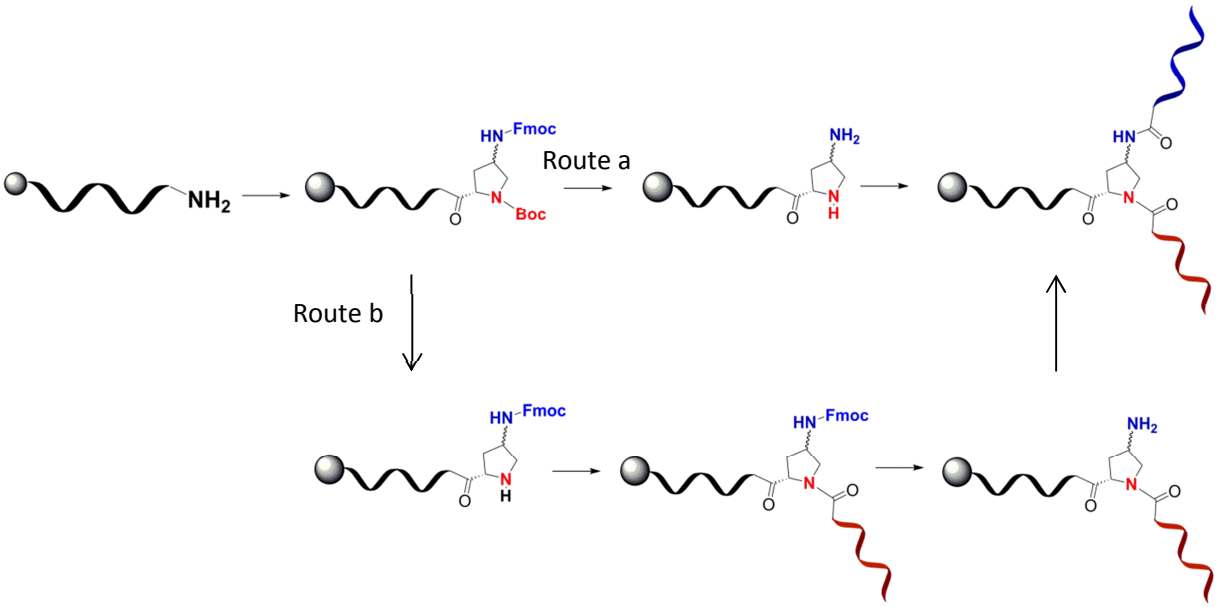


Scheme 5.1: Solid phase synthesis of branched peptides using tBoc chemistry

5.3.1a *Design Considerations and Synthetic Stategies*

In order to synthesize branched peptides, amino acid monomers with two amine groups are generally used. Naturally occurring and proteinogenic aminoacid, lysine is often used for this purpose.[16] 4(*R*/*S*)-Aminoproline is an analogue of lysine with a constrained cyclic sidechain with two amine groups and one carboxylic acid. Extension of the peptide chain from both the amine groups in such an amino acid allows the synthesis of branched peptides, where two peptide arms (Y and Z) branch out at the N terminus of a linear stem segment (X) that is still bound to the solid support at its C-terminus, as shown in Scheme 5.1.

The branching peptide arms could be elongated from the core simultaneously or sequentially one branch after another (Scheme 5.2). Simultaneous elongation (route a) leads to identical peptide sequences in two of the three branches. It required fewer steps as compared to the other route and so was relatively faster.



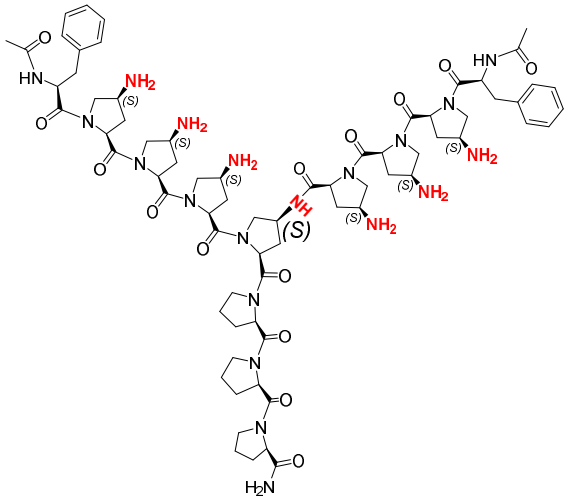
Scheme 5.2: Strategies to synthesize peptide branches on solid support – simultaneous elongation of the peptide branches (route a) and sequential elongation of peptide branches one after the other (route b).

In sequential elongation route, one of the peptide arms was elongated after selectively deprotecting one of the amines in the core unit (route b). After the synthesis of the first branch it was either N-capped or left with its N-terminus protected. The second amine group in the core was then deprotected by removing the orthogonal protecting group and the second peptide branch was then synthesized following the usual solid-phase peptide synthesis protocol. Even though the monomers, (4*S*)-*amp* and (4*R*)-*Amp* are orthogonally protected and are well equipped for either of the two routes, to initially test the concept of chiral branching peptide, the simpler option of *route a* was chosen in the present work. It will also help us understand the initial structure-property relationship without much complication.

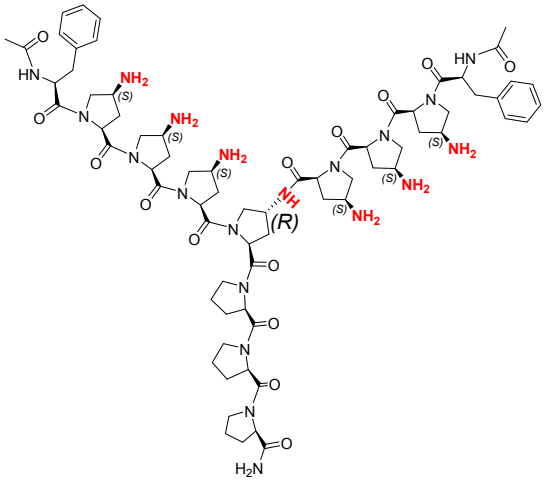
5.3.1b *Solid Phase Synthesis of Branched Peptides*

The protocol followed for the synthesis of branched peptides was similar to the ones used for the linear peptides as described in Chapter 2, except for a few steps following the incorporation of branching core. The commercially available MBHA resin was allowed to swell and was treated with 20% DIPEA (in DCM). A lower loading of the resin enhances the efficacy of coupling. Hence, the loading capacity of the resin was reduced to 0.1 mmol/g by partial coupling of the first proline residue and capping all the unreacted free amines on the resin with acetic anhydride. After incorporation of three proline residues following the routine protocol (Scheme 5.2), the branching core, either (4*S*)-*amp* or (4*R*)-*Amp* was added. Both primary amine and secondary amine on the incorporated amino acid was deprotected. First N(1)-t-Boc was removed by treatment with 50% TFA (in DCM). The N^4-Fmoc was later removed using 20% piperidine (in DMF). After washing the resin thoroughly, the two free N termini are simultaneously elongated to produce the two aminoproline branches. Addition of 4(*S*)-aminoproline monomer to the growing chain using the standard t-Boc protocol resulted in

coupling of both amino functions and produced the branched polyproline peptides. Phenylalanine was added at the N-termini of the branches as the concentration of the peptides could be calculated by measuring the absorbance of its side chain at 257 nm. The peptides were capped with acetic anhydride and cleaved from the resin using TFMSA/TFA in the presence of scavengers, ethanedithol and thioanisole. The N-capped peptides were thus obtained as C-terminal amides.



(4*S*)-*amp*$^{\lambda}$-(*amp*$_3$)$_2$ **P12**



(4*R*)-*Amp*$^{\lambda}$-(*amp*$_3$)$_2$ **P13**

Figure 5.5: Peptides (**P12-P13**) used in the present study.

TABLE 5.1: HPLC retention time and MALDI-TOF mass spectral analysis of the peptides

	Peptide	HPLC RT (min)	Molecular Formula	Calc. Mass	Obs. Mass
P12	AcNH-*Phe*-(***amp***)$_3$-***amp***-(*Pro*)$_3$CONH$_2$ | AcNH-*Phe*- (***amp***)$_3$	12.2	$C_{72}H_{102}N_{20}O_{14}$	1470.79	1471.81 (M+1)
P13	AcNH-*Phe*-(***amp***)$_3$-***Amp***-(*Pro*)$_3$CONH$_2$ | AcNH-*Phe*- (***amp***)$_3$	10.1	$C_{72}H_{102}N_{20}O_{14}$	1470.79	1471.75 (M+1)

The branched peptide **P12** with (4*S*)-*amp* as branching residue and two tripeptide units (4*S*)-amp_3 as branches is referred to with the following notation, (4*S*)-$amp^{\curlywedge}$-$(amp_3)_2$ (**P12**). Similarly, the peptide **P13** with (4*R*)-*Amp* as branching residue is represented as (4*R*)-$Amp^{\curlywedge}$-$(amp_3)_2$ (**P13**). The peptide arm Pro_3 is common among both the peptides studied here and is therefore not referred to in the notation.

5.3.1c *Purification and Characterization of Peptides*

The peptides were purified using the routine reverse phase HPLC using a semipreparative C18 column. A linear gradient system between water and acetonitrile was used similar to the ones used for linear peptides. The purity of the peptides was finally checked using C18 analytical column. The integrity of the purified peptides was confirmed by MALDI-TOF spectrometry using DHB as matrix.

The HPLC retention time, calculated and observed mass of the peptides are listed in the table 5.1. The HPLC chromatograms and MALDI-TOF mass spectra are shown in Appendix B.

5.3.2 Conformational Studies of Branched Peptides

The 4-aminoprolyl polypeptides with repeating units of 4(*R*/*S*)-aminoproline has been shown to have interesting solvent dependent conformational properties, dictated by the configuration at C4. The conformational properties of C4(*S*)-NH_2 substituted linear polyaminoprolyl peptide **P3** were explored earlier in Chapter 3. In this chapter, an attempt is made to employ this conformational feature to generate chiral branched polyprolyl peptides. The influence of the stereocenter at C4 is assessed by comparing the circular dichroism spectra of the peptides (4*S*)-$amp^{\curlywedge}$-$(amp_3)_2$ (**P12**) and (4*R*)-$Amp^{\curlywedge}$-$(amp_3)_2$ (**P13**).

In buffer (pH 7), both the peptides, **P12** and **P13** showed typical PP-II like CD spectra with a positive n→π* band in the 220 nm -225 nm region and a negative π→π* band at 205 nm (Figure 5.6A). No shift in the position of the negative bands was seen among the two peptides. However, the mean residue ellipticity showed considerable differences. The branched peptide **P12** showed a more intense positive and negative band as compared to the branched peptide **P13**. This revealed that when (4*S*)-*amp* was used as branching point, PP-II conformation was more stable in aqueous buffer. With this as a branching core producing more ordered trigonal structures as compared to (4*R*)-*Amp* core.

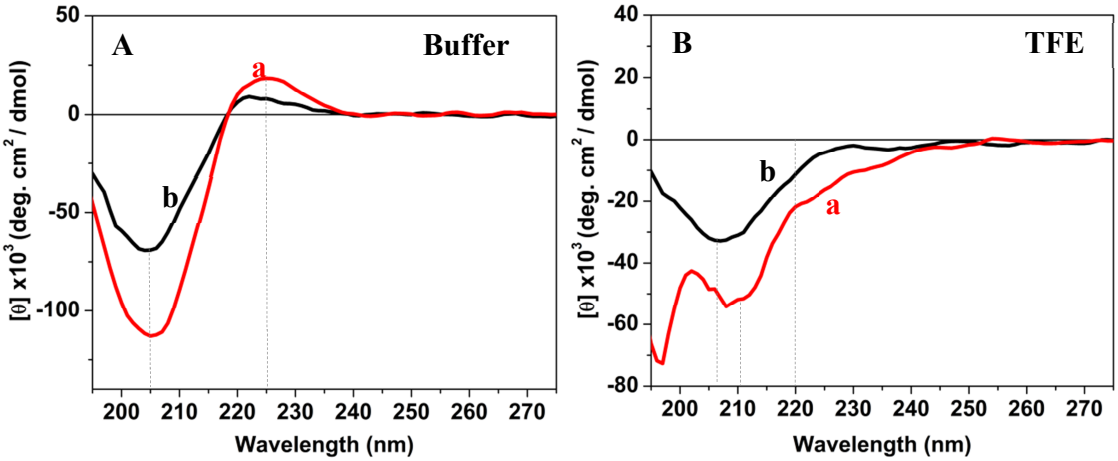


Figure 5.6: Solvent dependent conformational changes in the branched peptides (**P12**-**P13**). Circular dichroism spectra of the peptides, (4*S*)-*amp*$^{\lambda}$-(*amp*$_3$)$_2$ (**P12**) (trace **a**), and (4*R*)-*Amp*$^{\lambda}$-(*amp*$_3$)$_2$ (**P13**) (trace **b**) in buffer (A) and TFE (B).

In TFE, a loss of PP-II stability was found in both the peptides, (4*S*)-*amp*$^{\lambda}$-(*amp*$_3$)$_2$ (**P12**) and (4*R*)-*Amp*$^{\lambda}$-(*amp*$_3$)$_2$ (**P13**). The CD spectral signature of PP-II conformation was found to be perturbed in both the peptides, indicating that the conformational transition in the aminoprolyl peptide arms Y and Z was retained even in the branched peptides. However, the role of the branching core was evident in Figure 5.6B, which showed that **P12** had a stronger negative signal at 220 nm as compared to **P13**. The shift of the negative band towards longer wavelengths

was more pronounced in the case of **P12** (4*S*)-*amp*$^{\curlywedge}$-(*amp*$_3$)$_2$ than **P13** (4*R*)-*Amp*$^{\curlywedge}$-(*amp*$_3$)$_2$. However, the typical CD signature for β-sheet was not observed, probably due to the non-participating *Pro*$_3$ arm X, which was not expected to show any change in the CD spectra during 12 hour incubation time in the solvent after preparation of the solution.

These results suggested that even on incorporation of (4*S*)-*amp* into the polyproline peptides, it somewhat still retained its solvent dependent conformational properties. It was also suggestive that the chirality of the branching core influences the overall conformation of the molecule. The peptide **P12** showed more ordered and more stable PP-II structure in buffer and in TFE, it showed greater perturbation as compared to the branched peptide **P13** with (4*R*)-*Amp* at the core.

5.3.3. Morphological Study of Self-Assembled Branched Polyproline Peptides

Linear homooligomers of (4*S*)-*amp* exhibited interesting solvent dependent self-assembling properties (Chapter 3). In TFE, C4(*S*)-NH_2 substituted polyaminoprolyl peptides formed long nanofibers of 15-20 nm diameter with a left-handed helical twist as shown in section 4.3.1 of Chapter 4. However in water, they did not show any regular morphology. Such a behavior was found to corroborate with the CD spectral properties of the peptides. In TFE, the (4*S*)-*amp*$_n$ peptides showed β-sheet like CD pattern and nanofibrous morphology. However, in aqueous buffer, it showed a CD signature that was typical of PP-II conformation. In water, these peptides produced spherical particles with irregular and ill-defined features.

In branched peptides, the linear arms Y and Z contain trimeric (4*S*)-*amp*$_3$ segment, each of which are derived from peptide **P1.** The CD spectra of the peptides suggested that the branched architecture did not hinder the solvent dependent conformational change in the

peptide's branches Y and Z. In order to examine whether branched architecture favored or disfavored the self-assembly of (4*S*)-*amp* into fibres, they were studied using FESEM.

The samples for FESEM were prepared as described in Chapter 4 for linear peptides. The peptides (2μL) dissolved in the appropriate solvent was dropped on a clean Si wafer after a 12 hour incubation of the solution at room temperature. The dried film was obtained after evaporation of solvent under ambient conditions for 12 hours and under high vacuum for 4 hours. For FE-SEM studies, the peptide assemblies on the Si wafer were sputter-coated with a thin layer of gold prior to imaging.

5.3.3a *Solvent Dependent Self-Assembly of* (4*S*)-*amp*$^{\lambda}$-(*amp*$_3$)$_2$ ***(P12)***

The morphology of the peptide was studied by imaging the supramolecular structures formed by the peptides in different solvents. A 2 μL aliquot of 200 μM solution of the peptide made in milliQ water with no added salt, in 10 mM phosphate buffer containing 10 mM NaCl or in TFE, were left to stand for 12 hours and then drop-cast on a clean Si wafer. The films were then dried as described above prior to imaging.

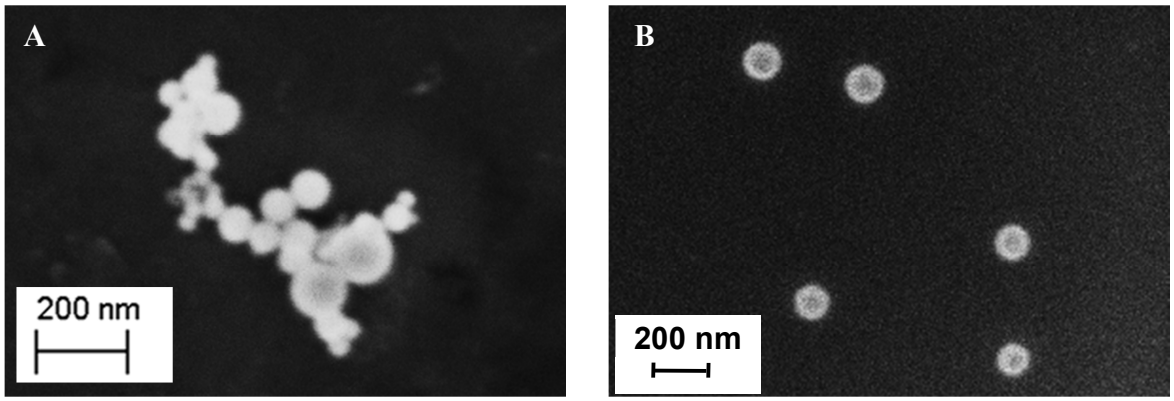


Figure 5.7: FE-SEM images of morphologies formed by peptide **P12** (4*S*)-*amp*$^{\lambda}$-(*amp*$_3$)$_2$ in water (A) and in 10 mM phosphate buffer containing 10 mM NaCl, pH 7.0 (B).

In water and in 10 mM phosphate buffered saline, the peptides were found to show spherical particles (Figure 5.7). In water the size of the particles varied from 20 nm to 200 nm. In buffer, the sizes of the particles were more homogenous around 50 nm diameter in size. In water, the particles were clumped, while in buffer, the particles were well isolated.

In TFE, the peptide **P12** (4*S*)-*amp*$^{\lambda}$-(*amp*$_3$)$_2$was found to have fibrous morphology (Figure 5.8). The fibres are almost similar to the nanofibrous morphology formed by linear peptides. Particularly, the fibres showed a left handed helix, similar to the linear peptides with similar twist angle to that observed in linear peptides. In addition to the fibres and their bundles, there were also many toroidal structures, and loops (Figure 5.8B). Although such structures are not predominantly observed with linear peptide, (4*S*)-*amp*$_9$ (**P3**) their occurrence were more frequent with the branching peptide **P12** (4*S*)-*amp*$^{\lambda}$-(*amp*$_3$)$_2$.

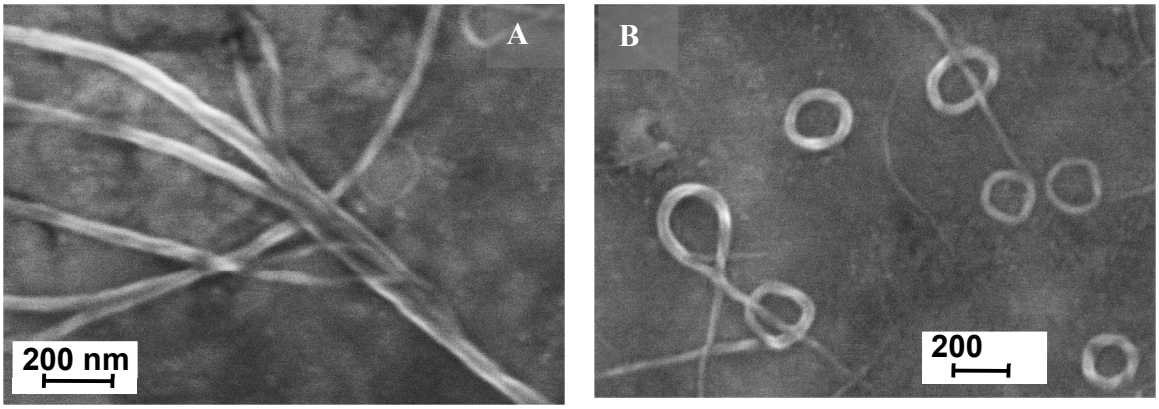


Figure 5.8: FE-SEM images of morphologies formed by peptide **P12** (4*S*)-*amp*$^{\lambda}$-(*amp*$_3$)$_2$ in TFE showing nanofibers with helical twists (A) and loops and ring like structures (B).

The effect of concentration on the self-assembly of the branched peptide was evaluated. At different concentrations (50 μM to 250 μM) in TFE after incubating for a period of 12 hours, and taking 2 μL aliquots for FESEM imaging.

At 50 μM, the peptides showed spherical particles of sizes in the range 20 nm to 200 nm (Figure 5.9A). At 100 μM, aggregates of the particles with similar size distribution were seen (Figure 5.9B). As the concentration was increased to 150 μM and higher, the nanofibres and bundles of fibres were observed (Figure 5.9C-E).

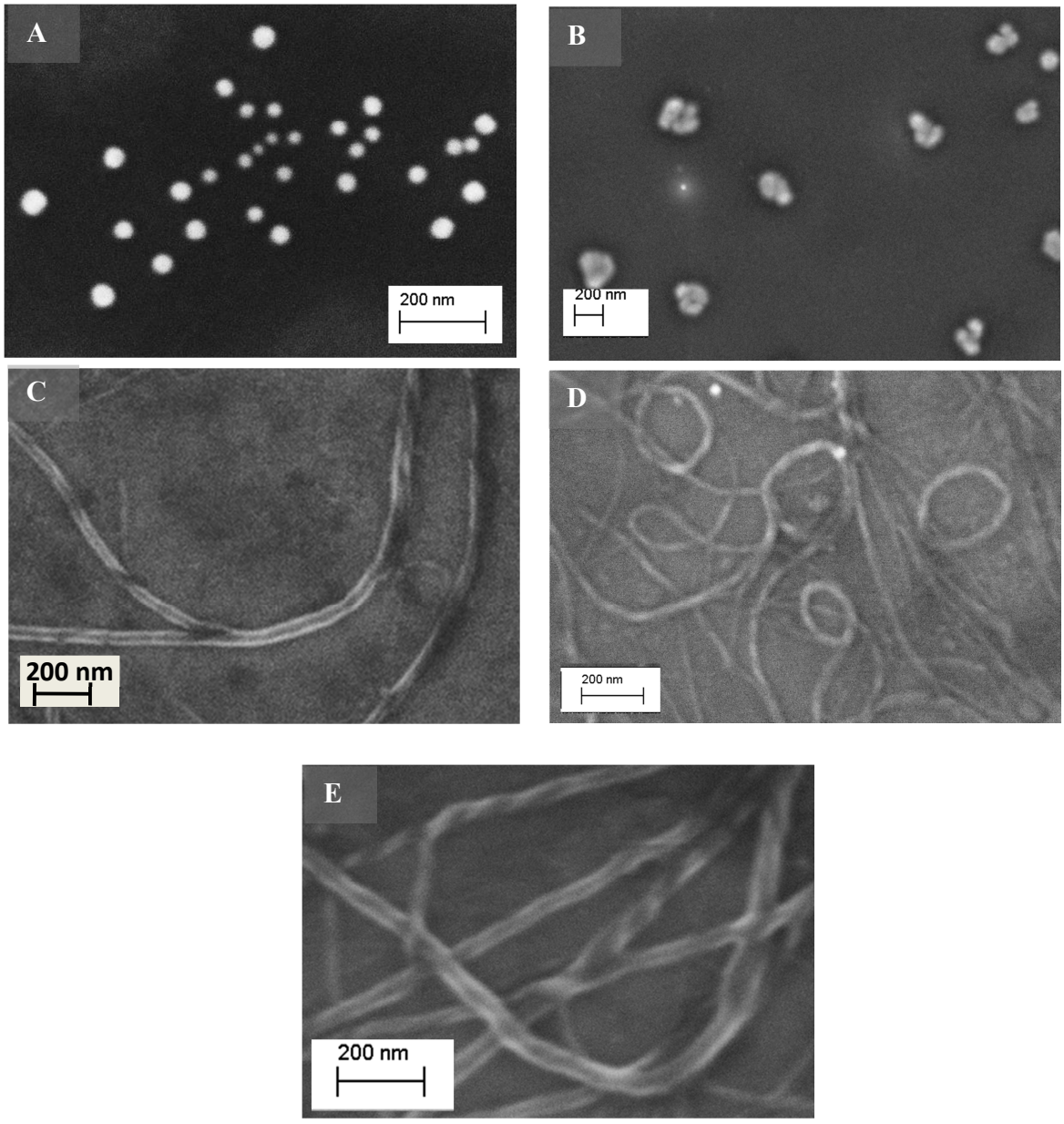


Figure 5.9: FE-SEM images of morphologies formed by peptide (4*S*)-*amp*$^{\lambda}$-(*amp*$_3$)$_2$ (**P12**) in TFE at different concentrations: 50 μM (A), 100 μM (B), 150 μM (C), 200 μM (D), and 250 μM (E).

5.3.3b *Solvent Dependent Self-Assembly of* (4*R*)-*Amp*$^{\curlywedge}$-(*amp*$_3$)$_2$ (**P13**)

In peptide (4*R*)-*Amp*$^{\curlywedge}$-(*amp*$_3$)$_2$ (**P13**), two of the three peptide arms (Y and Z) contained trimeric (4*S*)-*amp*$_3$ units, with the branching core of (4*R*)-*Amp.* The effect of the configuration at C4 of the chiral core in the peptide on self-assembly on the morphology of the supramolecular structures formed by the peptide was studied.

Samples prepared from 200 μM solutions of the peptide in water or phosphate buffer (pH 7) were imaged. The 4(*R*)-core peptide **P13** showed spherical particles of different sizes (Figure 5.10A). While in phosphate buffer, the peptide showed larger spherical particles of relatively narrow distributions (Figure 5.10B). This was similar to the morphological properties observed with (4*S*)-*amp*$^{\curlywedge}$-(*amp*$_3$)$_2$ (**P12**) as seen in Figure 5.7. However, the particles were much better defined compared to that formed by **P12**.

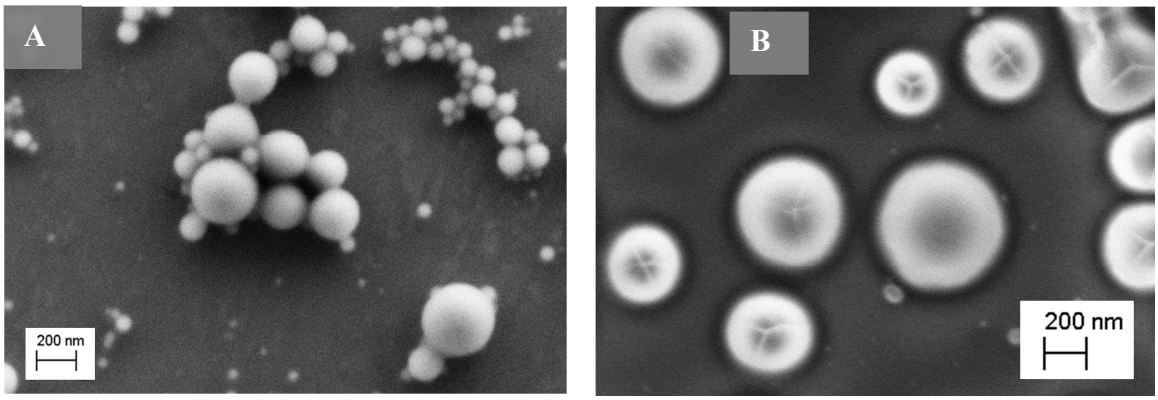


Figure 5.10: FE-SEM images of morphologies formed by peptide (4*R*)-*Amp*$^{\curlywedge}$-(*amp*$_3$)$_2$ (**P13**) in water (A) and in 10 mM phosphate buffer containing 10 mM NaCl, pH 7.0 (B).

In TFE, large aggregates of spherical particles were observed. The size of the particles ranged from 20 nm to about 200 nm (Figure 5.11A). A large variation in size was seen in these samples with regions populated by isolated small particles of about 20 nm in size (Figure 5.11B).

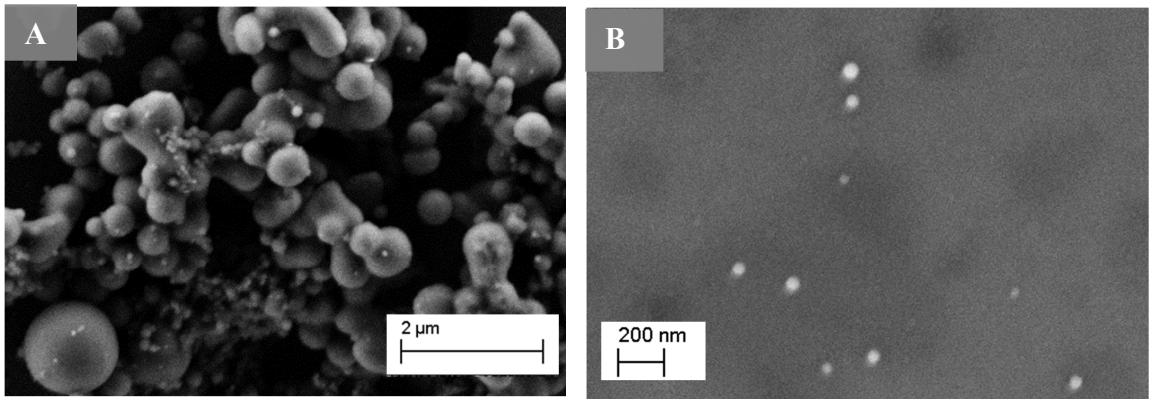


Figure 5.11: FE-SEM images of morphologies formed by peptide (4*R*)-*Amp*$^{\lambda}$-(*amp*$_3$)$_2$ (**P13**) in TFE showing aggregates of spherical particles of different sizes (A) and isolated smaller particles (B).

5.3.3c *Effect of the Chiral Core on Self-Assembly of Branched Peptides*

The peptides (4*S*)-*amp*$^{\lambda}$-(*amp*$_3$)$_2$ (**P12**) and (4*R*)-*Amp*$^{\lambda}$-(*amp*$_3$)$_2$ (**P13**) differ only in the stereochemistry of the aminoproline core used as the branching unit. In water and in buffer, the peptides showed similar morphology indicating the insignificant effect of the core in dictating the resulting nature of nanoparticles. However, the morphology observed in TFE with the peptide **P13** was found to be markedly different as the ones seen with that of **P12**. While **P12** produced well-formed nanofibers of 20 nm to 30 nm in diameter with left handed helical twist, **P13** was found to produce irregular aggregates. The nature of the core configuration at C4 from C4(*S*) to C4(*R*) thus influences the formation of ordered fibrous structures in TFE.

The supramolecular assemblies of (4*S*)-*amp*$^{\lambda}$-(*amp*$_3$)$_2$ (**P12**) resembled those obtained with linear peptide (4*S*)-*amp*$_9$ (**P3**). The length of the individual linear aminoprolyl segments in the peptides in the branching arms Y and Z was identical to that of linear peptide (4*S*)-*amp*$_3$ (**P1**). While the short trimeric peptide **P1** was unable to show any regular morphology in TFE,

integrating those units into a branched structure was found to drive them to ordered self-assembly. However, this also depended on the stereochemistry of the core at C4 position.

5.4 Summary

In this chapter, the branched polyproline peptides (4*S*)-*amp*$^{\lambda}$-(*amp*$_3$)$_2$ (**P12**) and (4*R*)-*Amp*$^{\lambda}$-(*amp*$_3$)$_2$ (**P13**) were constructed using 4(*R*/*S*) aminoproline as branching unit.

- The peptides were designed in such a way that one of the stem (X) contained the free amidated C-terminus and two branches (Y and Z) acetylated N terminus.
- The branching peptide arms bearing three (4*S*)-*amp* residues were synthesized by simultaneous elongation strategy.

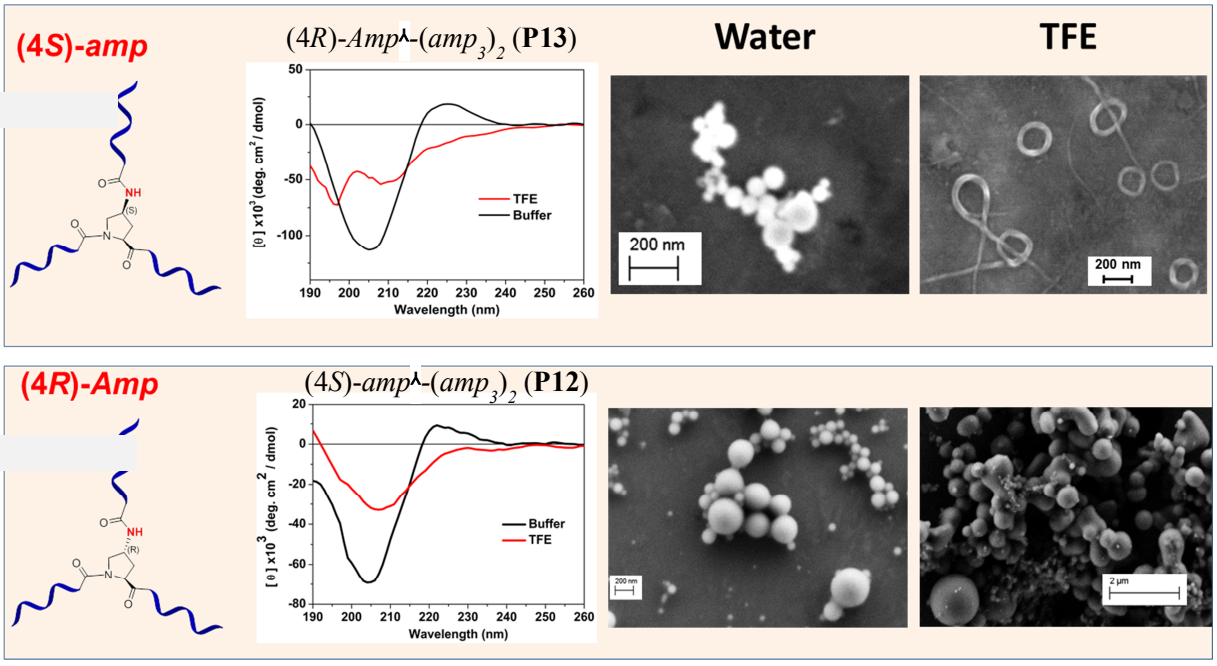


Figure 5.12: Comparison of CD spectra and morphologies formed by branched peptides (4*S*)-*amp*$^{\lambda}$-(*amp*$_3$)$_2$ (**P12**) and (4*R*)-*Amp*$^{\lambda}$-(*amp*$_3$)$_2$ (**P13**) in different solvents

- The circular dichroism spectra showed that both the peptides formed PP-II structure in aqueous phoshphate buffer (pH 7.0). In TFE, the PP-II form was found to be destabilized with the formation of β-sheet like conformation of the aminoprolyl arms Y and Z. In water, the peptides assembled into spherical structures and showed no differences in their morphology.
- In TFE, (4*S*)-*amp*$^{\curlywedge}$-(*amp*$_3$)$_2$ (**P12**) assembled into fibres and (4*R*)-*Amp*$^{\curlywedge}$-(*amp*$_3$)$_2$ (**P13**) formed irregular spherical aggregates.
- The change in morphology was attributed to the chiral core effecting the intermolecular interactions between the branched aminoprolyl peptide arms.
- The results suggested that a branched structure promotes self-assembly of the nanofibers as compared to linear topology, with the morphology dependent on the stereochemistry at C4 of the 4-aminoproline at the branching point.

5.5 Experimental

5.5.1 Solid Phase Peptide Synthesis

The general procedure used to synthesize the peptide were the same as the ones in Chapter 2, except for the loading value of the resin, which was reduced to 0.1 mmol/g.

5.5.1a *Synthesis of peptides*

Peptides were synthesized manually using a sintered (G2) reaction vessel equipped with a Teflon stopcock. All the materials used were of peptide synthesis grade (Novabiochem) and was used without further purification. Analytical grade DMF was purchased from (Merck, India) and stored over 4Å molecular sieves for 2 days

before using for peptide synthesis. Similarly DCM was distilled over CaH_2 and stored over 4 Å molecular sieves. Coupling reactions were carried out using *in situ* active ester method, by HBTU as coupling reagent, HOBt as recemization suppresser and DIPEA as catalyst.

Resin functionalization

Commercially available MBHA (4-methyl benzhydrylamine) resin (Novabiochem, 100-200 mesh) the hydrochloride salt was neutralized performed prior to amino acid coupling and the following steps were done for synthesis (100 mg scale). The resin was washed and swollen in dry DCM for atleast 1 hr. The DCM was drained and 50% solution of DIPEA in DCM was added (3 x 3ml; 10 min each) followed by thorough washing with DCM. Further washing and swelling with dry DMF for 1 hr.

Synthesis protocol

Boc–strategy was used for synthesis on MBHA resin for acid-labile protecting groups

- DCM wash (4 x 5 ml)
- 50% TFA in DCM (2 X 5 ml; 10 min each) for deprotection of t-Boc group
- 5% DIPEA in DCM (3 X 5 ml; 5 min each) for neutralization of TFA salt
- DCM, MeOH wash (3 x 3 ml each)
- Kaiser's/Chloranil test
- DCM, DMF wash (3 x 3 ml each)
- Coupling reaction (3 eq. each of aminoacid, DIPEA, HOBt and HBTU in 10eq. volume of DMF)

- Kaiser's/Chloranil test

These cycles ware repeated for every amino acid. The coupling and deprotection reactions were monitored by a combination of Kaiser's (ninhydrin) test and chloronil test. In case of negative test after coupling the re-coupling was performed with same aminoacid followed by capping of the unreacted amino groups using Ac_2O, DIPEA & DMF (1:1:1), in case coupling does not go to completion even after re-coupling. A linear peptide chain with arms X containing the aminoproline with a side chain amine protected with Fmoc at the end of the sequence was thus synthesized. Both N1-tBoc and N^4-Fmoc groups were removed and two peptide chains were extended from the aminoproline core from simultaneously using Boc-strategy.

Kaiser's test

Kaiser's was used to monitor the t-Boc/Fmoc deprotection and coupling reactions in the solid phase peptide synthesis using three solutions. Solution A: Ninhydrin (5.0 g) dissolved in ethanol (100 ml) Solution B: Phenol (80.0 mg) dissolved in ethanol (20 ml) Solution C: KCN (2 ml, 0.001 M aqueous solution) added to 98 ml pyridine

- Few beads of resin to be tested were taken in a test tube and washed 3 times with ethanol.
- 3-4 drops of each of the three solutions described above were added to it
- The test tube was heated to 120 °C for 4-6 min
- The successful deprotection was indicated by blue resin beads while colourless beads indicate the completion of coupling step.

Chloranil test

A few beads of resin were taken in a glass test tube (5 ml capacity) and were washed with methanol followed by toluene. To this three drops of saturated chloranil solution in toluene and 200 µl of acetone were added. The mixture was shaken for 2-3 minutes. Blue or green color is observed on the resin beads if free amines are present.

5.5.1b *Peptide cleavage from resin*

Finally after the last coupling the resin was washed with DMF (5 x 5 ml), DCM (5 x 5 ml), then with toluene (5 x 5 ml) and methanol (5 x 5 ml) then flushed with N2-gas for 3 mins. The resin along with the sintered flask was dried in vacuum desiccator over KOH and P_2O_5 for 6 hrs.

The resin MBHA (10 mg) with peptides attached to it was stirred with TFA (200 µL) and deionized water (10 µL) in an ice bath for 10 min. TFMSA (16 µL) was added slowly with vigorous shaking to dissipate the heat generated. The reaction mixture was stirred for 1.5 hrs at room temperature. The resin was removed by filtration under reduced pressure and washed with TFA (3 x 1 mL). The combined filtrate was concentrated, the product was precipitated with cold dry ether and the peptide was isolated by centrifugation (5 times at 5000 rpm) as white powder. Peptides which had Fmoc-protection in side groups were removed by 20% piperidine/DMF treatment and dried properly before cleavage.

5.5.2 High Performance Liquid Chromatography (HPLC)

Peptides were purified by reverse phase-HPLC on Agilent Technologies 1260 Infinity equipped with Photodiode array detector (PDA). Semi-preparative RP-C18 columns (250x10 mm, 10 μm) of was used for peptides. The solvent system comprised of MeCN:Water (5:95) with 0.1% TFA for solution A and for solution B MeCN: Water (50:50), 0.1% TFA. A gradient of 0-100% at a flow rate of 3 mL/min was used to elute the peptide and the eluant was monitored at 220 nm. The peak corresponding to the peptide was collected and the fractions were freezed. Subsequently these peptides were concentrated by using speed vacuum. The purity of the final peptides were further analyzed on the Phenomenex Analytical RP-C18 (250 x 4 mm, 5 μm) column by using a gradient flow of 0 to 100% B in 30 min at a flow rate of 1 mL/min. The absorbance of the eluant was monitored at its corresponding wavelength and the purity was obtained from the integrator output. The purities of the hence purified peptides were found to be more than 95%. The overall yields of the peptides are given in table 5.1

Table 5.2: Overall yields of the peptides used in the present study

	Peptide	Overall Yield (%)
P12	(4*S*)-*amp*$^{\lambda}$-(*amp*$_3$)$_2$	15
P13	(4*R*)-*Amp*$^{\lambda}$-(*amp*$_3$)$_2$	19

5.5.3 MALDI-TOF Characterization

MALDI-TOF mass spectra were obtained on either Voyager-Elite instrument (Perspective Biosystems Inc., Farmingham, MA) equipped with delayed extraction or on Voyager-De-STR (Applied Biosystems) instrument. 2,5-Dihydroxy benzoic acid (DHB) and α-

cyano-4- hydroxycinnamic acid (CHCA) both were used as matrix for peptides of which DHB was found to give satisfactory results. A saturated matrix solution was prepared with typical dilution solvent (50:50:0.1 Water: MeCN: TFA) and spotted on the metal plate along with the oligomers. The metal plate was loaded to the instrument and the analyte ions are then accelerated by an applied high voltage (15-25 kV) in reflector mode, separated in a fieldfree flight tube and detected as an electrical signal at the end of the flight tube.

5.5.4 Circular Dichroism (CD) Spectroscopy

CD spectrometric study was carried out on JASCO J-815 spectropolarimeter using cylindrical, jacketed quartz cell (10 mm path length), which was connected to Julabo-UC25 water circulator. For reproducible data, each set of spectra were measured using at least three individually prepared solutions. CD spectra were recorded using a spectral bandwidth of 1.0 nm at 25 °C with a time constant of 1 s and a step resolution of 1 nm. All the spectra were corrected for respective buffer condition and are typically averaged over 3-6 scans. A quartz cell with a path length of 1 mm was used with solutions containing approximately 0.25 mL (50 to 250 μM).

All peptides had same peptide concentration (50-250 μM) for CD measurements done in Na-phosphate buffer (pH 7.0). The data processing and curve fitting were performed using Origin 8.0 software. All spectra were collected at 25^{o} C with a 1 nm resolution and a scan rate of 50 nm/min. Spectra are the averages of 6 scans.

5.5.5 Field Emission Scanning Electron Microscopy (FESEM)

Appropriate volumes of the peptides were taken into microfuge tube from stock solution and water was evaporated by using speed vac. Desired solvent was added to it and solution was vortexed for 1 min and centrifuged. 2 μL of supernatant solution was then drop

casted on clean silicon vapor. Samples were allowed to dry at room temperature in vacuum desiccators and then coated with gold. Scanning electron microscopic imaging was performed using ZEISS ULTRA PLUS electron microscope.

5.6 Reference

1. Schroeder, Jr. H. W; Cavacini, L. Structure and Function of Immunoglobulins. *J Allergy Clin. Immunol.* **2010**, *125*, S41–S52.

2. Bernfield, M.; Kokenyesi, R.; Kato, M.; Hinkes, M. T.; Spring, J.; Gallo, R. L.; Lose, E. J. Biology of the Syndecans: A Family of Transmembrane Heparan Sulfate Proteoglycans. *Ann. Rev. Cell Biol.* **1992**, *8*, 365-93.

3. Shoulders, M. D.; Raines, R. T.; Collagen Structure and Stability. *Ann. Rev. Biochem*. **2009**, *78*, 929-958.

4. Vollmer, W.; Blanot, B.; de Pedro, M. A. Peptidoglycan structure and architecture *FEMS Microbiol. Rev.* **2008**, *32*, 149–167.

5. a) Pini, A.; Falciani, C.; Bracci, L. Branched Peptides as Therapeutics Current Protein and *Peptide Science* **2008**, *9*, 468-477. b) He, H.; Wang, H.; Zhou, N.; Yang, D.; Xu, b). Branched peptides for enzymatic supramolecular hydrogelation. *Chem. Commun*. **2018**, *54*, 86-89.

6. Tam, J. P.; Zavala, F. Multiple antigen peptide: A novel approach to increase detection sensitivity of synthetic peptides in solid-phase immunoassays. *J. Immunol. Methods* **1989**, *124*, 53-61.

7. Liu, S. P.; Zhou, L.; Lakshminarayanan, R.; Beuerman. R. W; Multivalent Antimicrobial Peptides as Therapeutics: Design Principles and Structural Diversities. *Int. J. Pept. Res. Ther*. **2010**, *16*, 199–213.

8. Minervini, A.; Siena, G.; Falciani, C.; Carini, M.; Bracci, L. Branched peptides as novel tumor-targeting agents for bladder cancer. *Expert Rev Anticancer Ther*. **2012**, *12*, 699-701.

9. Yoo, J.; Lee, D. Y.; Gujrati, V.; Rejinold, N. S.; Lekshmi, K. M.; Uthaman, S.; Jeong, C.; Park, I. K.; Jon, S.; Kim, Y. C. Bioreducible branched poly(modified nona-arginine) cell-penetrating peptide as a novel gene delivery platform. *J. Control. Release* **2017**, *246,* 142-154.

10. a) Crespo, L.; Sanclimens, G.; Montaner, B.; Tomás, R. P.; Royo, M.; Pons, M.; Albericio, F.; Giralt. E. Peptide Dendrimers Based on Polyproline Helices. *J. Am. Chem. Soc*. **2002**, *124*, 8876–8883. b) Crespo, L.; Sanclimens, G.; Royo, M.; Giralt, E.; Albericio, F. Branched Poly(proline) Peptides: An Efficient New Approach to the Synthesis of Repetitive Branched Peptides. *Eur. J. Org. Chem.* **2002**, *2002*, 1756-1762.

11. Siebler, C.; Trapp, N.; Wennemers, H. Crystal structure of (4*S*)-aminoproline: conformational insight into a pH-responsive proline derivative. *J. Pept. Sci*. **2015,** *21*, 208–211.

12. Rose, G. D.; Glerasch, L. M.; Smith, J. A. Turns in Peptides and Proteins. *Adv Protein Chem*. **1985**, *37*, 1-109.

13. Curran, T. P.; Chandler, N. M.; Kennedy, R. J.; Keaney, M. T. N-α-Benzoyl-Cis-4-Amino-L-Proline: A γ-Turn Mimetic. *Tetrahedron Lett.* **1996**, *37*, 1933-1936,

14. Bansode, N. D.; Madhanagopal, B.; Sonar, M. V.; Ganesh, K. N. Stereodependent and solvent specific formation of unusual β-structure through side chain-backbone H-bonding in C4(*S*)-(NH_2/OH/NHCHO)-L-prolyl polypeptides. *Biopolymers* **2017**,*108*, e22981

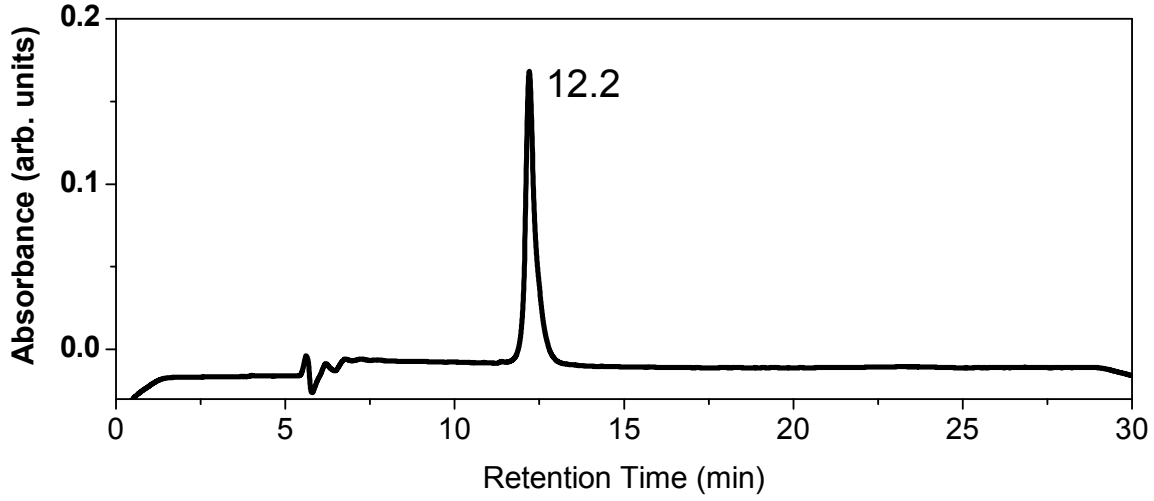
15. Bansode, N. D.; Sonar, M. V.; Ganesh, K. N. A nanofiber assembly directed by the non-classical antiparallel β-structure from 4*S*-(OH) proline polypeptide. *Chem. Commun*. **2016,** *52*, 4884-4887.

16. Shi, Z.; Zhou, C.; Liu, Z.; Totsingan, F.; Kallenbach, N. R. Amino Acid-Based Dendrimers. In *Amino Acids, Peptides and Proteins in Organic Chemistry.* Vol.4 – Protection Reactions, Medicinal Chemistry, Combinatorial Synthesis. Eds. Andrew B. Hughes, **2011** WILEY-VCH Verlag GmbH & Co. KGaA, Weinheim, pp 491-517.

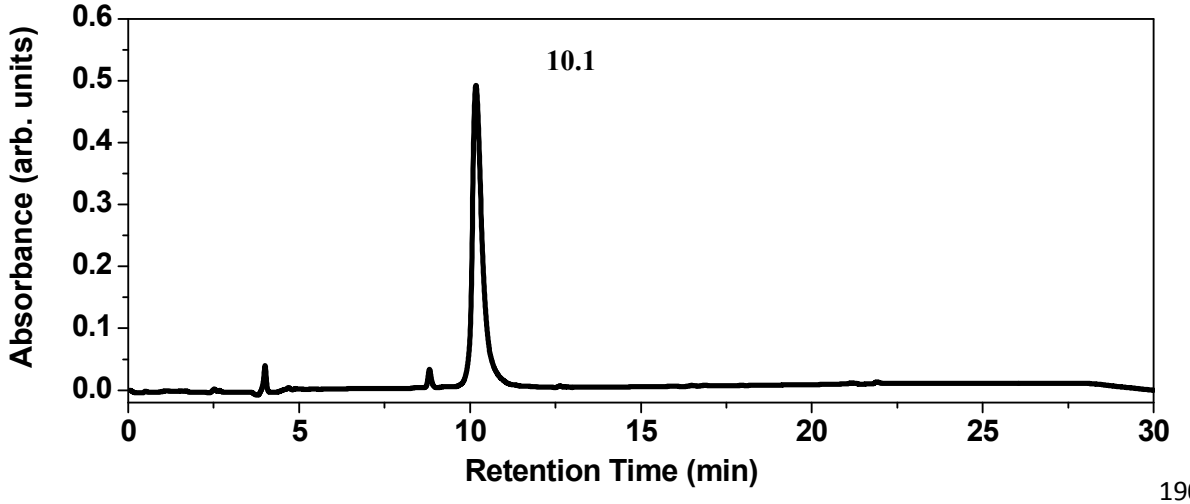
5.7 Appendix B

HPLC chromatograms of peptides

HPLC chromatogram of peptide **P12**

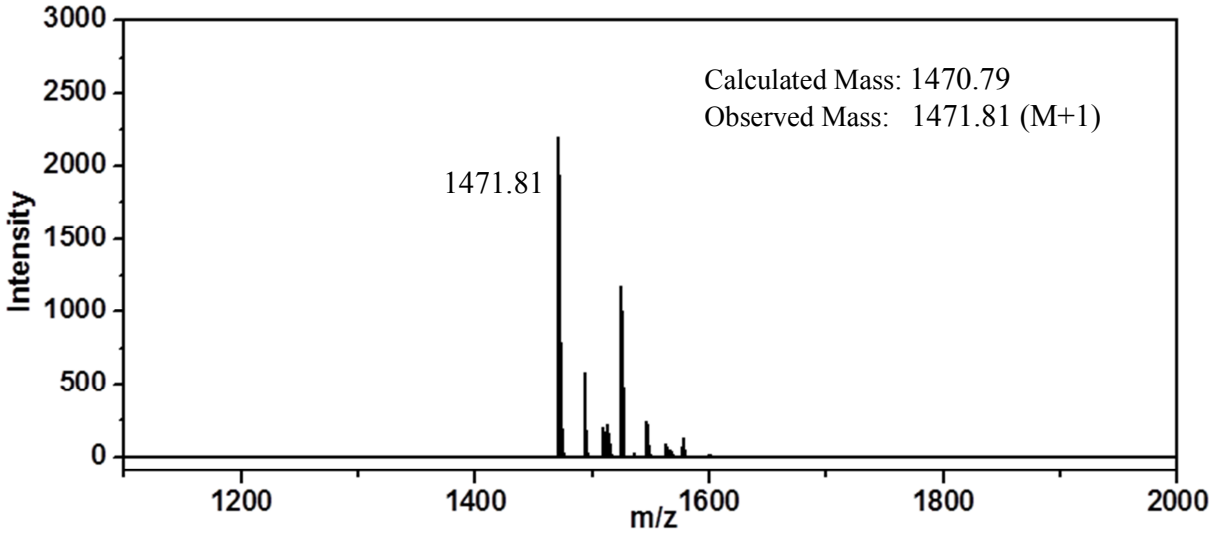


HPLC chromatogram of peptide **P13**

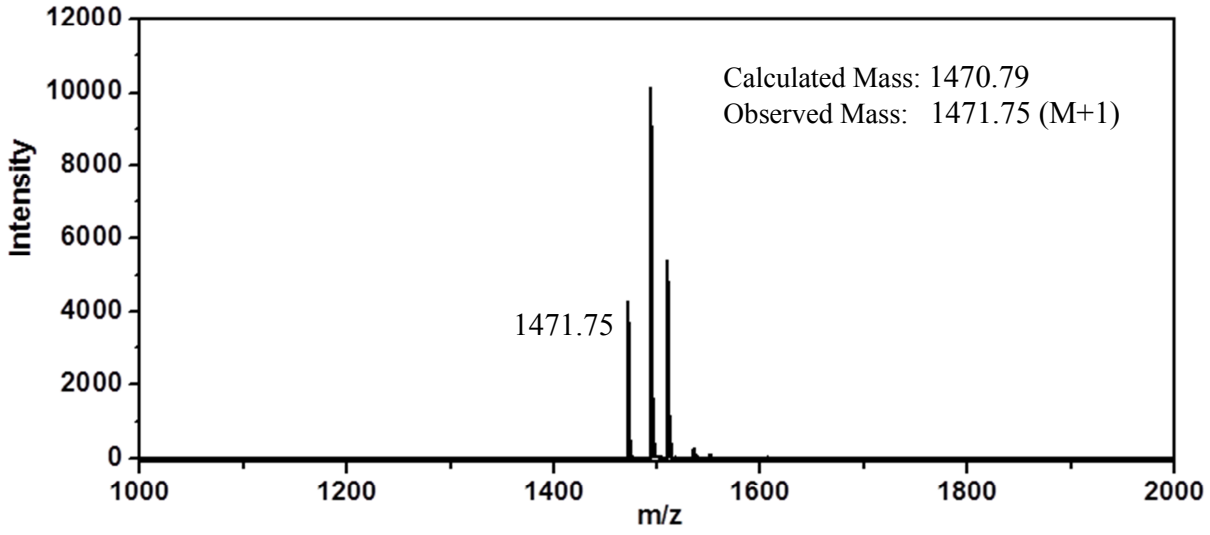


MALDI-TOF Spectra of Peptides

MALDI-TOF Spectrum of Peptide **P12**



MALDI-TOF Spectrum of Peptide **P13**



Chapter 6

Design, Synthesis, Biophysical Studies and Self Assembly of Branched Peptide Nucleic Acids

6.1 Introduction

Over the past few decades, there has been tremendous progress in the field of biomolecular self-assembly. Our understanding of the factors that influence the way peptides and DNA adopt particular defined conformations has empowered us to chemically mould them into nanostructures of arbitrary size and shape with better control and greater precision over their morphological features.[1]

The principles guiding the design of these self-assembling biomolecules into pre-determined morphology with specific functional outcomes are primarily based on molecular engineering of intermolecular side-chain to side-chain interactions. In the burgeoning field of nucleic acid nanotechnology, thousands of oligonucleotides are assembled into a diverse array of nanostructures of exemplary complexities with extraordinary precision by applying simple base-pairing rules given by Watson and Crick.[2] Recent developments in the field have demonstrated the potential of using programmable base-pairs for directed self-assembly. Peptides on the other hand have also been used for rational self-assembly.[3] Peptide based materials are arguably more versatile due to the large repertoire of building blocks with a variety of chemical functional groups. Directed self-assembly with peptides is, however, more complex than is the case with DNA/RNA. Still, there have been a few successful attempts at programming the supramolecular organisation of coiled coil peptides,[4] collagen[5] and ionic self-complementary peptides[6] by designing intermolecular sidechain – sidechain ionic bonds between strands with a well-defined secondary structure.[7]

In nature, there are many instances of protein based supramolecular assemblies with exceptional functional efficiency.[8] The enormous potential of peptide assemblies is therefore obvious. However, attempts to emulate the natural protein superstructures with peptides face

some formidable challenges. Among those major hurdles is the lack of a thorough understanding of the process of protein/peptide folding and the factors involved in determining the folding of the peptides of particular sequence into a specific secondary structure. As self-assembly with peptides is greatly affected by their secondary structures, this becomes a major limiting factor. The peptide sidechain interactions can be programmed as in nucleic acids by placing positively charged and negatively charged amino acids at defined positions in the backbone. However, for better specificity these strategies employing ionic bonds and hydrophobic interactions require complex designs. Comparatively, engineering molecular recognition through Watson-Crick base-pairing rules are simpler, superior and more robust.[9]

Combining the rich conformational dynamics of the peptide backbone and the robust base-pairing scheme of nucleic acids together would potentially yield superior self-assembling molecules. To this end, peptide DNA chimeras[10] and nucleolipids[11] have been synthesized and explored.

An imaginative approach is the use of peptide nucleic acids (PNA), which is a fusion of nucleobases on a polyamide chain.[12] PNAs were designed and synthesized to be a neutral, achiral mimic of DNA for various DNA/RNA binding applications.[12] Supramolecular assembly of PNAs into nanospheres, nanotubes and nanowires has been recently studied.[13-14] Sequence dependent programmable assembly of PNA into various nanostructures is still in its infancy. The battery of PNA analogs, reported over the past few decades provide a rich diversity in the constitution of their pseudopeptide backbone.[15] The nucleobases, which the PNAs have "inherited" from nucleic acids, allow specific molecular recognition through simple rules of complementarity programmable inter-strand interactions with high-fidelity. Thus, peptide nucleic acid based molecular self-assembly proves to be a promising alternative to construct

nanostructures of defined architectures and as models to enrich the guiding principles to develop more structurally complex and functional molecular nanodevices.

This chapter deals with branched peptide nucleic acids constructed with 4(*R/S*) aminoproline as scaffold at the branching point. Their synthesis, biophysical characterization and self-assembling properties under different conditions are discussed.

6.2 Rationale and Objectives

Having found that branched architecture aids self-assembly of peptides (Chapter 5), the design was extended to build branched PNA where the branching core was either (4*R*)-*Amp* or (4*S*)-*amp*, and the three arms, X, Y, and Z were tetrameric PNA strands.

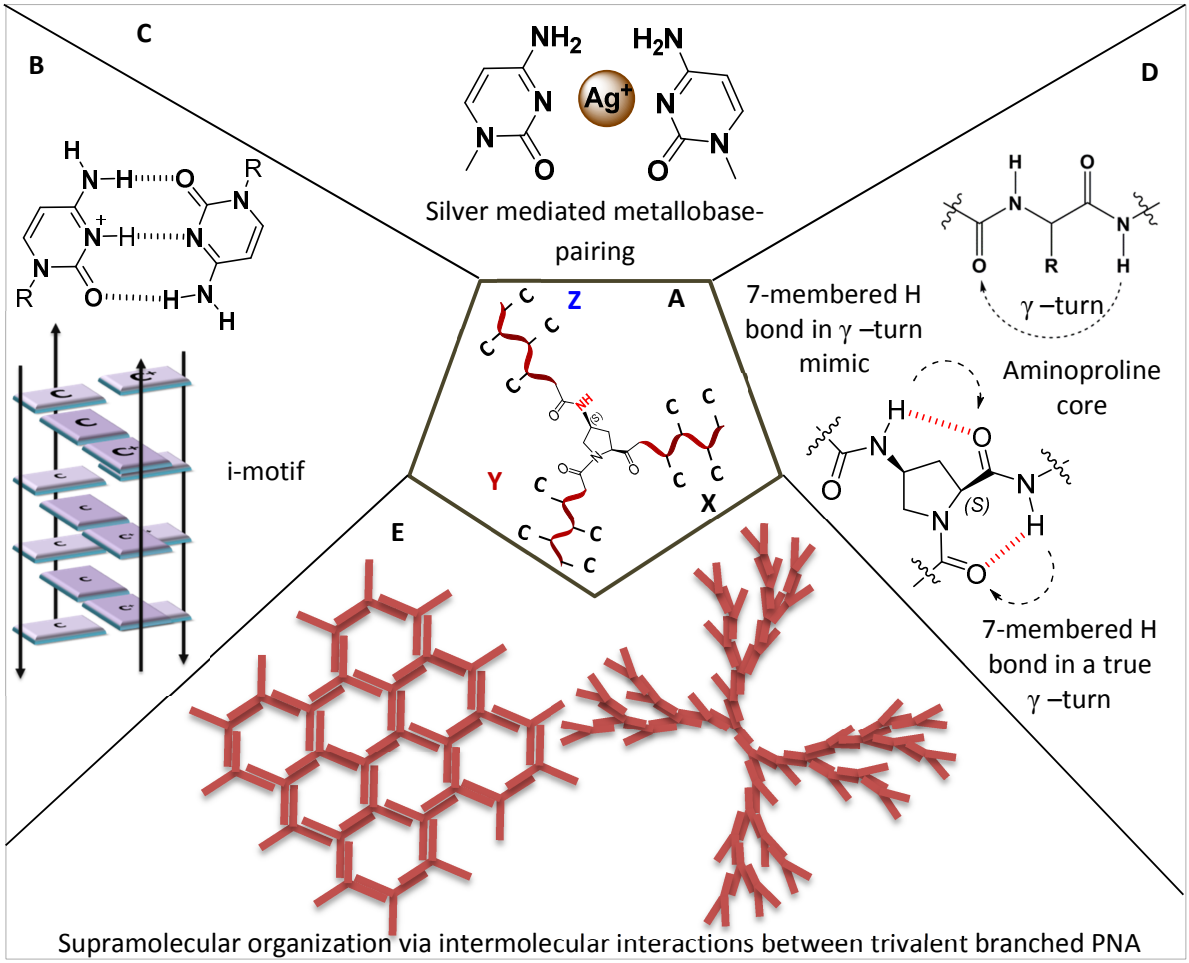


Figure 6.1: Structural, conformational and self-assembling properties of branched PNA

For the sake of simplicity, homooligomeric PNA strands were chosen as each of the three arms in the design of the branched molecule. Cytosines were chosen because in addition to specific binding to guanines through regular Watson-Crick base-pairing, they are also capable of forming pH dependent C-C^+ self-base pairing in i-motif structures,[16] and C-Ag^+-C metallo-base pairs[17] giving a much wider scope for self-assembly. Therefore, depending on the condition, the nature and strength of the interstrand interactions can be adjusted. It also allows control over the number of strands participating in the interactions. Since these are crucial for the way the molecule would pack together in an assembly, different conditions could be used to control the morphology of the supramolecular assemblies of these molecules.

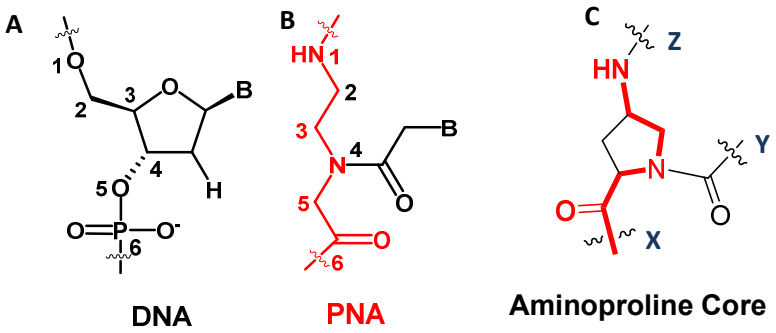


Figure 6.2: Comparison of the structure of DNA (A), PNA (B) and aminoproline core (C).

Here, the aminoproline core naturally integrates into trivalent branched PNA as it has built into it, a constrained PNA backbone that links PNA arms X and Z. Aminoprolines have been used to construct PNA analogs with constrained backbones to understand the role of conformational rigidity on the DNA binding properties of PNA.[18] Aminoproline unit can be considered to be a chimera with at least 3 different backbones built into it. As seen in the previous chapter, the aminoproline core links (i) X and Y arms by an α peptide backbone, (ii) X and Z arms are linked by a γ peptide backbone,[19] (iii) X and Z arms can also be thought of as being linked by a constrained amino ethyl glycyl-PNA backbone.[18] Therefore in terms of design,

an aminoproline can be an interesting bridge molecule between an α peptide and a γ peptide, or between an α peptide and a PNA.

Similar to the branched peptides, the chiral core with two stereo-centres at C2 and C4 is likely to influence the relative orientation of the three PNA arms attached to it. It could also be seen that the H bond donors and acceptors at the core of these branched PNA are quite different from the one in the previous branched polyproline.

In the branched polyproline peptides, the aminoproline core was linked to two of its peptide arms (X and Y) by tertiary amide links. In case of the branched PNA however, the aminoproline core is attached only to the arm X by tertiary amide bond. To the other two arms, Y and Z, it is linked via secondary amide linkage, each of which provides a H-bond donor and a H-bond acceptor. This is likely to have an influence on the flexibility and hence affect the conformational dynamics of the molecule. Notably, the aminoproline core in the branched PNA could form a gamma turn (Figure 6.1D). This is in addition to the potential trans-annular H-bond formation exhibited only by (4*S*)-*amp*, as discussed in Chapter 5. Prolines have a tendency to occur in turns and are often found to favor γ turns. Therefore, the orientation of the arms could be controlled by the core through formation of either (or both) of the two possible C_7 membered H bonds when (4*S*)-*amp* is used as the chiral branching core.

With a rich structural repertoire expected at the core and an environment specific tunability afforded by the oligocytosine PNA arms, it was expected that the branched PNA would exhibit pH, and metal ion specific conformational and self-assembling properties.

The specific objectives of the chapter include the following:

- Synthesis of branched PNA with (4*S*)-*amp* and (4*R*)-*Amp* as branching core and homotetramer of cytosine as the three PNA arms.
- Study the effect of the configuration at C4 of the aminoproline core on the conformation of the branched PNA molecule (i) under different pHs, (ii) in the presence of metal ions such as Ag^+ and, (iii) complementary DNA strands.
- Examine the self-assembly of the branched molecules through morphological studies.

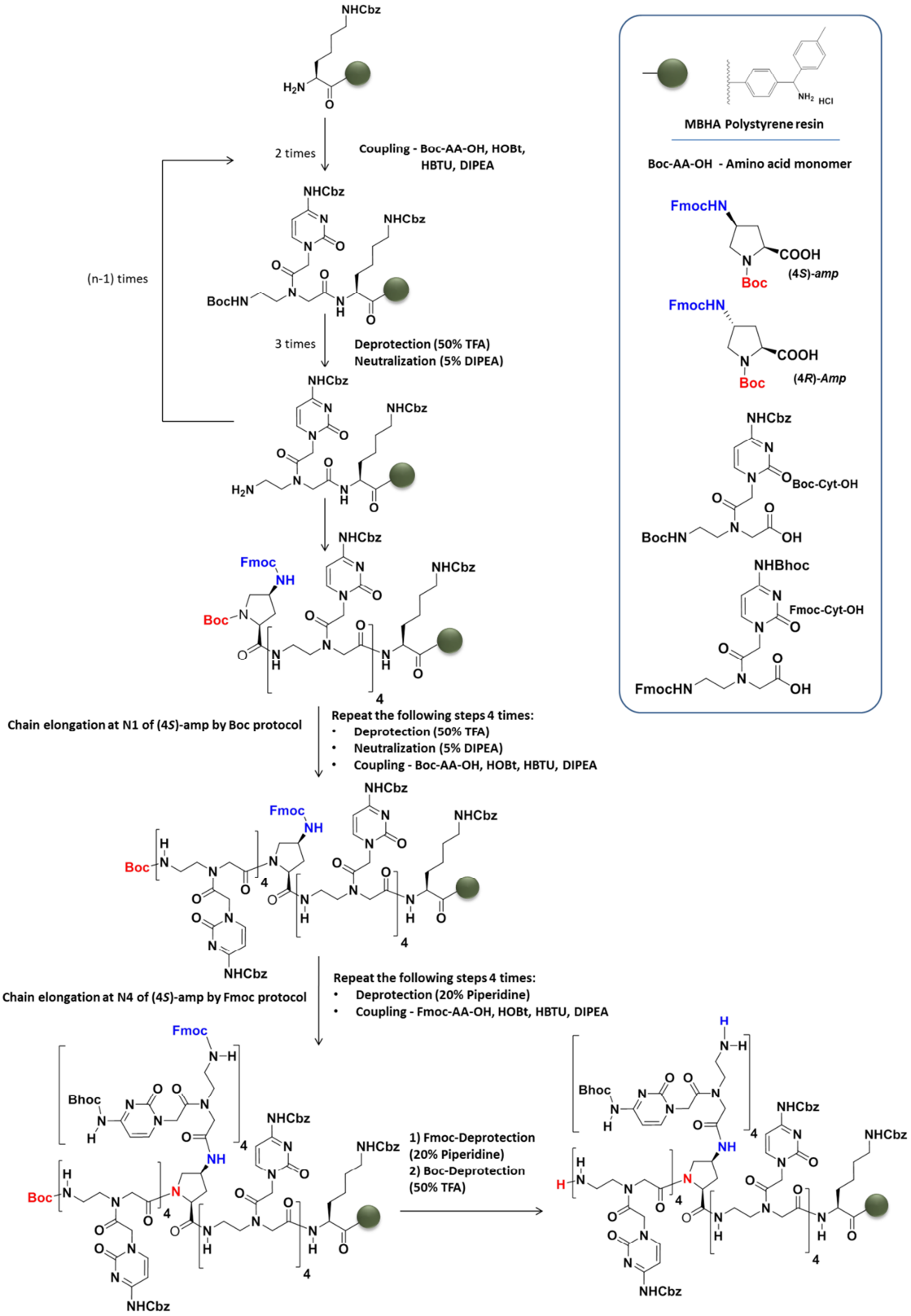
6.3 Results and Discussion

6.3.1 Synthesis of Branched PNA

Similar to the synthesis of branched peptides, branched PNAs were synthesized on solid support using MBHA resin. In order to study the effect of configuration at C4 of the aminoproline core, orthogonally protected aminoproline monomers (4*S*)-*amp* and (4*R*)-*Amp* were used.

6.3.1a *Synthetic Strategies*

For the synthesis of branched PNA molecules, both t-Boc and Fmoc strategies were employed. PNA monomers used for t-Boc strategy carried Cbz groups as orthogonal protecting groups, which is resistant to both basic (20% piperidine) and acidic (50% TFA) conditions. The monomers used for Fmoc strategy had the acid-sensitive protecting group (Bhoc) on the sidechain nucleobase amine groups. The 4(*R*/*S*)-aminoproline unit was added to create the branching point. Unlike the strategy used to synthesize branched peptides, branched PNA molecules were prepared not by elongating the two branching arms simultaneously, but by adopting sequential elongation route described in scheme 5.2. The latter strategy was preferred as attempts at elongating the branching PNA chains simultaneously yielded poor results. Sequential elongation strategy on the other hand was found to be more effective.



Scheme 6.1: Solid phase synthesis of branched PNA

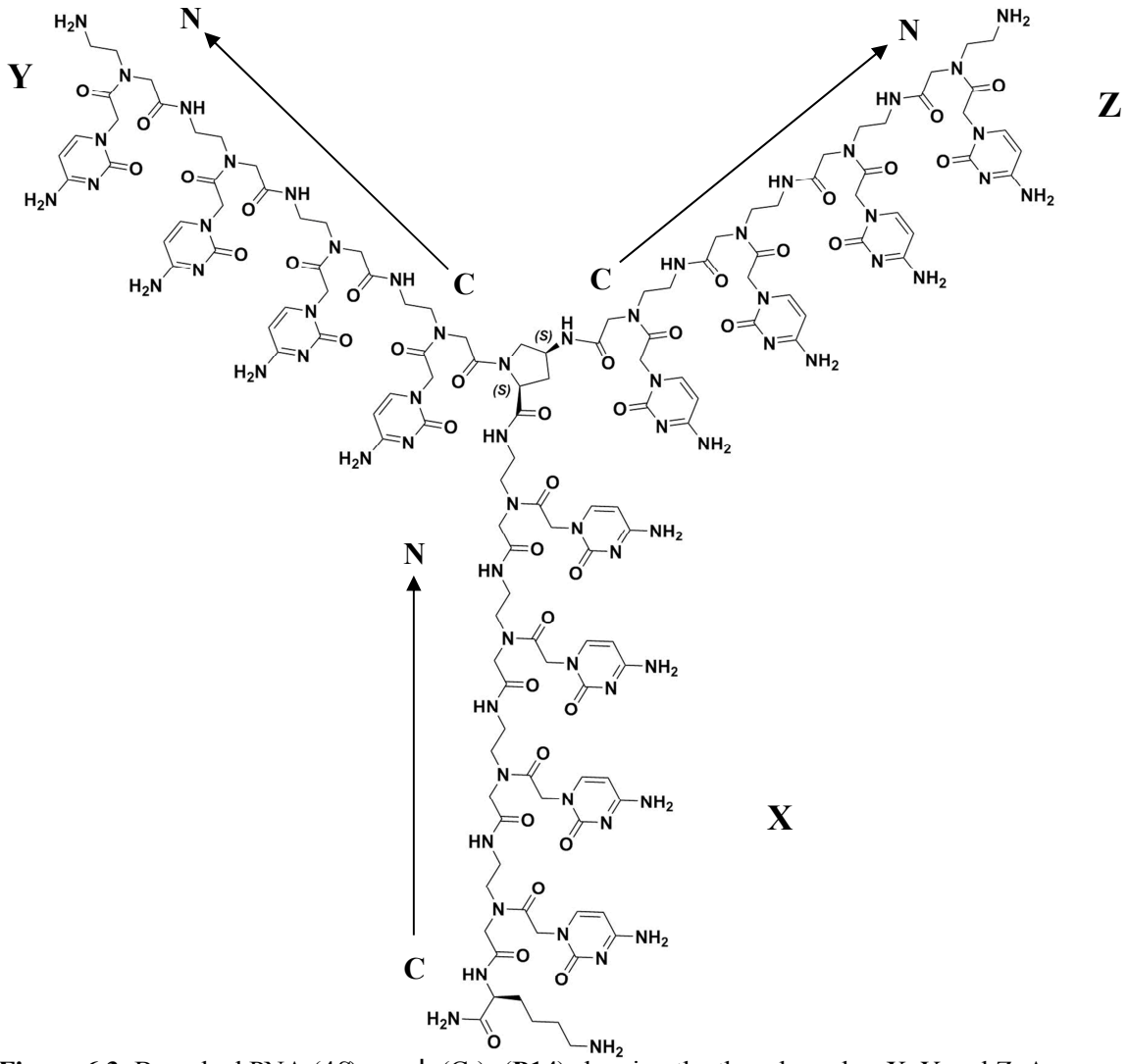


Figure 6.3: Branched PNA (4*S*)-*amp*$^{\curlywedge}$-$(C_4)_3$ (**P14**) showing the three branches X, Y and Z. Arrows shows the direction of synthesis of different PNA arms.

TABLE 6.1: HPLC retention time and MALDI-TOF mass spectral analysis of the PNAs

	PNA	HPLC RT (min)	Molecular Formula	Calc. Mass	Obs. Mass
P14	$(Cyt)_4$-*amp*-$(Cyt)_4$ $LysNH_2$ | $(Cyt)_4$ (4*S*)-*amp*$^{\curlywedge}$-$(C_4)_3$	12.60	$C_{131}H_{179}N_{65}O_{38}$	3272.29	3295.77 (M+Na)
P15	$(Cyt)_4$-*Amp*-$(Cyt)_4$ $LysNH_2$ | $(Cyt)_4$ (4*R*)-*Amp*$^{\curlywedge}$-$(C_4)_3$	12.75	$C_{131}H_{179}N_{65}O_{38}$	3272.29	3273.18 (M+1)

6.3.1b *Solid Phase Synthesis*

The N1 of the aminoproline core was deprotected with 50% TFA and the PNA arm Y was synthesized using t-Boc strategy which ends with the N-terminus residue carrying t-Boc protected primary amine (Scheme 6.1). The N^4 Fmoc was then removed on the aminoproline core and the PNA arm (Z) was extended by using Fmoc protocol. After the addition of 4 cytosine monomers the N-termini of both the branches were deprotected and the PNA was cleaved from the resin.

6.3.1c *Purification and Characterization of Branched Peptides*

The branched PNAs were purified using the reverse phase HPLC method on a semipreparative C18 column using linear gradient system of water and acetonitrile. The purity of the PNAs was then checked with C18 analytical column. The integrity of the purified PNAs was confirmed by MALDI-TOF spectrometry using DHB as matrix. Table 6.1 lists the HPLC retention time and molecular mass of the peptides obtained from HPLC analysis and MALDI-TOF spectrometry respectively. Representative HPLC chromatograms and MALDI-TOF mass spectra of branched PNAs are shown in Figure 6.4 and Figure 6.5 respectively.

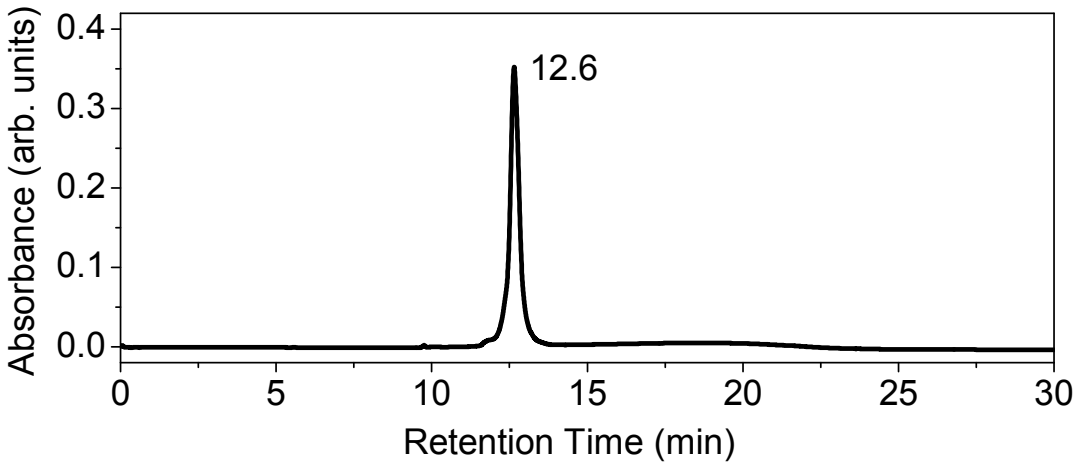


Figure 6.4: HPLC chromatogram of PNA **P14**

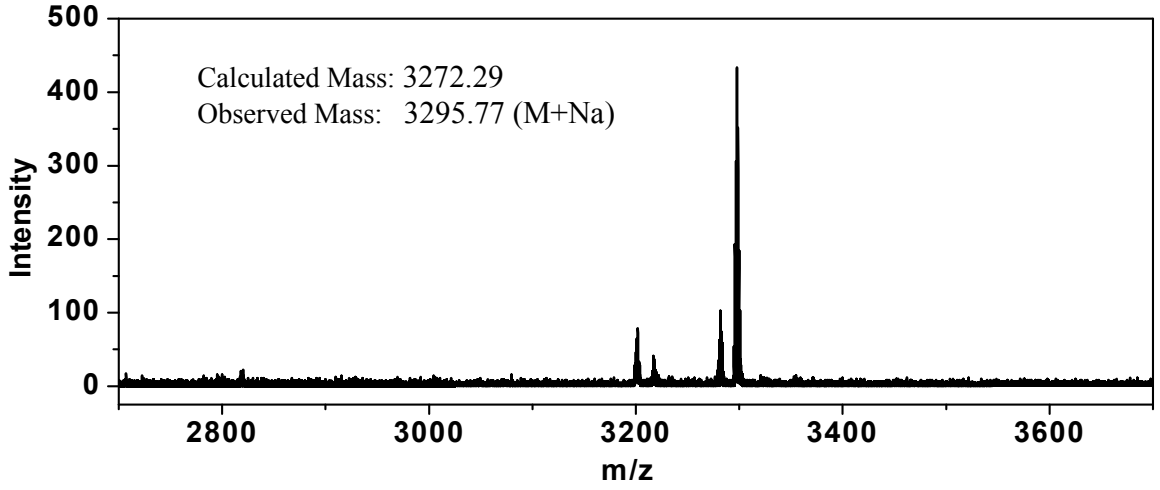


Figure 6.5: MALDI-TOF spectrum of PNA **P14**

The HPLC and MALDI-TOF spectra of all the PNA molecules in the present study are listed in Appendix C.

6.3.2 Conformational Studies of Branched PNA

The conformation of the branched peptides with 4(*R*/*S*)-aminoproline core, was found to be affected by the stereochemistry of the core in TFE (Chapter 5). In aqueous buffer, both (4*S*)-*amp* and (4*R*)-*Amp* residues as branching core showed predominantly PPII conformation. Here, conformational properties of branched PNAs under different pH, in the presence of complementary DNA, and under the influence of silver ions were monitored to ascertain the effect of core on the conformations adopted by these trivalent molecules under those conditions.

6.3.2a *Effect of pH on the Conformation of Branched PNA*

Single stranded PNA oligomers that are devoid of any chiral center generally do not show any characteristic CD spectra. Even when the PNA bears a C-terminal L-lysine or modified chiral backbone, single strand PNA molecules show weak chiro-optical properties on their own.[20] PNA oligomers of repeating cytosines have been shown to form i-motif structure in acidic

pH,[21] similar to DNA or RNA. An i-motif structure is formed when four strands of oligocytosines are bound together as a pair of intercalated duplexes (Figure 6.6). The duplexes are stabilized by a C-C^+ base pairing between the strands. The requirement of hemiprotonated cytosines ensure that i-motif conformation is formed only at a pH close to the pK_a of the N3 of cytosine.

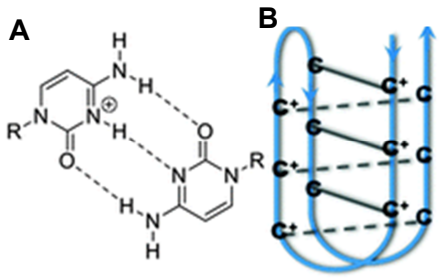


Figure 6.6: i-motif structure.[16d] A) The C-C^+ base pairing. B) Representation of interacted duplexes in an i-motif conformation formed by a continuous single strand.

PNA forms i-motif usually at lower pH compared to those of DNA i-motif,[21b] and it can be monitored by CD spectroscopy (Figure 6.7). A positive band at 295 nm in CD spectra is characteristic of i-motif structures.[16] In order to examine whether branched PNA molecules forms i-motif like structures, their circular dichroism spectra of the PNA solutions of concentration of 12 μM were recorded in 10 mM phosphate buffered saline at different pHs in the presence of 10 mM NaCl.

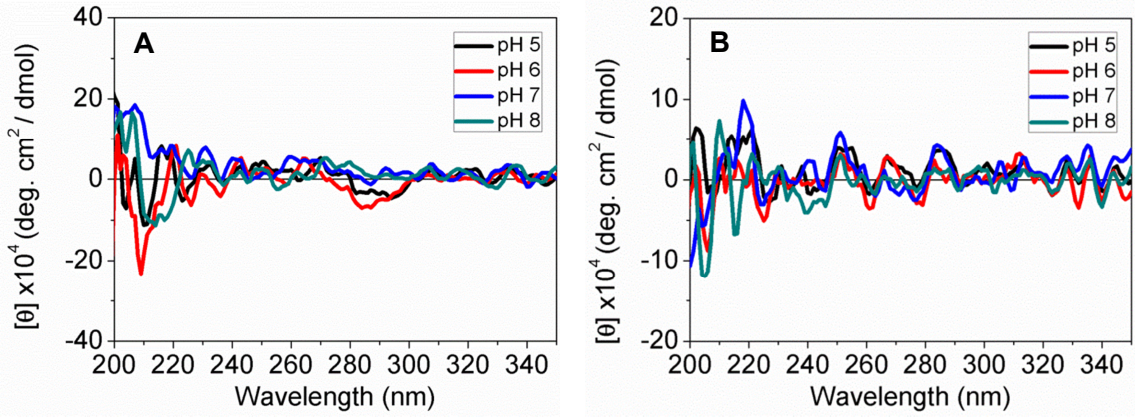


Figure 6.7: Circular dichroism spectra of PNA (4*S*)-*amp*$^{\curlywedge}$-$(C_4)_3$ (**P14**) (A) and PNA (4*R*)-*Amp*$^{\curlywedge}$-$(C_4)_3$ (**P15**) (B) in 10 mM phosphate buffered saline at pH 5-8.

Both the PNA molecules (4*S*)-*amp*$^{\lambda}$-$(C_4)_3$ (**P14**) and (4*R*)-*Amp*$^{\lambda}$-$(C_4)_3$ (**P15**) showed no characteristic bands in aqueous solutions of pH 5 to 8. There was a small negative band at 295 nm at pH 5-6 in case of PNA **P14**. Since the intensity of this band was too less as compared to the background, it was not possible to interpret anything about CD with respect to secondary structure.

6.3.2b *Effect of oligonucleotide dC_{12}*

PNA-DNA hybrid i-motif has been reported in the literature. In fact, it was shown that PNA prefers to form hybrid i-motif like structures with DNA with two strands of PNA and two strands of DNA.[22] To investigate whether the formation of a hybrid i-motif is favored by the branched PNA molecules with C-rich oligonucleotide strands, circular dichroism spectra of an equimolar mixture of the PNA and a homododecamer of cytosine (dC_{12}) was recorded at pH 5 and compared with the CD spectra of the same mixture at pH 7 and 8 (Figure 6.8).

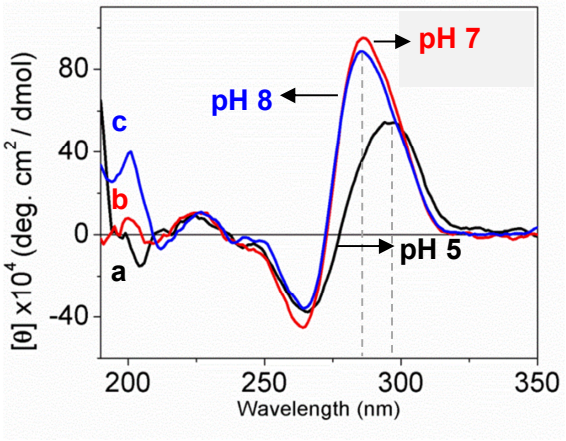


Figure 6.8: Circular dichroism spectra of PNA-DNA dC_{12} hybrids formed by (4*S*)-*amp*$^{\lambda}$-$(C_4)_3$ (**P14**) in 10 mM phosphate buffered saline at pH 5 (trace **a**), pH 7 (trace **b**) and pH 8 (trace **c**).

Aqueous solution of PNA/DNA mixture at neutral pH 7 and alkaline pH 8 showed similar spectral features (Firgure 6.5). There was a minor positive band at 225 nm band, a larger negative band at 265 nm and a strong positive band at 285 nm. Although the magnitudes of these

bands were slightly different, the overall CD signals at pH 7 and pH 8 showed no significant variations. This indicated that the PNA/DNA complexes existed in the same conformational state at neutral and alkaline pH.

However, at pH 5, the CD spectra of the PNA/DNA mixture revealed a clear shift in the position of the positive band to 295 nm, and the shift of this band suggested the formation of i-motif structure.

In order to rule out the formation of i-motif by dC_{12} alone, the CD spectra of DNA dC_{12} was recorded at pH 5, which showed a positive band at 290 nm. The equimolar mixture of PNA and DNA showed a distinct shift in the position of the prominent positive band at 295 nm (Figure 6.9). While a solution of DNA showed a band at 290 nm, the PNA/DNA mixture showed a band at 295 nm. This revealed that the PNA did indeed interact with the DNA strands and that the interaction of branched PNA with dC12 strands leads to formation of an i-motif like structure from the PNA:DNA hybrid. .

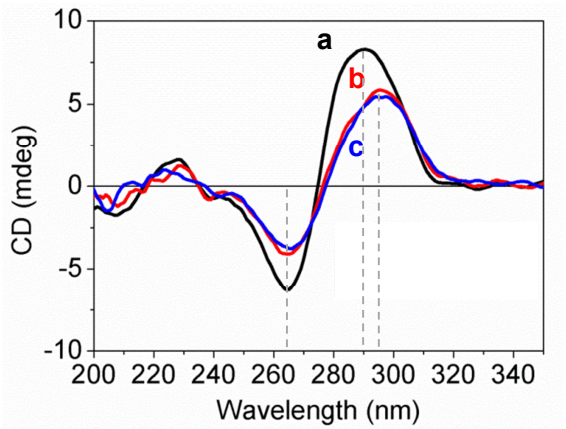


Figure 6.9: Circular dichroism spectra of DNA dC_{12} only (trace **a**), PNA-DNA dC_{12} hybrid formed by (4*S*)-*amp*^{A}-$(C_4)_3$ (**P14**) (trace **b**), (4*R*)-*Amp*^{A}-$(C_4)_3$ (**P15**) (trace **c**) in 10 mM phosphate buffered saline at pH 5.

Both the PNAs, (4*S*)-*amp*$^{\curlywedge}$-$(C_4)_3$, (**P14**) and (4*R*)-*Amp*$^{\curlywedge}$-$(C_4)_3$ (**P15**) showed similar CD spectra, indicating that the stereochemistry difference in core proline does not show up in CD spectra. Thus the configuration of the aminoproline core has little or no effect on the conformational behavior or binding properties of branched PNA dC_{12} DNA.

6.3.2b *Effect of Ag^+ on conformation of branched PNA*

Cytosine is known to have high affinity for various inorganic metal surfaces[23] and is shown to have superior binding properties with gold nanoparticles and silver nanoparticles.[24] Silver ions, in particular, are well known to induce C-Ag^+-C metallobase pairing. Formation of such metal ion mediated interactions between cytosines would result in the formation of PNA-PNA duplexes.[25] To monitor the metal induced PNA duplex formation and to check the effect of the chirality of aminoproline core on inducing such structures, CD spectra of the branched PNA molecules were recorded in water and in the presence of silver salt at stoichiometric concentrations.

In water, and in the absence of metal ions, the branched PNA showed negligible CD signals (Figure 6.9), with very weak bands in 200 nm - 230 nm range, perhaps arising from two chiral amino acids, C-terminus L-lysine, and the 4(*R*/*S*) aminoproline core. They were too weak to indicate any stable conformational properties of the branched PNA structure.

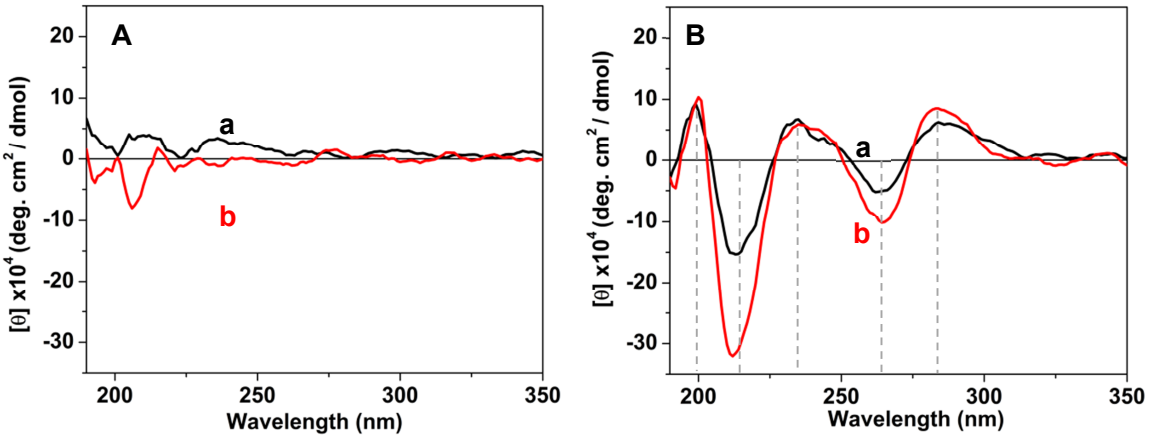


Figure 6.9: Circular dichroism spectra of PNA (4*S*)-*amp*$^{\lambda}$-$(C_4)_3$ (**P14**) (trace a) and (4*R*)-*Amp*$^{\lambda}$-$(C_4)_3$ (**P15**) (trace b) in the absence of Ag^+ (A) and in the presence of Ag^+ at [Cyt]:[Ag] of 1:1 (B) .

In the presence of stoichiometric amounts of aqueous silver nitrate, a well-formed CD spectral pattern was observed. The CD spectra of (4*S*)-*amp*$^{\lambda}$-$(C_4)_3$ (**P14**), and (4*R*)-*Amp*$^{\lambda}$-$(C_4)_3$ (**P15**) seen immediately after the addition of silver salt into the PNA solution is shown in the Figure 6.9B. A total of five bands were observed in the wavelength range of 190 to 325 nm, the bands showed an alternating positive and negative pattern. Similar pattern was observed with control PNA C_8 as well (Figure 6.10)

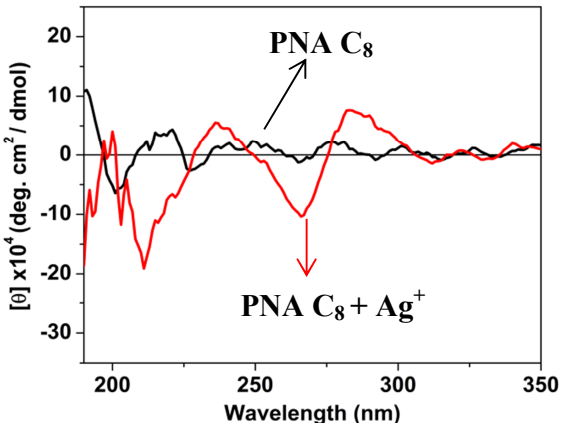


Figure 6.10: Circular dichroism spectra of aqueous solution of PNA C_8 without Ag^+ (black trace) and with equimolar Ag^+ (red trace).

The branched PNA (4*S*)-*amp*$^{\curlywedge}$-$(C_4)_3$ (**P14**) showed positive bands at 280 nm, 230 nm and 195 nm with approximately the same magnitude and negative bands at 260 nm and longer one at 210 nm. The same was shown by the 4(*R*)-analogue PNA (4*R*)-*Amp*$^{\curlywedge}$-$(C_4)_3$ (**P15**). While the magnitude of the bands at 195nm, 230 nm, 260 nm and 280 nm were similar for the two PNAs, the magnitude of the negative band at 210 nm was significantly different for the two chiral branched PNAs. In case of PNA (4*R*)-*Amp*$^{\curlywedge}$-$(C_4)_3$ (**P15**), the magnitude of the band at 210 nm was about two fold more intense as compared to PNA (4*S*)-*amp*$^{\curlywedge}$-$(C_4)_3$ (**P14**). This suggested that slight change in the conformation of the PNA is caused by the chiral core since it was the only structural difference between the two branched PNAs.

The CD spectra of the branched PNA with alternating positive and negative bands at 230 nm, 260 nm and 280 nm with nearly the similar magnitudes was atypical of PNA:DNA/RNA duplexes.[26] PNA molecules are achiral and in their single stranded form do not show any CD spectra.[20] When bound to complementary DNA/RNA, the PNA tends to adopt a helical conformation, the handedness of which was dictated by the complementary nucleic acid strand.[26-27] The PNA:PNA duplexes without any chiral substitutions in the backbone tend to adopt both left and right handed helices at about the same concentrations and this was found to result in the PNA duplexes showing no CD signals. Addition of a chiral amino acid like lysine at the C terminus is known to influence the helical handedness of the PNA backbone.[26-27] L-lysine at C terminus introduced a bias towards right handed helical sense in the PNA backbone. Similarly, introduction of modifications in the PNA backbone which renders it chiral also influenced the stability of one of the two possible helical senses in the PNA duplexes. Here, the

branched PNA has three PNA arms, each with a distinct chiral entity at their C-termini. PNA arm X has a L-Lys at its C-terminus. Arm Y and Z are bound to the chiral aminoproline to stereocenters C2(*S*) and C4(*R*/*S*) respectively. While addition of silver is known to bind two cytosine residues, resulting in the formation of duplexes mediated by C-Ag^{+}-C metallo basepairing,[17] similar interactions in PNA is hardly explored.

The CD signatures obtained for branched PNA (4*S*)-*amp*$^{\curlywedge}$-$(C_4)_3$ (**P14**) and (4*R*)-*Amp*$^{\curlywedge}$-$(C_4)_3$ (**P15**) are therefore a net sum of the CD features derived from the three PNA arms each forming either intramolecular or intermolecular duplexes mediated by Ag^{+} (C-Ag^{+}-C). The observed alternating positive and negative bands in the CD spectra could therefore be the resultant of the signals arising from each of the arms. Alternatively, cytosine rich sequences of DNA have been also shown to produce similar CD spectra in DNA.[28] In addition to this, the role of metal ions in enhancing the chiro-optical properties of PNA could not be ruled out either.

The CD spectra of the two branched PNAs, (4*S*)-*amp*$^{\curlywedge}$-$(C_4)_3$ (**P14**) and (4*R*)-*Amp*$^{\curlywedge}$-$(C_4)_3$ (**P15**) was found to undergo a time-dependent change (Fig 6.10 A-B). When the CD signals were monitored for a period of 1.5 hours, it was found that the two branched PNA molecules had distinct time dependent changes even though they showed similar spectra soon after addition of the metal ions into the PNA solution.

In case of branched PNA (4*S*)-*amp*$^{\curlywedge}$-$(C_4)_3$ (**P14**), an inversion of the signs of all the five bands were observed. The CD spectra at 90 minutes was almost a mirror image of the one obtained after 1 minute of addition of Ag^{+}. Time resolved CD spectra that captured this

transformation showed four isosbestic points between the five prominent bands. This indicated that the process involved two distinct species.

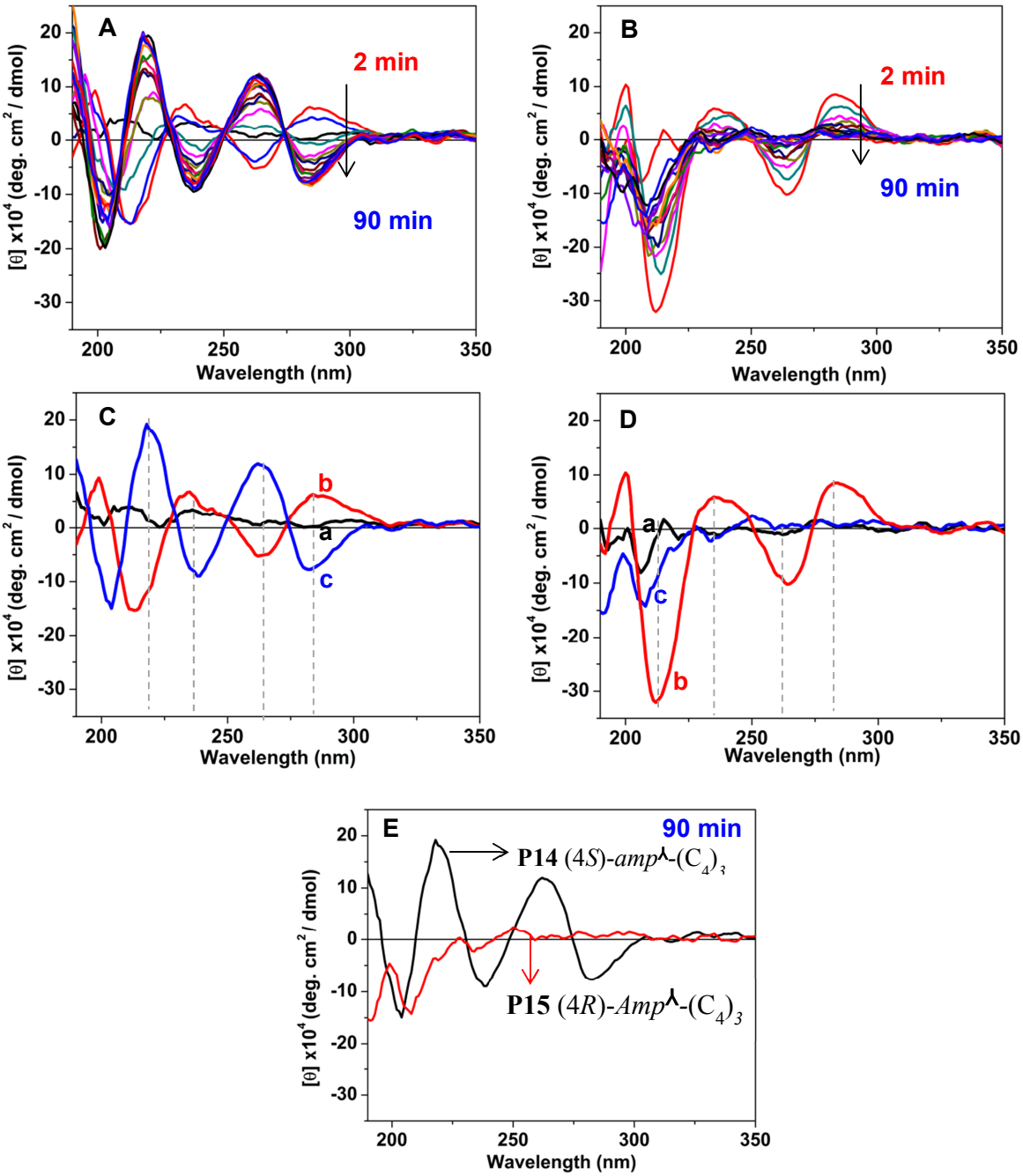


Figure 6.10: Time dependent circular dichroism spectra of PNA (4*S*)-*amp*$^{\lambda}$-$(C_4)_3$ (**P14**) (A and C) and (4*R*)-*Amp*$^{\lambda}$-$(C_4)_3$ (**P15**) (B and D) in the absence of Ag+ (trace a) and in the presence of Ag^+ at [Cyt]:[Ag] of 1:1 at time 2 min (trace b) and 90 minutes (trace c). (E) Comparison of CD spectra of PNA (4*S*)-*amp*$^{\lambda}$-$(C_4)_3$ (**P14**) (black trace) and (4*R*)-*Amp*$^{\lambda}$-$(C_4)_3$ (**P15**) (red trace) after 90 minutes.

The inversion in CD signals suggests that the branched PNA undergoes a change in its helical handedness. It was difficult to delineate the spectral contributions from individual PNA arms and identify whether all or only one/two of the PNA arms showed such a conformational dynamics. It was however, apparent that an overall change in chirality of the silver bound branched PNA occurred over a period of 90 minutes.

In case of (4*R*)-*Amp*$^{\lambda}$-$(C_4)_3$ (**P15**), the initial CD spectral pattern vanished within the same period of 90 minutes. A progressive decline in the intensity of all the bands was observed resulting in a featureless spectrum at 90 minutes (Figure 6.11). A total loss of CD signals could occur either due to loss of duplex structure and dissociation of the PNA strands into separate single strands with no distinct conformation, or as a result of an equilibrium between the two helical states with mirror image CD spectra, where they exist in solution in nearly equal concentrations.

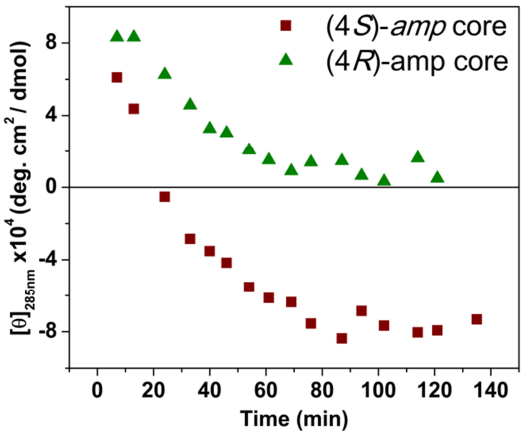


Figure 6.11: Change in molar ellipticity at 285 nm for PNA (4*S*)-*amp*$^{\lambda}$-$(C_4)_3$ (**P14**) (Brown square) and (4*R*)-*Amp*$^{\lambda}$-$(C_4)_3$ (**P15**) (green triangle).

Regardless of the process that leads to the observed behavior, it was evident that the chiral aminoproline core had a significant influence over the conformational dynamics of the branched PNA.

Ag^{+} induced conformational changes in the branched PNA molecules (4*S*)-*amp*$^{\lambda}$-$(C_4)_3$ (**P14**) and (4*R*)-*Amp*$^{\lambda}$-$(C_4)_3$ (**P15**) suggested the following:

- The chiral aminoproline core and its configuration at C4 has a significant influence on the overall conformation of the molecule.
- The strong and well-defined CD signals at 230 – 280 nm could have arisen from the formation of intermolecular or intramolecular PNA/PNA duplexes stabilized by Cyt-Ag^{+}-Cyt metallobase pair.
- The similarity in the initial CD spectral bands in both (4*S*)-*amp*$^{\lambda}$-$(C_4)_3$ (**P14**) and (4*R*)-*Amp*$^{\lambda}$-$(C_4)_3$ (**P15**) suggested that at 2 min stage, both the PNAs exhibited similar conformations.
- The rapid rate of formation of this species indicated that it was kinetically favoured.
- The gradual reversal of the signs of the bands in (4*S*)-*amp*$^{\lambda}$-$(C_4)_3$ (**P14**) indicated that interconversion of the initial form I, associated with a +ve 280 nm band, to its mirror image form II, associated with –ve 280 nm band.

The PNAs (4*S*)-*amp*$^{\lambda}$-$(C_4)_3$ (**P14**), and (4*R*)-*Amp*$^{\lambda}$-$(C_4)_3$ (**P15**), could exist in both form I and form II, which are different from each other in the helical handedness of one or two, or all the three PNA arms. The form I was kinetically favored and hence both the PNA resulted in the formation of this state immediately after addition of the silver ions. In the case of (4*S*)-*amp*$^{\lambda}$-$(C_4)_3$ (**P14**), form II was thermodynamically more stable and hence, a total interconversion between the two forms ensued. However, in the case of (4*R*)-*Amp*$^{\lambda}$-$(C_4)_3$ (**P15**), the two forms

did not differ in their energy and were favored equally. The result of which was an equilibrium between the two mirror image forms causing a cancellation of the CD signals arising from the two forms present in the solution.

The two PNA molecules differ in the aminoproline core. The (4*S*)-*amp* core in (4*S*)-*amp*$^{\lambda}$-$(C_4)_3$ (**P14**), has a preferred *endo* ring pucker which also would lead to formation of a trans-annular H bonding between the C4(*S*)-NH_2 group and the carbonyl oxygen of the same residue (Figure 6.12 A-B). (4*R*)-*Amp* core on the other hand, typically prefers *exo* ring pucker, in which the intra-residue H bond is not possible. The consequence of this could be that while (4*S*)-*amp* core has the possibility of a H bond that restricts the PNA arms Y and Z in (4*S*)–*amp* containing PNA (4*S*)-*amp*$^{\lambda}$-$(C_4)_3$ (**P14**), there is no such conformational restriction on PNA (4*R*)-*Amp*$^{\lambda}$-$(C_4)_3$ (**P15**).

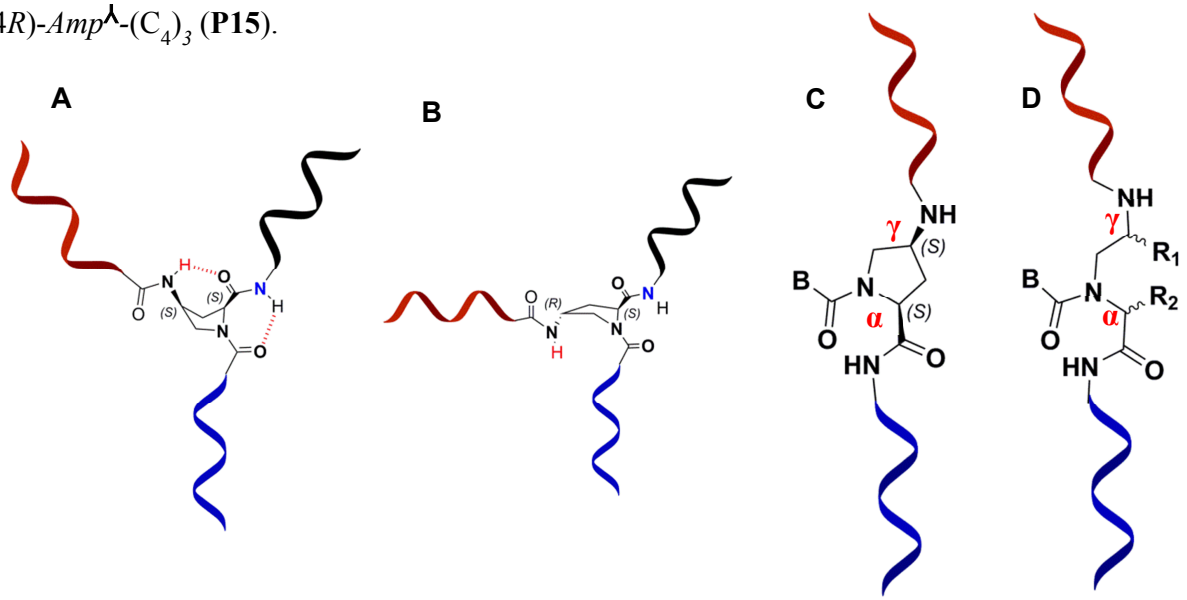


Figure 6.12: Comparison between the ring pucker of 4(*R*/*S*)-aminoproline core. (4S)-amp core prefers endo ring pucker (A) while (4R)-Amp core prefers exo ring pucker. C) Structure of aminoprolyl PNA and D) unmodified PNA backbone.

Thus the role of ring pucker and intraresidue H bond may assume importance in dictating the conformational dynamics of the two PNA molecules.

The three PNA arms are similar as they possess four cytosine nucleobases as sidechains. But, they are non-identical and have distinct C-termini. PNA arm X has a L-Lysine which is known to induce right handed helical sense in PNA-PNA duplex.[26-27] Chiral induction by C-terminal amino acid was known to be significant upto 8 residues and was therefore relevant to the present study. PNA arm Y also has an α-amino acid, L Proline at its C-termini and can be expected to have similar influence on the PNA handedness as was seen with L–Lysine. In case of PNA arm Z, it stems from a γ-amino acid.[19] The PNA arms X and Z could also be viewed as analogous to PNA bearing a constrained chiral modification in the middle of the backbone (Figure 6.12 C-D).[18]

As compared to α-substitutions, the γ-substitutions were known to have a stronger influence on the preference of helical handedness of the PNA.[20] The C4-substituted aminoproline core units, (4*S*)-*amp* and (4*R*)-*Amp* could therefore differentially affect the handedness of the PNA arm Z to a large extent.

Arm X has two chiral aminoacids – one L-Lysine at its C-terminus and a (2*S*,4*R*/*S*)-aminoproline at the N-terminus. Notably, the three prominent bands arising from the stacked base-pairs inverted in their sign but showed nearly the same magnitude. If we consider this system to have three PNA arms participating in metallobase pairing with similar propensity and contribute equally to the CD spectra, then the witnessed magnitude changes are plausible only under the two following scenarios. (i) When out of the 3 arms, one arm forms left handed helix, and another has a tendency for right handed helix, and the third undergoes a conversion from right to left (or vice versa). (ii) When all three arms undergo helix inversion.

Since the form I with a +ve band at 280 nm is likely to be kinetically favored state, it could involve at least a pair of the arms in an intramolecularly metallobase paired arrangement. A H bonding rearrangements at the core of PNA (4S)-*amp*$^{\lambda}$-$(C_4)_3$ (**P14**) could trigger an interconversion from the intramolecular metallobase pairs to intermolecular metallobase pairing allowing extended supramolecular assembly of the branched PNA molecules. In view of all these observations and inferences, the following model was proposed to explain the observed chiro-optical properties of the branched PNA.

1) The three PNA branches are unstructured and possessed no definite conformation in the absence of Ag^+ ions (Figure 6.13 A and D).
2) On addition of the silver ions, two of the arms form parallel intramolecular duplex by silver mediated C-Ag^+-C metallobase pairing (Figure 6.13 B and E).
3) With time, the intramolecular parallel duplex formed by two arms dissociate and the branches participate in intermolecular antiparallel duplexes, producing extended branched architectures (Figure 6.13 C).
4) The change in preference for the intramolecular duplex to intermolecular duplex is orchestrated by the H-bonding patterns and ring pucker of aminoproline core (Figure 6.13 C).
5) In case of (4*S*)-*amp*, the conversion to the open state suitable for intermolecular interaction is stabilized by the trans-annular H-bonding at the core residue favored during the C4-endo ring pucker. In case of (4*R*)-*Amp*, such a stabilizing factor is unavailable due to its configuration at C4. This renders both the open state and the closed state to be equally stable, when the branching core is (4*R*)-*Amp*. (Figure 6.13 F) On the other hand, (4*S*)-*amp* core favors the open state.

6) The change in the H-bonding pattern at the core and the ring puckers of the aminoproline unit manifests itself not only in the formation of two single stranded arms, ready to form metal mediated base-pairing with similar arms of the other molecules, but also in the reversal of preference for the helical handedness of PNA arm Z.

7) The result of these is the gradual change in the overall conformation of the molecule. This also suggests that PNA (4*S*)-*amp*$^{\lambda}$-$(C_4)_3$ (**P14**) with a proper shift in the preference from one state to another should produce ordered supramolecular assemblies as compared to PNA (4*R*)-*Amp*$^{\lambda}$-$(C_4)_3$ (**P15**) which is believed to not discriminate between the two states.

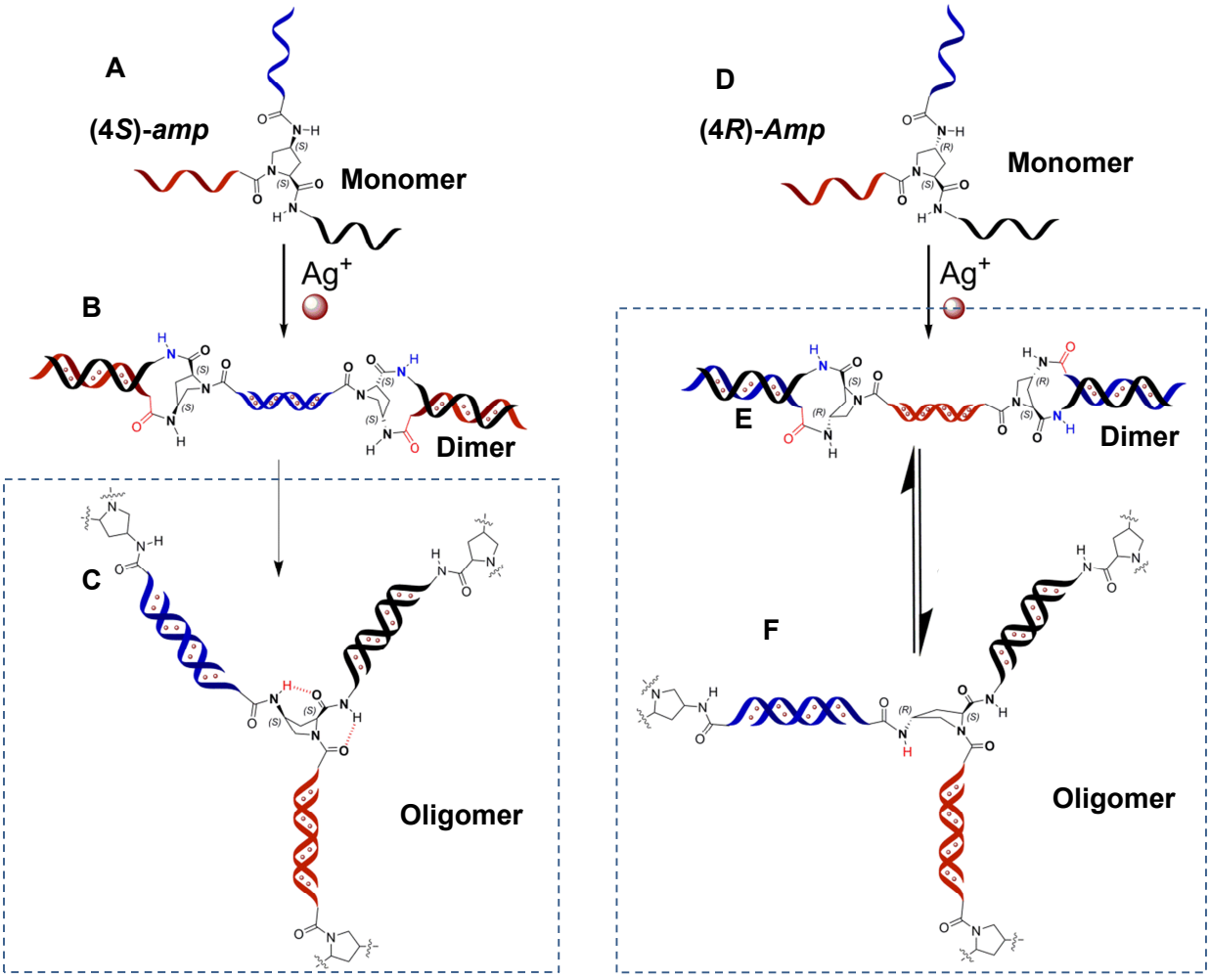


Figure 6.13: Plausible mechanism to explain the role of chiral aminoproline core in intramolecular to intermolecular interactions branched PNA

Since **P14** and **P15** differ only in their configuration at C4, from all previous studies of differences in their behavior, the only possible interpretation of their CD results is one that emerges from the above model.

6.3.3 Morphology of Self-Assembled Branched PNAs

The branched peptides constructed with 4(*R*/*S*) aminoproline core units exhibited stereodependent self-assembling properties in TFE, the solvent in which the (4*S*)-amp_3 branches showed stereospecific conformational changes (Chapter 5). Since peptide nucleic acids are superior to aminoprolyl polypeptides in their sequence dependent intermolecular interactions based on Watson-Crick base pairing and also because the PNA molecular recognition occurs in water, branched PNA molecules are construed to be better systems to test the deployability of 4(*R*/*S*)-aminoproline core as chiral hinge to control the self-assembling behavior of branched structures.

Similar to studies carried out with linear and branched peptides (Chapter 5), the morphology of self-assembling branched PNA was investigated using FESEM. The samples were prepared as described in the earlier chapters. Aliquots (2 μL) of the branched PNA solutions of appropriate concentration was taken on a clean Si wafer and allowed to dry in air under high vacuum for 4 hours. Prior to FESEM imaging, the dried films of the branched PNA, were sputter coated with gold for better contrast.

6.3.3a *Effect of pH on Self-Assembly of branched PNA*

The self-assembly of branched PNA was examined by preparing the samples from branched PNA solutions at a nucleobase concentration of 200 μM made in water or phosphate

buffer (10 mM) containing 10 mM NaCl at different pHs. The morphology of the particles were observed under FESEM.

In water, PNA (4*S*)-*amp*$^{\lambda}$-$(C_4)_3$ (**P14**) did not show any specific morphology (Figure 6.14A). In phosphate buffered saline at pH 7, the PNA **P14** was found to assemble into distinct spherical particles (Figure 6.14B). The particles were found to be homogenous in shape. The particles were of the size of about 50-100 nm. When the pH was reduced to 5, the PNA molecules were still found to assemble into spherical structures, relatively monodispersed and the particles had a diameter of about 1 μm (Figure 6.14 C). There were qualitatively fewer particles of diameter less than 100 nm. It was observed that the particles possessed a central hollow morphology.

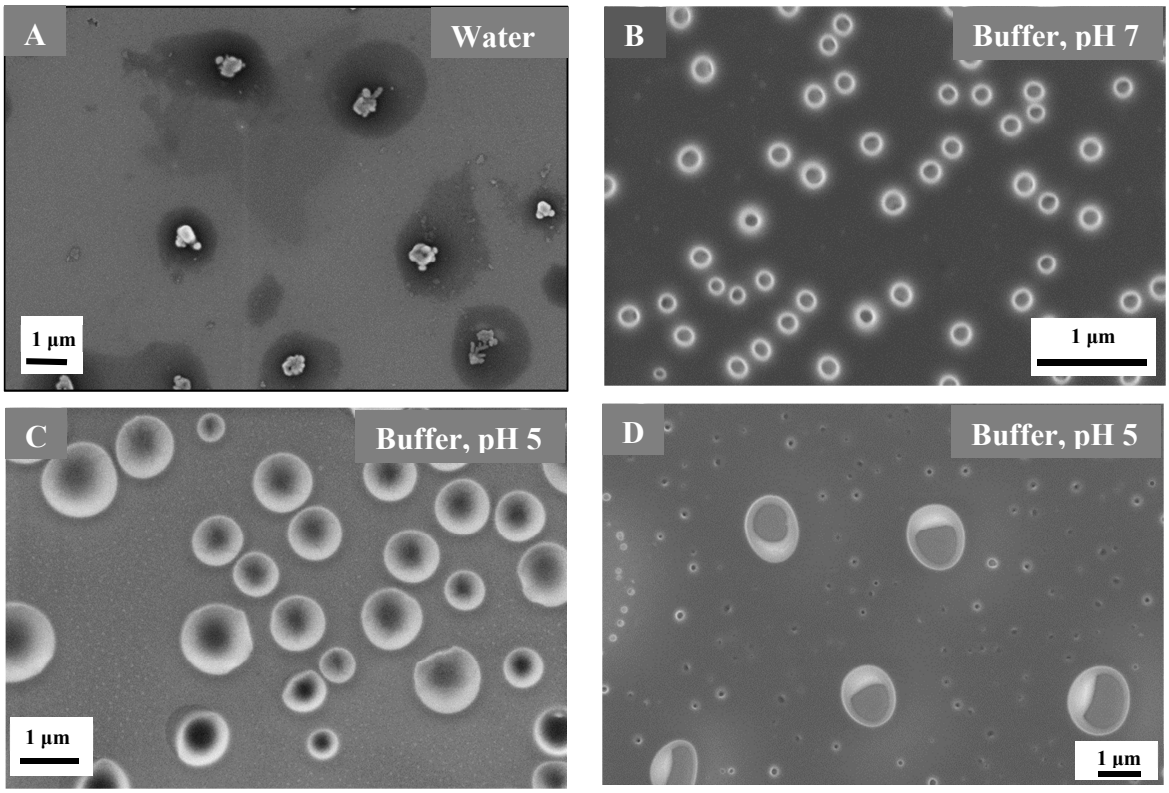


Figure 6.14: FESEM Images of (4*S*)-*amp*$^{\lambda}$-$(C_4)_3$ (**P14**) in water (A) in 10 mM phosphate buffered saline pH 7 (B) and pH 5 (C). Particles showing hollow morphology of the PNA in pH5 (D).

It is evident from figure 6.12D that particles were spherical capsule like structures with part of the outer layer broken off, perhaps due to dehydration under high vacuum conditions used for imaging. The morphologies are similar to that formed by liposomes and peptidosomes.[3]

The stereomeric PNA (4*R*)-*Amp*$^{\curlywedge}$-$(C_4)_3$ (**P15**) showed morphology similar to that observed with PNA (4*S*)-*amp*$^{\curlywedge}$-$(C_4)_3$ (**P14**) with irregular to ellipsoidal particles in water (Figure 6.15A). In phosphate buffer (at both pH 5 and pH 7), the branched PNA assembled into regular spherical particles. The morphology seen at pH 5 was not very much different from the one at pH 7. The size of the particles was found to be between 50 nm to 100 nm (Figure 6.15B-D).

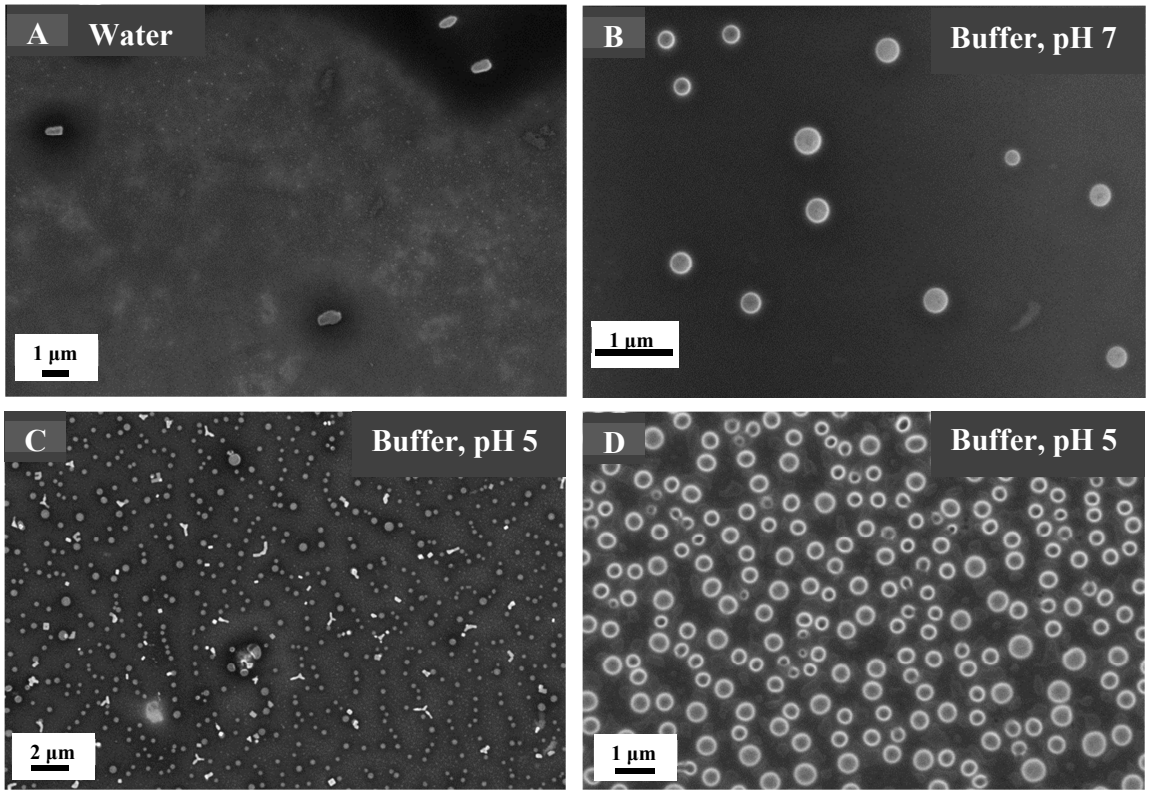


Figure 6.15: FESEM Images of PNA (4*R*)-*Amp*$^{\curlywedge}$-$(C_4)_3$ (**P15**) in water (A) in 10 mM phosphate buffered saline pH 7 (B) and pH 5 (C). Spherical particles of PNA in pH5 at a higher magnification (D).

6.3.3b *Effect of dG_{12} on Self-Assembly of branched PNA*

The advantage of using peptide nucleic acid strand as compared to simple peptides was the ease with which intermolecular interactions could be programmed using Watson-Crick base-pairing rules. Analogous to DNA nanotechnology, the peptide nucleic acid nanostructures could also be constructed by customizing the design principles used for directing self-assembly of DNA molecules to suit the PNA-DNA or PNA-PNA duplex geometry. In case of branched PNA (4*S*)-*amp*$^{\lambda}$-$(C_4)_3$ (**P14**), it was envisaged that the three arms could be crosslinked by complementary DNA molecules to stimulate the formation of supramolecular architecture. Therefore, the self-assembly of PNA (4*S*)-*amp*$^{\lambda}$-$(C_4)_3$ (**P14**) in the presence of complementary oligodeoxyguanosine dG_{12} was studied. PNA (4*S*)-*amp*$^{\lambda}$-$(C_4)_3$ (**P14**) (12 μM) was annealed with equimolar amounts (12μM) of dG_{12} and the hybrid solution (2μL) was spotted on a clean Si wafer and dried as described above. The samples were coated with gold before FESEM imaging.

The Figure 6.16 shows the morphology of PNA (4*S*)-*amp*$^{\lambda}$-$(C_4)_3$ (**P14**) in water with complementary oligonucleotide dG_{12}. The annealed complex of branched PNA and DNA showed a network like morphology with spherical particles interspersed between them (Figure 6.16A). No regular or any characteristic nanostructures were observed with dG_{12} alone under the same conditions. Comparison of the morphology of the DNA strand alone (Figure 6.16B) and branched PNA (4*S*)-*amp*$^{\lambda}$-$(C_4)_3$ (**P14**) alone (Figure 6.14A) and the PNA-DNA hybrid (Figure 6.16A), reveals that the DNA considerably influences the self-assembly of branched PNA. This

effect may arise from the intramolecular or intermolecular crosslinking of PNA arms by interspersing dG_{12} oligonucleotide strands.

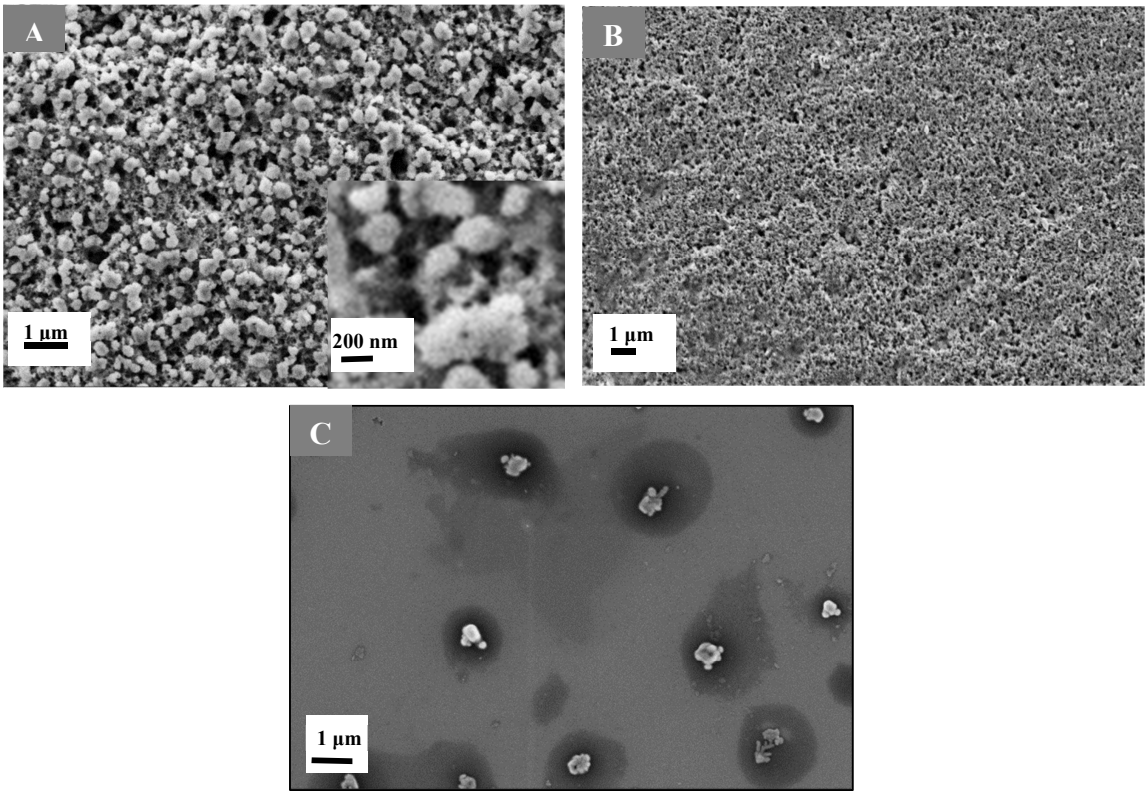


Figure 6.16: (A) FESEM Images of PNA-DNA hybrid formed by PNA (4*S*)-*amp*$^{\lambda}$-$(C_4)_3$ (**P14**) and dG_{12}. Inset shows magnified view. (B) Only dG_{12} in 10 mM phosphate buffered saline pH 7. (C) FESEM Image of only by PNA (4*S*)-*amp*$^{\lambda}$-$(C_4)_3$ (**P14**) in water, for comparison.

The absence of any regular morphology could be the consequence of random crosslinking of the PNA arms. Although the three arms XYZ are each unique, they carry the same sequence. When the oligonucleotide crosslinks these arms there are a possible total of 9 combinations of cross-linked pairs. This kind of heterogeneity hampers the ordered self-assembly process leading to the formation of seemingly featureless network like morphology.

6.3.3c *Effect of dC_{12} on Self-Assembly of Branched PNA*

Homo-oligomeric cytosines in DNA, RNA and PNA have been known to form i-motif structures at acidic pH.[21] The i-motif is a tetraplex formed by a stretch of cytosines involved in $C\text{-}C^+$ self-base-bairing. Such base pairs forming duplexes intercalate amongst each other to produce a 4-stranded i-motif structure. Since this requires one of the cytosines in the basepair to be protonated at N3, i-motifs are prevalent at acidic pH. However, recent reports suggest that even under physiological conditions, i-motifs are formed in the cells and is believed to be key for gene regulation.[30] Structurally, i-motif is more rigid than duplexes as it involves four strands and has been effectively used in supramolecular assembly of DNA.[31] A prominent example of its employment in soft materials science is the formation of DNA hydrogels.[30-31]

Analogous to studies with dC_{12} oligonucleotides, supramolecular assembly of branched PNA was studied with $dC_{12,}$ while maintaining the pH at 5.0 to facilitate the formation of i-motif. The samples were prepared by taking aliquot (2 μL) of a solution containing branched PNA (12μM) and dC_{12} (12 μM) in phosphate buffer (pH 5) and NaCl (10 mM) on a clean silicon wafer and allowing it to dry at room temperature. The solutions were allowed to age for 1 to 5 days.

Both PNA (4*S*)-*amp*$^{\curlywedge}$-$(C_4)_3$ (**P14**) (Figure 6.17A-B) and PNA (4*R*)-*Amp*$^{\curlywedge}$-$(C_4)_3$ (**P15**), (Figure 6.17C-D) were found to form nanotubes that were a few micrometers in length and about 100-200 nm in width. The sharp edges on the nanotubes indicated that the assembled structures were crystalline with well-defined facets. The cross-section of the nanotubes were to be mostly rectangular (Box in Figure 6.17B) accompanied by some with a hexagonal cross-section. On

closer observation (Box in Figure 6.17D), some of square shaped tubes showed minor facets that with stunted growth, suggesting that kinetics of the tube formation influenced its morphology.

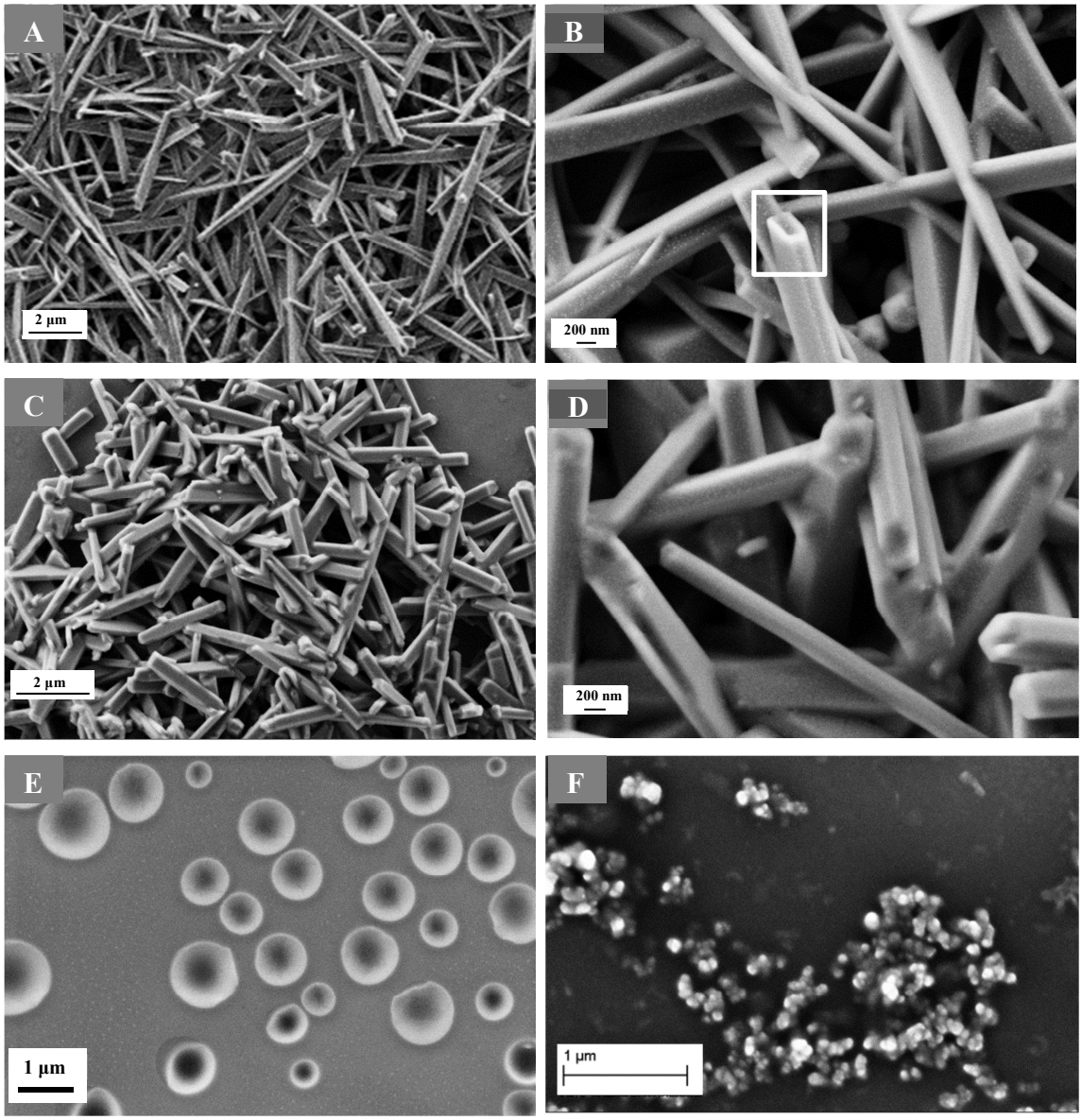


Figure 6.17: DNA/PNA nanotubes formed by PNA (4*S*)-*amp*ʎ-$(C_4)_3$ (**P14**) (A-B) and PNA (4*R*)-*Amp*ʎ-$(C_4)_3$ (**P15**) (C-D) with dC_{12} in 10 mM phosphate buffered saline pH 5. FESEM images of only PNA (4*S*)-*amp*ʎ-$(C_4)_3$ (**P14**) (E) and DNA dC_{12} in buffer (10 mM, pH 5) (F).

A time dependent study was carried out to probe the growth of the nanotubes (Figure 6.18). From a solution of PNA (4*R*)-*Amp*ʎ-$(C_4)_3$ (**P15**) and dC_{12} in phosphate buffered saline,

aliquots (2 μL) were drawn at different time points for a period of up to 5 days and the samples for FESEM were prepared as described above. The dried samples were coated with gold prior to imaging. The results of the study revealed the following.

On day 1, small crystallites were observed (Figure 6.18A). Many of these were well-formed octahedrons with triangular faces. Others were truncated octahedrons with additional square and trapezoidal faces (Figure 6.18B).

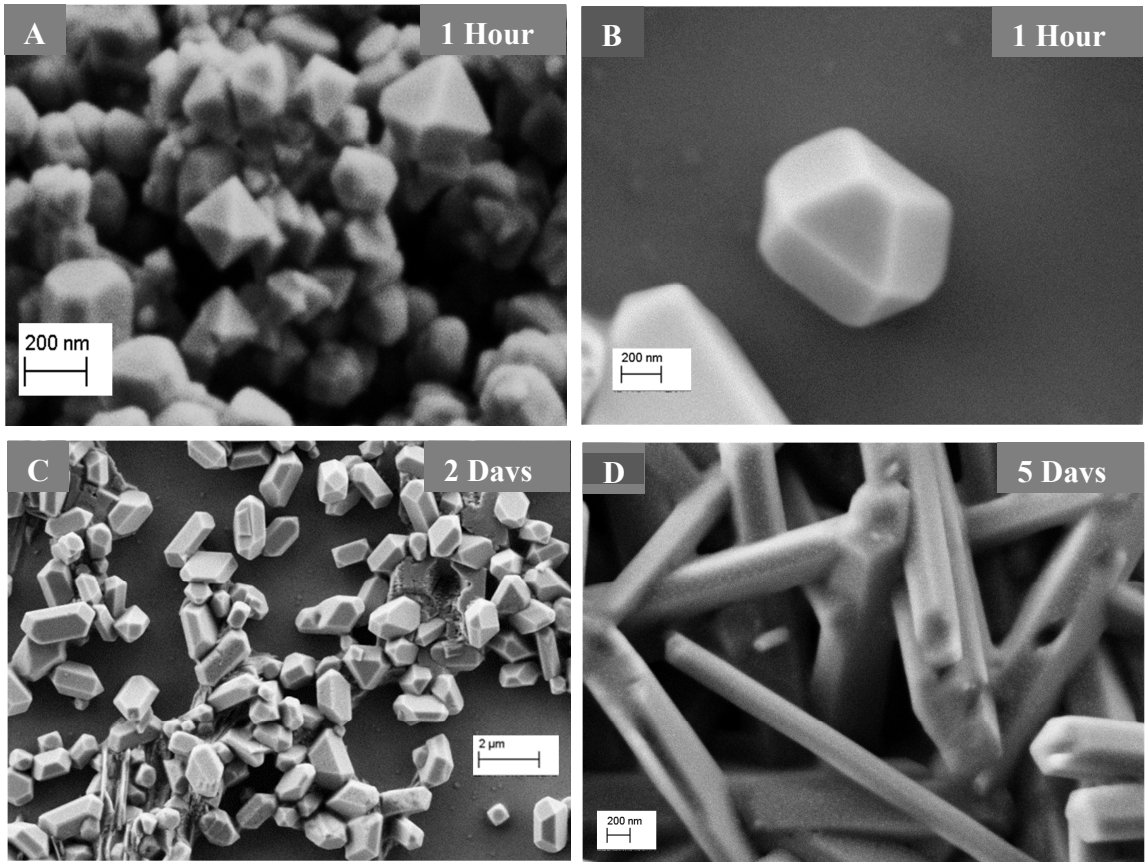


Figure 6.18: Growth stages of nanotubes formed by PNA (4*R*)-*Amp*$^{\lambda}$-$(C_4)_3$ (**P15**) with dC_{12}. Morphology of the particles in a solution of 12 μM PNA and DNA in 10 mM phosphate buffered saline pH 5 at different time points: within 1 hour (A); (B) is a close view of one particle; (C) after 2 days; (D) after 5 days.

On day 2, many of the crystals had grown in one direction more than the others producing elongated hexagonal prisms (Figure 6.18C). While the involvement of anisotropic growth was evident at this stage, the crystallites did not show any hollow nature.

On day 5, the fully grown long nanotubes were obtained. These tubes had either square cross-section or hexagonal cross-sections (Figure 6.18D). The hollowness of the tubes was clear from the open ends of the tubes. The time dependent study suggested that the nanotubes formed via a process that was similar to those observed with some hollow crystals.[32] The hollow morphology could therefore be a consequence of the differential growth rates at different facets of a seed crystal. The branched PNA and DNA pack together to form seed crystals in the first 24 hours. These crystals have an octahedron habit. Some of the crystal faces outgrow the others leading to anisotropic growth of the crystals into hexagonal sequence prisms. The progressive growth of the edges of these fast growing facets led to the formation of a dent, which eventually resulted in a tube like morphology with hollow interior and crystalline walls.[32]

6.3.3d *Effect of Ag^+ on Self-Assembly of Branched PNA*

Pyrimidines have been known to have affinity for transition metal ions.[33] In particular, there were many reports of silver selectively binding to cytosines to form C-Ag^+-C metallobase pair. An assembly of silver mediated metallobase-pairs into long contiguous molecular wires was recently reported.[34] In order to check whether supramolecular assembly of the branched (4*S*)-*amp*$^{\lambda}$-$(C_4)_3$ (**P14**), and PNA (4*R*)-*Amp*$^{\lambda}$-$(C_4)_3$ (**P15**) could be induced by silver ions through intermolecular interactions between different arms of the PNA molecules, the following studies were carried out.

To an aqueous solution of the branched PNA with specific cytosine concentration (0.5 mM to 2.5 mM), different volumes of freshly prepared aqueous solution of $AgNO_3$ was added to bring the concentration of silver to be 2 mM. The solutions were mixed by vortexing for approximately 1 min and left to stand for a period of typically 8 hours under ambient condition.

Aliquot (2 μL) of this was dropped on a clean Si wafer and the solvent was allowed to evaporate at room temperature for 12 hours. The film was put under high vacuum to ensure that it is totally dry. The drop cast PNA film was then sputter coated with a layer of gold for FESEM imaging.

When the PNA (4*S*)-*amp*$^{\curlywedge}$-$(C_4)_3$, (**P14**) and silver nitrate were taken in a concentration where the cytosine units and Ag^+ ions were present in equimolar concentrations, a regular and homogenous morphology was obtained. The branched PNA (4*S*)-*amp*$^{\curlywedge}$-$(C_4)_3$ (**P14**) assembled into four pointed nanostars up on complexation with Ag^+ ions (Figure 6.19).

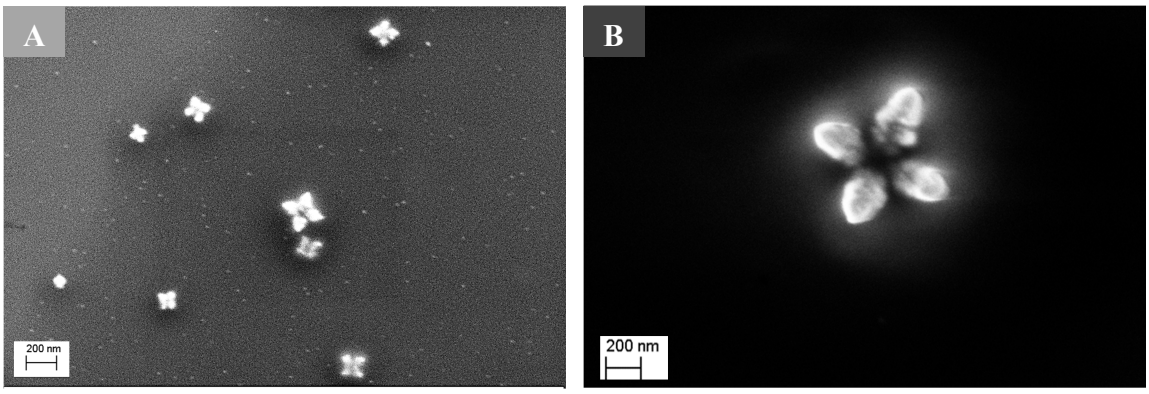


Figure 6.19: Self-assembly of PNA (4*S*)-*amp*$^{\curlywedge}$-$(C_4)_3$ (**P14**) with silver ions in water. PNA – Ag four-pointed stars formed in a solution of 2 mM cytosine concentration and 2 mM $AgNO_3$ (A). One of the nanostars showing the gaps between the four lobes.

These four pointed star like structures had four lobes arranged in a four-fold symmetry, where the long axis of the lobes intersect at the center, and each of these form right angles with those of its neighbours. The size of the lobes was about 200 nm along the long axis. In many of the structures, a void at the center was clearly noticeable and so was a cross shaped void that separates the lobes from one another (Figure 6.19B). The number of lobes forming the star shaped clusters was exclusively four. These exemplify the precision of the ordered assembly process behind the formation of complex with well-defined morphology.

Effect of concentration on morphology of Ag^+ - PNA complex

The changes in the [C]:[Ag^+] stoichiometry was found to influence the morphology of the silver PNA complex in the concentration range of cytosine from 0.5 mM to 2.0 mM, with the concentration of Ag^+ being 2.0 mM (Figure 6.20). At PNA (4*S*)-*amp*$^{\lambda}$-$(C_4)_3$ (**P14**):Ag^+ stoichiometry of 1:4, rod-like structures with 50 nm in width and lengths about 1-2 μm were obtained. Upon closer examination, these rods were found to be rough and porous (Figure 6.20F).

When the [C]:[Ag^+] ratio was increased to 1:2, rods start aggregating into longer structures (Figure 6.20B). When the stoichiometry [C]:[Ag^+] was changed to 1.5:2.0, the phase change occurred with rods assembling into four pointed nanostars (Figure 6.20C). These were heterogenous in size accompanied by some irregular aggregates. At equimolar concentration of cytosine and Ag+, as shown earlier, the complexes of branched PNA (4*S*)-*amp*$^{\lambda}$-$(C_4)_3$ (**P14**), with Ag assemble into very nice regular four-pointed nanostars (Figure 6.20D).

When the cytosine concentration increased further (stoichiometric ratio 2.5 mM : 2.0 mM) the nanostars became more prominent and start further aggregating together into large one dimensional thread like assemblies (Figure 6.20E). This indicated that the nanostructures can undergo further aggregation post-assembly, when the stoichiometry of PNA was more than that of silver. Thus during the initial periods, assembly seem to dominated by C:Ag+ interactions and at a later stage, it is influenced by self-assembly induced by PNA-PNA interactions.

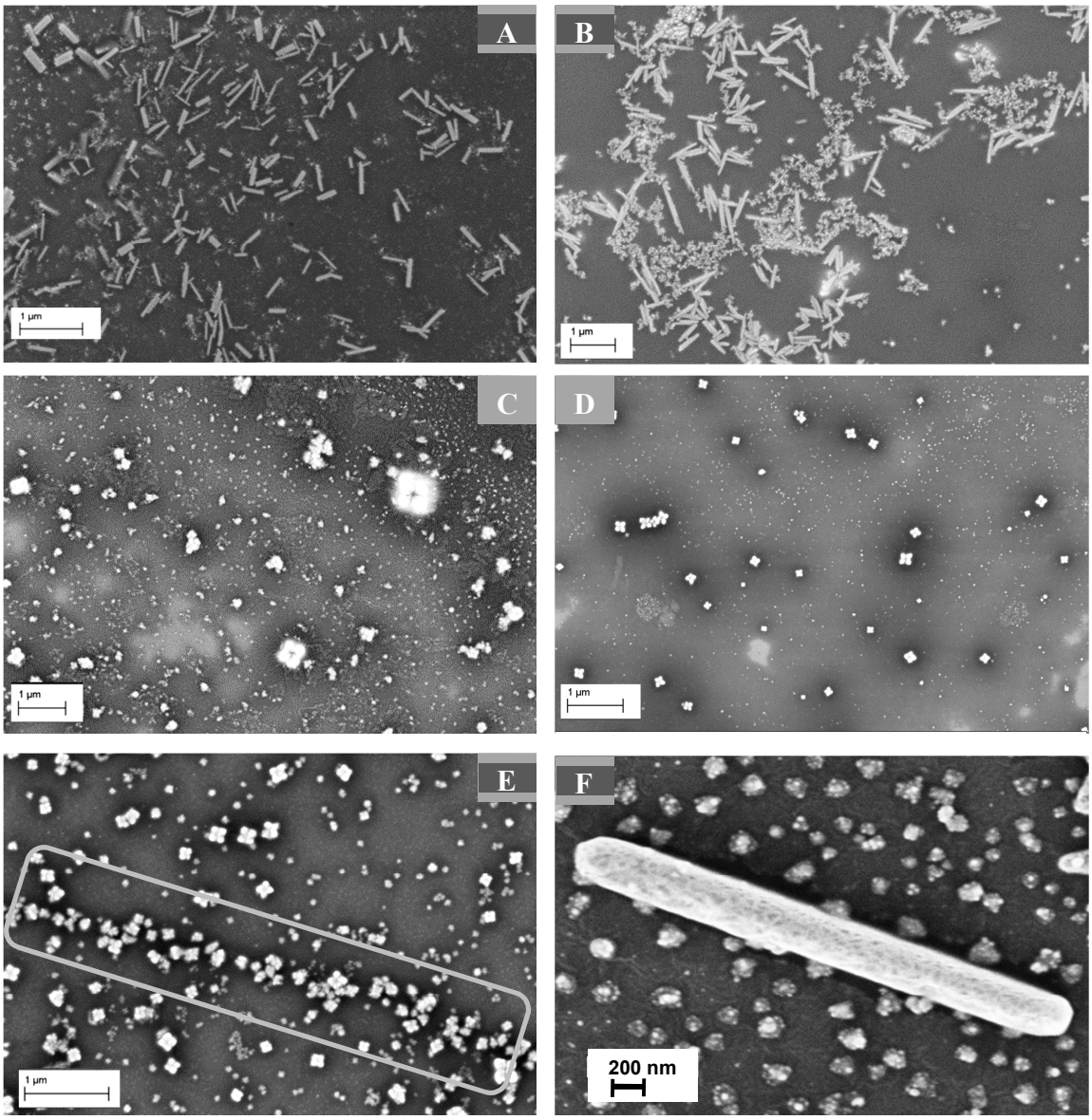


Figure 6.20: Effect of concetration ratio [C]:[Ag+] on the self-assembly of PNA (4*S*)-*amp*ʎ-$(C_4)_3$ (**P14**) with silver ions in water: [C]: [Ag+] was 0.5 mM : 2 mM (A), 1.0 mM : 2.0 mM (B), 1.5 mM : 2.0 mM (C), 2.0 mM : 2.0 mM (D), 2.5 mM: 2.0 mM. (E). (F) Porous rods formed by the PNA – Ag+ complex at 0.5 mM : 2.0 mM ratio.

Growth of Ag^+/PNA Nanostars

In order to understand the mechanism underlying the formation of silver nanostars, their growth was monitored over a period of 12 hours by time dependent FESEM imaging studies. To

an aqueous solution of PNA, freshly prepared $AgNO_3$ solution was added to bring the concentration of cytosine and Ag^+ to be 2 mM each. Aliquots (2 μL) taken out at different time points were deposited on a clean Si wafer to prepare the samples for FESEM studies. For the first sample, aliquot was taken soon after addition of $AgNO_3$, within the first 5 minutes. Subsequently, aliquots were retrieved at 3 hour, 6 hour, and 9 hour time points. The solvent from the drop was allowed to evaporate under high vacuum and the films were then left to stand for 12 hours under ambient conditions before imaging them under FESEM.

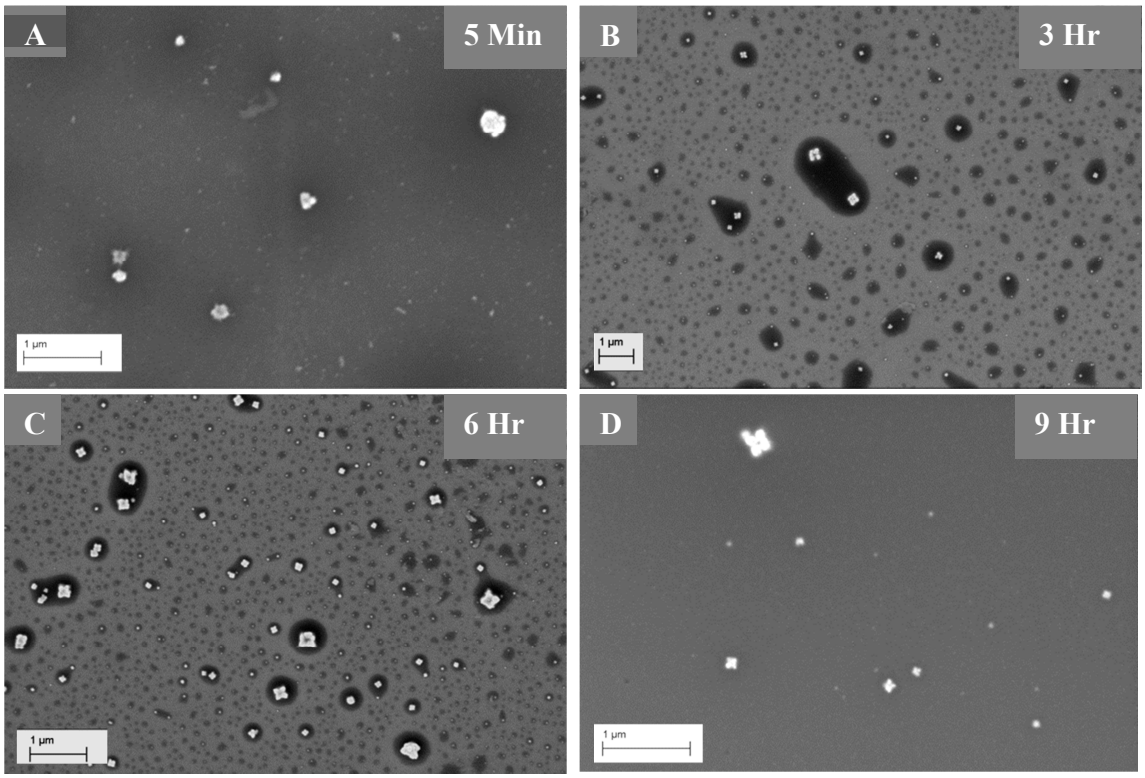


Figure 6.21: Time dependednt changes in morphology of PNA (4*S*)-*amp*^{A}-$(C_4)_3$ (**P14**) with silver ions in water: [C]: [Ag+] 2.0 mM : 2.0 mM. Particles and nanostructures formed within an hour (A), 3 hour (B), 6 hour (C) and 9 hours (D).

The 5 min sample showed many small particles (Figure 6.21A) where features of these particles were indiscernible with, some larger aggregates showing branched architecture but not well-defined in shape. At 3 hour, a few of the particles were found to be leading to the expected

four pointed star like morphology with well-defined features (Figure 6.21B), but many particles smaller than 20 nm were still present. At 6 hours, most particles were found to have the nanostar morphology with a very few emerging clusters as compared to sample at 3 hours. At 9 hours, formation of well-defined nanostars (Figure 6.21D) from clusters was complete with no tendency for further aggregation.

One of the possible mechanisms for nanostar morphology is that the PNA/Ag complex initially assemble into ellipsoidal particles that grow independently form clusters of 4 particles to produce the observed nanostars (Figure 6.23A). The time dependent FESEM studies however ruled out such a sequential process of assembly. Even within 1 hour, there were aggregates that showed tendency to evolve into nanostar architecture (Figure 6.23B). In none of the samples from the intervening time points, isolated and growing ellipsoidal lobes were found. In the final stages, at 9 hour, there were particles with exclusively 4 lobes. A sequential process of assembly should result in at least a few odd clusters with 2, 3 or 5 lobes. All the nanostars obtained were found to adhere to four fold symmetry, which is unlikely for a process that involves clustering of the pre-matured lobes. Further, the size of the all the lobes composing a nanostar are always nearly the same during the time period of this study. Thus the degree of precision and uniformity in morphological features, suggested that each of these star like particles synchronously grow as one entity and that they are not a sequential ensemble of separately pre-formed particles.

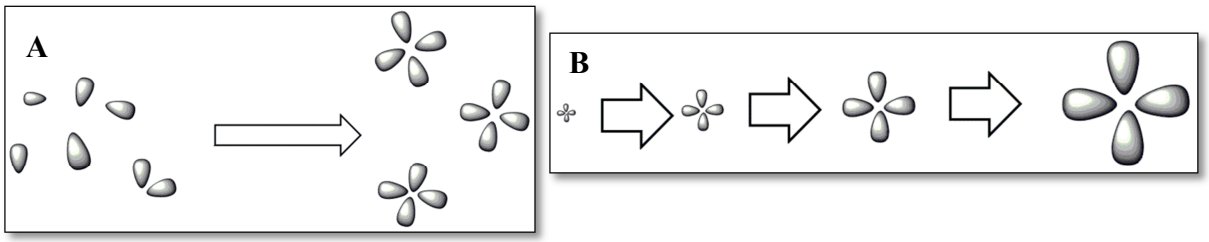


Figure 6.23: Two plausible mechanism of formation of four-point nanostars. A) The elliptical lobes form and grow independently and aggregate to form stars. B) The lobes grow synchronously as one branched entity.

When the core of branched PNA was (4*S*)-*amp*, silver induced the PNA (4*S*)-*amp*$^{\lambda}$-$(C_4)_3$ (**P14**) to assemble into regular four-pointed stars in water. To check the effect of chirality of the core branching unit, the self-assembly of complexes of Ag^+ with PNA (4*R*)-*Amp*$^{\lambda}$-$(C_4)_3$ (**P15**) was studied under the same condition. The samples for the FESEM imaging studies were prepared in the same way as described for (4*S*)-*amp*-$^{\lambda}$-$(C_4)_3$ (**P14**). The figure 6.22 shows that the morphology of Ag+ - PNA **P15** complexes taken in different concentration ranges from 1:4 to 1:1 ratio. Significantly, under these concentrations, it was observed that PNA **P15-**Ag+ complex forms small and irregular aggregates.

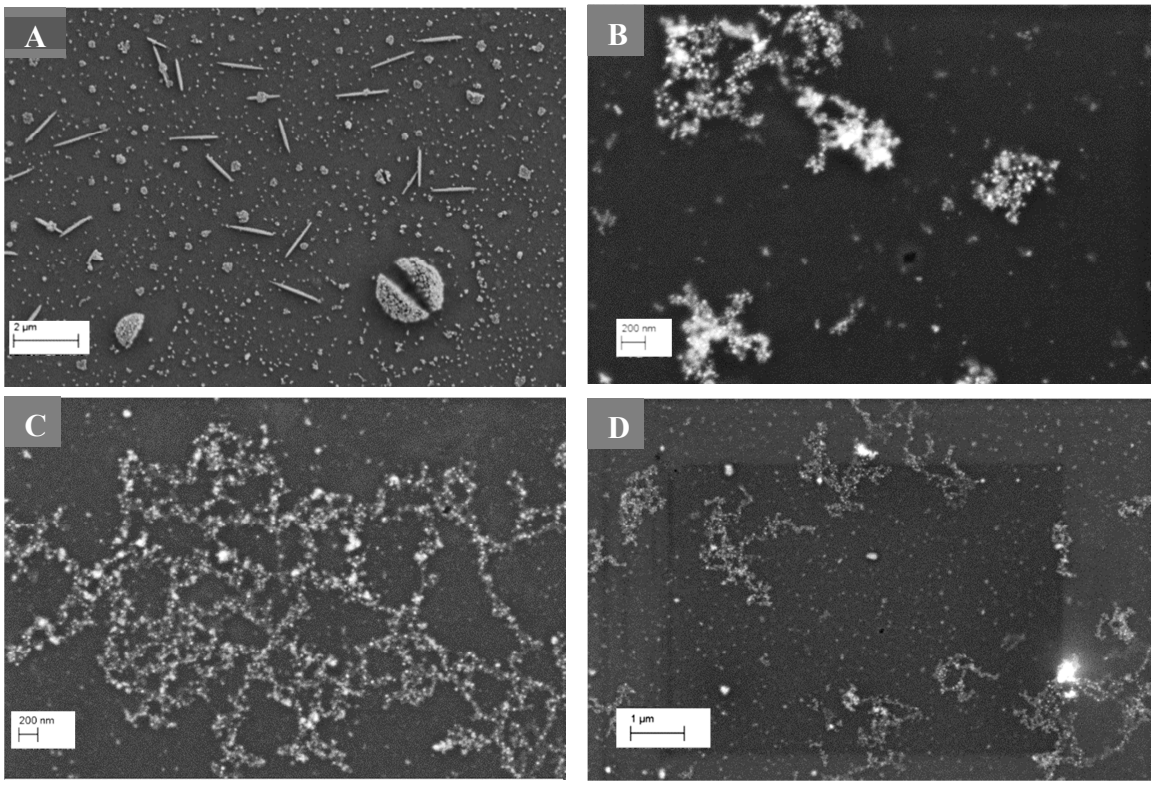


Figure 6.22: Effect of concetration ratio [C]:[Ag^+] on the self-assembly of PNA (4*R*)-*Amp*$^{\lambda}$-$(C_4)_3$ (**P15**) with silver ions in water: [C]: [Ag^+] was 0.5 mM : 2 mM (A), 1.0 mM : 2.0 mM (B), 1.5 mM : 2.0 mM (C), 2.0 mM : 2.0 mM (D).

In contrast to the regular well-defined morphology formed by **P14** (4*S*)-*amp*$^{\lambda}$-$(C_4)_3$ (**P14**), the PNA (4*R*)-*Amp*$^{\lambda}$-$(C_4)_3$ (**P15**) was unable to produce any shape-specific morphology. These results clearly showed the important influence of the stereo-configuration of the core in the self-assembly process of the dendritic type of molecules. It is notable that the circular dichroism studies of these two branched PNA also were remarkably different in the presence of silver ions. The CD results showed that PNA (4*S*)-*amp*$^{\lambda}$-$(C_4)_3$ (**P14**), attained a conformation soon after addition of Ag^+ ions into the solution, which gradually (90 min) reversed in its helical handedness. PNA (4*R*)-*Amp*$^{\lambda}$-$(C_4)_3$ (**P15**), on the other hand, initially attained a conformation similar to the one formed by (4*S*)-*amp*$^{\lambda}$-$(C_4)_3$ (**P14**) soon after exposure to Ag^+ ions and within 1.5 hours, **P15** underwent a reversal of handedness its conformation. However, unlike **P14**, the reversal was not complete and both the forms co-existed in nearly the same concentration resulting in total loss of CD signals. Such a biphasic conformational heterogeneity would seriously hamper the formation of ordered supramolecular structures. This was demonstrated by the formation of nanostructures with irregular and ill-defined morphology with (4*R*)-*Amp*$^{\lambda}$-$(C_4)_3$ (**P15**)-Ag^+ complex. These results clearly underline the role of chirality of the core aminoproline and especially the configuration at C4 in determining not only the conformational properties of the molecules, but also their self-assembling properties.

Role of Metal Ions on Self-Assembly of Branched PNA

Cytosines have been reported to form strong interactions with many metals.[32-34] This attribute of cytosine makes it interesting to study the complexation of branched PNA molecules

suitable with other metal ions in determining the self-assembling properties. In order to examine if the ability of nanostar formation is specific to only Ag^{+}, the self-assembly of (4*S*)-*amp*$^{\curlywedge}$-$(C_4)_3$ (**P14**) was studied in the presence of Hg^{2+}. Solutions of the PNA and metal ions were prepared where the concentration of cytosine and that of the metal ions were 2 mM each. From these solutions, the samples were prepared as described above for FESEM imaging (Figure 6.23).

Among the metals tested (Hg^{2+}, Cu^{2+} , Fe^{2+} , Au^{3+}, and Pb^{2+}), only Hg^{2+} was found to be able to produce a defined morphology, in contrast to only irregular structures were obtained with other metals. In the presence of Hg^{2+}, the PNA (4*S*)-*amp*$^{\curlywedge}$-$(C_4)_3$ (**P14**) formed long nanowires with a spherical cross-section.

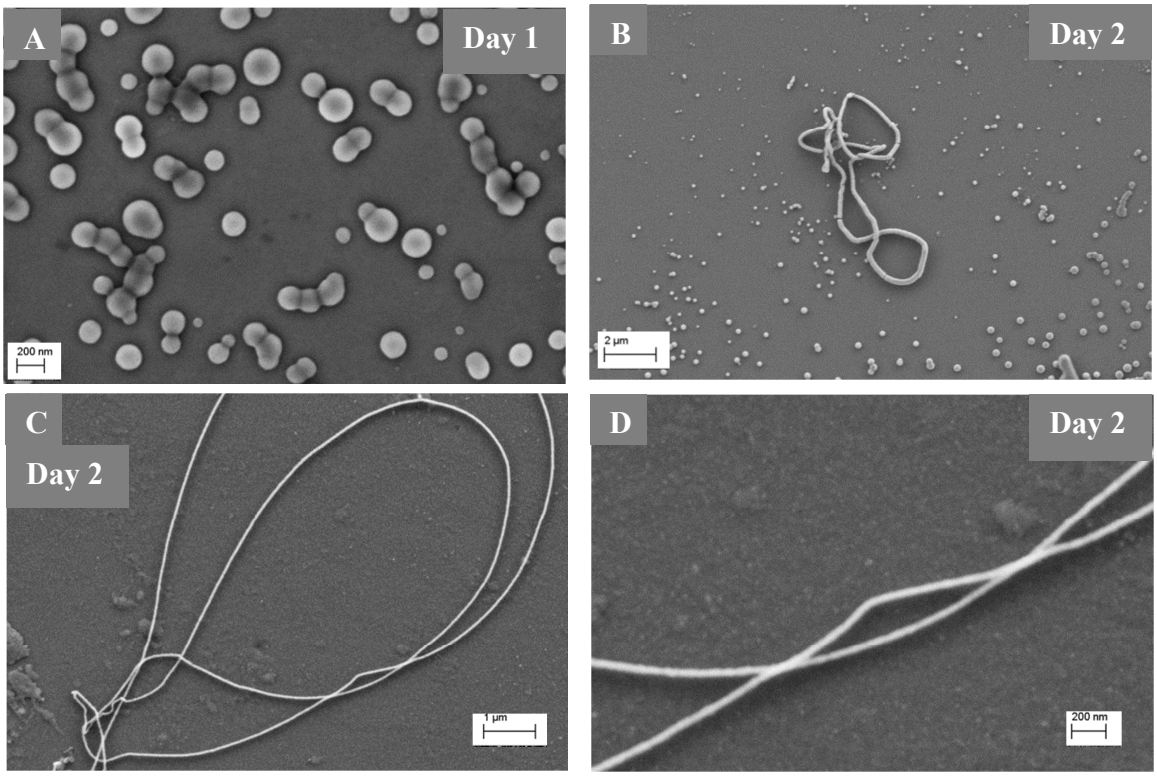


Figure 6.23: PNA / Mercury molecular wires. Spherical particles formed in a solution of PNA (4*S*)-*amp*$^{\curlywedge}$-$(C_4)_3$ (**P14**) and mercury on day 1 (A) and long wires formed after 2 days (B). Similar wires formed by PNA (4*R*)-*Amp*$^{\curlywedge}$-$(C_4)_3$ (**P15**) with Hg^{2+} in water (C and D).

Within one hour of addition of the metal salt, the solution was found to contain spherical nanoparticles of size around 50-200 nm, with PNA assembled into nanospheres induced by complexation with Hg^{2+} ions. These spheres then linearly fuse onto each other a period of 24 hours to impressively produce long supramolecular wires. Interestingly, PNA (4*R*)-*Amp*$^{\curlywedge}$-$(C_4)_3$ (**P15**) also produced a similar morphology of long nanowires with mercury ions. Thus, the influence of Hg^{2+} in the assembly of branched PNAs with either (4*R*)-*Amp* or (4*S*)-*amp* core was almost negligible. It is not clear at this stage how Hg^{2+} and Ag+ induce different effects on the self-assembly of PNA (4*S*)-*amp*$^{\curlywedge}$-$(C_4)_3$ (**P14**) and PNA (4*R*)-*Amp*$^{\curlywedge}$-$(C_4)_3$ (**P15**), which have chirally different proline cores.

6.4 Summary

In this chapter, branched peptide nucleic acids were constructed with (4*S*)-*amp* and (4*R*)-*Amp* as chiral branching core and their conformational properties and self-assembling behavior were studied.

- Using CD spectroscopy, the conformational properties of these molecules were studied at different pH. Such PNAs show no characteristic CD pattern on their own. However, in the presence of dC_{12} at pH 5, the PNAs (4*S*)-*amp*$^{\curlywedge}$-$(C_4)_3$ (**P14**) and (4*R*)-*Amp*$^{\curlywedge}$-$(C_4)_3$ (**P15**) CD spectra characteristic of i-motif structures of the PNA:DNA complexes.
- These hybrids were also found to assemble into hollow rectangular nanotubes. The nanotubes appeared to be crystalline and found to have grown from octahedral seed crystals over a period of 5 days.

- The branched PNAs showed chiral core dependent characteristic conformational behavior. While both (4*S*)-*amp*$^{\lambda}$-$(C_4)_3$ (**P14**) and (4*R*)-*Amp*$^{\lambda}$-$(C_4)_3$ (**P15**) form duplex on addition of silver ions, the conformation of **P14** and **P15** underwent changes over a duration of 90 minutes. The results indicated change of handedness of branched PNAs dependent on the chirality of the core.
- Stereochemistry dependent intra-molecular H-bonding properties were postulated to orchestrate the reversal of helical handedness of the silver mediated PNA duplexes. The chirality of the core also influenced the self-assembling properties.
- The four-point star like morphology formed by silver complexes with PNA (4*S*)-*amp*$^{\lambda}$-$(C_4)_3$ (**P14**) was not seen with PNA **P15** (4*R*)-*Amp*$^{\lambda}$-$(C_4)_3$.

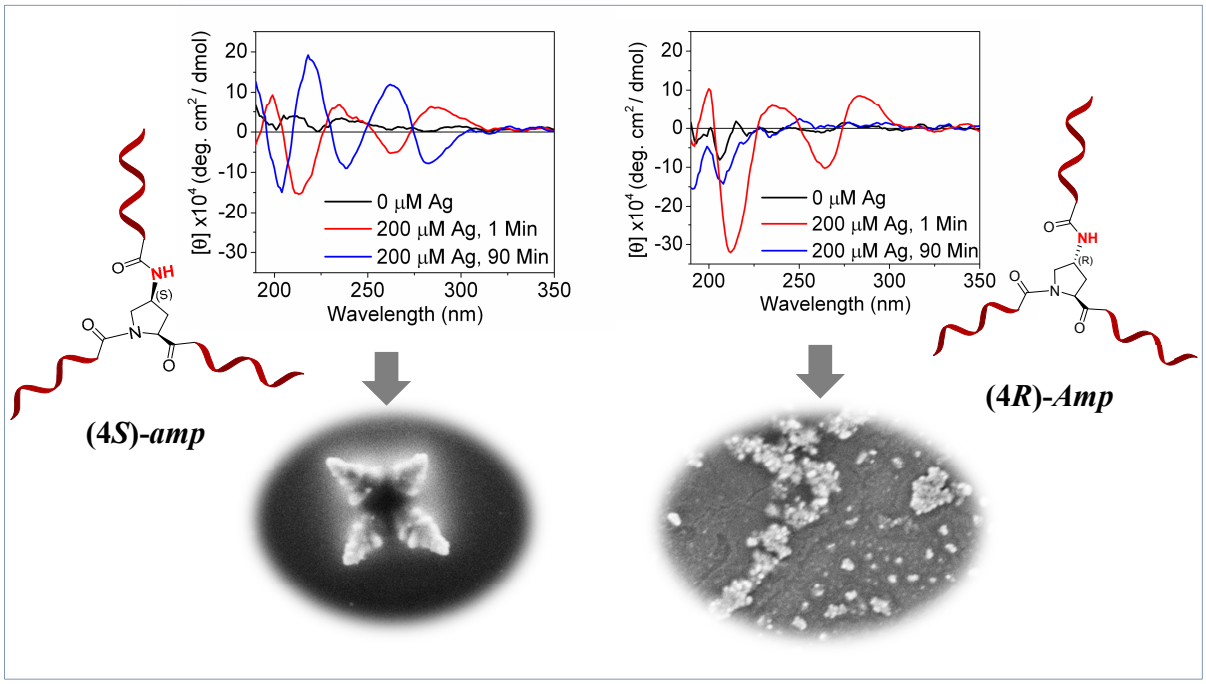


Figure 6.22: Stereodependent self-assembly of branched PNA

- The concentration dependent self-assembly studies revealed that the evolution of morphology of the nanostructures formed by the complex of Ag^+ and branched PNA was

dependent on the stoichiometry. The isolated four pointed nanostars formed at equimolar concentration of Ag^+ and Cytosine became porous rods at large Ag^+ concentration.

- On monitoring the growth of the nanostars it was found that they grew as a single entity and not clusters of separately formed elliptical particles.
- The branched PNAs were also found to assemble into spherical particles in the presence of Hg2+ ions in water, which then merged into one another to produce long molecular wires of many micrometers in length over a period of 2 days.

4-substituted aminoproline was known to have interesting properties due to the interplay of various stereoelectronic factors and H-bond forming ability. The rich conformational dynamics of aminoproline was exploited to synthesize branched PNA dendron-like molecules. These studies showed that a chiral control over the conformation and self-assembly could be achieved with these branched molecules. As a novel motif that brings together the strengths of peptide backbone based peptide nanotechnology and sequence dependent nucleic acid nanotechnology, these chiral branched PNA proved to be highly promising as a tool for directed self-assembly and for construction of dynamic nanodevices as demonstrated by the diverse nanostructures like nanospheres, hollow capsules, nanostars, and nanotubes, formed by these moleclues under various conditions in this thesis. Further investigations with the use of different sequences in the three arms of the PNA are likely to help gain useful insights into the supramolecular assemblies of these systems and widen the scope of the various self-assembly based applications.

6.5 Experimental

The DNA and RNA oligonucleotides were obtained commercially from IDT (integrated DNA technologies). All the chemicals were of analytical grade.

6.5.1 Solid Phase PNA Synthesis

The general procedure used to synthesize the PNA was the same as the ones in Chapter 2, except for the loading value of the resin, which was reduced to 0.1 mmol/g.

6.5.1a *Synthesis of PNA*

PNAs were synthesized manually using a sintered (G2) reaction vessel equipped with a Teflon stopcock. All the materials used were of peptide synthesis grade (Novabiochem) and was used without further purification. Analytical grade DMF was purchased from (Merck, India) and stored over 4Å molecular sieves for 2 days before using for peptide synthesis. Similarly DCM was distilled over CaH_2 and stored over 4 Å molecular sieves. Coupling reactions were carried out using *in situ* active ester method, by HBTU as coupling reagent, HOBt as recemization suppresser and DIPEA as catalyst. The aeg-PNA monomers were obtained from ASM Research Chemicals (Germany) and used as received.

Resin functionalization

Commercially available MBHA (4-methyl benzhydrylamine) resin (Novabiochem, 100-200 mesh) the hydrochloride salt was neutralized performed prior to monomer coupling and the following steps were done for synthesis (100 mg scale). The resin was washed and swollen in dry DCM for atleast 1 hr. The DCM was drained

and 50% solution of DIPEA in DCM was added (3 x 3ml; 10 min each) followed by thorough washing with DCM. Further washing and swelling with dry DMF for 1 hr.

Synthesis protocol

A combination of Boc–strategy and Fmoc strategy was used for synthesis on MBHA resin.

- DCM wash (4 x 5 ml)
- 50% TFA in DCM (2 X 5 ml; 10 min each) for deprotection of t-Boc group
- 5% DIPEA in DCM (3 X 5 ml; 5 min each) for neutralization of TFA salt
- DCM, MeOH wash (3 x 3 ml each)
- Kaiser's/Chloranil test
- DCM, DMF wash (3 x 3 ml each)
- Coupling reaction (3 eq. each of PNA monomer, DIPEA, HOBt and HBTU in 10eq. volume of DMF)
- Kaiser's/Chloranil test

These cycles ware repeated for every PNA monomer. The coupling and deprotection reactions were monitored by a combination of Kaiser's (ninhydrin) test and chloronil test. In case of negative test after coupling the re-coupling was performed with same monomer followed by capping of the unreacted amino groups using Ac_2O, DIPEA & DMF (1:1:1), in case coupling does not go to completion even after re-coupling. A linear PNA chain with arms X and Y containing the aminoproline with a sidechain amine protected with Fmoc in the middle of the sequence was thus synthesized. The sidechain Fmoc was deprotected with by 20 % piperidine in DMF and the branching PNA arm was synthesized using Fmoc-strategy.

- Wash with DMF 4 x 5 mL.
- 20% piperidine in DMF 2 x 5 mL (15 min for each) for deprotection of Fmoc group.
- Wash with DMF 3 x 5 mL, MeOH 3 x 5 mL, DCM with 3 x 5 mL and DMF 3 x 5 mL.
- Test for complete deprotection (Kaiser's test).
- Coupling reaction with PNA monomer, DIPEA, HOBt and HBTU (3 eq.) in DMF.
- Repeat of the coupling reaction.
- This cycle was repeated for every monomer.

Kaiser's test

Kaiser's was used to monitor the t-Boc/Fmoc deprotection and coupling in the solid phase peptide synthesis using three solutions. Solution A: Ninhydrin (5.0 g) dissolved in ethanol (100 ml) Solution B: Phenol (80.0 mg) dissolved in ethanol (20 ml) Solution C: KCN (2 ml, 0.001 M aqueous solution) added to 98 ml pyridine

- Few beads of resin to be tested were taken in a test tube and washed 3 times with ethanol.
- 3-4 drops of each of the three solutions described above were added to it
- The test tube was heated to 120 °C for 4-6 min
- The successful deprotection was indicated by blue resin beads while colourless beads indicate the completion of coupling step.

Chloranil test

A few beads of resin were taken in a glass test tube (5 ml capacity) and were washed with methanol followed by toluene. To this three drops of saturated chloranil solution in toluene and 200 µl of acetone were added. The mixture was shaken for 2-

3 minutes. Blue or green color is observed on the resin beads if free amines are present.

6.5.1b *Peptide cleavage from resin*

Finally after the last coupling the resin was washed with DMF (5 x 5 ml), DCM (5 x 5 ml), then with toluene (5 x 5 ml) and methanol (5 x 5 ml) then flushed with N2-gas for 3 mins. The resin along with the sintered flask was dried in vacuum desiccator over KOH and P_2O_5 for 6 hrs.

The resin MBHA (10 mg) with peptides attached to it was stirred with TFA (200 µL) and deionized water (10 µL) in an ice bath for 10 min. TFMSA (16 µL) was added slowly with vigorous shaking to dissipate the heat generated. The reaction mixture was stirred for 1.5 hrs at room temperature. The resin was removed by filtration under reduced pressure and washed with TFA (3 x 1 mL). The combined filtrate was concentrated, the product was precipitated with cold dry ether and the peptide was isolated by centrifugation (5 times at 5000 rpm) as white powder. Peptides which had Fmoc-protection in side groups were removed by 20% piperidine/DMF treatment and dried properly before cleavage.

6.5.2 High Performance Liquid Chromatography (HPLC)

Peptides were purified by reverse phase-HPLC on Agilent Technologies 1260 Infinity equipped with Photodiode array detector (PDA). Semi-preparative RP-C18 columns (250x10 mm, 10 μm) of was used for peptides. The solvent system comprised of MeCN:Water (5:95) with 0.1% TFA for solution A and for solution B MeCN: Water (50:50), 0.1% TFA. A gradient of 0-100% at a flow rate of 3 mL/min was used to elute the peptide and the eluant was monitored at 220 nm. The

peak corresponding to the peptide was collected and the fractions were freezed. Subsequently these peptides were concentrated by using speed vacuum. The purity of the final peptides were further analyzed on the Phenomenex Analytical RP-C18 (250 x 4 mm, 5 μm) column by using a gradient flow of 0 to 100% B in 30 min at a flow rate of 1 mL/min. The absorbance of the eluant was monitored at its corresponding wavelength and the purity was obtained from the integrator output. The purities of the hence purified peptides were found to be more than 95%.The overall yield of peptides are given in table 6.2.

Table 6.2: Overall yields of the peptides used in the present study

	Peptide	Overall Yield (%)
P14	(4*S*)-*amp*$^{\lambda}$-$(C_4)_3$	14
P15	(4*R*)-*Amp*$^{\lambda}$-$(C_4)_3$	15

6.5.3 MALDI-TOF Characterization

MALDI-TOF mass spectra were obtained on either Voyager-Elite instrument (Perspective Biosystems Inc., Farmingham, MA) equipped with delayed extraction or on Voyager-De-STR (Applied Biosystems) instrument. 2,5-Dihydroxy benzoic acid (DHB) and α-cyano-4-hydroxycinnamic acid (CHCA) both were used as matrix for peptides of which DHB was found to give satisfactory results. A saturated matrix solution was prepared with typical dilution solvent (50:50:0.1 Water: MeCN: TFA) and spotted on the metal plate along with the oligomers. The metal plate was loaded to the instrument and the analyte ions are then accelerated by an applied high voltage (15-25 kV) in reflector mode, separated in a fieldfree flight tube and detected as an electrical signal at the end of the flight tube.

6.5.2 Circular Dichroism (CD) Spectroscopy

CD spectrometric study was carried out on JASCO J-815 spectropolarimeter using cylindrical, jacketed quartz cell (10 mm path length), which was connected to Julabo-UC25 water circulator. For reproducible data, each set of spectra were measured using at least three individually prepared solutions. CD spectra were recorded using a spectral bandwidth of 1.0 nm at 25 °C with a time constant of 1 s and a step resolution of 1 nm. All the spectra were corrected for respective buffer condition and are typically averaged over 3-6 scans. A quartz cell with a path length of 1 mm was used with solutions containing approximately 0.25 mL (50 to 250 μM).

The PNA solutions of concentrations (typically, 12 μM) were prepared from a stock solution for CD studies in 10 mM sodium phosphate buffers of appropriate pH. For acidic pH 5, 0.2M HCl was added to adjust the pH. For all the DNA interaction studies, the solutions of oligonucleotides of appropriate concentrations were mixed with the PNA solution taken in buffer (10 mM sodium phosphate buffer and 10 mM NaCl) and incubated at room temperature for 8 hours. The data processing and curve fitting were performed using Origin 8.0 software. All spectra were collected at 25^{o} C with a 1 nm resolution and a scan rate of 50 nm/min. Spectra are the averages of 6 scans, except for time dependent studies where 3 scans were averaged.

6.5.3 Field Emission Scanning Electron Microscopy (FESEM)

Appropriate volumes of the peptides were taken into microfuge tube from stock solution and water was evaporated by using speed vac. Desired solvent was added to it and solution was vortexed for 1 min and centrifuged. 2 μL of supernatant solution was then drop casted on clean silicon vapor. Samples were allowed to dry at room temperature in vacuum

desiccators and then coated with gold. Scanning electron microscopic imaging was performed using ZEISS ULTRA PLUS electron microscope.

6.6 Reference

1. Yin, P.; Choi, H. M. T.; Calvert, C. R.; Pierce, N. A. Programming biomolecular self-assembly pathways. *Nature* **2008,** *451*, 318-322.

2. Seeman, N. C; Sleiman, H. F. DNA nanotechnology. *Nat. Rev. Mater*. **2017**, *3*, 17068.

3. Santisa, E. D.; Ryadnov, M. G. Peptide self-assembly for nanomaterials: the old new kid on the block, *Chem. Soc. Rev.* **2015**, *44,* 8288-8300. b) Mandal, D.; Shirazi, A. N.; Parang, K. Self-Assembly of Peptides to Nanostructures, *Org. Biomol. Chem*. **2014**, *12*(22), 3544–3561. c)Hartgerink, J. D.; Beniash, E.; Stupp, S. I. Self-assembly and mineralization of peptide-amphiphile nanofibers. *Science* **2001,** *294*, 1684-1688. d) Gaitzsch, J.; Karu, K.; Battaglia G. Peptoidosomes as nanoparticles from amphiphilic block alpha-peptoids using solid-phase-synthesis. *Eur. Polym. J.* **2015**, *73*, 447–454.

4. Lapenta, F.; Aupič, F.; Strmšeka, Z.; Jerala, R. Coiled coil protein origami: from modular design principles towards biotechnological applications. *Chem. Soc. Rev*. **2018**, *47*, 3530-3542.

5. Gleaton, J.; Chmielewski, J.; Thermally Controlled Collagen Peptide Cages for Biopolymer Delivery. *ACS Biomater. Sci. Eng.* **2015**, *1*, 1002–1008. b) Hsu, W.; Chen, Y.; Horng, J. C. Promoting Self-Assembly of Collagen-Related Peptides into Various Higher-Order Structures by Metal − Histidine Coordination. *Langmuir* **2012**, *28*, 3194 −3199. c) Przybyla, D. E.; Chmielewski, J. Higher-Order Assembly of Collagen Peptides into Nano- and Microscale Materials. *Biochemistry* **2010**, *49*, 4411–4419.

6. Chen, P. Self-assembly of ionic-complementary peptides: a physicochemical viewpoint *Colloids and Surfaces A: Physicochem. Eng. Aspects* **2005**, *261*, 3–24.

7. a) Jalan, A. J.; Hartgerink, J. D. Pairwise interactions in collagen and the design of heterotrimeric helices. *Curr. Opin. Chem. Biol.* **2013**, *17*, 960–967. b) Jiang, T.; Xu, C.; Liu, Y.; Liu, Z.; Wall, J. S.; Zuo, X.; Lian, T.; Salaita, R.; Ni, C.; Pochan, D.; Conticello, V. P. Structurally Defined Nanoscale Sheets from Self-Assembly of Collagen-Mimetic Peptides. *J. Am. Chem. Soc.* **2014**, *136*, 4300–4308.

8. Pieters, B. J. G. E.; Eldijk, M. B.; Nolte, R. J. M; Mecinovic, J. Natural supramolecular protein assemblies. *Chem. Soc. Rev*. **2016**, *45*, 24-39.

9. Zhang, F.; Nangreave, J.; Liu, Y.; Yan, H. Structural DNA Nanotechnology: State of the Art and Future Perspective. *J. Am. Chem. Soc.* **2014**, *136*, 11198 −11211.

10. Lou, C.; Martos-Maldonado, M. C.; Madsen, C. S.; Thomsen, R. P.; Midtgaard, S. R.; Christensen, N. J.; Kjems, J.; Thulstrup, P. W.; Wengel, J.; Jensen, K. J. Peptide–oligonucleotide conjugates as nanoscale building blocks for assembly of an artificial three-helix protein mimic. *Nat. Commun.* **2016***, 7*, 12294.

11. a) Li, X.; Kuang, Y.; Xu, B. Soft "Molecular trinity" for soft nanomaterials: Integrating nucleobases, amino acids, and glycosides to construct multifunctional hydrogelators Soft *Matter***, 2012**,*8*, 2801-2806. b) Datta, D.; Tiwari, O.; Ganesh, K. N. New archetypes in self-assembled Phe-Phe motif induced nanostructures from nucleoside conjugated-diphenylalanines. *Nanoscale* **2018**, *10*, 3212-3224.

12. Egholm, M.; Buchardt, O.; Nielsen, P. E.; Berg, R. H. Peptide nucleic acids (PNA). Oligonucleotide analogs with an achiral peptide backbone. *J. Am. Chem. Soc*. **1992**, *114,* 1895–1897. b) Lundin, K. E.; Good, L.; Strömberg, R.; Gräslund, A.; Smith, C.I. Biological Activity and Biotechnological Aspects of Peptide Nucleic Acid. *Adv. Genet.* **2006**, *56,* 1-51.

13. a) Ellipilli, S.; Vasudeva M. R.; Ganesh, K. N. Perfluoroalkylchain conjugation as a new tactic for enhancing cell permeability of peptide nucleic acids (PNAs) via reducing the nanoparticle size. *Chem. Commun*. **2016,** *52*(3), 521-524. b) Vernille, J. P.; Kove, L. C.; Schneider, J. W. Peptide Nucleic Acid (PNA) Amphiphiles: Synthesis, Self-Assembly, and Duplex Stability *Bioconjugate Chem*. **2004**, *15*, 1314–1321. c) Molecular self-assembly using peptide nucleic acids Berger, O.; Gazit, E. *Biopolymers* **2017**, *108* (1), e22930.

14. Berger, O.; Adler-Abramovich, L.; Levy-Sakin, M.; Grunwald, A.; Liebes-Peer, Y.; Bachar, M.; Buzhansky, L.; Mossou, E.; Forsyth. V. T.; Schwartz, T.; Ebenstein, Y.; Frolow, F.; Shimon. L. J.; Patolsky, F.; Gazit, E. Light-emitting self-assembled peptide nucleic acids exhibit both stacking interactions and Watson-Crick base pairing. *Nat. Nanotech*. **2015**, *10*, 353–360.

15. Kumar, V. A; Ganesh, K. N. Conformationally Constrained PNA Analogues: Structural Evolution toward DNA/RNA Binding Selectivity. *Acc. Chem. Res*. **2005**, *38*, 404–412.

16. a) Guéron, M.; Leroy, J. L. The i-motif in nucleic acids. *Curr. Opin. Struct. Biol.* **2000**, *10,* 326–331. b) Day, H. A.; Huguin, C.; Waller, Z. A. E. Silver cations fold i-motif at neutral pH *Chem. Commun*. **2013**, *49*, 7696.

17. a) Tanaka, K.; Tengeiji A.; Kato T.; Toyama N.; Shionoya M.A. Discrete Self-Assembled Metal Array in Artificial DNA *Science* **2003**, *299*, 1212-1213. b) Tanaka K.; Yamada Y.; Tengeiji A.; Kato T.; Toyama N.; Takezawa Y.; Yori M.; Shiro M.; Shionoya M. Artificial metallo-DNA: structural control and discrete metal assembly. *Nucleic Acids Res Suppl*. **2003**, *3*, 121-122.

18. Gangamani, B. P.; Kumar, V. A.; Ganesh, K. N. Chiral analogs of peptide nucleic acids: synthesis of 4-aminoprolyl nucleic acids and DNA complementation studies using UV/CD spectroscopy. *Tetrahedron* **1999**, *55*, 177–192.

19. Seebach, D.; Beck, A. K.; Bierbaum, D. J. The world of beta- and gamma-peptides comprised of homologated proteinogenic amino acids and other components. *Chem. Biodivers*. **2004**, *8*, 1111-1239.

20. Sforza, S.; Haaima, G.; Marchelli, R.; Nielsen, P. E. Chiral Peptide Nucleic Acids (PNAs): Helix Handedness and DNA Recognition.Eur. *J. Org. Chem*. **1999**, 197-204.

21. a) Manzini, G.; Yathindra, N.; Xodo, L. E. Evidence for intramolecularly folded i-DNA structures in biologically relevant CC-repeat sequences. *Nucleic Acids Res*. **1994,** *22*, 4634-4640. b) Gade, C. R.; Sharma, N. K. Hybrid DNA i-motif: Aminoethylprolyl-PNA (pC5) enhance the stability of DNA (dC5) i-motif structure. *Bioorg. Med. Chem. Letts.* **2017,** *27*, 5424–5428. c) Sharma, N. K. & Ganesh, K. N. PNA C-C+i-motif: superior stability of PNA TC8 tetraplexes compared to DNA TC8 tetraplexes at low pH. *Chem. Commun.* **2005**, 4330–4332.

22. Modi, S.; Wani, A. H.; Krishnan, Y. The PNA–DNA hybrid I-motif: implications for sugar–sugar contacts in i-motif tetramerization. *Nucleic Acids Res.* **2006**, *34*, 4354–4363. b) Krishnan, Y.; Stephens, E.; Balasubramanian, S. A PNA_4 Quadruplex. *J. Am. Chem. Soc.* **2004**, *126*, 5944–5945.

23. Chang Lu, C,; Huang, Z.; Liu, B.; Liu, B.; Ying, Y.; Liu. J. Poly-cytosine DNA as a High-Affinity Ligand for Inorganic Nanomaterials. *Angew. Chem. Int. Ed*. **2017,** *56*, 6208 –6212.

24. Gourishankar, A.; Shukla, S.; Ganesh, K. N.; Sastry, M. Isothermal Titration Calorimetry Studies on the Binding of DNA Bases and PNA Base Monomers to Gold Nanoparticles. *J. Am. Chem. Soc.* **2004**, *126*, 13186–13187.

25. Jayarathna, D. R.; Stout, H. D.; Achim, C. Metal Coordination to Ligand-Modified Peptide Nucleic Acid Triplexes. *Inorg. Chem*. **2018**, *57*, 6865–6872.

26. Swasey, S. M.; Leal, L. E.; Acevedo, O. L.; Pavlovich, J.; Gwinn, E. G. Silver (I) as DNA glue: Ag+- mediated guanine pairing revealed by removing Watson-Crick constraints *Sci. Rep*. **2015**, *5*, 10163.

27. Sugiyama, T.; Kittaka, A.Chiral Peptide Nucleic Acids with a Substituent in the N-(2-Aminoethy)glycine Backbone. *Molecules* **2013**, *18*, 287-310.

28. Santamar-Diaz, N.; Mendez-Arriaga, J. M.; Salas, J. M.; Galindo, M. A. Highly Stable Double-Stranded DNA Containing Sequential Silver(I)-Mediated 7-Deazaadenine/Thymine Watson–Crick Base Pairs. *Angew. Chem. Int. Ed*. **2016**, *55*, 6170 –6174.

29. Zikich, D.; Liu, K.; Sagiv, L.; Porath, D.; Kotlyar A. I-motif nanospheres: unusual self-assembly of long cytosine strands. *Small* **2011**, *7*, 1029-1034.

30. Zeraati, M.; Langley, D. B.; Schofield, P.; Moye, A. L.; Rouet, R.; Hughes, W. E.; Bryan, T. M.; Dinger, M. E.; Christ, D. I-motif DNA structures are formed in the nuclei of human cells. *Nat. Chem*. **2018**, *10*, 631–637.

31. a) Dong, Y.; Yang, Z.; Liu, D. DNA nanotechnology based on i-motif structures. *Acc. Chem. Res.* **2014**, *47*, 1853-1860. b) Cheng, E.; Xing, Y.; Chen, P.; Yang, Y.; Sun, Y.; Zhou, D.; Xu, L.; Fan, Q.; Liu, D. A pH-Triggered, Fast-Responding DNA Hydrogel. *Angew. Chem. Int. Ed.* **2009**, *48*, 7660 –7663.

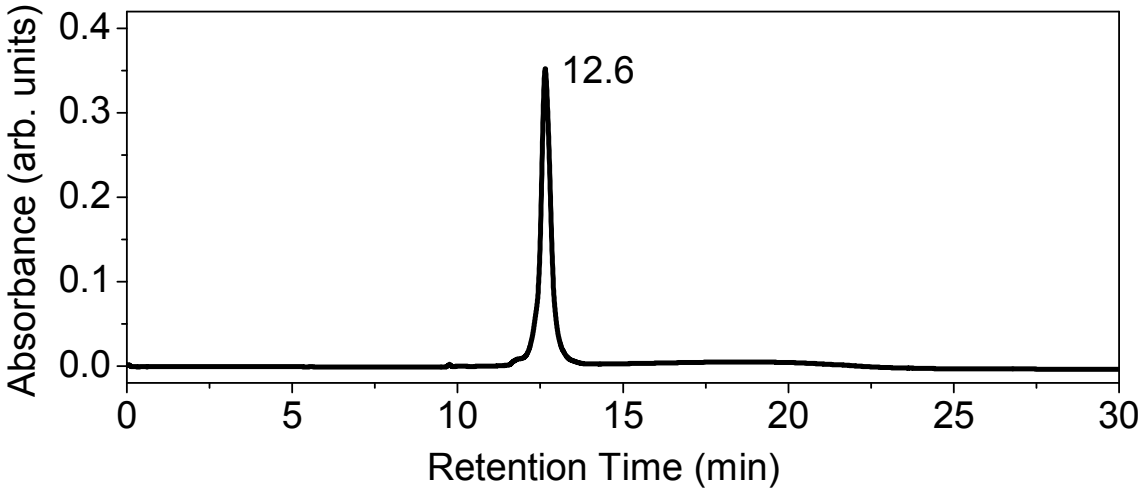
32. Ring crystals of oligonucleotides: Growth stages and X-ray diffraction studies. Mandal, P. K.; Chandrasekaran, A. R.; Madhanagopal, B.; Venkadesha, S.; Gautham, N. *J. Cryst. Growth* **2012,** *354*, 20-26.

33. Lippert, B.; Miguel, P. J. S. The Renaissance of Metal − Pyrimidine Nucleobase Coordination Chemistry. *Acc. Chem. Res.* **2016**, *49*, 1537 −1545.

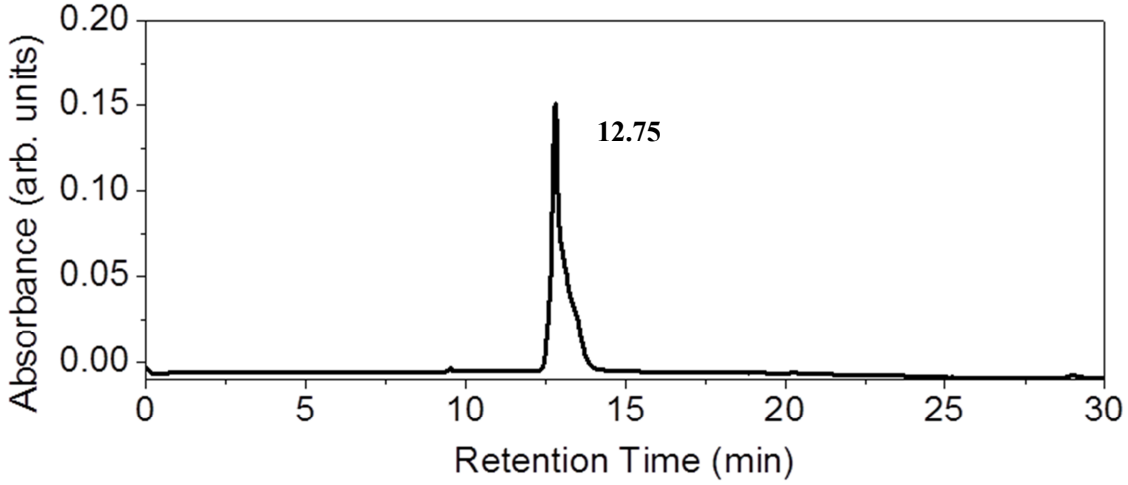
34. Kondo, J.; Tada, Y.; Dairaku, T.; Hattori, Y.; Saneyoshi, H.; Ono, A.; Tanaka, Y. A metallo-DNA nanowire with uninterrupted one-dimensional silver array. *Nat. Chem*. **2017**, *10*, 956-960.

6.7 Appendix C

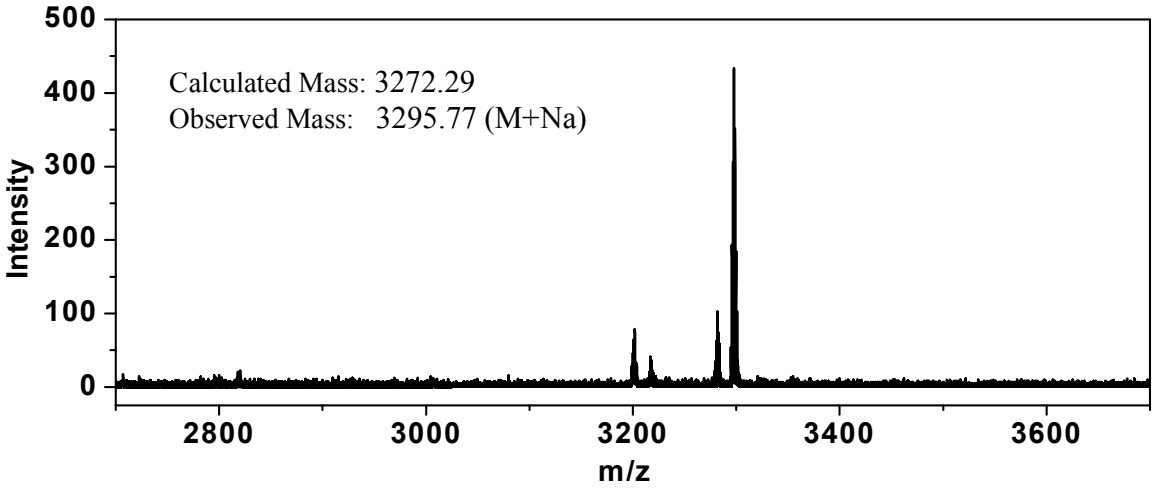
HPLC chromatogram of (4*S*)-*amp*$^{\lambda}$-$(C_4)_3$ (**P14**)



HPLC chromatogram of (4*R*)-*Amp*$^{\lambda}$-$(C_4)_3$(**P15**)



MALDI-TOF Spectrum of (4*S*)-*amp*$^{\lambda}$-$(C_4)_3$ (**P14**)



MALDI-TOF Spectrum of (4*R*)-*Amp*$^{\lambda}$-$(C_4)_3$ (**P15**)

